THÈSE

En vue de l'obtention du

DOCTORAT DE L'UNIVERSITÉ DE TOULOUSE

Délivré par :

Institut National Polytechnique de Toulouse (Toulouse INP)

Discipline ou spécialité :

Science et Génie des Matériaux

Présentée et soutenue par :

Mme NELLY WAHYUNI
le lundi 12 novembre 2018

Titre :

Absorption and Luminescence Properties of beta-carotene with Antioxidant and Modified Kaolinite and Its Application in OLED

Ecole doctorale :
Sciences de la Matière (SDM)

Unité de recherche :
Laboratoire de Chimie Agro-Industrielle (L.C.A.)

Directeur(s) de Thèse :
M. ZEPHIRIN MOULOUNGUI
M. GEORGES ZISSIS

Rapporteurs :
M. AMANE JADA, CNRS
M. DIVINE NDE BUP, UNIVERSITE DE BAMENDA

Membre(s) du jury :
Mme KATHLEEN MOINEAU, CNRS TOULOUSE, Président
M. BELKACEM ZEGHMATI, UNIVERSITE DE PERPIGNAN, Membre
M. GEORGES ZISSIS, UNIVERSITE TOULOUSE 3, Membre
M. THAMRIN USMAN, UNIVERSITAS TANJUNGPURA, Membre
M. ZEPHIRIN MOULOUNGUI, INRA TOULOUSE, Membre

ACKNOWLEDGMENTS

My Husband, SARYUDI
Our Lovely Children, AYA FITRIA QOLBI and
TITAN ARRAYAN FIKRI

Thanks for all your love, understanding and support

My Parents, M. ALI MOCHTAR and ZUKIAH
SUKARJO and DALIYEM
Family of 101, LIANA AISYAH and ACHMAD NASRULLAH
AND ALL MY FAMILY

ACKNOWLEDGMENTS

Absorption and Luminescence Properties of Carotenoids with Antioxidant and Modified Kaolinite and Its Application in OLED

Summary

Energy crises, especially fossil fuel-based energy, lead to increased use of new energy and renewable energy. In addition, research is also directed towards more efficient energy use through the development of energy storage materials such as batteries, and the use of energy-efficient materials. An OLED (organic light-emitting diode) is a light-emitting diode (LED) and is known for their high potential in a display, signage, and lighting applications.

Carotenoids constitute an important class of linear π-conjugated molecules that exhibit a high degree of electronic delocalization and ultrafast dynamic. The dye that is used as a photosensitizer plays an important role in the operation of DSSCs or other bifunctional material.

In this research, we studied the photostability of the carotenoid compound (β-carotene and fucoxanthin) using natural antioxidant and modified kaolinite. In this work, the carotenoid stability by the carotenoid compound/antioxidant binary is studied for the first time. Photostability of β-carotene can be enhanced by antioxidant and modified kaolinite. Photoprotection efficiency of β-carotene by curcumin was higher than fucoxanthin. Modified kaolinite decreased photodegradation of β-carotene by shielded and protected from direct UV irradiation.

Antioxidant fucoxanthin and curcumin decreased the electrochemical gap of the binary material. The electrochemical gap of carotene/curcumin is -1.61 eV, carotene/fucoxanthin is -1.75 eV compare to the only β-carotene -2.04 eV. Fucoxanthin can keep the first oxidation stage of β-carotene. Therefore at the binary compound, electron was still reversible, but not for curcumin.

Fucoxanthin in OLED devices NPD/Fx/ETL reduced significanly the EQE (%) almost 80% in Alq_3 and 76% in BAlq. OLED device: NPD(50nm)/Fx(1nm)/Alq3(85nm) yielded an effeciency quantum external yield, EQE = 0.12% and CIE (0.4160, 0.5302). Fabrication OLED using β-carotene as HTL and curcumin as EL layer resulted yellow color , EQE = 0.02%, with the composition MoO_3(15nm)/NPD(40nm)/Car(10nm)/Cur(15nm)/Alq_3(70nm)/Ca(100nm). For application of β-carotene in OLED device, its perfomance can be improved by using curcumin at the fabrication

Keywords: antioxidant, beta-carotene, fucoxanthin, kaolinite, OLED, photostability

Propriétés d'absorption et de luminescence du caroténoïdes à l'aide un antioxydant et le kaolin modifié et son application dans les diodes électroluminescentes organiques (OLED)

Résumé

Les crises énergétiques, en particulier celles liées aux combustibles fossiles, conduisent à une utilisation accrue des nouvelles énergies renouvelables. De plus, les recherches visent également à utiliser des matériaux de stockage de l'énergie qui sont plus efficace, tels que les batteries, et à utiliser des matériaux économes en énergie. Une OLED (diode électroluminecente organique)) est une diode émettrice la lumière (LED) qui sont connues grâce leur potentiel élevé dans les applications d'affichage, de signalisation et d'éclairage.

Parmi ces matériaux organiques, les caroténoïdes constituent une classe importante de molécules linéaires conjuguées qui présentent un degré de délocalisation électronique élevé et de dynamique ultra-rapide. Le colorant joue un rôle important dans le fonctionnement des cellules solaires à pigment photosensible (CSPP) ou d'autres matériaux bi fonctionnels.

Dans cette recherche, nous avons étudié la photo stabilité des caroténoïdes (β-carotène et fucoxanthine) à l'aide du kaolin modifié et de l'antioxydant. La photostabilité du β-carotène et de la fucoxanthine peut être améliorée par la kaolinite modifiée et l'antioxydant.

La fabrication OLED utilisant la fucoxanthine n'est pas suffisante à cause de la bande interdite de la fucoxanthine (Fx) qui est très grande et peut être un isolant. NPD (50 nm) / Fx (1 nm) / Alq$_3$ (85 nm) a un EQE de 0,12% et un CIE (0,416 ; 0,5302). Les dispositifs OLEDs en utilisant le ß-carotene comme couche de transport du trou et la curcumine comme couche émettrice ont donné une couleur jaune avec un EQE de 0,02%.

Mots-clés: antioxydant, bêta-carotène, curcumine, fucoxanthine, kaolinite, OLED, photostabilité

Studi Absorpsi dan Emisi Karotenoid dengan Antioksidan dan Kaolinit Termodifikasi serta Aplikasinya di Organic Light Emitting Diode (OLED)

Ringkasan

Krisis energi, terutama energi berbasis bahan bakar fosil, memacu pada penggunaan energi baru dan terbarukan. Selain itu, beberapa penelitian juga diarahkan untuk penggunaan energi yang lebih efisien dan penggunaan bahan hemat energi. OLED (organik light-emitting diode) adalah dioda pemancar cahaya (LED) dan sedang giat dikembangkan karena banyak diaplikasikan sebagai layar elektonik, sensor, dan lampu.

Karotenoid merupakan golongan organik terpenting dari molekul linear π-terkonjugasi karena delokalisasi elektroniknya yang tinggi dan dinamis ultra cepat. Pewarna yang digunakan sebagai fotosensitizer memainkan peranan penting dalam aplikasinya di solar sel berbasis photosensitizer atau bahan bifungsional lainnya.

Penelitian ini bertujuan untuk meningkatkan photostabilitas dari senyawa karotenoid (β-karoten dan fucoxanthin) menggunakan antioksidan dan kaolinit yang dimodifikasi. Hasil penelitian menunjukkan bahwa antioksidan dan kaolinit yang dimodifikasi dapat meningkatkan fotostabilitas β-karoten.

OLED dengan komposisi NPD(50nm)/Fx(1nm)/Alq3(85nm) menghasilkan EQE 0.12% dengan CIE (0.4160, 0.5302). Perakitan OLED menggunakan kombinasi β-carotene sebagai *hole transport layer* (HTL) dan kurkumin sebagai *emitting layer* (EL) menghasilkan emisi berwarna kuning dengan EQE sebesar 0.02%.

Kata kunci: antioksidan, karotenoid, beta-karoten, fucoxanthin, kaolinite, OLED, photostabilitas

TABLE OF CONTENTS

LIST OF FIGURES

x

xiii

LIST OF TABLES

GENERAL CONCLUSIONS AND FUTURE WORK

GENERAL INTRODUCTION

Energy crises, especially fossil fuel-based energy, lead to increased use of new energy and renewable energy. This encourages researchers to develop new and renewable types of energy. In addition, research is also directed towards more efficient energy use through the development of energy storage materials such as batteries, and the use of energy-efficient materials. Organic electronics are still a young area of technology that comprises applications as diverse as illuminants, photovoltaics, printed electronics and batteries. Organic material converse light to electrical current (photovoltaics) and electrical current to light (light diodes). Organic light emitting diode (OLED)-based electronic devices are one that is developed today. An OLED (organic light-emitting diode) is a light-emitting diode (LED) in which the emissive electroluminescent layer is a film of organic compound that emits light in response to an electric current (Zissis and Bertoldi, 2014). OLEDs are known for their high potential in display, signage, and lighting applications (Zmija *et al*., 2009; Kathirgamanathan *et al*., 2012; Karzazi, 2014., Scholz *et al*., 2015). According to IDTechEx, the OLED display market grew from 6 billion U.S. $ in 2012 to over 10 billion U.S. $ in 2013. The market is expected to grow to about 17.5 billion U.S. $ in 2015 and 25 billion U.S. $ in 2017. Around 33% of electricity is utilized due to the present lighting system (Thejo Kalyania and Dhoble, 2012).

An OLED is a device that emits light under application of an external voltage. There are two main classes of OLED devices: those made with small organic molecules and those made with organic polymers. OLEDs have the unique properties of lightweight, flexible, transparent and colour tune ability, which makes them an ideal modern light source.

Natural electronics is an area of research that searches for naturally occurring or naturally derived biomolecules to replace traditional synthesized materials in solid-state organic electronics (Irimia-Vladu, 2014). Biomolecules

often have natural electrical and optical properties that are fine-tuned to improve device performance (Irimia-Vladu *et al*., 2011; Hagen *et al*, 2006; Steckl *et al*., 2011, Gomez *et al*., 2014; Soltani Rad *et al*., 2015). Using biomolecules also support renewable and environmentally responsible electronics, with potentially a concomitant reduction in cost (Muhl *et al*., 2014).

OLED displays are based on component devices containing organic electroluminescent material (made by small molecules or polymers) that emits light when stimulated by electricity. An OLED is a solid-state semiconductor device that is 100 to 500 nanometres thick and consists of a conducting layer and an emissive layer, all together sandwiched between two electrodes and deposited on a substrate. The conducting layer is made of organic plastic molecules that transport "holes" from the anode. The emissive layer is a film of organic compound that transport electrons from the cathode and emits light in response to an electric current. The conduction in organic layer is driven by delocalization of π electrons caused by conjugation over all or part of the organic molecule (Kathirgamanathas *et al*, 2012).

Some researchers have developed organic materials for OLED as Tris-bipyridine ruthenium (II) complexes (Gao and Bard, 2000), Eu (III) complexes (Pietraszkiewicz *et al*., 2013). Lin *et al*, (2014) have studied the effect of functional groups sulfonyl, phosphine-oxide, and carbonyl to the stability of organic materials for OLED.

Organic materials which have carbonyl functional groups can improve the stability of the OLED. Among these organic materials, carotenoids constitute an important class of linear π-conjugated molecules that exhibit high degree of electronic delocalization and ultrafast dynamic (Vivas *et al*., 2011). The β-carotene is one of the potential natural organic compound used as biofunctional electronic, as organic field effect transistors (OFETs) and organic photovoltaics (OPVs) (Głowacki *et al*., 2011; Suryana *et al*., 2013). The molecular structures of carotenoids present donor-p-acceptor forms which are

very promising candidates for this applications. Bouchouit *et al* (2015) studied the non linear optical properties of some caretonoid compound and concluded the nonlinear optical properties of the studied pigments decrease in the order of β-carotene > violaxanthin > xanthophyll. Such behaviour is becaused the β-carotene is a highly conjugated compound and possesses hydrocarbon lacking functional groups. The molecular structure of β-carotene does not consist of oxygen atoms. In comparison with β-carotene, xanthophyll is oxidized derivative of carotenes and it contains hydroxyl groups. Contrary to the carotenes, hydroxyl groups substitute some hydrogen atoms and/or oxygen atoms substitute some pairs of hydrogen atoms. Xanthophyll is also more polar than carotenes.

The long chain of alternating double bonds (conjugated) is responsible for the orange color of β-carotene. Their absorption of blue–green light corresponds to an electronic transition from the $1A_g^-$ ground state (S_0) to the $1B_u$ state (S_2) (Larsen *et al*., 2003). The π-electrons in the chain are delocalized, loosely held and easily excited by low energy visible light.

The information about HUMO-LUMO is particularly important if we want to understand the modification of the $S_0 \rightarrow S_2$ transition energies of β-carotene as sensitizer. The highest unoccupied molecular orbital- lowest unoccupied molecular orbital (HUMO-LUMO) of β-carotene were 5.84 eV and 3.54 eV (Glowaski *et al*., 2011). These HUMO-LUMO energy changes provide important information about the various physical and organic reaction of β-carotene. The sensitizing dye which has the higher absorption coefficient and lower $S_0 \rightarrow S_2$ transition energy will give higher photoelectric conversion efficiencies of dyes sensitized solar cells (Ruiz-Anchondo *et al*., 2010).

The dye that is used as a photosensitizer plays an important role in the operation of DSSCs or other bifunctional material. The efficiency of the cell is critically dependent on the absorption spectrum of the dye and the anchorage of the dye to the surface of the semiconductor (El-Agez *et al*., 2012). Much work

has been concentrated on organic dyes and organic metal complexes. Life time of the sensitizer is on the other challenging in this research field.

Photostability of β-carotene has studied by some researchers. Its complexation with humic acids (as a π–π interaction) was able to strongly affect its chemical properties due the higher photostability (Martini *et al*., 2010). The thin layer of opaque minerals (Martian regolith) can protect the degradation of β-carotene caused directly by irradiation (Vítek *et al*., 2009). Barazzouk *et al.* (2012) reported that antioxidants increased photostability of Chlorophyll-a. The UV stability of β-carotene can be improved by the addition of a photostabiliser which absorbs light below 465 nm (Morabito *et al*., 2011; Sattar *et al*., 1977).

Light, in particular ultraviolet irradiation (UV), but also visible and near infra red irradiation (IR) are the major sources to generate reactive oxygen species (ROS) such as singlet oxygen, radicals or peroxides. (Photo) oxidative stress is a complex process. To a large extent it is linked to the presence of air oxygen, its transformation into reactive species and their chemical reaction with oxidation-sensitive compounds. Light in the presence of a sensitizer often initiates oxidative stress or autoxidation. It is well known that under light exposure β-carotene can form lipophilic ROS like peroxyl radicals and lipoperoxides that further degrade β-carotene itself (Rudolph *et al*., 2014). As an effect of UV irradiation the C=C and C-C bonds of the hydrocarbon chain break leading to a loss of colour (Morabito *et al*., 2011).

Antioxidants may be molecules that can neutralize free radicals by accepting or donating electron(s) to eliminate the unpaired condition of the radical. The antioxidant molecules may directly react with the reactive radicals and destroy them, while they may become new free radicals which are less active, longer-lived and less dangerous than those radicals they have neutralized. They may be neutralized by other antioxidants or other mechanisms to terminate their radical status. Many antioxidants have aromatic ring structures and are able to delocalize the unpaired electron (Lü *et al*., 2010).

Many natural and synthetic compounds have been investigated over the decades for their efficacy to protect against oxidative stress (Heo and Jeon, 2009). Antioxidants from natural sources are preferred by consumers due to the concerns about the toxic and carcinogenic effects of synthetic antioxidants.

Plants, including fruits, vegetables, and spices are already well known sources that contained a wide range of antioxidants. They contain a wide variety of antioxidant compounds, such as phenolics (phenol and polyphenols), flavonoids, carotenoids, steroids and thiol compounds (Lotito and Frei, 2006). Recently, there has been increased interest in the antioxidant capacity of algae. Seaweed was reported to contain a range of antioxidants that are highly beneficial such as fucoxanthin (Yan *et al*., 1999; Chuen Fung, 2012; Waghmode and Kumbar, 2015; Zaelani *et al*., 2015). Fucoxanthin is a major xanthophyll which exhibits potential antioxidant activity (Sudhakar *et al*., 2013) and an orange-color carotenoid (Beppu *et al*., 2012).

The other potential antioxidant compound is curcumin, the yellow pigment of turmeric and curry (Curcuma longa Linn) (Barzegar and Moosavi-Movahed, 2011). Curcumin has attracted much attention due to its significant medicinal potential and also its antioxidant properties (Silva-Buzanello *et al*., 2016). The contribution of each part of the curcumin molecule for the whole antioxidant activity has been subject of some debate. The predominant mechanism depends on the electron withdrawing character of the free radical itself and also on the solvent polarity or through the phenolic hydroxyl group.

West Kalimantan, Indonesia and Africa have abundances of minerals like quartz and kaolin clay (Mbaye *et al*., 2014; Destiarti *et al*., 2017). The application of kaolin a widely used industrial clay material, depend on its surface reactivity. Its common application e.g. filler in polymer, rubber, paper, cosmetic, medicines (Zsirka *et al*., 2015). Kaolin can also be used as adsorbents, catalysis, composites, nano-hybrids, and electrode coating (Araujo *et al*., 2014; Dedzo and Detellier, 2014; Matusik *et al*, 2011; Matusik and Matykowska, 2014; Tonlé *et al*., 2011, Samyn *et al*., 2015). Solid electrolyte

for Li-ion batteries was made from amorphous nacrite clay hybrid from Tunisia (Jaafar *et al*., 2014). These applications, however, require modifications of the surface and their structure.

The improvement of properties of kaolinite can be done by two main different treatment such as (a) physical modification, and (b) chemical treatment with acid, bases or organic compound. Physical modification with thermal/ microwave treatment, involved alteration of chemical composition and crystalline structure by the high temperature. In chemical modification with acid, bases, or organic compound, usually by alteration of structure, surface functional groups and surface area (Kumar *et al*., 2013).

Some researchers used thermal treatment and or chemical treatment to improved kaolinite properties. Thermal treatment, usually by calcination, produce metakaolinite which is more reactive than the origin ones. Calcinating kaolin at 600°C continuing activating by HCl has material with specific surface area 219 m^2/g (Belver *et al*., 2002). Other activation condition are using H_2SO_4 (Hattab *et al*., 2013), CH_3COOH, H_3PO_4, HCl, HNO_3 and base NaOH (Kumar *et al*., 2013). Acid activated with H_2SO_4 of metakaolinite increased their dielectric permittivity. It can be used for filling the plastic or rubber-coating material on wires (Izci, 2014).

Based on the background described, the aim of this PhD research are :

(1)   Characterization of natural clay from Congo, Gabon and Indonesia

(2)   Modification and characterization of kaolin clay

(3)   Study photostability of β-carotene with antioxidant and modified kaolinite

(4)   Fabrication of OLED using biomolecules

In general, this thesis is consist of eight part:

General Introduction : decribe the background, purposes and goal of this research.

Chapter I	: this chapter decribed fabrication OLED, state of the art of research using biomolecule, photostability of β-carotene using antioxidant and modified kaolin. This chapter also give information about clay, especially kaolin clay: structure, properties, modification and application.
Chapter II	: chapter methodology consist of the procedures were done in this research, analysis and characterization of the materials. The main concept of the instrumentation, also described.
Chapter III	: this is the first chapter of the result. This part is focus on the characterization of natural clay from West Kalimantan, Indonesia and from Gabon and Congo, Africa.
Chapter IV	: this chapter decribed the modification of two types of kaolin; nacritic from Congo and kaolinite from Indonesia. Nacritic kaolin was modifed by NH_3 (NH_4OH base) and kaolinite using $ZnCl_2$.
Chapter V	: this part discussed about photostability of carotenoid molecules with antioxydant (fucoxanthin and curcumin) and modified kaolinite from West Kalimantan, Indonesia.
Chapter VI	: this chapter described fabrication OLED using biomolecules.
Conclusions and Future work	: this part give the whole conclusions and the perpectives base on the results.

References

Araujo, F.R., Baptitta, J.G., Marcal, L., Ciuffia, K.J., Nassara, E.J., Calefi, P.S., Vivcente, M.A., Trujilano, R., Rives, V., Gilc, A., Korilic, S., and De Faria E.H. (2014) Versatile heterogeneous dipicolinate complexes grafted into kaolinite: Catalytic oxidation of hydrocarbons and degradation of dyes. *Catalysis Today*, **227**, 105-115.

Barazzouk, S., Bekalé, L., and Hotchandani, S. (2012) Enhanced photo stability of chlorophyll-a using gold nanoparticles as an efficient photoprotector. *Journal of Materials Chemistry*, **22**, 25316-25324.

Barzegar, A. and Moosavi-Movahedi, A.A. (2011) Intracellular ROS protection efficiency and free radical-scavenging activity of curcumin. *PLoS ONE*, **6** (10), 26012.

Belver, C., Banares., Munoz. M.A., and Vicente, M.A. (2002) Chemical activation of kaolinite under acid and alkaline conditions. *Chemical Materials*, **14**, 2033-2043.

Beppu, F., Hosokawa, M., Niwano, Y., and Miyshita, K. (2012). Effects of dietary fucoxanthin on cholesterol metabolism in diabetic/obese KK-Ay mice. *Lipid and Health Diseases*, **11** (112), 1-8.

Chong, M.N., Vimonses, V., Lei, S., Jin, B., Chow, C., and Saint, C. (2009) Synthesis and Characterisation of Novel Titania Impregnated Kaolinite Nano-Photocatalyst. *Microporous and Mesoporous Materials,* **117**, 233–242.

Chuen-Fung, A.Y. (2012) The Fucoxanthin content and antioxidant properties of undaria pinnatifida from Marlborough Sound, Auckland University of Technology University, New Zealand,Thesis.

Dedzo, G.K. and Detellier, C. (2014) Intercalation of two phenolic acids in an ionic liquid-kaolinite nanohybrid material and desorption studies. *Applied Clay Science*, **97-98**, 153-159.

Destiarti, L., Wahyuni, N., and Yani, A. (2013) Synthesis of zeolite A from Capkala kaolin by varying mass of aluminium oxide: XRD spectrum and CEC. *The 2nd Proceeding the 2nd International Conference of the Indonesian Chemical Society*, 77-82.

Destiarti, L. Wahyuni, N., Prawatya, Y., and Sasri R. (2017) Synthesis and characterization of mangan oxide coated sand from Capkala kaolin. *International Conference on Chemistry, Chemical Process and Engineering (IC3PE) AIP Conf. Proc.* 1823, 020023-1–020023-5.

El-Agez, T.M., El Tayyan, A.A., Al-Kahlout, A., Sofyan, A., Taya, S.A. and Abdel-Latif, M.S. (2012) Dye-Sensitized solar cells based on ZnO films and natural dyes. *International Journal of Materials and Chemistry*, **2** (3), 105-110.

Gao, F.G. and Bard, A.J. (2000) Solid-State Organic Light-Emitting Diodes Based on Tris(2,2'-bipyridine)ruthenium(II) Complexes. *Journal of American Chemical Society*, **122**, 7426-7427.

Głowacki, E.D., Leonat, L., Voss, G., Bodea, M., Bozkurt, Z., Irimia-Vladu, M., Bauerf, S. and Sariciftci, N.S. (2011) Natural and nature-inspired semiconductors for organic electronics. Proceeding of SPIE 8118.

Gomez, E.F., Venkatraman, V., Grote, J.G., and Steckl, A.J. (2014) DNA bases thymine and adenine in bio-organic light emitting diodes. *Scientific Report*, **4**, 7105.

Hagen, J.A., Li, W., Steckl, A.J., and Grote, J.G. (2006) Enhanced emission efficiency in organic light-emitting diodes using deoxyribonucleic acid complex as an electron blocking layer. *Applied Physical Letters*, **88**, 171109.

Hattab, A., Bagane, M., and Chlendi M. (2013) Characterization of Tataouinen's raw and activated clay. *Chemical Engineering & Process Technology*, **4** (4), 1-5.

Haq, A., Iqbal, Y., and Khan M.R. (2009) Phase and microstructure characterization of kaolin clays from North Western Pakistan. *Journal of Pakistan Materials and Society*, **3** (2), 77-90.

Hiendro, A., Hadary, F., Rahmalia, W., and Wahyuni, N. (2012) Enhanced Perfomence of bixin sensitized solar cells with activated kaolinite. *International Journal of Engineering Research and Innovation,* **4**, 40-44.

Heo, S-J. and Jeon, Y-J. (2009) Protective effect of fucoxanthin isolated from Sargassum siliquastrum on UV-B induced cell damage. *Journal of Photochemistry and Photobiology B Biology*, **95** (2), 101-107.
http://www.oled-info.com/idtechex-sees-10-billion-oled-display-market-2013-will-reach-25-billion-2017 (accesed 6th February 2018)

Irimia-Vladu, M. (2014) ''Green'' electronics: Biodegradable and biocompatible materials and devices for sustainable future. *Chemical Society Reviews*, **43**, 588–610.

Irimia-Vladu, M., Sariciftci, N.S., and Bauer, S. (2011) Exotic materials for bio-organic electronics. *Journal Materials Chemistry*, **21**, 1350–1361.

Izci, E. (2014) Structural and dielectric properties of acid activated metakaolinite. Abstract for 11th GeoRaman International Conference, June 15-19 St. Louis, Missouri, USA.

Jaafar, N., Naamen, S., Ben Rhaiem, H., and Ben Haj, A.A. (2014) Elaboration of amorphous-clay hybrid: ($Al_2Si_2O_7$. $1/2Li_2O$) designed as a single ion conducting solid electrolyte for Li-ion batteries. *American Journal of Chemistry*, **5**, 1261.

Karzazi, Y. (2014) Organic light emitting diodes: devices and applications. *Journal of Materials and Enviromental Science,* **5** (1), 1-12.

Kathirgamanathan, P., Surendrakumar, S., Antipan-Lara, J., Ravichandran, S., Chan, Y.V., Arkley, V., Ganeshamurugan, S., Kumaraverl, M., Paramswara, G., Partheepan, A., Reddy, V.G., Bailey, G., and Blake, A.J. (2012) Lithium schiff-base cluster complexes as electron injectors: Synthesis, crystal structure, thin film characterisation and their performance in OLEDs. *Journal of Materials Chemstry*, **22**, 6104.

Kumar, S., Panda, A.K., and Singht, R.K. (2013) Preparation and characterization of acids and alkali treated kaolin clay. *Bulletin of Chemical Reaction Engineering & Catalysis*, **8** (1): 61- 69.

Larsen, D.S., Papagiannakis, E., Van Stokkum, I.H.M., Vengris, M., Kennis, J.T.M., and Van Grondelle, R. (2003) Excited state dynamics of β-carotene explored with dispersed multi-pulse transient absorption. *Journal of Applied Physic*, **109**, 103529.

Lin, N., Qiao, J., Duan, L., Wang, L., and Qiu, Y. (2014) Molecular understanding of the chemical stability of organic materials for OLEDs: A comparative study on sulfonyl, phosphine-oxide, and carbonyl-containing host materials. *Journal of Physical Chemistry C*, **118**, 7569−7578.

Lotito, S.B., Frei, B. (2006) Consumption of flavonoid-rich foods and increased plasma antioxidant capacity in humans: cause, consequence, or epiphenomenon. *Free Radical Biology and Medical*, **41**, 1727–1746.

Lü, J.M., Lin, P.H., Yao, Q., and Chen, Q. (2010) Chemical and molecular mechanisms of antioxidants: experimental approaches and model systems. *Journal of Cellular and Molecular Medicine*, **14** (4), 840-860.

Matusik, J., Stodak E., and Baranowski, K. (2011) Synthesis of polylactide/clay composites using structurally different kaolinites and kaolinite nanotubes. *Applied Clay Sciences*, **51**, 102-109.

Matusik, J. and Matykowska, L. (2014) Behavior of kaolinite intercalation compounds with selected ammonium salts in aqueous chromate and arsenate solutions. *Journal of Molecular Structure*, **1071**, 52-59.

Mbaye, A., Diop, M.A.K., Miehe-Brendle, C.A.K., Senocq, J., Maury, F., and Francis. (2014) Characterization of natural and chemically modified kaolinite from Mako (Senegal) to remove lead from aqueous solutions. *Clay Minerals*, **49**, 527-539.

Morabito, K., Steeley, K.G., Shapley, N.C., Mello, C., Li, D., Calvert, P., and Tripathi, A. (2011) Proximal effects of ultraviolet light absorbers and polymer matrix in the photostability of β-carotene. *Dyes and Pigments*, **92**, 509-516.

Mühl, S. and Beyer, B. (2014) Bio-organic electronics–Overview and prospects for the future. *Electron*, **3**, 444-461.

Pietraszkiewicz, M. Maciejczyk, M.I. Samuel, D., and Zhang, S. (2013) Highly photo and electroluminescent 1,3-diketonate Eu(III) complexes with spiro-fluorene xantphos dioxide ligands: Synthesis and properties. *Journal of Material Chemistry C*, **1**, 8028.

Rahmalia W. (2016) Paramètres *de performances de photo-électrodes de TiO₂/Kaolinite et d'Electrolyte à base de carbonates biosourcés dans la cellule Sensibilisée par la bixine*. Institut National Polytechnique de Toulouse (INP Toulouse).These, 188 pp.

Rudolph, T., Eisenberg, S., Grumelard, J., and Herzog, B. (2014) State-of-the-art light protection against reactive oxygen species. *International Journal for Applied Science*, **3**, 10-14.

Ruiz Cruz, M.D. (1996) Dickite, nacrite, and posible dickite/nacrite mixed-layers from the Betic Cordilleras (Spain). *Clay and Clay Minerals*, **44** (3), 357-369.

Ruiz-Anchondo, T., Flores-Holguín, N., and Glossman-Mitnik, D. (2010) Natural carotenoids as nanomaterial precursors for molecular photovoltaics: A computational DFT study. *Molecules*, **15**, 4490-4510.

Samyn, P., Schoukens, G., and Stanssens, D. (2015) Kaolinite nanocomposite platelets synthesized by intercalation and imidization of poly(styrene-*co*-maleic anhydride). *Materials,* **8**, 4363-4388.

Sattar, A, de Man, J.M., Alexander, J.C. (1977) Wavelength effect on light-induced decomposition of Vitamin A and β-carotene in solutions and milk fat. *Canadian Institute of Food Science and Technology Journal*, **10**, 56-60.

Scholz, S., Kondakov, D., Lüssem, B., and Leo, K. (2015) Degradation mechanisms and reactions in organic light-emitting devices. *Chemical Reviews*, **115**, 8449−8503.

Silva-Buzanello, R.A., Souza, M.F., Oliveira, D.A., Bona, E., Leimann, F.V., Cardozo, L.F. Araújo, P.H.H., Ferreira, S.R.S., and Gonçalves, O.H. (2016) Preparation of curcumin-loaded nanoparticles and determination of the antioxidant potential of curcumin after encapsulation. *Polímeros,* **26** (3), 207-214.

Soltani Rad, M.N., Sharbati, M.T., Behrouz, S., and Nekoei, A. R. (2015) Fabrication of non-doped red organic light emitting diode using naturally occurring curcumin as a donor-acceptor-donor (D-A-D) emitting layer with very low turn-on voltage*. Iranian Journal of Science & Technology*, **39A3***,* 297-304.

Steckl, A.J., Spaeth, H., You, H., Gomez, E., and Grote, J. (2011) DNA as an optical material. *Optical Photon News*, **22**, 34–39.

Suryana, S., Khoiruddin., and Supriyanto, A. (2013) Beta-carotene dye of Daucus carota as sensitizer on dye-sensitized solar cell. *Materials Science Forum*, **737**, 15-19.

Thejo Kalyania, N. and Dhobleb, S.J. (2012) Organic light emitting diodes: Energy saving lighting technology—A review. *Renewable and Sustainable Energy Reviews*, **16**, 2696-2723.

Tonlé, I.K., Letaif, S., Ngameni, E., Walcarius, A., and Detellier, C. (2011) Square wave voltammetric determination of lead (II) ions using a carbon paste electrode modified by a thiol-functionalized kaolinite. *Electroanalysis*, **23**, 245-252.

Vítek, P., Jehlička, J., Bezděk, J., Francŭ, E. (2009) Degradation of β-carotene under uv-rich irradiation conditions: implication for martian environmental. 40th Lunar and Planetary Science Conference.

Vivas, M.G., Silva, D.L., de Boni, L., Zalesny, R., Bartkowiak, W., and Mendonca, C.R. (2011) Two-photon absorption spectra of carotenoids compounds. *Journal of Applied physics*, **109**, 103529.

Waghmode, A.V. and Kumba, R.R. (2015) Phytochemical screening and isolation of fucoxanthin content of Sargassum ilicifolium. *International Journal of Pure and Applied Biosciences,* **3** (6), 218-222.

Wong, I.Y.H., Koo, S.C.Y., and Chan, C.W.N. (2011) Prevention of age related macular degeneration. *International Journal of Optic and molecules*, **31**, 73-82.

Yan, X., Chuda, Y., Suzuki, M., and Nagata, T. (1999) Fucoxanthin as the major antioxidant in Hijikia fusiformis a common edible seaweed. *Bioscience, Biotechnology and Biochemistry*, **63** (3), 605-607.

Yip, W.H., Joe, L.S., Mustapha, W.A., Maskat, M.Y., and Said, M. (2014) Characterisation and stability of pigments extracted from *Sargassum binderi* obtained from Semporna, Sabah. *Sains Malaysiana,* **43** (9), 1345–1354.

Zailanie, K., Kartikaningsih, H., and Kalsum, U. (2015) Effect of *sargassum filipendula* fucoxanthin against HeLa cell and lymphocyte proliferation. *Journal of Life Science and Biomedical,* **5** (2), 53-59.

Zissis, G. and Bertoldi, G. (2014) Status Report on Organic Light Emitting Diodes (OLED). 2014 Status Report on Organic Light Emitting Diodes (OLED). JRC Science and policy Report, 1-33.

Zsirka, B., Horvath, E., Mako, E., Kurdi, R., and Kristof, J. (2015) Preparation and characterization of kaolinite nanostructure: Reaction pathways, morphology and structural order. *Clay minerals*, **50**, 329-340.

Zmija, J. and Maachowski, M.J. (2009) Organic light emitting diodes operation and application in displays. *Archives of Materials Science and Engineering,* **40** (1), 5-12.

CHAPTER I

BIBLIOGRAPHY

CHAPTER I

BIBLIOGRAPHY

This chapter will describe the OLEDs concept, natural organic compound as a dyes, antioxidant, clay and kaolin. In this research we use two antioxidants : fucoxanthin and curcumin. Antioxidants and modified kaolin were used to improve the photostability of β-carotene.

1.   Organic light emitting diode (OLED)

OLED is a cutting edge technology of using organic materials (small molecular or polymeric) to generate light (Zhou, 2007). The basic structure of an OLED consists of a stack of organic layers sandwiched by a transparent conducting anode and a metallic cathode. With suitable driving voltage applied to the diode, holes are injected from the anode and electrons from the cathode. Both holes and electrons are driven by the electric field and meet in the recombination zone, and their recombination results in electroluminescence (EL).

Organic electroluminescent materials have been the subject of intense research for use in light emitting diodes (LEDs). When compared with liquid crystal displays (LCDs), OLEDs require lower energy input, have a wider viewing angle with improved color contrast, and can be made much thinner.The electroluminescence (EL) of organic compounds was first demonstrated in 1953 by Bernanose but was not significantly developed until 1987 when Tang and Van Slyke constructed a device employing aluminum tris(8-hydroxyquinoline) as the luminescent material. The first example of a polymer-based OLED was published by Friend *et al* in 1990 in which poly(p-phenylene-vinylene) (PPV) was used as the emissive layer. Since this discovery, many conjugated polymers have been developed for use in LEDs including poly(1,4-phenylene) (PPP), poly(thiophene), and polyfluorene.

Organic LEDs have a more complex structure than inorganic ones for two main reasons. Firstly, the low-carrier mobility and the electrical

conduction process impose a new device structure; secondly, the much different carrier mobility between electron transport material (n-type) and hole transport material (p-type), the last being several orders of magnitude higher. In turn, the benefits of using an organic-based self-emissive layer that allows very thin film devices (in some cases below 100 nm), the much sought after flexibility result in devices with unique properties that move the interest of the scientific community.

Chauhan *et al* (2014) resumed the advantages of OLED, such as: (1) large area diffuse light, source, (2) thin, flat, lightweight, (3) form freedom in design, (4) fast switch-on, fully dimmable, (5) many colors, includes whites, (6) robust source (no wires inside), (7) transparent, mirror-like, black or white appearance, (8) low voltage technology, (9) potentially high efficiency, (10) green product (energy efficient, recyclable), and (11) potentially cheap fabrication. Therefore, OLED devices using in many application such as, light (Pang *et al*., 2014), display (Ammermann *et al*., 1995), sensor (Shinar and Shinar, 2008), and organic printed electronics (Sekine *et al*., 2014).

1.1 Principle of OLED

OLEDs are carrier injection devices, where organic thin film sandwiched between electrodes. If direct-current voltage is applied, holes and electrons recombine in the light emitting layer, and light will be emitted. The basic device structure includes a glass substrate on which a transparent electrode (ITO, etc.) is formed (Figure 1.1).
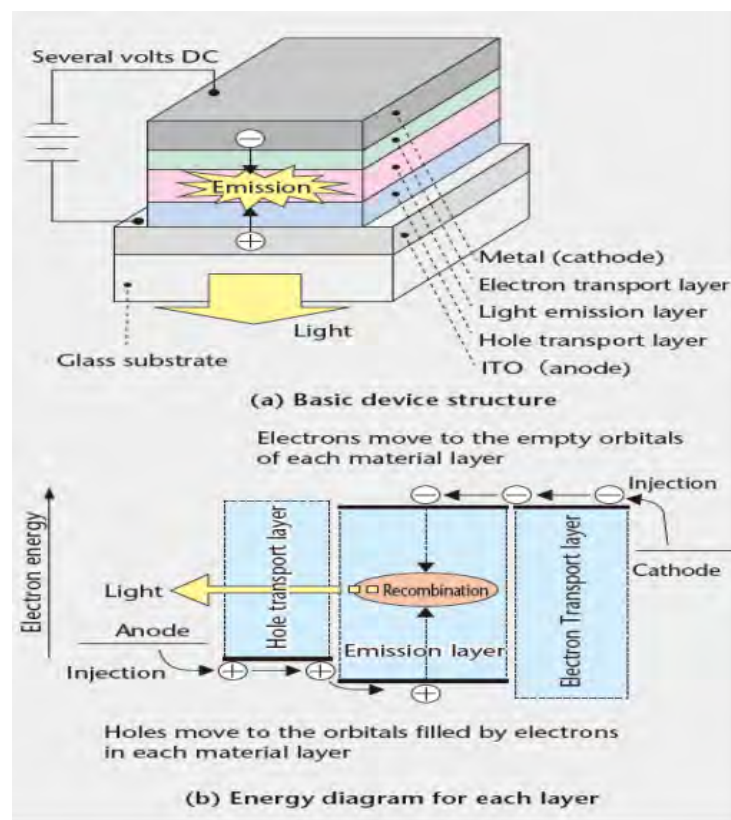
Figure 1.1: Principle of electroluminescence (Shimizu, 2014)

1.2   Fabrication of OLED

The OLED device is of interest not only for the practical use but also for the basic research. By fabricating this device, we can study the electrical behavior of the insulating organic compounds and measure their electro-luminescence (EL) spectra (Tajima *et al*., 2003).

The traditional LED from inorganic semiconductors is typically a p-n junction, were a hole injected from anode and an electron injected from cathode diffuses in the respective semiconductor type to recombine at the interface resulting in light emission. In this kind of semiconductors, the carrier mobilities are relatively In a similar way to that we found for inorganic semiconductors, the organic LEDs performance depends on the injection/transport and recombination of electrical charge. For this, the general structure is usually comprised by a hole transport material (also called hole

transport layer-HTL) and an electron transport material (electron transport layer-ETL), needed to deliver the charge to an active material between them (in a "sandwich" structure), usually called emissive layer-EL. The choice of HTL and ETL is clearly dependent on the physical and electronic properties of the EL, in particular the location of the HOMO and LUMO levels. In fact, we expect that the interface between HTL and EL will also act as an electron blocking region, and, of course, that the interface between ETL and EL can act as hole blocking region. This strategy is not surprising because increasing the carrier concentration inside the EL helps the electron– hole recombination and therefore the efficiency. This simple system addresses the so-called carrier confinement and is one of the most important configuration issues in organic-LEDs developments. Figure 1.2 shows a schematic of this general architecture.
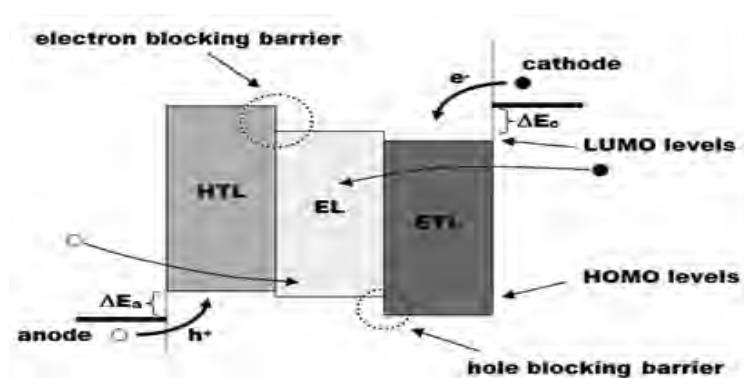
Figure 1.2: Typical OLED structure

Figure 1.2 represented the typical OLED structure with the hole transport layer (for hole injection/transport), electron transport layer (for electron injection/ transport), and emissive layer. The ideal cathode and anode levels, in respect to the materials LUMO and HOMO levels, are shown. The interfaces at HTL/EL and EL/ETL act as electron and hole barriers, respectively, as desired for a correct carrier confinement inside the EL.

Composed of two substrate layers on the outside emissive and conductive layer lie between the cathode and the anode layers. A current is applied across the LED, where electrons move from cathode to anode. The cathode gives

electrons to the emissive layer, where the anode withdraws these electrons from the conductive layer. The emissive layer becomes rich innegative charge while the conductive layer becomes more positively charged .The two charges recombine in the emissive layer, creating a drop in energy levels of the electrons. The drop in energy levels results in radiation that is on the visible spectrum, emitting light.

For a basic understanding of organic electroluminesence phenomena, as well as for the fabrication of efficient organic LEDs, a division in low-molecular-weight and high-molecular-weight organic materials is useful. There are no sharp limits for the molecular weight for organic molecules to be classified as either a low or a high-molecular-weight material. Usually, the term high molecular- weight materials refers to polymers made up of molecules that exceed the length other molecules by a factor of about 10^2. Well resolved molecules formed from tens of monomer units, termed oligomers, stand for the intermediate category between low- and high-molecular-weight materials. The main advantages of low-molecular-weight materials for electroluminesence organic devices include a high fluorescent quantum yield, ease of film formation by vacuum vapour deposition, high purification and crystal growth capability and a wide election of material design. Crystallization of initially amorphous samples, production of exciplexes with other materials, and often high chemical reactivity create serious problems in their application to stable electroluminesence systems. On the other hand, high-molecular-weight materials allow for the easy preparation of thin films by casting, and show a high resistance to crystallization. The difficulties in purification procedures and, mostly, a low fluorescent quantum yield, in addition to a complex structure, are drawbacks in their application to organic electroluminesence devices (Jan Kalinowski, 1999).

One of the key challenges on the path to developing the next generation of high-performance OLEDs is the design and synthesis of readily processible and thermally robust emissive and charge transport materials with improved

multifunctional properties. OLEDs are double charge injection devices, requiring the simultaneous supply of both electrons and holes to the electroluminescent material sandwiched between two electrodes. ((Kulkarni *et al*, 2004). Most highly fluorescent or phosphorescent organic materials of interest in OLEDs tend to have either p-type (hole-transport) or n-type (electron transport) charge transport characteristics (Figure 1.3). In terms of the device-fabrication process, solution-processible small molecular luminescent materials which ia possess the advantages of high purity (vs. polymers) and low procession cost (vs. vacuum deposition) (Yu *et al*., 2015).
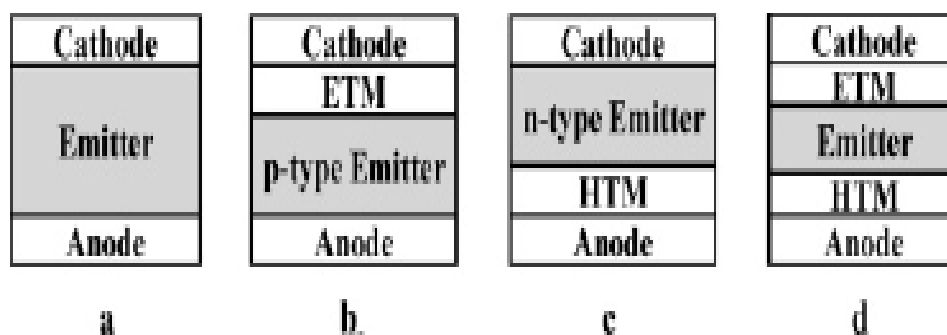
Figure 1.3: Common OLED architectures with a hole-transport material (HTM) and an electron-transport material (ETM)

In general, material which are usually used in oled fabrication are anode, cathode, HIL, HTL, EL, ETL, and substrate (Thejo Kalyania and Dhobleb, 2012). Some material are usually used in OLED fabrication are listed in Table 1.1:

a. Substrate: this is usually clear plastic, glass, or metal foil, which is a transparent and conductive substrate with high work function (ϕw ≈ 4.7– 4.9 eV).

b. Anode: this is as a transparent electrode to inject holes into organic layers. Important   requirement of this layer is that it must have low roughness and with high work function.

c. Hole injection layer (HIL): The materials with high mobility, electron blocking capacity and high glass transition temperature can be used as HIL.

d. Hole transport layer (HTL): Hole transporting layer plays an important role in transporting holes and blocking electrons, thus preventing electrons from reaching the opposite electrode without recombining with holes.

e. Emissive layer (EML): The layer in between HTL and ETL is a good emitter of visible photons, generally known as emissive layer (EML). This layer can be a material made of organic molecules or polymers with high efficiency, lifetime and color purity.

f. Electron transport layer (ETL): This layer should have good electron transporting and hole blocking properties.

Table 1.1: Materials in OLED (Thejo Kalyania and Dhobleb, 2012).

Layer of OLED's	Materials generallly used in different layer of OLED's
Anode	High work function: ITO, IZO, ZNO; TCP (PANI, PEDOT); Au, Pt, Ni, p-Si; ITO; Surface treatment; Plasma (O_2, NH_3); Solution (Aquaregia); Thin insulator AlO_x, SiO_x; RuO_x
Cathode	Low work function: Mg:Ag; Li:Al; Ca, etc; Thin insulator: LiF; MgO_x
HIL	HOMO level: TPD, NPD, PPV, PVK, etc
ETL	LUMO level: Alq_3, PBD, BCP, etc
EML: Dopants	Alq_3, CPB, Balq, coumarin, Ir $(ppy)_3$, etc

OLED devices/displays can be fabricated in two ways namely vacuum deposition technique and solution techniques including spin coat technique, ink jet technique, casting, etc. Vacuum deposition is the widely used technique, but it is time consuming as high vacuum state is to be obtained and is difficult to deposit over large area. In contrast solution techniques have currently gained momentum as they consume less time easy to deposit thin layer thin film can be deposited over a large area (Thejo Kalyania and Dhobleb, 2012)

1.3   Efficiency of OLED

Organic electroluminescence (OEL) is the emission of light from organic materials in an electric field. The luminescent materials that are the most important elements in OLEDs devices include small molecule materials and polymer materials. The main requirements for OLEDs luminous materials are high photoluminescence quantum yields (PLQYs) in the solid state, high carrier mobility (both n and p type), excellent film-forming property (pinhole-free), good thermal and oxidative stability, and good color purity (adequate CIE coordinates) (Yu *et al*., 2015).

The EL quantum efficiency is the most essential parameter for an OLEDs device, regardless of the distinct visual sensitivity of different emission color. Of particular importance is the external quantum efficiency (η_{ext}), which is defined by the ratio of the number of emitted photons outside the device to an apparent number of charges injected into the device. It is expressed by the following equations (Tsutsui, 1997):

$$\eta_{ext} = \gamma \ \eta r \ \varPhi f \ \chi \qquad (1.1)$$

$$\chi = \frac{1}{2n^2} \qquad (1.2)$$

where γ is the charge balance factor (i.e., the number of excitons formed within the device per injected charge carrier) η_r is the efficiency of production of radiative transition excitons; Φ_f is the solid-state photoluminescence efficiency of the emitters; and χ is the light out-coupling efficiency in which n is the refractive index of the emitting organic materials, which usually assumed to be ~1.5.

1.4   Emitting layer

1.4.1 General concept of absorption and emission of light by material

To account adequately for the processes of absorption and emission of light, it is necessary to assume that radiant energy can only be absorbed in definite units, or quanta. The energy, E, carried by any one quantum is proportional to its frequency of oscillation, that is:

$$E = h\nu = hc/\lambda$$

where ν is the frequency, λ the related wavelength and h = Planck's constant (6.624×10^{-27} ergs/seconds).

The energy of a single quantum is too small for convenience and it is usual to talk of the energy associated with N quanta (where N = 6.023×10^{23} the number of single molecules in a gram molecule), which is called an Einstein. Thus, if in a photochemical reaction one molecule reacts for each quantum absorbed, then the absorption of one einstein is sufficient energy for the reaction of one gram mole. Since the amount of energy per einstein is proportional to the frequency of the radiation, it varies enormously over the range of the electro-magnetic spectrum.

At room temperature most molecules occupy the lowest vibrational level of the ground electronic state, and on absorption of light they are elevated to produce excited states. The simplified diagram below shows absorption by molecules to produce either the first, S1, or second S2, excited state **(Figure 1.4)**.

Luminescence is the emission of light from any substance, and occurs from electronically excited states. Luminescence is formally divided into two categories—fluorescence and phosphorescence—depending on the nature of the excited state. In excited singlet states, the electron in the excited orbital is paired (by opposite spin) to the second electron in the ground-state orbital. Consequently, return to the ground state is spin allowed and occurs rapidly by emission of a photon. The emission rates of fluorescence are typically 108 s–, so that a typical fluorescence lifetime is near 10 ns (10×10^{-9}s).. It is valuable to consider a 1-ns lifetime within the context of the speed of light. Light travels 30 cm, or about one foot, in one nanosecond. Many fluorophores display subnanosecond lifetimes (Lakowicz, 2006)

Fluorescence is a spectrochemical method of analysis where the molecules of the analytes are excited by irradiation at a certain wavelength and emit radiation of a different wavelength. The emission spectrum provides

information for both qualitative and quantitative analysis. As shown in Figure 1.4, when light of an appropriate wavelength is absorbed by a molecule (i.e., excitation), the electronic state of the molecule changes from the ground state to one of many vibrational levels in one of the excited electronic states. The excited electronic state is usually the first excited singlet state, S1. Once the molecule is in this excited state, relaxation can occur via several processes. Fluorescence is one of these processes and results in the emission of light.
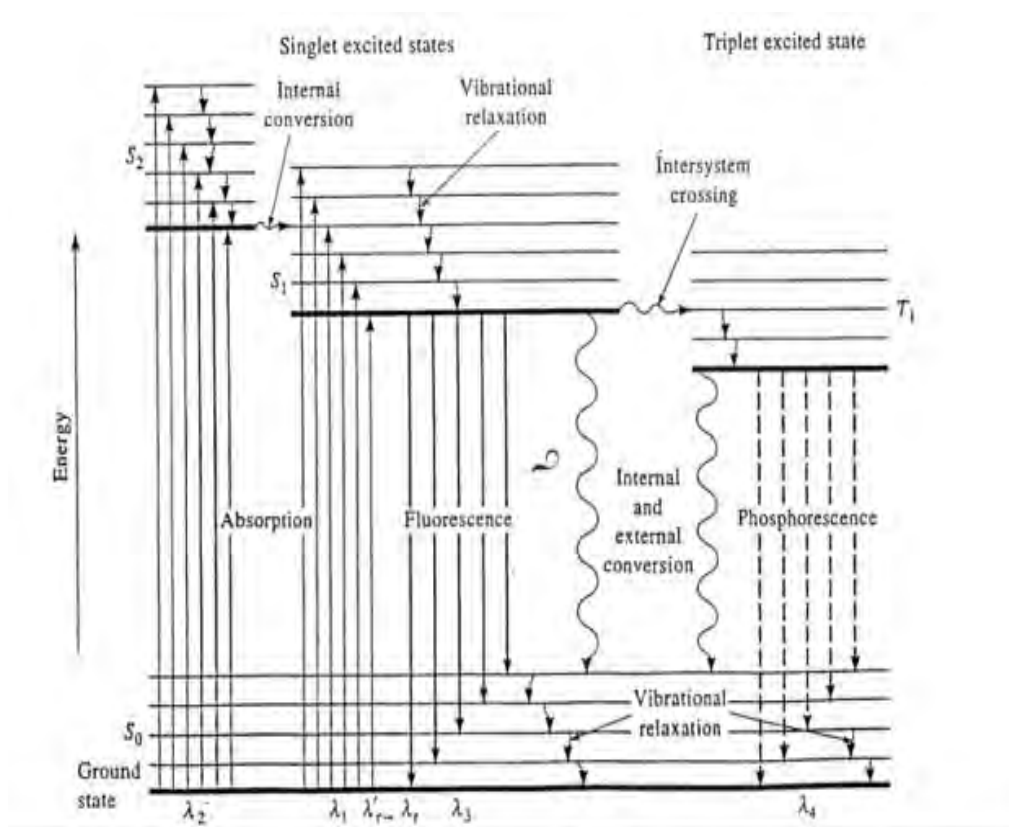
Figure 1.4: Electronic transition energy level diagram

Following absorption, a number of vibrational levels of the excited state are populated. Molecules in these higher vibrational levels then relax to the lowest vibrational level of the excited state (vibrational relaxation). From the lowest vibrational level, several processes can cause the molecule to relax to its ground state. The most important pathways are: (Skoog *et al* ., 2006)

1. Collisional deactivation (external conversion) leading to nonradiative relaxation.

2. Intersystem Crossing (10-9s): In this process, if the energy states of the singlet state overlaps those of the triplet state, as illustrated in Figure 1.4, vibrational coupling can occur between the two states. Molecules in the single excited state can cross over to the triplet excited state.

3. Phosphorescence: This is the relaxation of the molecule from the triplet excited state to the singlet ground state with emission of light. Because this is a classically forbidden transition, the triplet state has a long lifetime and the rate of phosphorescence is slow (10^{-2} to 100 sec).

4. Fluorescence: Corresponds to the relaxation of the molecule from the singlet excited state to the singlet ground state with emission of light. Fluorescence has short lifetime (~10^{-8} sec) so that in many molecules it can compete favourably with collisional deactivation, intersystem crossing and phosphorescence. The wavelength (and thus the energy) of the light emitted is dependent on the energy gap between the ground state and the singlet excited state.

5. Internal Conversion: Direct vibrational coupling between the ground and excited electronic states (vibronic level overlap) and quantum mechanical tunnelling (no direct vibronic overlap but small energy gap) are internal conversion processes. This is a rapid process (10^{-12} sec) relative to the average lifetime of the lowest excited singlet state (10^{-8} sec) and therefore competes effectively with fluorescence in most molecules.

1.4.2 Organic material as emitting layer in OLED

There are three most successful approaches for reducing the energy band gap in organic compounds including: (i) extending the π-conjugation, (ii) tuning bond-length alternation in the π-system by stabilizing a quinoidal character, and (iii) introducing appropriate donor-acceptor (D-A)

functionalities in a molecule (push-pull effect) (Roncali, 1997; Van Mullekom *et al*, 2001).

The D-A structure is almost a common feature found in many red or deep-red fluorescent chromophores (Chakraborty *et al*., 2005; Thomas *et al*., 2004; Kato *et al*., 2004). The D-A chromophores usually used in OLEDs emitting layer are divided into three main categories:

(i)   single head donor-acceptor chromophores (D-A),

(ii)   double-head donor-acceptor-donor (D-A-D) chromophores, and

(iii)   double-head acceptor-donor- acceptor (A-D-A) chromophores.

Figure 1.5 illustrated the examples molecules from each categories.
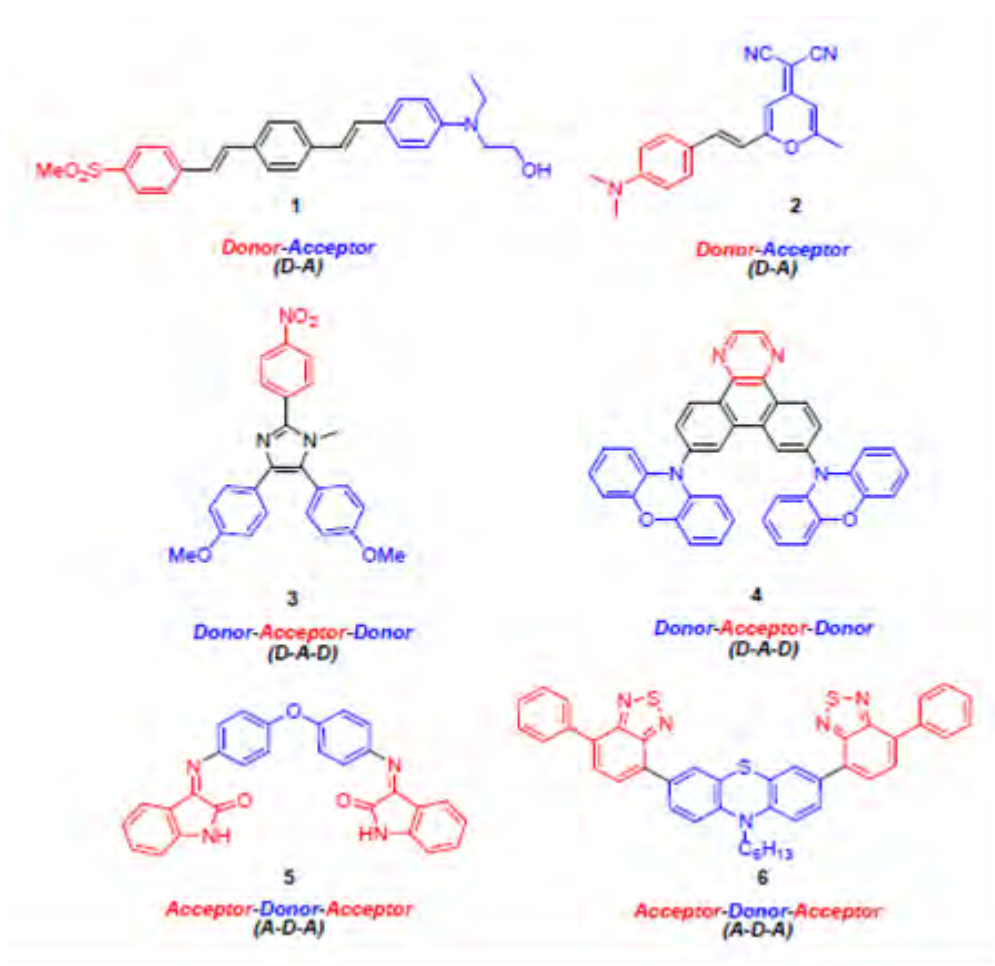
Figure 1.5: The chemical structure of chromophores type
(Soltani *et al.*, 2015)

1.4.3 Biomolecule organic diode (BIODE) and natural dyes in OLED

The first report on using biomolecule as emitting layer in OLED was initiated by Tajima *et al* (2003), whose yielded the EL spectra from cytochrome c. They obtained emission spectrum band of cytochrome c was 690 nm at applied voltage during the EL measurement 8 V. Figure 1.6 represented the divice of OLED using cytochrome c and the molecular structure of cytochrome c .
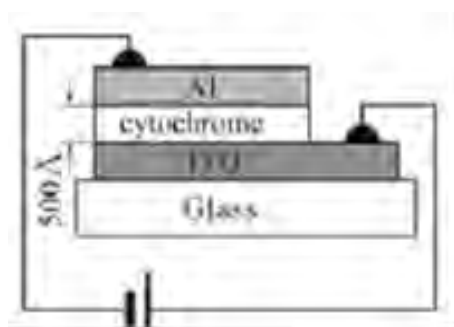
(a)
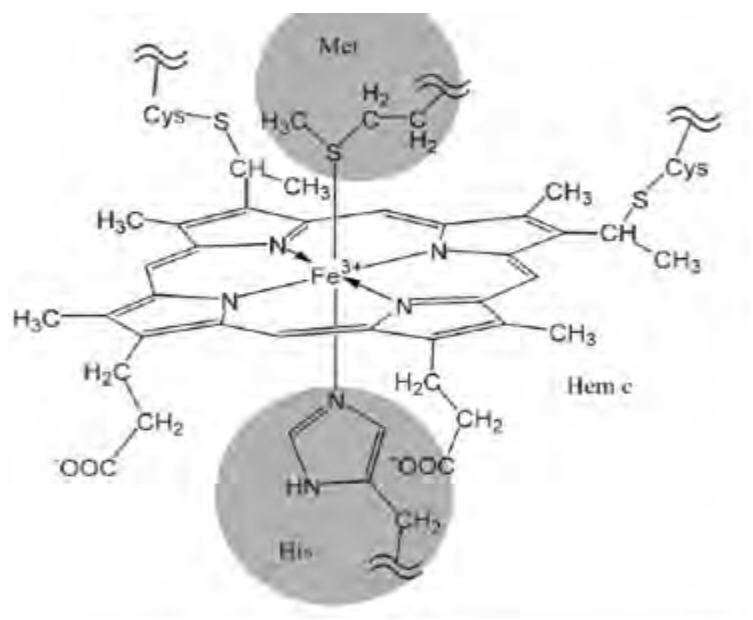
(b)

Figure 1.6: The schematic view of the device structure an chemical structure of hem c (iron porphyrin) in cytochrome c. (His: methionine, and His: histidine)

They also fabricated OLED using other biomolecules: ITO/biomolecule/Al junctions using chlorophyll a, cytochrome c, myoglobin, hemin, Vitamin B_{12}. Structure of those biomolecules are represented in Figure 2.7. This oled type is called biomolecular light-emitting diode (BIODE). The quantum efficiencies of the fabricated OLED were of the order of 1×10^{-7} at applied voltage of around 10V (Tajima *et al*, 2006).
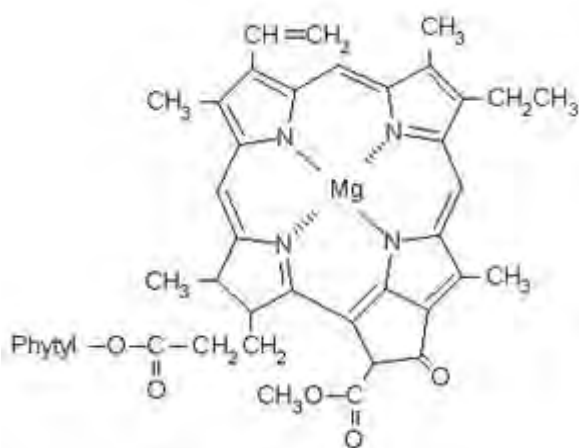
chlorophyll a
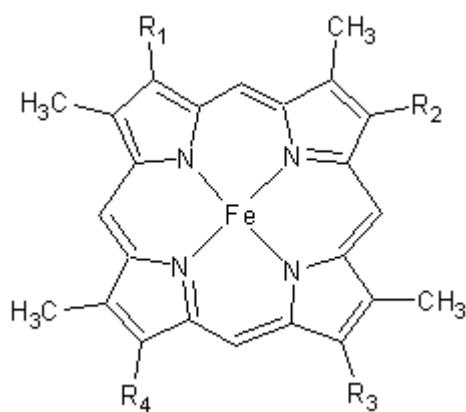
cytochrome c
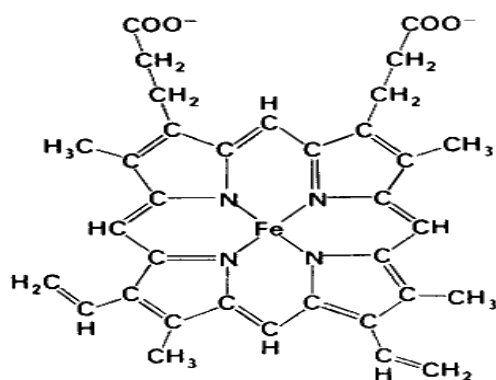
Myoglobin
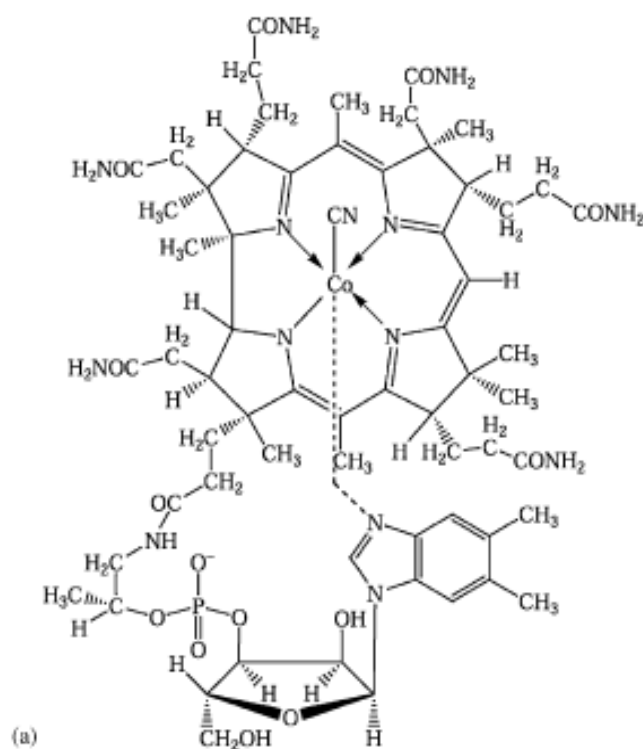
Vitamin B$_{12}$

Figure 1.7: Structure biomolecules using in BIODE

The other BIODE was made by Ohtani *et al* (2011). They used chloropylls which were extracted from spinach. They fabricated ITO(150nm)/PPV-chlorophylls (100 nm)/ Al (150 nm), and the area of this

OLED was 2 x 2 mm^2. Here, PPV (poly [(m-phenylenevinylene)-alt-(2,5-dihexyloxy-p-phenylenevinylene)] as host active material and chloropylls as doped material. The maximum EL intensity maximum (approximately at 680 nm) when doping density of chlorophyll a was 5 wt% and the injection current was about 2 mA and applied voltage of about 8V.

The application of the donor-acceptor (D-A) type of chromosphor of curcumin was done by Soltani Rad *et al* (2015). Structure of curcumin molecule and the OLED structure are reperesented in Figure 1.8a. The configuration of the multilayer fabricated was ITO/4,4'-Bis(N-carbazolyl)-1,1'-biphenyl (CBP) (45 nm)/ Curcumin (35 nm)/ 1,4-phenylenebis(triphenyl silan) (HGH$_2$) (10 nm)/ Alq$_3$(35 nm)/LiF(1 nm) /Al (100 nm), as shown in Figure 1.8b. A maximum external quantum efficiency (EQE) of ηEQE=0.029% was obtained for device based on A-D-A and device has an emission at 612 nm. The fabricated curcumin-OLED in this study also showed very low turn-on voltages at 0.5-1 V.

(a)

(b)
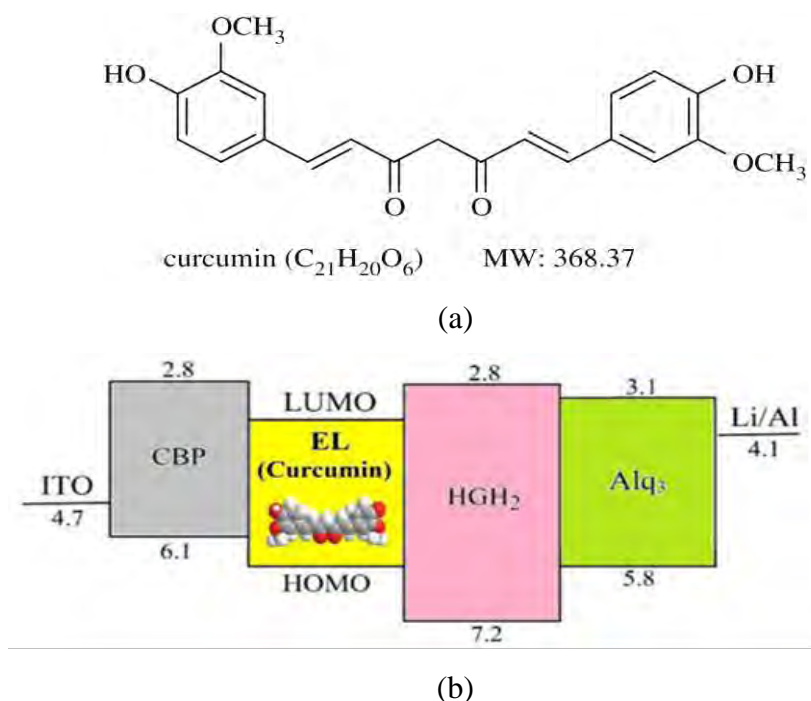
Figure 1.8: (a) Structure of curcumin and (b) schematic energy level (in eV) diagram of multi layer fabricated OLED using curcumin (Soltani Rad *et al*., 2015)

Gomez *et al*. (2014) used DNA bases thymine and adenine in bio-organic light emitting diodes (Figure 1.9). Adenine (A) and thymine (T) were deposited as electron-blocking/hole-transport layers (EBL/HTL) that resulted in increases in performance over the reference OLED containing the standard EBL material NPB. A-based OLEDs reached a peak current efficiency and luminance performance of 48 cd/A and 93,000 cd/m^2, respectively, while T-based OLEDs had a maximum of 76 cd/A and 132,000 cd/m^2. By comparison, the reference OLED yielded 37 cd/A and 113,000 cd/m^2. The enhanced performance of T-based devices is attributed to a combination of energy levels and structured surface morphology that causes more efficient and controlled hole current transport to the emitting layer.
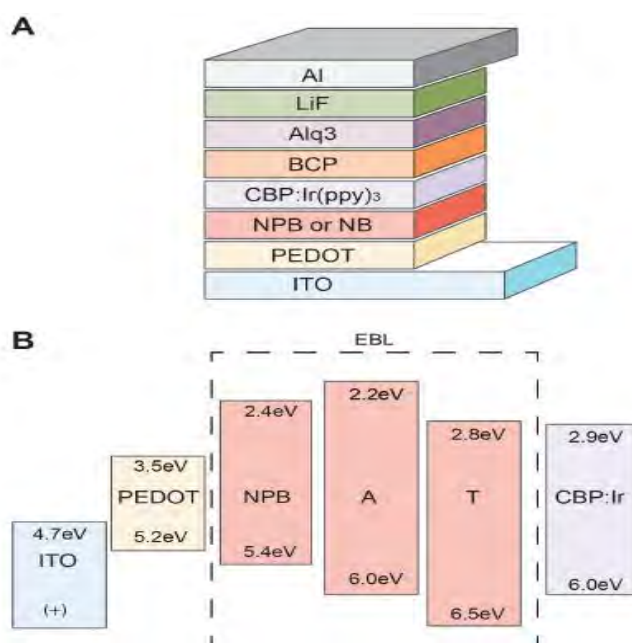
Figure 1.9: The device configuration of the OLED (A) the EBL contains NPB (reference device) or a nucleobase (A or T) and (B) molecular orbital energy levels for the EBL materials and the levels of adjacent materials.

2.   Natural organic compound: β-carotene

β-carotene is one of the colourful carotenoids with antioxidant activity. It is a strongly-colored red-orange pigment present in many plants and fruits, like carrots, pumpkins, or sweet potatoes. β-carotene is the pro-vitamin of vitamin A and is widely used as a colorant in foods and beverages. It is a non-polar highly conjugated lipophilic hydrocarbon compound (Figure 1.10). The eleven conjugated C=C double bonds serve as a chromosphore moiety in the molecule, which is responsible for the light absorption and the colour of β-carotene (Morabito *et al*., 2011). Accordingly, β-carotene has a characteristic UV-VIS spectrum, in which the position of the principal absorption maximum (λ_{max}) depends on the configuration (Cerón-Carrasco *et al*., 2010) and oxidation of the molecule (Laughlin *et al*., 2002; Cao-Hoang *et al*., 2011) as well as on the type of the solvent used (Laughlin *et al*., 2002; Marx *et al*., 2003; Chetkovic and Markovic, 2008) according to the changes in transition energies between the ground and excited states.
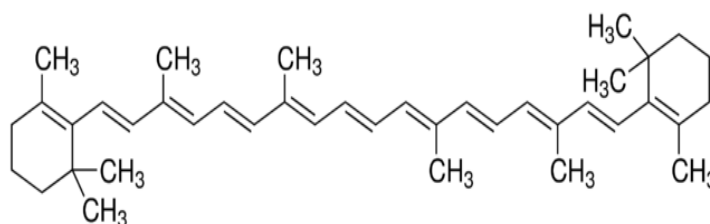
Figure 1.10: Molecular structure of β-carotene (Delgado-Vargas *et al*., 2000)

The melting point of β-carotene is higher than 180 °C, but melting is not reversible and the true melting point cannot be determined. Pure crystalline β-carotene (purified by fractional dissolution) is black but undergoes fast direct oxidation by air in the crystal phase 5 even at low temperatures (-80 °C) in dark. Oxidation results in a change of colour to orange or red, the powder becomes similar in appearance and composition to laboratory samples available commercially ((Laughlin *et al*., 2002).

The oxidation of β-carotene with molecular oxygen is an autocatalytic free radical process which leads to the formation of different epoxycarotenoids, apocarotenals, small molecular mass products, and some oligomeric/polymeric materials, some of them representing the key aroma compounds in certain flowers, vegetables, and fruits (Zeb, 2013; Mordi *et al.,* 1993). The initial site of the oxygen attack on the β-carotene molecule occurs at the terminal double bonds resulting in predominant formation of epoxides These and long chain β-apocrotenals formed in the first stage of oxidation decompose to lower molecular mass carbonyl-containing compounds in further oxidation reactions ((Mordi, 1992); Rodríguez *et al*., 2007). The pathway of cleavage of the molecule (central or random) is affected by the surrounding medium (type of solvent), as well as the absence or presence of a phenolic antioxidant (Yeum *et al*., 2009). Phenolic antioxidants, like BHT and α-tocopherol, inhibit the oxidation of β-carotene (Ozhogina and Kasaikina , 1995; Siems *et al*., 2005).

The β-Carotene is more resistant to heat than to oxygen (Marty and Berset, 1990; Qiu *et al*., 2009). As an effect of UV irradiation the C=C and C-C bonds of the hydrocarbon chain break leading to a loss of colour (Morabito *et al*., 2011). The UV stability of β-carotene can be improved by the addition of a photostabiliser which absorbs light below 465 nm (Morabito *et al*., 2011; Sattar *et al*., 1977).

In the last decade, π-conjugated molecules have emerged as potential candidates for applications in photonic devices due to its easy handling, environmental stability and structural flexibility (Chakrabarti and Ruud, 2009; Belfield *et al.,* 2004). Among these materials, carotenoids constitute an important class of linear π-conjugated molecules that exhibit high degree of electronic delocalization and ultrafast dynamics. Marder *et al* (1997) studied the third-order optical nonlinearities in polarized carotenoids using third harmonic generation. They observed the enhancement of the optical nonlinearity as the intramolecular charge transfer increase from the polyenic chain to the acceptor moiety.

Energy level of β-carotene is represented at Figure 1.11 (Gonzales Vivas *et al*.,2011):
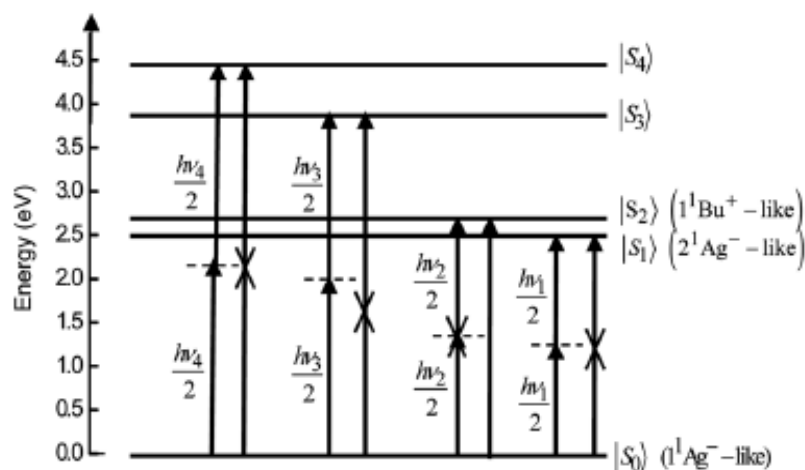
Figure 1.11: Energy level of β-carotene

A significant disadvantage of using organic chromophores in nonlinear optical (NLO) is that they are susceptible to photodegradation. Consequently, in order to develop robust, photochemically stable chromophores, it is important to understand the processes and mechanisms by which photodegradation occur and develop strategies to reduce the photodegradation. It has been suggested that chromophore ground state bleaching at high optical intensities will reduce the average occupancy of the chromophore triplet state and lead to a reduced rate of singlet oxygen generation and, hence, to increased photostability (Gupta, *et al*., 2008).

Williams *et al* (2011) reported the β-carotene enhanged the photostability of thin films containing PYR-3(2-{3-Cyano-4-[3-(1-decyl-1H-pyridin-4-ylidene)-propenyl]-5,5-dimethyl-5H-furanylidene}-malononitrile) and amorphous polycarbonate (APC). β-carotene can enhance the photostability of NLO chromophores by a number of physical processes. The first is shown in Figure 1.12 (left and middle), where incident light leads to excitation to the PYR-3 singlet S_1 excited state. This is followed by fluorescence as well as intersystem crossing (ISC) to the excited triplet state, T_1, which has a long

33

lifetime that typically ranges from milliseconds to seconds. The intersystem crossing can be mediated by oxygen via $S_1 + {}^3O_2 \rightarrow T_1 + {}^3O_2$ or $S_1 + {}^3O_2 \rightarrow T_1 + {}^1O_2$, where ${}^3O_2$ is triplet oxygen and ${}^1O_2$ is singlet oxygen. It can relax back from T_1 to S_0 by $T_1 + {}^3O_2 \rightarrow S_0 + {}^3O_2$ or $T_1 + {}^3O_2 + S0 + {}^1O_2$ (Birks, 1970).

The singlet oxygen generated in this process can react with the chromophore and can result in its decomposition or the decomposition of nearby chromophores. However, if a beta-carotene molecule is nearby, it is possible that there can be energy transfer from the PYR-3 T_1 state to the beta-carotene triplet state that leaves PYR-3 in the ground S_0 state. Beta-carotene can then relax back from the triplet to the singlet state via a multiphonon process. In solutions, this occurs very efficiently via collisions with the solvent. However, it is not clear if this process is very effective in polymer/beta-carotene films. It is also possible that ${}^1O_2$ generated by PYR-3 can be relaxed back to ${}^3O_2$ by energy transfer to β-carotene, as shown in Figure 1.12. This process is believed to occur efficiently in solutions containing beta-carotene and ${}^1O_2$, where the energy difference between the beta-carotene triplet and singlet states is less than the energy difference between the singlet and triplet oxygen states (1 eV) (Viljanen, *et al*., 2002). It is also possible that singlet oxygen generated by PYR-3 simply degrades β-carotene which is not the most desired process.
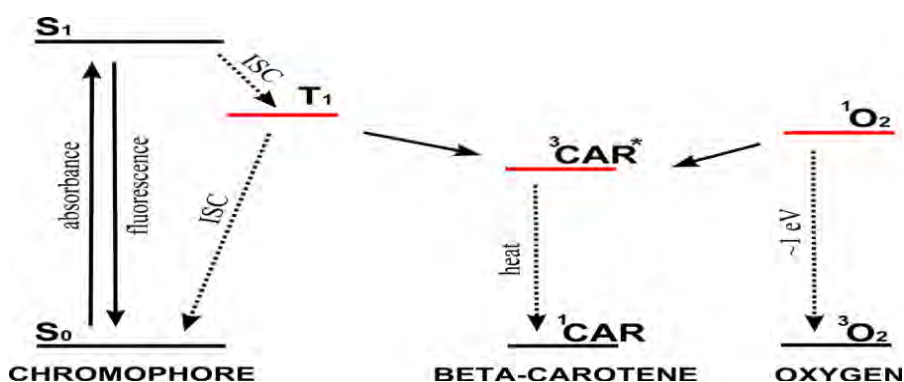
Figure 1.12 : Energy level diagram showing excitation of the PYR-3 chromophore with β-carotene

Figure 1.12 showing excitation of the PYR-3 chromophore (left) to the S_1 state, intersystem crossing (ISC) to the T_1 state, energy transfer to beta-carotene (middle) that leaves PYR-3 in the ground S_0 state and beta-carotene in the triplet excited state, and finally multi-phonon decay from the beta-carotene excited triplet state to the singlet ground state. Also shown is another possible mechanism, where ISC generates singlet oxygen. This can be followed by energy transfer from singlet oxygen (right) to β-carotene (middle) that leaves oxygen in the lower energy triplet state and multi-phonon relaxation from the beta-carotene triplet state to the singlet ground state.

3. Antioxidant

3.1 General concept of antioxidant

Antioxidants may be molecules that can neutralize free radicals by accepting or donating electron(s) to eliminate the unpaired condition of the radical (Lü *et al*., 2010). Recently, there has been a considerable interest infinding natural antioxidants from plant materials to replace synthetic antioxidant in food products (Taher and Sarmidi, 2015) or medical (Zaelani *et al*, 2015).

3.2 Fucoxanthin

Seaweeds are macroscopic, marine, saltwater-dwelling a primitive type of plants which form an important component of marine living resources (Rout and Kumar, 2015). According their pigmentation, the seaweeds broadly grouped into chlorophyceae (green algae), the phaeophyceae (brown algae) and the rhodophyta (red algae).

Fucoxanthin (Figure 1.13), a major marine carotenoid, occurs abundantly in some macro and microalgae and contributes more than 10% of the estimated total production of carotenoids in nature. This pigment is bound to several proteins and, together with chlorophyll-a (Chl*a*), forms fucoxanthin-Chl*a*-protein complexes in the thylakoids, where it acts as a primary carotenoid to harvest light and transfer energy. This protein has been extensively

investigated in microalgae, including P. *tricornutum*, for its role in photosynthesis. However, it is not known whether this pigment functions as a secondary carotenoid relating to photo-oxidative protection. The fucoxanthin has been found to have a number of therapeutic activities, including anticancer, antihypertensive, anti-inflammatory, and antiobesity effects (Maeda *et al*, 2008; Kim *et al*., 2012; Zaelani *et al*, 2015).
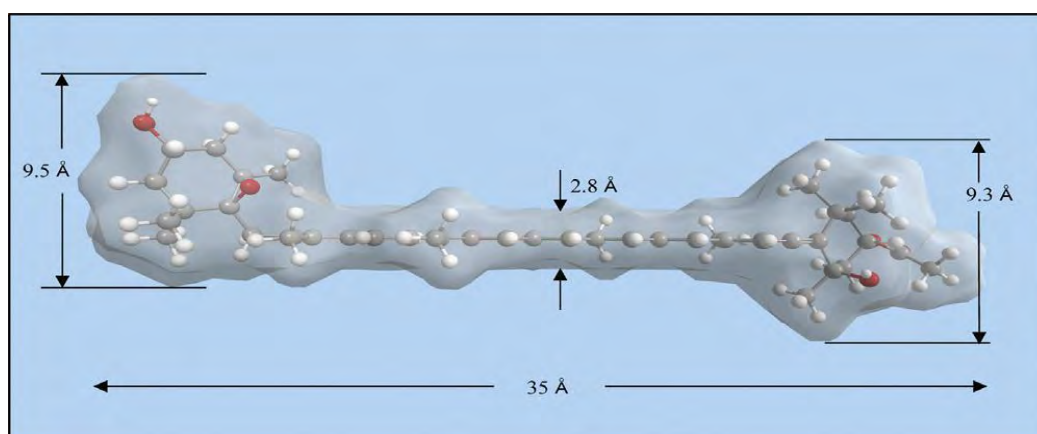
Figure 1.13: Chemical structure and dimension of Fucoxanthin
(Kita *et al*., 2015)

Fucoxanthin standard (Figure 1.14) has absorption peaks in the wavelength range 350-750 nm (methanol: water (1: 9, v / v)) to the absorption peak at 423 nm wavelength region (Yip *et al*., 2014). Fucoxanthin Also has its own fluorescence properties (green color) and can be used as a fluorescent marker in various diagnostic purposes in the future (Sudhakar *et al*, 2013). Pigment fucoxanthin extracted from Sargasasum Banderi have stability at pH = 5-7 on the storage conditions in a dark place below 4 ℃ (Yip *et al*. 2014).

Fucoxanthin extracted from various species of brown algae, resulting yield varied from 39.6 µg/g -15 mg/g. The yield of the resulting fucoxanthin also depends on conditions such as the type of solvent, duration and temperature of the extraction (Table 1.2).
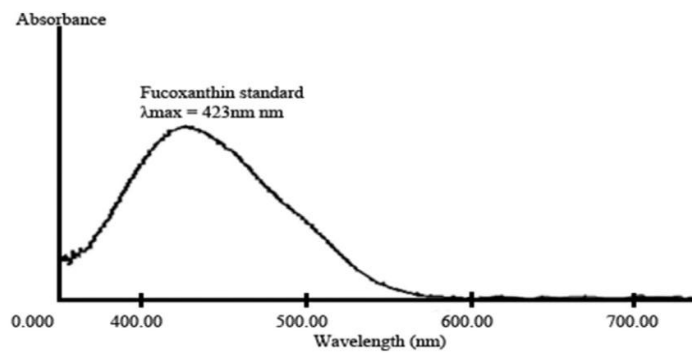
Figure 1.14: Absorption peaks of fucoxanthin standard

Indonesia as an archipelago with 17,504 islands and a number of long reach 81,000 km coastline has huge potential for the development of commodity seaweed. The development activities have been conducted and start from Nanggroe Aceh Darussalam to Papua. The potential commodity cultivation of seaweed Indonesia reached 769,452 hectares. From that total area, only about 50% was utilized around 384,733 hectares. But it will continued until 10 million tons can be achieved (Warta exports, 2013).

Table 1.2: Extraction fucoxanthin from algae

Sources	Species	Condition extraction		% Yield	Application	Ref
		Wet/dried	Solvent			
Brown algae: Java	Sargassum sp	wet	100% acetone	107.2 µg/g		Indrawati *et al*, 2015
Brown seaweed	Sargassum filipendula	wet	DMSO (1:10 w/v)		Anticancer	Zaelani *et al*, 2015
Brown Seaweed	Himanthalia elongata		n-hexana,dietyl eter, chlorofom		Antioxidant, antibacteria	Rajauria and Abu-ghanna, 2013
Brown Seaweed					Antioxidant, antiobesity, anticancer	Muthuirullappan and Francis, 2013
Brown seaweed, Micro-algae					Antioxidant, antiinflamatory, anticancer, anti-obesity	Peng *et al*, 2001
Brown Seaweed, India	Sarrgassum: illifolium, longifolium, wihgtii, Padina gymaspea, Turbinaria ornafa	Dried	90% acetone	0.23µg/g	Antioxidant	Sudhakar *et al*, 2013
Brown algae Malaysia	Sargassum binderi	dried	100% methanol			Hii *et al*, 2013
Brown algae, Fuji-China	Laminaria japonica	dried	methanol		Antioxidant	Liu *et al*, 2015
Brown algae Malaysia	Sargassum binderi, sargassum duplicatum	dried	Acetone:methanol (7:3 v/v)	1.01 + 0.1 mg		Novendri *et al*, 2011
Sea weed Wakanal, Japan	Undaria piannatifia	dried	Acetone/methanol (70:30 v/v)		Antioxidant for meat colour chicken	Sasaki *et al*, 2008
Sea weed comercial	Undari pinnatifida	dried	acetone		Antioxidant, anti-diabetic	Iwasaki *et al*, 2012

3.3 Curcumin

Curcumin is an orange yellow crystalline powder with three coloring components in various portions which are all dicinnamoyimethane derivatives (Mainum and Shashikala, 2014). The derivatives of curcumin are: (i) 1, 7-Bis-(4-hydroxy- 3-methoxyphenyl)-hepta-1, 6-diene- 3, 5 dione = diferuloyl methane (Chemical formula: $C_{21}H_{20}O_6$, Formula weight: 368), (ii) 1-(4-hydroxyphenyl)-7-(4-hydroxy 3- methoxyphenyl)-hepta-1,6-diene-3, 5 dione = phydroxycinnamoyl ferulo methane (Chemical formula: $C_{20}H_{18}O_5$, Formula weight: 338), and (iii) 1, 7-Bis-(4-hydroxyphenyl) - hepta-1, 6-diene-3, 5dione=p, pdihydroxy dicinnamoyl methane (Chemical formula: $C_{19}H_{16}O_4$, Formula weight: 308). The main compound of curcuminoids: curcumin,

demethoxycurcumin, and bisdemethoxycurcumin are represented at Figure 1.15 (Himesh *et al.*, 2011; Kulkarni *et al.*, 2012)
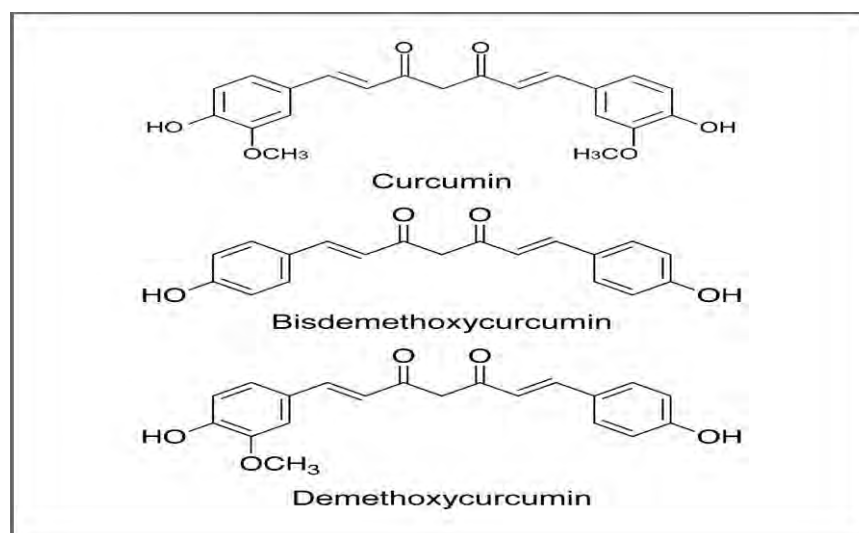
Figure 1.15: Molecular structure of the main compound in curcumin

Curcumin can be extracted from turmeric (Curcuma longa) (Kulkarni *et al.*, 2012; Kandasamy and Subramanian, 2013; Van Nong *et al.,* 2016) or Curcuma xanthorriza rhizomes (Taher and Sarmidi, 2015). The common method are using maceration, percolation and soxhlet extraction techniques (Himesh *et al.*, 2011). The other method was using UAE, ultrasonic assisted extraction (Rouhani *et al.*, 2009). It was found that the yield of ultrasound-assisted extraction was approximately three times higher than the traditional method. Laokuldilok *et al*,. (2015) used microwave assisted to extract the bioactive compounds from turmeric (Curcuma longa). The contents of curcumin, demethoxycurcumin and bisdemethoxycurcumin of extracts obtained from MAE (Microwave-assisted extraction) were in range of 163.00-183.77, 91.73-99.48 and 46.36-53.35 mg/g extract, respectively which were higher than soxhlet extraction.

There are several reports in the literature indicating a variety of pharmacological activities of curcuminoids such as anti-inflammatory, antibacterial, antimicrobial, antifungal, antiparasitic and antimutagenic and as

modest inhibitors of HIV 1 and HIV 2 proteases (Reddy and Lokesh, 1992; Srimal, 1997; Sanphui *et al*., 2011; Agarwal and Sung, 2009; Jayaprakasha *et al*., 2005, Shanmugam and Bhavani, 2014). Curcumin is also a prominent candidate for treating cystic fibrosis, Alzheimer's and malarial diseases in addition to cancer (Maheshwari *et al.* 2006; Yallapu *et al*. 2012).

Due to environmental awareness and harmful effects of either toxicity or non-biodegradable nature of synthetic dyes, natural colorants are thinking globally due to the fact that the majority of the sources are safer, more environmental friendly, curcumin also used`as natural dyes in textile (Hasan *et al*, 2014). Soltani Rad *et al*. (2015) used curcumin as emitting layer in OLED. They reported the absorption and photoluminesence of curcumin in pure methanol were 424 nm and 555 nm,respectively (Figure 1.16). Curcumin has an EL (electroluminesence) peak emission wavelength at $\lambda = 612$ nm and this wavelength is comparable to other previously reported chromaphores, for instance: 630 and 700 nm (Sharbati *et al*, 2011), 600 to 905 nm (Sharbati *et al*, 2010), 700 nm (Yao *et al*., 2014), 486 to 529 nm (Takahashi *et al*, 2014), 566 to 678 (Lee *et al*., 2011) and 692 to 815 (Yang *et al*., 2008).
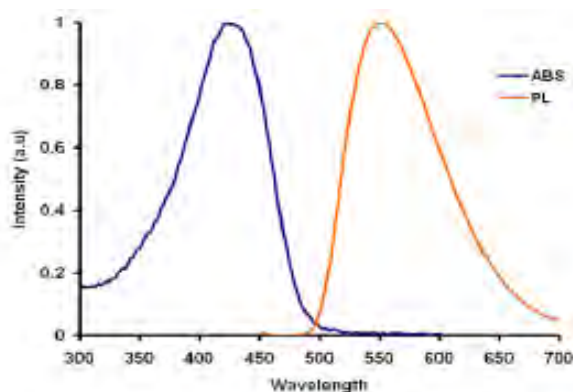
Figure 1.16: Absoprtion (ABS) ans photoluminesence (PL) of curcumin in methanol

4.   Clay

Clay is a natural mineral group of crystalline philosilicates with a layered structure and is smaller than 2 micrometers in size. According to Mason and Moore (1982), the clay mineral structure consists of two constituent units. The first unit forms a tetrahedral sheet of silicon and oxygen. The other constituent units form octahedral sheets of aluminum or magnesium with oxygen or hydroxide. Clay minerals of the 1:1 and 2:1 types are represented in Figure 1.17 (Leroy and Revil, 2004).
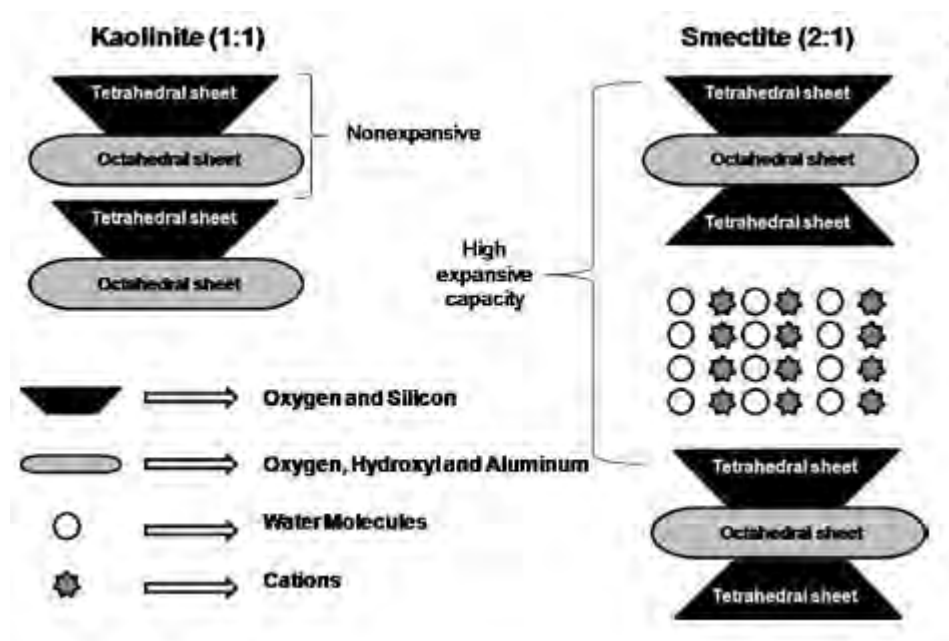
Figure 1.17: Models of a 1:1 (Kaolinite) and 2:1 (Smectite) sheet structures

Technical applications are encountered in the paper industry, in ceramics, in brick production and in the chemical industry. In addition, clays are used for cleaning purposes "fuller's earth" (Murray, 2000). Clays also are used in medical and cosmetic (Awad *et al*., 2017; Dias Moraesa *et al*., 2017).

Clay minerals are classified into eight major groups, on the basis of layer type (1:1 or 2:1), layer charge and type of interlayer, as presented in triple layer clay minerals (2:1) at Table 1.3.

Table 1.3: Classification of layered silicate minerals
(Brindley and Brown, 1980)

Layer type	Group	Sub grup	Species
1:1	Sepentine- Kaolin	Serpentines Kaolins	Lizardite, Antigorite, Chrysotile, Kaolinite, Dickite, Nacrite
2:1	Talc-Pyrophilillite	Talcs Pyrophyllite	Talc, Willemseite Pyrophyllite
	Smectite	Saponite Monmorrilonites	Saponite, Hectorite Monmorrilonite, Beidellite
	Vermicullite	Trioctahedral Vermicullite	Trioctahedral Vermicullite
		Dioctahedral Vermicullite	Dioctahedral Vermicullite
	Mica	Trioctahedral Mica Dioctahedral Mica	Plogophite, Biotite, Lepidolite
			Muscovite
	Brittle Mica	Trioctahedral Brittle Mica	Clintonite
		Dioctahedral Brittle Mica	Margarite
	Chlorite	Trioctahedral Chlorite	Clinochore
		Dioctahedral Chlorite	Donbassite
		Di,trioctahedral Chlorite	Cookeite
2:1	Sepiolite-Palygorskite	Sepiolites	Sepiolite
Inverted Ribbons		Palygorskites	Palygorskites

The industrial applications of the three most important clay mineral types are varied and in most instances quite different. This is primarily because of differences in their physical and chemical properties, which are dependent on structure and composition. A summary of some of the important characteristics and properties of kaolins, smectites, and palygorskite are shown in Table 1.4 (Murray, 2000).

Table 1.4: Some important properties of clay minerals that relate to their applications

Kaolin	Smectite	Palygorskite
1:1 layer	2:1 layer	2:1 layer inverted
White or near white	Tan, olive green, gray, or white	Light tan or gray
Litte substitution	Octahedral and tetrahedral substitution	Octahedral substitution
Minimal layer charge	High layer charge	Moderate layer charge
Low base exchange	High base exchange capacity	Moderate base exchange capacity
Pseudo-hexagonal flakes	Thin flakes and laths	Elongate
Low surface area	Very hight surface area	High surface area
Very low absorption capacity	High absorption capacity	High absorption capacity
Low viscosity	Very high viscosity	high viscosity

4.1   Kaolin

The name kaolin is derived from the Chinese term "Kauling" meaning high ridge, the name for a hill near Jauchau Fu, China, where this material was mined centuries ago for ceramics. The main constituent, kaolinite, is a hydrous aluminum silicate of the approximate composition $2H_2O$-Al_2O_3-$2SiO_2$. Structurally, kaolinite consists of alumina octahedral sheets and silica tetrahedral sheets stacked alternately and has the theoretical formula $(OH) Si_4Al_4O_{10}$ and the theoretical composition 46.54% SiO_2, 39.5°/0 Al_2O_3, 13.96% H_2O. The shape of a perfectly ordered kaolinite crystal is pseudohexagonal, but ordering may range from a high degree, to a poorly ordered crystal where shape is non-determinant (Prasad *et al*., 1991).

Kaolins are generally classified as primary or secondary deposits. Primary kaolins are formed by the alterations of crystalline rocks such as granite and are found in the location where they were formed. Secondary kaolin deposits are sedimentary in nature and are formed by the erosion of primary deposits (Prasad *et al*., 1991).

The kaolin group is divided in three polytypes (kaolinite, nacrite, dickite) in addition to halloysite their hydrated analogue. Kaolinite, dickite, and nacrite have the same chemical composition of 46.54% SiO_2, 39, 50% Al_2O_3 and 13.96% H_2O with the chemical formula $Al_2SiO_2O_5(OH)_4$. Halloysit has the chemical formula $Al_2SiO_2O_5(OH)_4.2H_2O$. Identification of kaolin polytypes can be done by X-Ray diffraction, infra red-spectroscopy, and differential thermal analysis (Shen *et al*., 1994; Ruiz Cruz, 1996; Buatier *et al*., 1996). The crystallographic of kaolin group (Ruiz Cruz., 2007) is shown in Table 1.5.

Tabel 1.5: The crystallographic of kaolin group

	Sistem	Space grup	Parameter sel
Kaolinite	Triclinik	C1	a= 5,156 Å α = 91,697° b =8,945 Å ß = 104,862° c = 7,05 Å Y = 89,823°
Dickite	Monoklinik	Cc	a = 5,138 Å ß = 96,74° b = 8,918 Å c = 14,389 Å
Nacrite	Monoklinik	Cc	a = 8, 908 Å ß = 113,7° b = 5,146 Å c = 15,697 Å
Halloysite	Monoklinik	CC	a = 5,14 Å ß = 96° b = 8,90 Å c = 14,70 Å

The morphology of the kaolin group can be identified with scanning electron microscope (SEM). Halloysite has a tubular shape, speris. Kaolinite is more varied morphology, plate, pseudohexagonal, or vermicular. While, dickite particles are blocky or platty. Nacrite is identified by a thin hexagonal particle shape (Figure 1.18).

44
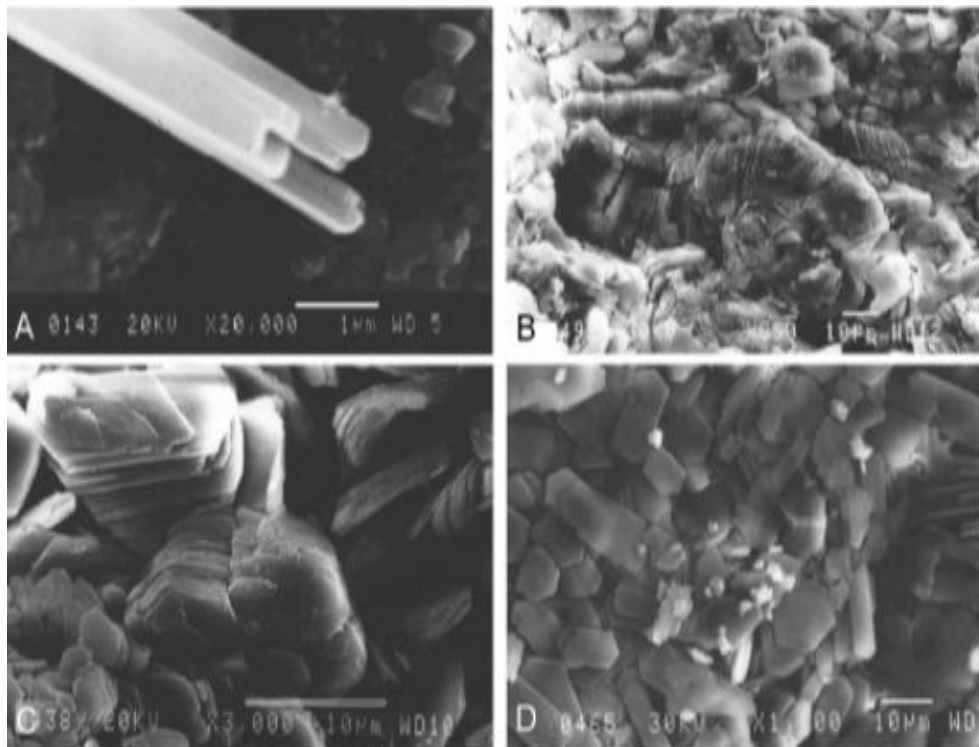
Figure 1.18: The morphology of grup kaolin halloysite (A), kaolinite (B), dickite (C), and nacrite (D) (Ruiz Cruz, 2007)

4.1.1 Kaolinite

Kaolinite normally appears as stacked pseudohexagonal platelets,<2 μm in size, with a common booklet-like shape. Each platelet is considered as an arrangement of several layers, each of which consists of two basal (001) planes: the tetrahedral silica sheet, with O atoms bonded to Si atoms, and called the "siloxane surface", and the octahedral alumina sheet, with OH groups bonded to Al, called the "aluminol surface". Both sheets share the O atoms (Figure 1.19). Each kaolinite layer is considered as a strong dipole, where the siloxane surface is hydrophobic and dominated by negative charges, while the aluminol surface exhibit positive charges and is hydrophilic. Thus, the individual layers of kaolinite are strongly bonded by hydrogen and dipolar interactions (Awad et *al*., 2017).
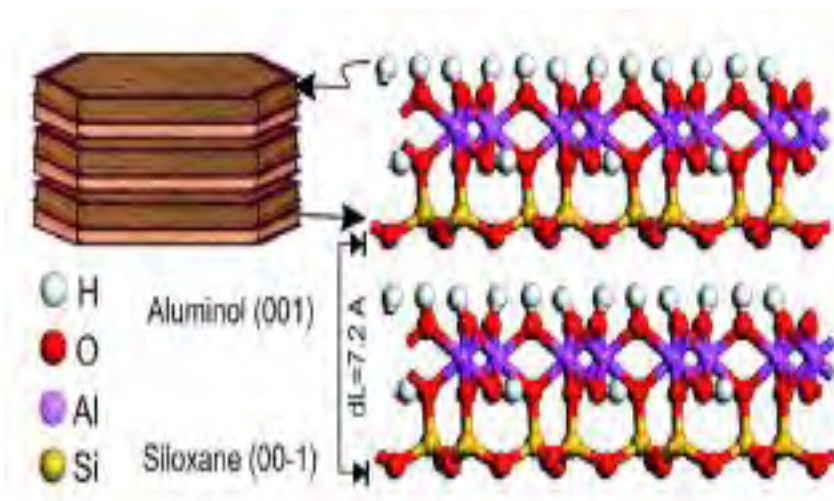
Figure 1.19: Molecular simulation model of kaolinite structure (1 ×2 ×2 unit cells) showing siloxane and aluminol surfaces

Fatimah *et al* (2014) sintesed TiO_2/ kaolinite as a membran for water disinfektan. Kaolinite was used as adsorbent for some metal ion such as $Cd^{2+,}$ $Cu^{2+,}$ Pb^{2+}, and Zn^{2+} (Srivastava *et al*., 2005; Mbaye *et al*., 2014; Chai *et al*., 2017).

4.1.2 Nacrite

Nacrite is the rarest kaolin polymorph and thherefore regarded nacrite as the typical high-temperature polymorph (Buhmann, 1988). The nacrite layer (7.186 Å) is slightly thicker than the dickite (7.162 Å) and kaolinite (7.124 Å) layers. Within the limits of accuracy of the kaolinite and nacrite structures, this difference appears due to a slightly greater interlayer separation in nacrite (2.92Å) than in dickite (2.89 Å) and kaolinit (2.84 Å). This suggests that the packing of layer is less favorable in nacrite because of the strain the directed interlayer bonds. The thicker layer is compensated by a shorter lateral repeat distance in nacrite (8.909 Å) than the corresponding repeats in kaolinite (8.932 Å) and dickite (8.940 Å). The nacrite structure is based on a 6R stacking sequence of kaolin layers, in which each successive layer is shifted relative to the layer below by of the 8.9 lateral repeat along the - X direction of the resultant unit cell (Figure 1.20) (Blount *et al*,. 1969).

46
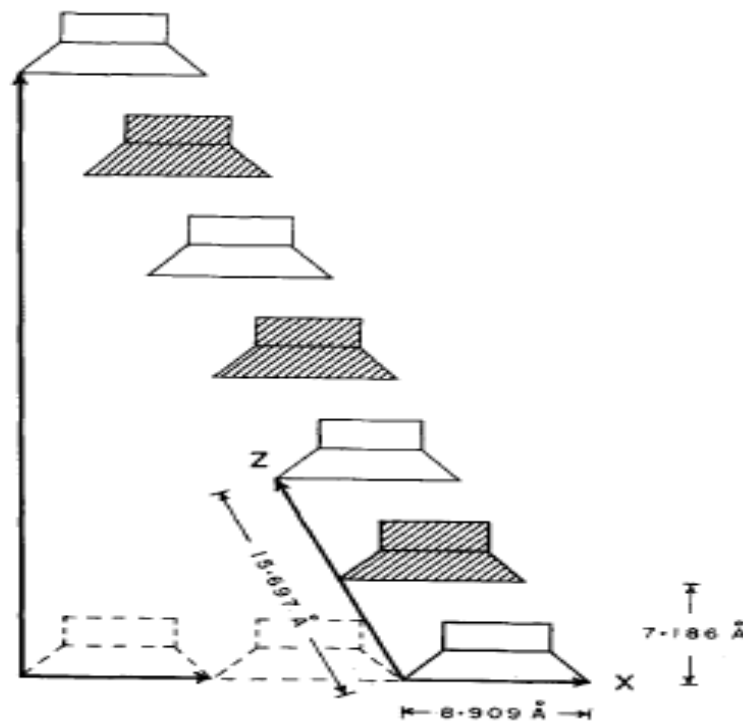
Figure 1.20: Layer sequence in nacrite

Jaafar *et al* (2014) used amorphous nacrite clay hybrid from Tunisia as solid electrolyte for Li-ion batteries, while Xu and co-workers (2016) synthesized nacrite-nanoroll and used it for reinforcing tensile and tear strength of its composite with linear low-density polyethylene (LLDPE).

4.2 Activation and modification of kaolin and its characterization

The applications of kaolin, a widely used industrial clay raw material, depend on its surface reactivity (Zsirka *et al*., 2015). There are broadly two different treatments or modification methods of clay minerals studied by different researchers such as (1) physical modification (thermal or microwave treatment) which involves alteration of chemical composition and crystalline structure by the effect of high temperature, (2) chemical modification (by acids, bases, organic compounds) which is usually by the alteration of structure, surface functional groups and surface area (Hussin *et al*., 2011).

However, the improvement of the properties of kaolin by chemical methods is difficult because of the high passivity of this material. Thus, it is not significantly affected by acid or alkaline treatments, even under strong conditions (concentrated solutions and/or high temperatures). Metakaolinite, a metastable phase obtained by calcination of kaolinite, has been reported to be more reactive under chemical treatments (Xu, *et al*., 1999). Metakaolins are obtained by calcination of kaolins at temperatures between 550-950 °C (Belver *et al*., 2002; Ilić *et al*., 2010; Jaafar *et al*., 2015; Rahmalia, 2016).

Acid treatment is one of the most common chemical treatments for clay minerals and has been used to increase the specific surface area and the number of acidic centers, modify the surface functional group and to obtain solids with high porosity (Hiendro *et al*., 2012). The other researchers using alkali such as NaOH (Granizo *et al*., 2000), KOH (Belver *et al*., 2002). Mbaye *et al* (2014) reported that kaolinite organically modified by grafting with 3-aminopropyltriethoxysilane (APTES) improved significantly its retention ability of heavy metal Pb (II) from solutions.

References

Abhishek, P., Kulkarni., Christopher, J., Babel, A.T., and Jenekhe, S.A. (2004) Electron transport materials for organic light-emitting diodes. *Chemical Materials*, **16** (23), 4556-4573.

Agarwal, B.B. and Sung, B. (2009) Pharmacological basis for the role of curcumin in chronic diseases: an age-old spice with modern targets. *Trends Pharmacology Sciences*, **30**, 85-90.

Ammermann, D,. Böhler, A., and Kowalsky, W. (1995) Multilayer Organic Light Emitting Diodes for Flat Panel Displays. Annual report Institut Hochfrequenztechnik, TU Braunschweig, 47-58.

Awad, M.E., López-Galindo, A., Setti, M., El Rahmanya, M.M., and Iborra, C.V. (2017) Kaolinite in pharmaceutics and biomedicine (Review). *International Journal of Pharmaceutic*s, **533**, 34–48.

Belfield, K.D., Morales, A.R., Kang, B.S., Hales, J.M., Hagan, D.J., Van Stryland, E.W., Chapela, V.M., and Percino. (2000) Synthesis of two-photon

absorbing unsymmetrical fluorenyl-based chromophores. *Journal of Chemical Materials*, **16**, 4634.

Birks, J.B. (1970) Photophysics of Aromatic Molecules . Wiley-Interscience, New York.

Blount, A.M., Threadgold, I.M., and Bailey, S.W. (1969) Refinement of the crystal structure of nacrite. *Clays and Clay Minerals*, **17**, 185-194.

Brindley, G.W. and Brown, G. (1980) Crystal Structures of clay Minerals and Their X-ray Identification. Monograph 5, Mineralogical Society.

Buatier, M.D., Potdevin, J.L., Lopez, M., and Petit, S. (1996) Occurrence of nacrite in the Lodève basin (France). *European Journal of Mineral*, **8**, 847-852.

Buhmann, D. (1998) An occurance of authigenic nacrite. *Clays and Clay Minerals*, **36** (2), 137-140.

Cao-Hoang, L., Fougère, R., and Waché, Y. (2011) Increase in stability and change in supramolecular structure of β-carotene through encapsulation into polylactic acid nanoparticles. *Food Chemistry*, **124**, 42-49.

Chai, W., Huang, Y., Su, S., Han, G., Liu, J., and Yijun, C.Y. (2017) Adsorption behavior of Zn(II) onto natural mineral minerals in wastewater. A comparative study of bentonite and kaolinite. Physicochemical Problems of Mineral Processing, **53**, 264−278.

Chakrabarti, S. and Ruud, K. (2009) Large two-photon absorption cross section: Molecular tweezers as a new promising class of compounds for nonlinear optics. *Physical Chemistry Chemical Physics*, **11**, 2592–2596.

Cerón-Carrasco, J.P., Requena, A., and Marian, C.M. (2010) Theoretical study of the low-lying excited states of β-carotene isomers by a multireference configuration interaction method. *Chemical Physic*, **373**, 98-103.

Cvetkovic, D. and Markovic, D. (2008) Stability of carotenoids toward UV-irradiation in hexane solution. *Journal of Serbia Chemistry Society*, **73** (1), 15–27.

Dias Moraesa, J.D., Alina Bertolinob, S.R., Cuffinic, S.L., Ducartd, D.F., Bretzkee, P.E., and Leonardia, G.R. (2017) Clay minerals: Properties and applications to dermocosmetic products and perspectives of natural raw materials for therapeutic purposes—A review. *International Journal of Pharmaceutics*, **534**, 213–219.

Delgado-Vargas, F., Jiménez, A.R., and Paredes-López, O. (2000) Natural pigments: Carotenoids, anthocyanins, and betalains-characteristics, biosynthesis, processing, and stability.*Critical Reviews in Food Science and Nutrition,* **40** (3), 173–289.

Fatimah, I., Hasanah, U.A., and Putra, H.P. (2014) Preparation of bifunctional ceramic membrane based on TiO_2/kaolinite for water desinfection. *Journal of Materials and Enviromental Sciences,* **5** (6), 1976-1981.

Gomez, E.F., Venkatraman, V., Grote, J.G., and Steckl, A.J. (2014) DNA bases thymine and adenine in bio-organic light emitting diodes. *Scientific Report*, **4**, 7105.

Gupta, G., Steier, W.H., Liao, Y., Luo, J., Dalton, L.R., and Jen, A.K. (2008) *Journal of Physic Chemistry C*, **112**, 8051.

Granizo, M.L., Blanco-Varela, A., and Palomo. (2000) Influence of the starting kaolin on alkali-activated materials based on metakaolin. Study of the reaction parameters by isothermal conduction calorimetry. *Journal of Materials Science*, **35**, 6309 – 6315.

Hasan, M.M., Hossain, M.B., Azim, M.A., Ghosh, A.Y., and Reza, M.S (2014) Application of purified curcumin as natural dye on cotton and polyester. *International Journal of Engineering & Technology*, **14** (05), 17-23.

Hiendro, A., Hadary, F., Rahmalia, W., Wahyuni, N. (2012) Enhanced performance of bixin sensitized solar cells with activated kaolinite. *International Journal of Engineering Research and Innovation,* **4**, 40-44.

Hii, S.L., Choong, P.Y., Woo, K.K., and Wong, C. L. (2010) Stability studies of fucoxanthin from sargassum Binderi. *Australian Journal of basic and Applied Sciences*, **4**(10), 4580-4584.

Himesh, S., Sharan, P.S., Mishra, K., Govind, N., and Singhai, A.K. (2011) Qualitative and quantitative profile of curcumin from ethanolic extract of curcuma Langa. *International Research Journal of Pharmacy*, **2** (4), 180-184.

Hussin, F., Aroua, M.K., and Daud, W.M. (2011) Textural characteristics, surface chemistry and activation of bleaching earth: A review. *Chemical Engineering Journal*, **170**, 90–106.

Ilić, B.R., Mitrović, A.A., and Miličić, L.R. (2010) Thermal treatment of kaolin clay to obatin metakaolin. *Hemijska Industija*, **64** (4), 351–356.

Jaafar, N., Naamen, S., Ben Rhaiem, H., and Ben Haj, A.A. (2015) Functionalization and structural characterization of a novel nacrite-LiCl nanohybrid material. *American Journal of Analytical Chemistry*, **6**, 202-215.

Jayaprakasha, G.K., Jaganmohan, L.R., and Sakariah, K.K. (2005) Chemistry and biological activities of C. longa. *Trends in Food Sciences and Technology,* **16**, 533-48.

Kalinowski, J. (1999) Electroluminescence in organics. *Journal of Physics D: Applied Physics*, **32**, 179- 142.

Kandasamy, J. and Subramanian, M. (2013) Validation method for estimation of curcumin from different varieties of curcuma longa. *International Journal of Pharma and Bio Sciences*, **4**(1), 1004-1010.

Kita, S., Fuji, R., Richard, J., Cogdell, R.J., and Hashimoto, H. (2015) Characterization of fucoxanthin aggregates in mesopores of silica gel: Electronic absorption and circular dichroism spectroscopies. *Journal of Photochemistry and Photobiology A: Chemistry,* **313**, 3–8.

Kulkarni, S.J, Maske, K.N., Budre, M.P., and Mahajan, R.P. (2012) Extraction and purification of curcuminoids from Turmeric (curcuma longa L.*). International Journal of Pharmacology and Pharmaceutical Technology*, **1** (2), 81-84.

Laokuldilok, N., Kopermsub, P., Thakeow, P., and Utama-ang, N. (2015) Microwave assisted extraction of bioactive compounds from turmeric (Curcuma longa). *Journal of Agricultural Technology,* **11** (5), 1185-1196.

Laughlin, R.G., Bunke, G.M., Eads, C.D., Laidig, W.D., and Shelley, J.C. (2002) Preparation and physical characterization of pure β-carotene. *Chemical Physic and Lipids*, **115**, 63-76.

Lee, K.H., Kim, Y.K., and Yoon, S.S. (2011). Donor-acceptor-donor type red fluorescent emitters containing adamandane-substituted julolidines for OLEDs. *Bulletin of Korean Chemical Society*, **32**, 2787–2790.

Leroy, P. and Revil, A.A. (2004) Triple-layer model of the surface electrochemical properties of clay minerals. *Journal of Colloid andInterface Sciences,* **70**, 371–380.

Lowell, S, and Shield, J.E. (1984) Powder Surface Area and Porosity (Particle Technology Series), 3nd ed, Chapman and Hall, London,.

Lü, J.M., Lin, P.H., Yao, Q., and Chen, Q. (2010) Chemical and molecular mechanisms of antioxidants: experimental approaches and model systems. *Journal of Cellular and Molecular Medicine*, **14** (4), 840-860.

Maeda, H., Tsukui, T., Sashima, T., Hosokawa, M., and Miyashita, K. (2008) Seaweeds carotenoid, fucoxanthin as a multi-functional nutrients. *Asia Pacific Journal of Clinic and Nutritions*, **17**, 196-199.

Maheshwari, R.K., Singh, A.K., Gaddipati, J., and Srimal, R.C. (2006) Multiple biological activities of curcumin: a short review. *Life Sciences*, **78**, 2081.

Mainum, S.H. and Shashikala P. (2014) Extraction, nanoformulation and evaluation of curcumin. *International Journal of Pharmacognosy*, **1** (8), 520-527.

Marder, S.R., Torruellas, W.E., Desce, B.M., Ricci, V., Stegeman, G.I., Gilmour, S., Bredas, J.L., Li, J., Bublitz, G.U., and Boxer, S.G. (1997) Large molecular third-order optical nonlinearities in polarized carotenoids, *Science,* **276**, 1233-1235.

Marx, M., Stuparic, M., Schieber, A., and Carle, R. (2003) Effect of thermal processing on trans-cis-isomerization of β-carotene in carrot juices and carotene-containing preparations. *Food Chemistry*, **83**, 609-617.

Marty, C. and Berset, C. (1990) Factors affecting the thermal degradation of all-trans-β-carotene. *Journal of Agriculture and Food Chemistry*, **38**, 1063-1067.

Mbaye, A., Diop, C.A.K., Miehe-Brendle, Senocq, J.F., and Maury, F. (2014) Characterization of natural and chemically modified kaolinite from Mako (Senegal) to remove lead from aqueous solutions. *Clay Minerals*, **49** (4), 527-539.

Morabito, K., Steeley, K.G., Shapley, N.C., Mello, C., Li, D., Calvert, P., and Tripathi, A. (2011) Proximal effects of ultraviolet light absorbers and polymer matrix in the photostability of β-carotene. *Dyes and Pigments*, **92**, 509-516.

Mordi, R.C., Walton, J.C., Burton, G.W., Highes, L., Ingold, K.U., Lindsay, D.A., and Moffatt, D.J. (1993) Oxidative degradation of β-carotene and β-apo-8'-carotenal. *Tetrahedron*, **49**, 911-28.

Mordi, R.C. (1992) Mechanism of β-carotene degradation. *BJ Letter*, 310.

Murray, H.H. (2000) Traditional and new applications for kaolin, smectite, and palygorskite: a general overview. Applied Clay Science, 17, 207–221.

Muthuirulappan, S. and Francis, S.P. (2013) Anti-cancer mechanism and possibility of nano-suspension formulation for marine algae product fucoxanthin. *Asian Pacific Journal of Cancer Prevention*, **14**, 2213-2216.

Ohtani, N., Kitagawa, N., and Matsuda, T. (2011) Fabrication of organic light-emitting diodes using photosynthetic pigments extracted from spinach. *Japananese Journal of Applied Physisc,* **50**, 1-3.

Ozhogina, O.A. and Kasaikina, O.T. (1995) β-carotene as an interceptor of free radicals. *Free Radical Biology and Medicine*,**19**, 575-581.

Pang, H., Michalski, L., Weaver, M.S., Ma, R., and Brown, J.J. (2014) Thermal behavior and indirect life test of large-area OLED lighting panels. *Journal of Solid State Lighting*, **1**,7-9.

Peng, J., Yuan, J.P., Wu, C.F., and Wang, J.H. (2011) Fucoxanthin, a marine carotenoid present in brown seaweeds and diatoms: Metabolism and bioactive relevant to human health. *Drugs*, **9**, 1806-1828.

Prasad, M.S., Reid, K.J., and Murray, H.H. (1991) Kaolin: processing, properties and applications. *Applied Clay Science*, **6**, 87-119.

Qiu, D., Chen, Z-R., and Li, H-R. (2009) Effect of heating on solid β-carotene. *Food Chemistry*, **112**, 344-349.

Rajauria, G. and Abu-Ghannam. N. (2013) Isolation and Partial Characterization of Bioactive Fucoxanthin from Himanthalia elongate Brown Seaweed: A TLC-Based Approach. *International Journal of analytical Chemistry,* Volume 2013, Article ID 80257.

Reddy, A.C.P. and Lokesh B.R. (1992) Studies on spice principles as antioxidants in the inhibition of lipid peroxidation of rat liver microsomes. *Molecular Cells and Biochemistry*, **111**, 117-124.

Rodriguez, E.B. and Rodriguez-Amaya, D.B. (2007) Formation of apocarotenals and epoxycarotenoids from β-carotene by chemical reactions and by autoxidation in model systems and processed foods. *Food Chemisry*, **101**, 563-720.

Roncali, J. (1997) Synthetic principles for bandgap control in linear π-conjugated systems. *Chemical Reviews*, **97**, 173–206.

Rouhani, S., Alizadeh, N., Salimi, S., and Haji-Ghasemi, T. (2009) Ultrasonic assisted extraction of natural pigments from thizomes of curcuma longa L. *Progress in Color Colorants and Coating*, **2**, 103-113.

Rout, S. and Kumar, A. (2015) A review on the potentiality of marine seaweeds as a medical sources. *World Journal of Pharmacy and Pharmaceutical Sciences*, **4** (10), 458-476.

Ruiz Cruz, M.D. (1996) Dickite, nacrite and possible dickite/nacrite mixed-layers from the Betic cordilleras (SPAIN). *Clays and Clay Minerals*, **44** (3), 357-369.

Ruiz Cruz, M.D. (2007) genesis and evaluation of kaolin-group mineral during the diagenisis and the beginning of methamorphism.

Sanphui, P., Goud, N.R., Khandavilli, U.B.R., Bhanoth, S., and Nangia, A. (2011) New polymorphs of curcumin. *Chemical Communications*, **47**, 5013.

Sattar, A., de Man, J.M., and Alexander, J.C. (1977) Wavelength effect on light-induced decomposition of Vitamin A and β-carotene in solutions and milk fat. *Canadian Institute of Food Science and Technology Journal*, **10**, 56-60.

Sekine, C., Tsubata, Y., Yamada, T., Kitano, M., and Doi, S. (2014) Recent progress of high performance polymer OLED and OPV materials for organic printed electronics. *Science and Technology of Advanced Materials*, **15**, 034203.

Sharbati, M.T., Panahi, F., and Gharavi, A. (2010) Near-infrared organic light-emitting diodes based on donor-pi-acceptor oligomers. *Photonics Technology Letters*, **22**, 1695–1697.

Sharbati, M.T., Soltani Rad, M.N., Behrouz, S., Emami, F., and Nekoie, A. (2011). Fabrication and electrical characterization of red organic light emitting diode using an isatin derivative as an organic chromophore. *Optical Engineering*, **50**, 44002–44006.

Shanmugam and Bhavani, P. (2014) Studies on the comparison of phytochemical constituents and antimicrobial activity of curcuma longa varieties. *International Journal of Current Microbiology and Applied Science*, **3** (9), 573-581.

Shen, Z.Y., Wilson, M.J., Fraser, A.R., and Perason, M.J. (1994) Nacritic clay associated with the Jiangshan-Shaoxing deep fault in Zhejiang Province, China. *Clays and Clay Minerals*, **42** (5), 576-581.

Shimizu, T.   (2014) Trends in research on organic light emitting diode. *Broadcast Technology*, **58**, Autumn.

Shinar, J. and Shinar, R. (2008) Organic light-emitting devices (OLEDs) and OLED-based chemical and biological sensors: An overview. *Journal of Physics D: Applied Physics*, **41**, 133001.

Siems, W., Wiswedel, I., Salerno, C., Crifò, C., Augustin, W., Schild, L., Langhans, C-D., and Sommerburg, O. (2005) β-Carotene breakdown products may impair mitochondrial functions— potential side effects of high-dose β-carotene supplementation. *Journal of Nutrisition and Biochemistry*, **16**, 385–397.

Srimal, R.C. (1997) Turmeric: a brief review of its medicinal properties. *Fitoterapia*, 68, 483-493.

Srivastava, P., Singh, B., and Angove, M. (2005) Competitive adsorption behavior of heavy metals on kaolinite. *Journal of Colloid and Interface Science*, **290**, 28–38.

Taher, Z.M. and Sarmidi, M.R. (2015) Optimization processing parameters for curcuma xanthorriza oleoresin yield and its antioxidant activity. *International Journal of Biotechnology for Wellness Industries*, **4**, 97-102.

Tajima, H., Ikeda, S., Matsuda, M., Hanasaki, N., Oh, J.W., and Akiyama, H. (2003) A light-emitting diode fabricated from horse-heart cytochrome c . *Solid State Communications*, **126**, 579–581.

Tajima, H., Shimatani, K., Komino, T., Ikeda, S., Matsuda, M., Ando, Y., and Akiyama, H. (2006) Light-emitting diodes fabricated from biomolecular compounds. *Colloids and Surfaces A: Physicochemical and Engineering Aspects,* **284–285**, 61–65.

Takahashi, T., Shizu, K., Yasuda, T. ,Togashi, K., and Adachi, C. (2014). Donor–acceptor-structured 1,4- diazatriphenylene derivatives exhibiting thermally activated delayed fluorescence: design and synthesis, photophysical properties and OLED characteristics. *Science and Technology of Advanced Materials*, **15**, 034202.

Thejo Kalyania, N. and Dhobleb, S.J. (2012) Organic light emitting diodes: Energy saving lighting technology—A review. *Renewable and Sustainable Energy Reviews*, **16**, 2696– 2723.

Tsutsui, T. (1997) Progress in electroluminescent devices using molecular thin films. *Mrs Bulletin*, 39–45.

Van Mullekom, H.A.,Vekemans, J.M., Havinga, E.E., and Meijer, E.W. (2001). Developments in the chemistry and band gap engineering of donor–acceptor substituted conjugated polymers. *Materials Science and Engineering*: *Review*, **32**, 1–40.

Van Nong, H., Xuan Hung, L., Nam Thang, P., Duc Chinh, V., Van Vu, L., Tien Dung, P., Van Trung, T., and Thu Nga, P. (2016) Fabrication and vibration characterization of curcumin extracted from turmeric (Curcuma longa) rhizomes of the northern Vietnam. *SpringerPlus*, **5,** 1147.

Viljanen, K., Sundberg, S., Ohsima, T., and Heinonen, M. (2002) Carotenoids as antioxidants to prevent photooxidation. *European Journal of Lipid Sciences and Technology*, **104**, 353.

Xue, B.,Wang, H., Xia, M., Wang, X., Yang, K., Chi, Q., Li, F., and Jiang, Y. (2016) Preparation of nacrite nanorolls and their reinforcing effect in LLDPE matrix. *Polymer Composite*, 1-9.

Yallapu, M.M., Jaggi, M., and Chauhan, S.C. (2012) Curcumin nanoformulations: a future nanomedicine for cancer. *Drug Disc Today*, **17**, 71.

Yang, Y., Farley, R.T., Steckler, T.T., Eom, S.H., Reynolds, J.R., Schanze, K.S., and Xue, J. (2008). Near infrared organic light-emitting devices based on donor-acceptor-donor oligomers. *Applied Physics Letters*, **93**, 163305-163308.

Yao, L., Zhang, S., Wang, R., Li, W., Shen, F., Yang, B., and Ma, Y. (2014). Highly efficient near-infrared organic light-emitting diode based on a butterfly-shaped donor–acceptor chromophore with strong solid- state fluorescence and a large proportion of radiative excitons. *Angewandte Chemie International Edition*, **53**, 2119-2123.

Yeum, K-J., Dos Anjos. F.A.L., Smith, D., Krinsky, N.I., and Russell, R.M. (2000) The effect of α-tocopherol on the oxidative cleavage of β-carotene. *Free Radical Biology and Medicine*, **29**, 105-114.

Yu, T., Liu, L., Xie, Z., and Ma, Y. (2015) Progress in small-molecule luminescent materials for organic light-emitting diodes. *Science China Chemistry*, **58** (6), 907–915.

Zeb, A. (2013) Oxidation and formation of oxidation products of β-carotene at boiling temperature. *Chemical Physics and Lipids*, **165**, 277-281.

Zhou, Z. (2007) Combinatorial fabrication & studies of small molecular organic light emitting devices (OLEDs) and structurally integrated OLED-based chemical and biological sensors. Iowa State University. Ames, Iowa. 121 pp

Zsirka, B., Horvath, E., Mako, E., Kurdi, R., and Kristof, J. (2015) Preparation and characterization of kaolinite nanostructure: Reaction pathways, morphology and structural order. *Clay minerals*, **50**, 329-340.

CHAPTER II

METHODOLOGY

CHAPTER II
METHODOLOGY

1. Preparation and modification the raw clay

There are five samples of raw clay that we used in this research, two samples were from Indonesia and three samples were from Central Africa. Here, clay from Congo Brazzaville and Gabon were characterized.

1.1 Kaolin from Indonesia

The raw kaolin used came from Capkala (Bengkayang) and Sintang region, West Kalimantan province, Indonesia (Figure 2.1). The separation and purification was done to the rawa kaolin by aqueous decantation (3 times) and centrifugation at 6000 rpm for 10 minutes to increase clay fraction. The chemical composition of this fraction was follows: SiO_2 51.82%; Al_2O_3 43.91%; MgO 1.19%, TiO_2 0.91%; Fe_2O_3 0.87%; CaO 0.10%; and loss by ignition.

Figure 2.1: West Kalimantan, Indonesia

1.2 Clay from Centra Africa

The raw clay from Congo Brazzaville and Gabon (Figure 2.2). The Congo's clay used in this research was collected from Mouibeyi, a village near Loubomo river and 5 km from Dolisie at Congo-Brazzaville, Africa. Samples were taken by digging the soil at 2 m depth. The soil was cleaned from the roots of the plant and sieved 100 mesh then purified by washing with distilled water 3 times, centrifugation at 6000 rpm for 15 minutes to separate clay and quartz fractions. The clay fraction was dried and sieved to produce the particle size of 125 μm, characterized and identified as natural clay (NN).

Figure 2.2:   Location map showing Moubeyi region, Congo Brazzaville and Gabon

1.3 Modification nacrite with solution ammonium hydroxide

This modification methode was adapted from Rahmalia (2016). Natural clay from Mouibeyi was calcined at 600°C for 6 hours (NC). The chemical activation was carried out by adding 20 g of the natural clay to 50 mL solution of 5 M ammonium hydroxide and stirred under atmospheric pressure and room temperature for 8 hours. The clay suspension was then filtered from the solution and washed with distilled water until neutral, dried in oven at 102°C. This process were repeated 3 times, and then the activated clay was grounded in mortar pestle to powder form (NA). Chemical activating was conducted by NH_4OH 30-33% from Sigma Aldrich .

1.4 Modification kaolinite with solution zinc chloride

Kaolinite from Capkala, West Kalimantan (250 mesh) was calcined in a furnace at 600°C for 6 hours to produce metakaolinite and then modified with $ZnCl_2$. Five grams of metakaolinites were modified by interacted with 125 mL $ZnCl_2$ 0.08 M and stirred for six hours. The mixture was decanted to separate the solid fraction and then dried. Chemical reagent, $ZnCl_2$ was from Sigma Aldrich.

2. Characterization of clay

The natural, calcined, and activated clay were characterized by X-Ray diffraction (XRD), X-Ray fluoresence (XRF), Spectroscopy infra red (FTIR), Thermal gravimetry analysis/differential thermal analysis (TGA/DTA), Scanning Electron Microscopy (SEM) and nitrogen adsorption.

2.1 X-Ray diffraction (XRD)

The X-Ray powder diffraction pattern were obtained by using a Philips BRUKER and employing CuK-alpha filtered radiation and the patterns were analysis by the Bruker-D8 Software.

In this technique the primary X-rays are made to fall on the sample substance under study. Because of its wave nature, like light waves, it gets diffracted to a certain angle. This angle of diffraction, which differs from that of the incident beam, will give the information regarding the crystal nature of the substance. The wavelength of the X-rays can be varied for the application by using a grating plate.

The diffraction of X-rays is a good tool to study the nature of the crystalline substances. In crystals the ions or molecules are arranged in well-defined positions in planes in three dimensions. The impinging X-rays are reflected by each crystal plane. Since the spacing between the atoms and hence the planes can't be same or identical for any two chemical substances, this technique provides vital information regarding the arrangement of atoms and the spacing in between them and also to find out the chemical compositions of crystalline substances. The sample under study can be of either a thin layer of crystal or in a powder form. Since, the power of a diffracted beam is dependent on the quantity of the corresponding crystalline substance, it is also possible to carry out quantitative determinations (Goldstein, 2003)

2.2 X-Ray fluoresence (XRF)

The XRF analysis of the samples were done by using PANanalytical Epsilon 3. In XRF, X-Ray produced`by source irradiate the sample. In most cases, the source is an X- ray tube but alternatively it could be synchrotron or a radioactive material. The elements present in the sample will emit fluoresence X-ray radiation with discrete energies (equivalent to color in optical light) which is characteristic for the elements. A different energy isequivalent to the diffrennt color. By measuring the energy (determining the colors) of radiation emmited bt the sample it is possible to determine which elements are present (qualitative analysis). By measuring the intensities of the emmited energies (colors), it is possible to mesure how much of the element is present in the sample (quantitaive analysis) (Brouwer, 2010).

2.3 Spectroscopy infra red (FTIR)

Infrared spectra were recorded in the region 4000-400 cm^{-1} in Perkin-Elmer SHIMADZU infrared spectrometer, using KBr pellet technique. Infrared spectroscopy is most commonly used spectroscopic method. There are a number of reasons for its great success and dissemination. The method is rapid, sensitive, easy to handle and provides many different sampling techniques for gases, liquids and solids. Important aspects are the convenient qualitative and quantitative evaluation of the spectra.

The concept of characteristic vibrations is used for qualitative analysis of polyatomic molecules. In organic compounds, characteristic vibrations occur usually between 4000 and 1500 cm^{-1}. Inorganic compounds containing heavy atoms may exhibit characteristic vibrations at much lower frequencies. Characteristic vibrations are based on motions, mostly stretching vibrations, that are localized in and characteristic of typical functional groups. While individual bands are not sufficient to confirm the identity of a molecule, they provide useful information about the type and abundance of the substructures that make up a molecule. All frequencies of organic compounds below 1500 cm^{-1} involve molecular vibrations, usually bending motions, that represent a characteristic fingerprint of the entire molecule or large fragments of the molecule. The comparison of the spectrum of an un-known compound with spectra stored in spectral libraries together with correspondingsearch programs are an excellent possibility for qualitative analysis (Gauglitz and Vo-Dinh, 2003).

2.4 Thermoanalytical analysis

Thermoanalytical analysis is a technique in which the temperature difference between a substance and a reference material is measured as a function of temperature whilst the substance and reference material are subjected to the same controlled temperature programme. There are some technique base on thermoanalitycal, such as diffrensial thermal analysis

(DTA), thermogravimetric analysis (TGA), differential scanning calorimetric (DSC), etc.

DTA, a technique requires the use of a reference material, which is a known substance, usually inactive thermally (inert material) over the temperature range interest. Important features of the reference material are that the thermal characteristic (specific heat, conductivity etc.) and the particle size should be very similar to that of the sample. The most commonly used reference materials: calcined α-Al_2O_3, calcined MgO, a part of the sample precalcined to 1000°C, calcined quartz-free kaolinite, and quartz. TG is a technique in which the mass of a substance is measured as a function of temperature while the substance is subjected to a controlled temperature programme (Földvári, 2011).

DTA/TGA were performed on Mettler-Toledo AG Analytical. The all measurements were carried out at heating rate 10°C/min under flow of N_2 from room temperature until 800°C. For DSC, those were performed on Mettler-Toledo AG Analytical. The all measurements were carried out at heating rate 10°C/min under flow of N_2 from room temperature until 400°C.

2.5 Scanning electron microscopy (SEM-EDS)

The SEM were taken on JEOL-JSM 7100 F, using an accelerating voltage of 10 kV. The samples were deposited on a samples holder with adhesive carbon foil and sputtered with gold. EDS makes use of the X-ray spectrum emitted by a solid sample bombarded with a focused beam of electrons to obtain a localized chemical analysis. All elements from atomic number 4 (Be) to 92 (U) can be detected in principle, though not all instruments are equipped for 'light' elements (Z < 10). Qualitative analysis involves the identification of the lines in the spectrum and is fairly straightforward owing to the simplicity of X-ray spectra. Quantitative analysis (determination of the concentrations of the elements present) entails measuring

line intensities for each element in the sample and for the same elements in calibration standards of known composition (Goldstein, 2003).

2.6 Gas sorption analysis

N_2-gas adsorption techniques are best suited for investigation of materials with fine pores in the range from about 2–300 nm. Subcritical N_2-gas adsorption experiments are performed using various procedures. In most applications, the amount of gas adsorbed is determined using a discontinuous static volumetric method. A degassed evacuated sample is exposed to N_2 at liquid-N_2 temperature. The quantity of adsorbed gas on the solid surface is measured at discrete pressure (P) steps over the relative equilibrium pressure (P/P_0) range of 0.0075 to 0.995 at constant temperature, where P_0 is the condensation pressure at the temperature of the experiment. The experiment systematically increases pressure up to the condensation pressure (adsorption branch) followed by reduction of pressure from P_0 (desorption branch) and the data are reported as the adsorption isotherm: quantity of gas adsorbed per mass expressed as moles or volume in $cm^3.g^{-1}$ (S.T.P.) as a function of relative equilibrium pressure (P/P_0) (Anovitz, 2015).

The shape of the isotherm and its hysteresis pattern provide useful information about the physisorption mechanism, the solid and gas interactions, and can be used to qualitatively predict the types of pores present in the adsorbent.

A number of models is used to quantify surface area, the most common of these is that developed by Brunauer, Emmett, and Teller which is an extension of the Langmuir model of monolayer adsorption to multilayer adsorption. The fundamental assumption is that the forces active in the condensation of the gases also are responsible for the binding energy in multi-molecular adsorption. By equating the rate of condensation of gas molecules onto an already adsorbed layer to the rate of evaporation from that layer and

summing for an infinite number of layers, the following linear expression can be written (Lowell and Shield, 1984):

$$\frac{P}{V_a(P_0-P)} = \frac{1}{V_m C} + \frac{C-1}{V_m C}\left(\frac{P}{P_0}\right)$$

(2.1)

where Va is the volume of gas adsorbed, P/P_0 is the relative pressure, Vm is the volume of adsorbate as a monolayer and C is the BET constant. A plot of $P/(Va(P_0 - P))$ versus P/P_0 can yield a straight line with the intercept i = $1/V_m C$, slope s = $(C - 1)/V_m C$ and volume of a monolayer V_m = 1/(s + i). The values of C and V_m can be obtained from linear regression of the data.

The total surface area (St) can then be derived from:

$$S_t = \frac{V_m N_{Av} A_{cs}}{M}$$

(2.2)

where N_{Av} is Avogadro's number (6.023 x 10^{23}), M is the molecular weight of the adsorbate and A_{cs} is the adsorbate cross sectional area (16.2 A^2 for N_2). The specific surface area, (S) is then determined from total St by dividing by the sample weight. One can use either the singlepoint BET method, typically taken at a P/P_0 value of 0.3, or a multi-point BET (minimum of three points) with the realization that some error will be introduced by using the former approach, the magnitude of which will scale as the value of C decreases.

Total pore volume can be derived from the amount of vapor adsorbed (V_{ads}) at a relativepressure close to unity (assuming pores are filled with liquid adsorbate, V_{liq}).

$$V_{liq} = \frac{P_a V_{ads} V_m}{RT}$$

(2.3)

where Pa is ambient pressure, R is the gas constant and T is temperature in K. Average pore radius (rp) can be estimated from the pore volume assuming a cylindrical pore geometry using this relationship.

Textural analysis of samples in this reserach were carried out from the corresponding nitrogen adsorption-desorption isoterms at 77 K (BET method). BET apparatus from BEL JAPAN, BEL SORPMAX. The nitrogen adsorption data were obtained using 0.2 g of sample. The samples were degassed 1 h at 90°C with rate 4°C/min. The BET analysis procedure is automated and

operates with static volumetric technique. The isotherms were used to determine the specific surface area using BET equations.

3. **Characterization of β-carotene, fucoxanthin, and curcumin using UV-spectrophotemeter**

All the organics chemicals and biomolecules were from Sigma Aldrich: β-carotene, fucoxanthin, and acetone, except curcumin was from Phodé, Albi-France.

The absorption spectrum of β-carotene, fucoxanthin, and curcumin was measured using UV-spectrophotometer (SHIMADZU 1800). UV-Visible absorption spectroscopy involves measuring the absorbance of light by a compound as a function of wavelength in the UV-visible range. When a molecule absorbs a photon of UV-Vis light, the molecule is excited from its ground state to an electronic excited state. In general a compound will absorb in the visible region if it contains at least five conjugated chromophoric and auxochromic groups (Sauer *et al*., 2011)

The wavelength which is most strongly absorbed by a compound is called its λ_{max} and can be measured by UV-visible spectroscopy. Ultraviolet and visible spectrometry is almost entirely used for quantitative analysis; that is, the estimation of the amount of a compound known to be present in the sample. The sample is usually examined in solution.

Lambert (1760) generally is credited with the first mathematical formulation of this phenomenon, although it now appears that Bouguer first stated it in 1729. The mathematical expression is:

$$T = I/I_0 = e^{-kb} \tag{2.4}$$

where Io is the incident intensity, I is the transmitted intensity, e is the base of natural logarithms, k is a constant, and b is the path length (usually in centimeters).

Beer's law is identical to Bouguer's law, except that it is stated in terms of concentration. The amount of light absorbed is proportional to the number of

66

absorbing molecules through which the light passes. Combining the two laws gives the Beer-Bouguer-Lambert law:

$$T = I/I_0 = e^{-kbc}$$ (2.5)

where c is the concentration of the absorbing species (usually expressed in grams per liter or milligrams per liter). This equation can be transformed into a linear expression by taking the logarithm and is usually expressed in the decadic form. Mathematically, the correlation of absorbanc, percentage transmittance T and concentration by the expression which is well known as Beer's Law (Owen, 1996; Kumar, 2006).

$$A = -\log T = -\log (I/I_0) = \log (I_0/I) = \varepsilon bc$$ (2.6)

where is ε the molar absorption or extinction coefficient.

4. Photostability of β-carotene

4.1 Photostability with antioxidant

The 2.5 ppm of β-carotene in acetone was interacted with of fucoxanthin and curcumin with variation in concentration. The solutions were irradiated with UV light 365 nm (fluks = 1.6 W/m^2) until 9 h. The measurements were carried out in quartz cuvette. Each irradiation interval time, about 3 mL of the solution was taken and analysis with UV-spectrophotometer. The same condition was done to the β-carotene solution with and without UV-irradiation. The solutions were stored in dark room or inside the refrigerator when it is not in use. All the experiments were carried out in the presence of air. Absorption spectra of β-carotene were measured using UV-spectrophotometer (SHIMADZU 1800) from 350-550 nm. The rate photodegradation and half-life time was calculated using pseudo-first order reaction data. The percentage photostability provided to β-carotene by antioxidant then was calculated using the formula as described (Claes, 1960) :

$$\frac{E_3 - E_2}{E_1 - E_2}$$ (2.7)

where E_1, E_2, and E_3 are, respectively, the concentration (or absorbance) of β-carotene at 452 nm before irradiation, after irradiation without antioxidant, and after irradiation in the presence of antioxidant.

4.2 Photostability with modified kaolinite

2.5 ppm of β-carotene (BC) in acetone was interacted with kaolin (K), calcined kaolinite (Mkaol) and modified kaolinite (MK) with the composition of BC/MK = 40 mL/1 g) for hour and then irradiated by UV light at 365 nm (flux = 1.6 W/m^2) until nine hours. Before analysis, the effluent was centrifuged for 5 minutes at 5000 rpm. Concentration of β-carotene was calculated with standard curve equation, y = 0.2786x + 0.167 (x = concentration of β-carotene, y = absorbance, and correlation coefficient, R^2 = 0.997). The rate photodegradation and half-life time was calculated using pseudo-first order reaction data. The percentage photostability provided to β-carotene by antioxidant then was calculated using the formula as described by Claes (1960) in equation 2.7.

5. Electrochemical analysis

Cyclic voltammetry (CV) is a methodology widely used by organic photovoltaic (OPV) researchers to obtain the HOMO and LUMO levels. There is little consensus in the OPV community on how this technique is used and how the measurements relate to the vacuum scale. In standard experiments, the CV technique usually involves the application of forward and reverse linear potential scans to a stationary working electrode immersed in a solution containing the redox active species under investigation. The experiment is usually conducted in a solution of supporting electrolyte, which is at a much higher concentration than that of the redox material. When the material has accessible oxidations, an anodic wave will appear on the positive forward scan, and a corresponding cathodic wave will be detected on the reverse scan. For redox couples exhibiting fast electron transfer, which are usually referred to as

Nernstian or reversible couples, and assuming that the two oxidation states (Ox/Red) are stable in the time scale of the experiment, the maximum (peak) currents in these two related waves should be approximately the same. The formal potential reflects the relative stabilities of Ox and Red, which in turn are influenced by medium and solvation effects (Bard *et al*., 2001).

Information provided by the electrochemical method are the oxidation (reduction) potentials (π_{ox} and π_{red}, respectively) of molecules dissolved in non-aqueous solvents of high electric permittivity (e.g., acetone, acetonitrile, dimethylformamide, etc) (Sworakowski *et al*., 2016). In this research, Cyclic voltametry (CV) measurement of biomolecules in CH_2Cl_2 (dicloromethane) solution were used to evaluate electrochemical characteristics. Cyclic voltammetry experiments were done on an EG&G Princeton Applied Research potentiostat/galvanostat (model 273A). Data were collected and analyzed by the Pgstat electrochemical analysis system software on a PC computer. A three-electrode cell was used in all experiments. Platinum wire electrodes were used as both counter and working electrodes and $Hg/Hg_2Cl_2/Cl^-$ as saturated colome electrode (SCE) The solution electrochemistry was performed on 1 mM solutions of each dicloromethane (DCM) solvent. An electrolyte solution of 0.1 M TBAPF6 in DCM was used in the electrochemical cell. The solutions were purged with ultra high purity Argon before the experiment, and a blanket of Argon was used during the experiment. Electrochemistry was done at a scan rate of 100 mV/s. Electrochemical potential gap (eV) is calculated from this equation:

$$E_{gap}^{el} = |onset_{red} - onset_{ox}| \qquad (2.8)$$

The corelation of electrochemical potentials with orbital energies is according to the equations as follows (Cardona *et al*., 2011):

$$E_{HOMO} = -\left(E_{|onset,ox\,vs.Fc^+/Fc|} + 5.39\right)(eV) \qquad (2.9)$$

$$E_{LUMO} = -\left(E_{|onset,red\,vs\,Fc+/Fc|} - 5.39\right)(eV) \qquad (2.10)$$

6. Fabrication organic light emitting diode (OLED)

Fabrication OLED using Specbos 1201-JETI equipment by Technische Instrument GmbH. Preparation and fabrication of OLED under N_2 atmosphere in glove chamber.

Fabrication OLEDs were done using evaporating method. All the materials such as hole transport layer (HTL), emitter layer (EL), and electron transport layer (ETL) were putted at sources pot at the glove chamber. ITO glass were deposited by HTL, EL, and ETL, sequentially. The thickness of each layer were controlled by arrange the mean rate deposition at the control panel. Evaporation temperature of the dyes are 140°C.

The OLED devices then were tested their electricals behavior and light emission before continuing to the optical measurement. Figure 2.3 are shown evaporation chamber and control panel at fabrication OLED.

    (a) Evaporation chamber   (b) Controller panel

Figure 2.3: Evaporation chamber and controller panel
at OLED fabrication

References

Anovitz, L.M. (2015) Characterization and analysis of porosity and pore structures. *Reviews in Mineralogy & Geochemistry*, **4** (80), 61-164.

Anonim-2000. An Introduction to Fluorescence Spectroscopy. PerkinElmer Ltd.

Bard, A.J. and Faulkner, L.R. (2001) Electrochemical Methods: Fundamentals and Applications Wiley , New York.

Brouwer, P. (2010) Theory of XRF. PANalytical, BV, Netherland.

Claes, H. (1960) Interaction between chlorophylls and carotenes with different chromophoric groups. *Biochemical and Biophysical Research Communications*, **3,** 585-590.

Cardona, C.M., Li, W., Kaifer, A.E., Stockdale, D., and Bazan, G.C. (2011) Electrochemical considerations for determining absolute frontier orbital energy levels of conjugated polymers for solar cell applications. *Advances Materials,* **23**, 2367–2371.

Földvári, M. (2011) Handbook of thermogravimetric system of minerals and its use in geological practice. Geological Institute of Hungary.

Gauglitz, G. and Vo-Dinh, T. (2003) Handbook of spectroscopy. Wiley-Vch Verlag GmbH & Co. KGaA, Weinheim.

Goldstein, J.I. (2003) Scanning electron microscopy and x-ray micronalysis, 3rd ed, Plenum Press, New York.

Lowell, S. and Shield, J.E. (1984) Powder Surface Area and Porosity (Particle Technology Series), 3nd ed, Chapman and Hall, London.

Owen, T. (1996) Fundamentals of UV-visible spectroscopy; Hewlett-Packard Company, Germany.

Rahmalia, W. (2016) Paramètres de performances de photo-électrodes de TiO_2/kaolinite et d'électrolyte a base de carbonates biosourcés dans la cellule solaire sensibilisée par la bixine. Thèse, Institut National Polytechnique de Toulouse, France.

Russ, J.C. (1984) Fundamentals of Energy Dispersive X-ray Analysis, Butterworths. London.

Sauer, M. Hofkens, J., and Enderlein, J. (2011) Handbook of Fluorescence spectroscopy and Imaging. Wiley-Vch Verlag GmbH & Co. KGaA, Weinheim.

Sworakowski, J., Lipinski, J., and Janus, K. (2016) On the reliability of determination of energies of HOMO and LUMO levels in organic semiconductors from electrochemical measurements. *Organic Electronics*, **33**, 300-310.

.

CHAPTER III

CHARACTERIZATION OF NATURAL CLAY

CHAPTER III

CHARACTERIZATION OF NATURAL CLAY

Central Africa and Indonesia have the same characteristic in climates and natural resources, becaused they are located in the equatorial region. Clay is one of the natural resouces that can be found there. There are five samples of clays will be characterized in this chapter. Two of them came from Indonesia. Samples from Central Africa are from Congo Brazzaville and Gabon. Identification of one clay from Gabon is separated in other subchapter, because its physical properties is very different from the other samples.

1.   Introduction

Clays have several industrial applications in areas such as construction, agricultural, textile, paper, pharmaceutical, ceramic, electrical, nuclear energy, and petroleum industries. Clays are best studied and identified using the following: X-ray diffraction, X-ray fluorescence, energy-dispersive X-ray analysis, electron diffraction, differential thermal analysis, infra red spectroscopy, and electron microscopy (Obaje *et al*., 2013).

Clay minerals are classified into eight major groups, on the basis of layer type (1:1 or 2:1), layer charge and type of interlayer, as presented in triple layer clay minerals (2:1). The industrial applications of the clay mineral types are varied and depend on their physical and chemical properties, which are correlated on structure and composition (Murray, 2000).

A natural clay consists of one or different type of clay minerals together with some impurities. The most common impurities in natural clay are quartz, calcite, feldspar, mica and organic matter while hydrated iron oxide, ferrous carbonate and pyrite are being the minor impurities. The factors that affect most of the physical properties of clay are particle size, shape, cation exchange capacity and the type of impurities present which are intimately related to the applications of the clay minerals. The other important properties are surface

chemistry, surface area, and surface charge. These, along with color and brightness, affect many use properties such as low and high shear viscosity, absorption, plasticity, green, dry and fired strength, casting rate, permeability, and bond strength (Murray, 2000). Clay particle sizes are in the micrometer to nanometer range length scale (Saikia *et al*., 2010).

Kaolin, $Si_2Al_2O_5(OH)_4$ is a dioctahedral clay mineral of 1:1 layered structure with poly-types namely kaolinite, dickite and nacrite, and the polymorph halloysite (Buatier *et al*, 1996; Haq *et al*., 2009). A single layer of kaolinite comprises planes of O_6, Si_4, O_4, $(OH)_2$, Al_4 and $(OH)_6$ stacked one over the other.

2.   Characterization natural clay from Central Africa and Indonesia,

The natural clays were characterized by XRD, XRF, FTIR, TGA/DTA, SEM and nitrogen absorption. The X-Ray powder diffraction pattern were obtained by using a Philips BRUKER and employing CuK-alpha filtered radiation and the patterns were analysis by the Bruker-D8 Software. IR spectra were recorded in the region 4000-400 cm^{-1} in Perkin-Elmer SHIMADZU infra red spectrometer, using KBr pellet technique. The XRF analysis of the samples were done by using PANanalytical Epsilon 3. Thermal Analysis were performed on Mettler-Toledo AG Analytical. The all measurements were carried out at heating rate 10°C/min under flow of N_2 from room temperature until 800°C. Textural analyses were carried out from the corresponding nitrogen adsorption-desorption isoterms at 77 K (BET method). BET apparatus from BEL JAPAN, BEL SORPMAX. The nitrogen adsorption data were obtained using 0.2 g of sample. The samples were degassed 1 h at 90°C with rate 4°C/min. The BET analysis procedure is automated and operates with static volumetric technique. The isotherms were used to determine the specific surface area using BET equations. The SEM were taken on JEOL-JSM 7100 F, using an accelerating voltage of 10 kV. The samples were deposited on a samples holder with adhesive carbon foil and sputtered with gold.

2.1   Physical properties

The physical properties of the natural clays are represented at Figure 3.1. Clay's color from West Indonesia (Capkala and Sintang) and clay from Gabon are white tend to grey. These clay's color are significantly different with clay from Congo. The Congo's clay seem like brown-green. Kaolin is usually white or near white in color. The largest use of kaolin is for coating paper. Whiteness is the one of some properties that is important to the paper manufacturer include dispersion, viscosity both low and high shear, brightness, gloss, smoothness, adhesive demand, film strength, ink receptivity, and print quality (Murray, 2000). In relation to color, the whiteness of kaolin is normally directly correlated with Fe and Ti minerals (Al-Shameri and Rong, 2009; Awad *et al*., 2017).

Figure 3.1: Clay from Indonesia, Congo Brazzaville and Gabon

2.2. Structural characterization (IR and XRD)

A number of works has been carried out on the quantitative clay mineral analysis using infra red spectroscopy. Vibrational spectroscopic investigations yield useful information about hydration characteristics, interlayer cations and moisture content in clays. The structural differences of kaolin can be detected by spectroscopic method. The FTIR spectroscopy applied to clay mineralogy lies in its ability to characterize the functional group and fingerprint region of very small quantities of samples (Saikia *et al*., 2010).

In general, the constituent units of clay minerals include hydroxyl groups, tetrahedral silicate/aluminate anions, octahedral metal cations, and

interlayer cations. In IR-spectra, OH-stretching modes lie in the spectral region of 3400-3750 cm^{-1}. Metal-O-H bending modes occur in the 600-950 cm^{-1} region. Si-O and Al-O stretching modes are found in the 700- 1200 cm^{-1} range. Si-O and Al-O bending modes dominate the 150-600 cm^{-1} (Vaculíková and Plevová, 2005).

Figure 3.2 is the IR spectra of four clays samples. The FTIR technique investigates OH vibrations, whose absorption bands appear at different frequencies depending on the cations directly linked to the hydroxyls. This permits the determination of cation distribution around hydroxyls and thus allows assessing short-range cation ordering. The band position is compared with the Gadsden (1975) and Aroke *et al.* (2013) and possible assignments of the samples are presented in the Table 3.1.
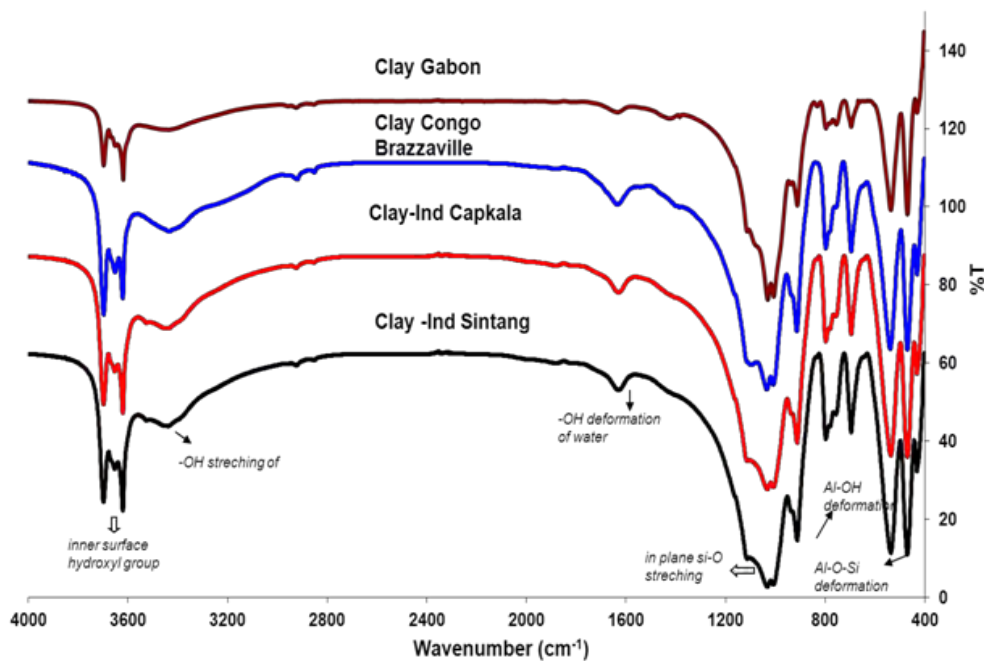
Figure 3.2: Spectra infrared of natural clay

The general features of the stretching absorption bands are well established that all the samples are clay, from the appereance band in range 1030-1035 cm^{-1}. This peak correlated to the Si-O streching in clay, kaolin. This a typical spectrum of kaolin show three bands around 3670-3620 cm^{-1}

(Djomgoue and Njopwouo, 2013), and these characteristic bands are observed in the studied kaolin samples as mentioned at the Table 3.1. The studied kaolin samples exhibit the bands near the three characteristic bands at 3669, 3645 and 3620 cm^{-1}. The bands between 3450 and 3670 cm^{-1} are attributed to the OH stretching mode. The band observed at around 3620 cm^{-1} has been ascribed to the inner hydroxyls, and the bands observed at around the other three. The absorption bands observed at 3420-3445 cm^{-1} vibrational mode of the hydroxyl molecule, which is observed in almost all the natural hydrous silicates. The H-O-H bending of water is observed at 1620-1642 cm^{-1}. In the 1000 cm^{-1} and 500 cm^{-1} region, main functional groups were Si-O and Al-OH. Muscovite and possibly quartz interference could be observed at 1031-1038 cm^{-1} for the studied kaolin (Saikia *et al*., 2010). The Al-OH absorption peak was identified at 891-915 cm^{-1} for the studied sample. The band at 914-936 cm^{-1} corresponding to Al-OH bending vibrations of kaolin, the doublet at 780-798 cm^{-1} is due to Si-O-Si inter tetrahedral bridging bonds in SiO_2 and OH deformation band of gibbsite at 1000 cm^{-1} are finger prints of the typical vibrational modes which are recognized easily.

The OH deformation of water is found in between 1620-2642 cm^{-1}. The kaolin samples exhibits the C-H stretching bands in between 2850–2958 cm^{-1} indicating polyatomic Cn-H-O entitles with C bonded to two or three H. The strongest -CH band in between 2920-2931 cm^{-1} assigned to symmetrical stretch of C-H mode of -CH_2 group. The band between 2850-2867 cm^{-1} is assigned to anti symmetrical stretch of –CH_2 group. Another peak is found at 2954 cm^{-1} in one kaolin sample due to symmetric stretch of –CH_3 group.

Table 3.1: Infrared band positions of the studied clay samples compare to kaolin type

Assignments	Wavenumber (cm^{-1})					
	Kaolin [a]	**Kaolin** [b]	**CIS**	**CIC**	**CC**	**CG**
Al---O-H stretching	3670-56	3700 3660	3698 3654	3697 3653	3697 3653	3697
OH Stretching, crystalline hydroxyl	3645	3620	3620	3620	3629	3619
H-O-H stretching, absorbed water			3436	3435	3432	3434
C-H stretching	2907		2920 2850	2908 2834	2914 2849	
H-O-H bending of water			1627	1631	1635	1639
C-H stretching						1425
-	1117-05	1130 1110		1112		1113
Si-O quartz					1098	
Si-O stretching, Clay minerals	1035-30	1030	1032	1032	1033	1030
Si-O stretching	1019-05	960	1007	1007	1007	1006
OH deformation, linked to $2Al^{3+}$	918-09	846	912	912	913	911
OH deformation, linked to Al^{3+}, Mg^{2+}	800-784	805	796	753	796	796
Si-O quartz	700-686	675 630	694	697	695	697
Fe-O, Fe_2O_3 Si-O-Al	542-35		538	538	538	535
Si-O-Si bending	475-68		469 430	469	469 430	469

[a] Gadsen, 1975 [b] Aroke *et al*., 2013
CIS = clay-Indonesia Sintang; CIC = clay Indonesia Capkala;
CC= clay Congo Brazzaville ; CG= Clay Gabon

Kaolin has four polimorph: kaolinite, dickite, nacrite, and halloysite. The –OH stretching for the kaolin polymorph are shown in Table 3.2. Van der Marel (1969) reported that polymorphism of kaolin can identified in -OH stretching bands. Kaolinite has two peaks at 3693 and 3620 cm^{-1}, nacrite has four peaks at 3700, 3650, 3627 and 3620 cm^{-1}, dickite four peaks at 3708,

3656, 3627 and 3622 cm^{-1}, and halloysite at 3695, 3668, 3654, and 3621 cm^{-1}. For halloysite, two of the peaks are weaks (3666 and 3654 cm^{-1}). But, it seem to hard to identify mineral type of kaolin using FTIR, because, the samples are natural and composed with others mineral, such as muscovite, quartz, and gibsite. For the next step, these samples will be characterized by X-ray difractometer.

Table 3.2: The -OH stretching band of kaolin polymorph

Assignments	Wavenumber (cm^{-1})							
	CIS	CIC	CC	CG	Kaolinite (a)	Nacrite (b)	Dickite (c)	Holloysite (d)
Al---O-H stretching	3698 3654	3697 3653	3697 3653	3697	3695	3714 3647	3688 3642	3695 3668 3654
OH stretching, crystalline hydroxyl	3620	3620	3629	3619	3620		3615	3621

[a] Madejova, 2003. [b] Jaafar *et al*., 2015. [c] Prost *et al*., 1989. [d] Van der Marel., 1969.

Typically, clays have a hexagonal structure oriented perpendicularly to the C axis. The inter layers distance varies according to the type of clay. First order X-ray Bragg reflection did not totally identify the minerals present in the clay. The compounds complexity caused a multiple reflection of higher orders (n = 2, 3, 4, . . .) promoting the superposition of the first order peaks with those of higher orders (Senoussia *et al*., 2016). XRD diagrams shown that all samples consist of kaolin (Figure 3.3). Clay from Indonesia, from Capkala (CIC) and Sintang (CIS) are kaolinite type. These kaolin are consist of kaolinite, muscovite, and quartz. Kaolinite mineral in CIS is lower than CIC.

Samples from Indonesia and Gabon (CIS, CIC, and CG) are consist of kaolinite with different intensity, while sample from Congo Brazzaville (CC) is nacritic. Kaolinite, muscovite, and quartz are identified in CG, but the majority is almost still quartz. The intensity of muscovite is higher than kaolinite. It seem that this clay is muscovite type assosiated with kaolinite and quartz.

According to Brindley and Brown (1980), muscovite is a dioktahedral type of mica. The structural layer type is 2:1.
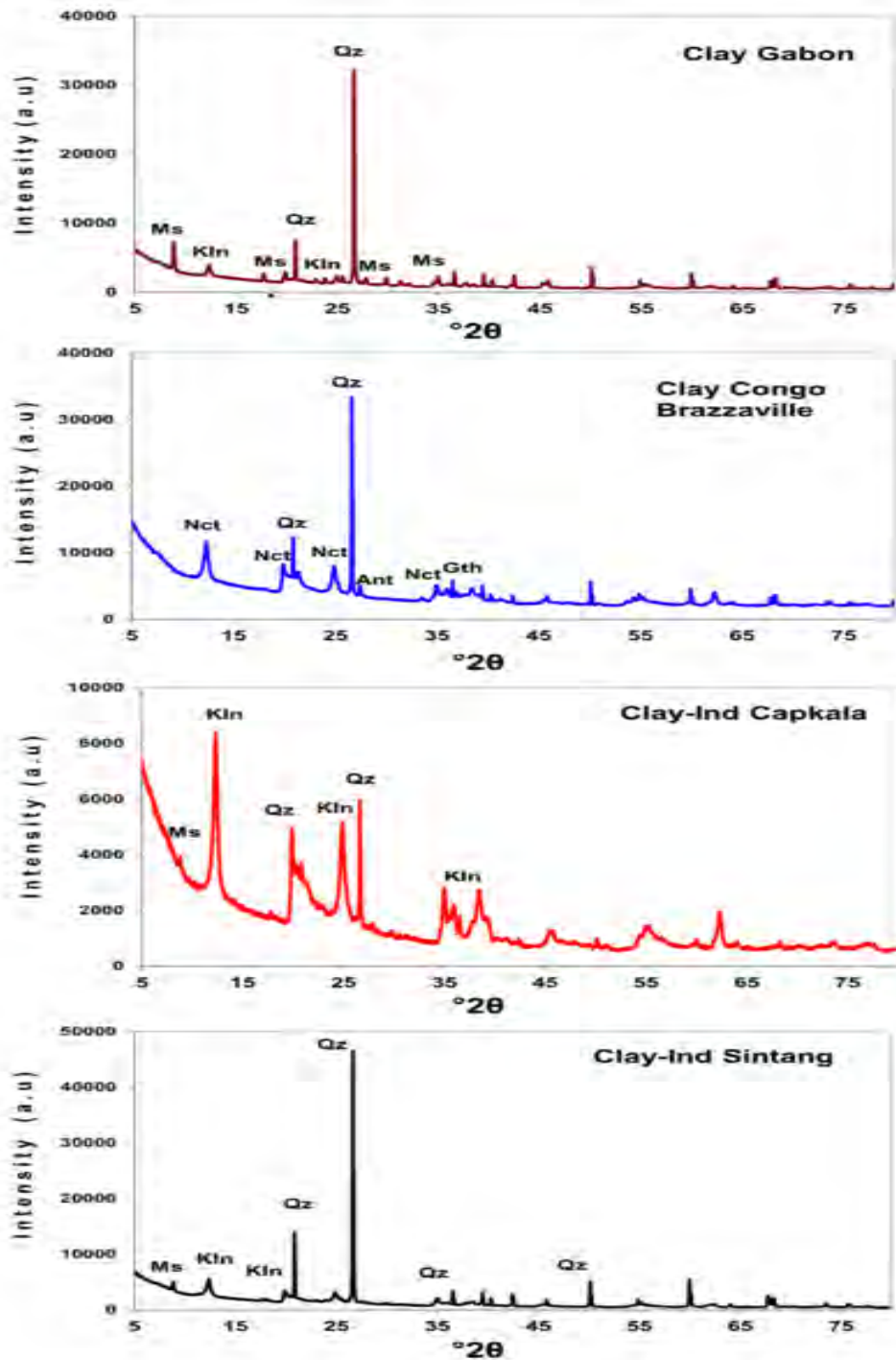
Figure 3.3: Spectra XRD of natural clay (Ms: muscovite; KIn: kaolinite; Qz: quartz; Nct: nacrite; Ant; anatase; Gth: goethite)

The d_{001} muscovite mica (Figure 3.4) is a monoclinic with a=0.51906 nm, b= 0.9008 nm, c =2.0047 nm, β = 95.757°, space group C 2/c (de Poel *et al*,. 2014). Natural muscovite, with ideal composition of $KAl_2(Si_3AlO_{10})(OH)_2$, is a 2:1 phyllosilicate silicate mineral. Each layer is composed of two tetrahedral sheets and one dioctahedral sheet, sandwiched between two tetrahedral sheets. In tetrahedral sheets, silicon atoms randomly occupy approximate 75% of the tetrahedral sites, and aluminum atoms occupy the remaining sites. In dioctahedral sheets, 2/3 octahedral sites areoccupied by aluminum atoms, and the rest sites are vacant. It is common that Si^{4+} and Al^{3+} are replaced by isomorphic low charge cations, accordingly the host layers are negatively charged and alkali ion, mainly K^+, is attracted in the interlayer to counter balance the charge of the layers. Muscovite layers have severe charge deficiency, therefore unlike silicates with moderate deficiency, e.g. smectites, the interlamellar cations in muscovite are no expandable, and can not be exchanged easily, or no charge defective silicates, e.g. talc, strong Coulombic interaction couples the adjacent layers beside van der Waals forces (Jia *et al*., 2015).
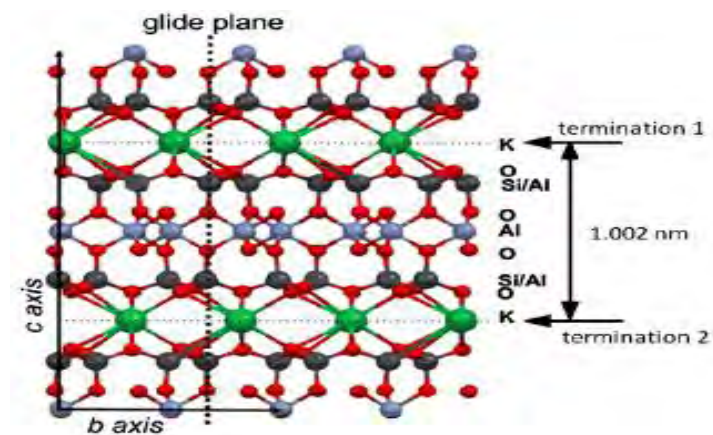
Figure 3.4: Ball and stick model of muscovite mica

Muscovite mica is widely used because of its flatness which is is a suitable substrate material for the self-assembly of molecular layers of thin films, for example of Pt, a substrate for the imaging of graphen (de Poel *et al*,.

2014). A thin film muscovite mica in ITO was used in solar cells. ITO/mica retains its low electric resistivity even after continuous bending of 1000 times and has high efficiency (Ke *et al*., 2016). Naturally, muscvite is not expandable layer phylosilicate type, but modification by calcined follow by ion exchange using Li^+ increased the basal spacing of muscovite from 0.99 nm to 1.21 nm. The lower energy of Li^+ allowed trimethyloctadecylammoniumchloride (OTAC) exhange it and muscovite to expand greatly. The distance between the adjacent aluminosilicate layers of the muscovite increased from 0.32 nm to 2.25 nm (Jia *et al*., 2015). This result give another perpective in application of muscovite as like as monmorillonite or vermiculite. Microcrystal muscovite has a series of excellent properties such as low-cost, ultrafine particle size, heat-durability, alkali-resistance and salt-resistance.

The nacrite mineral in CC assosiated with small quantity of anatase and goethite, but high portion of quartz. The amount of goethite correlated to the color of CC in Figure 3.1. Only CC has a high quantity of kaolinite mineral compare to the three others. The natural clays then analyzed their morphology by SEM-EDX and gas sorption analyzer.

2.3 Morfological and textural characterization (SEM-EDX and gas sorption analysis)

The morphology of all the natural clays with different magnification are shown in Figure 3.5 and the and SEM-EDX at Table 3.3. The kaolinite crystals are pseudo-hexagonal along with plates, some larger books, and vermicular stacks (Murray, 2000). Both are kaolinite and muscovite are platy crystal (Robertson and Enggleton, 1991; Singh and Gilkes, 1991).

SEM of clay from Congo Brazzaville shown nacrite layer in the arrow direction. From the EDX analysis, the Fe contain of this clay is higher than the others clay (Table 3.3). It is corrrelated to the color of this clay at Figure 3.1.

Table 3.3: Percentage mass of the element

Element	Percentage of mass (%)			
	Clay Gabon	**Clay Congo Brazzaville**	**Clay-Ind Sintang**	**Clay-Ind Capkala**
C	8.23	18.2	2.9	14.2
O	50.86	48.15	46.72	45.2
Mg	0.36	-	0.30	-
Al	15.31	10.85	18.6	17.8
Si	16.64	13.95	26.56	19.0
K	1.96	0.65	2.62	0.9
Ti	-	0.7	0.84	1.1
Fe	2.95	7.45	1.46	1.9
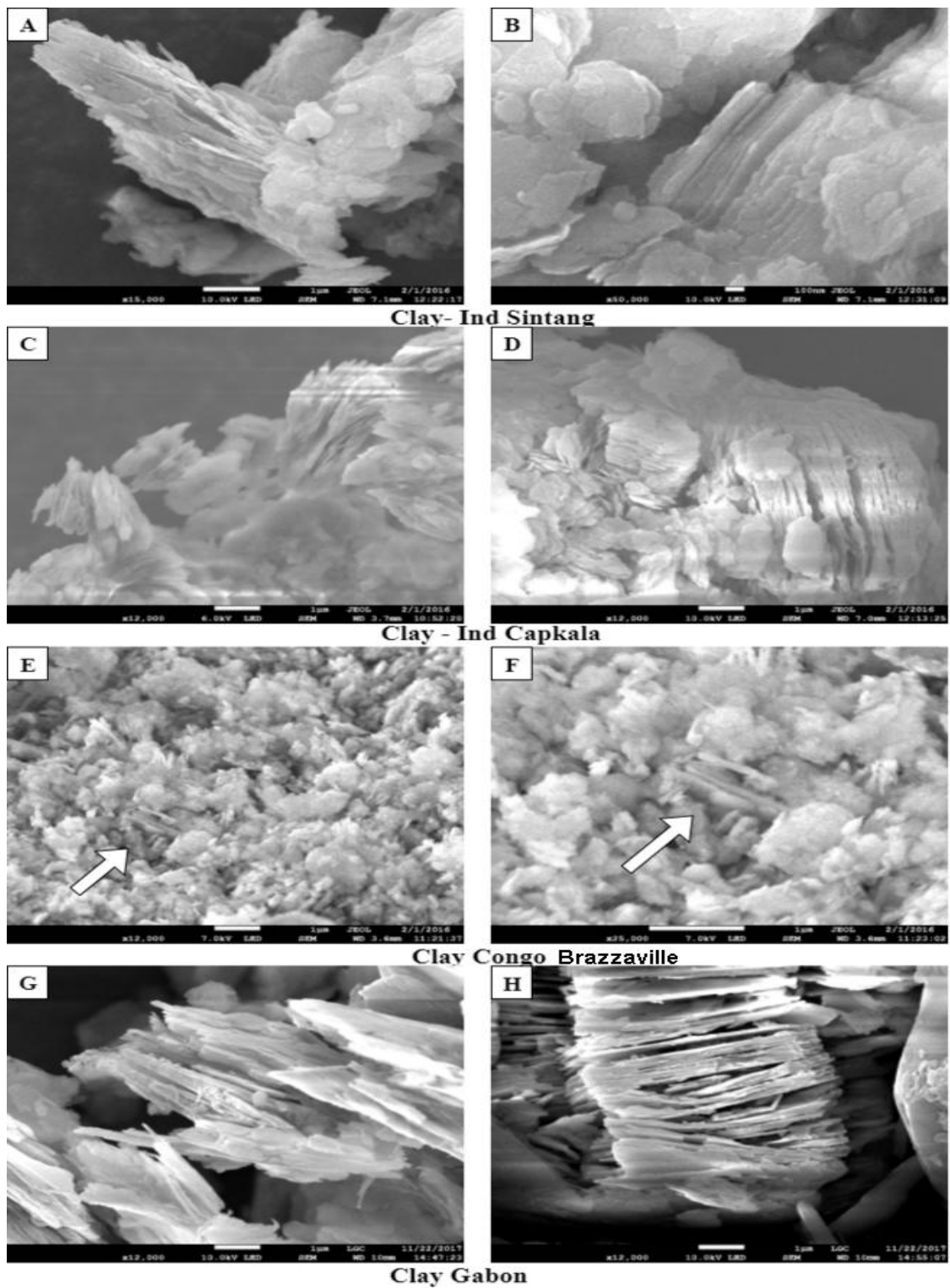
Figure 3.5: SEM of clay from Sintang-Ind (A, B), Capkala-Ind (C, D), Congo Brazaville (E, F), and Gabon (G, H)

According to Singh and Gilkes (1991) whose studied weathering of mica concluded that muscovite had mostly altered to kaolinite with minor amounts of halloysite occurring between kaolinite plates. The possibility of the the book layer is consist of platy of kaolinite and muscovite. Kaolinite could inherit directional information from muscovite by growing epitaxially on the surface of residual layers of muscovite, or by topotactic replacement of muscovite layers by kaolinite layers (Figure 3.6).
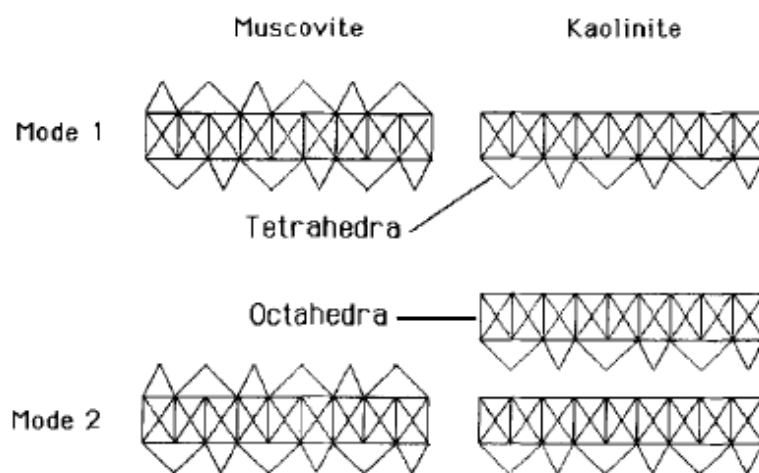
Figure 3.6: Two modes of topotactic transformation of chromian muscovite (fuchsite) to kaolinite by stripping of tetrahedral sheets (Mode 1) and by the insertion of octahedral sheets (Mode 2)

Kaolinite is an aluminosilicate formed by the alteration of K-feldspar such as microcline and micas such as muscovite as shown in equations 3.1 and 3.2 (Ekosse, 2005).

$$2KAl_3Si_3O_{10}(OH)_2 + 2H^+ + 3H_2O \rightarrow 3Al_2Si_2O_5(OH)_4 + 2K^+ \qquad (3.1)$$

    K-feldspar   kaolinite

$$2KAlSi_3O_8 + 2H^+ + 9H_2O \rightarrow Al_2Si_2O_5(OH)_4 + 2K^+ + 4H_4SiO_4 \qquad (3.2)$$

    muscovite   kaolinite
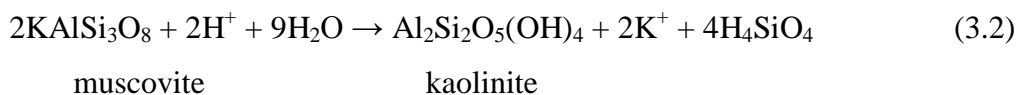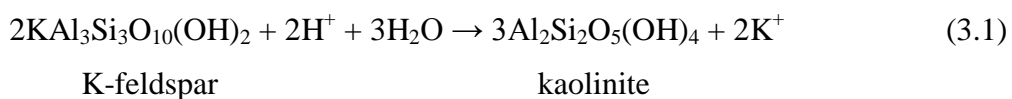
The surface area of the clays: CIS, CIC, and CC shown the average surface are in range 22-38 m^2/g (Table 3.4). These surface area are higher than the average kaolin, because kaolinite associated with muscovite which has higher surface area. Compared with other clay minerals, the low sorption capacity of kaolinite is attributed to its low specific surface area (around 8–15 m^2/g) and surface charge of the particle (Murray, 2007). As the ratio of surface area of basal to edge face (aspect ratio) is typically high for muscovite (~20) and other platty clay (e.g., kaolinite and smectite (Nosrati *et al*., 2012). Surface area of CG is highest than the others correlated to higher muscovite contain in this clay.

Table 3.4 : BET surface area, total pore volume and mean pore volume

Clay	Surface area (m^2/g)	Total pore volume (cm^3/g)	Mean pore volume (nm)
Clay-Ind Capkala	35.414	0.2006	22.660
Clay-Ind Sintang	22.888	0.12109	21.161
Clay Congo Brazzaville	30.540	0.1589	20.810
Clay Gabon	38.670	0.2960	30.606

3.   Kaolin from Gabon

3.1   Characterization

XRD of the other kaolin sample from Gabon shown that there are peaks with high crystalinity and the others are broder (Figure 3.7). The slim peak corresponds to the quartz (Qz), and the broader one may be organic compound. The basal spacing of the unidentified molecule is 0.582 nm, and the other 0.395 nm. Even, in Gabon this material usually call as 'red kaolin', but from XRD analysis, there is no clay mineral.
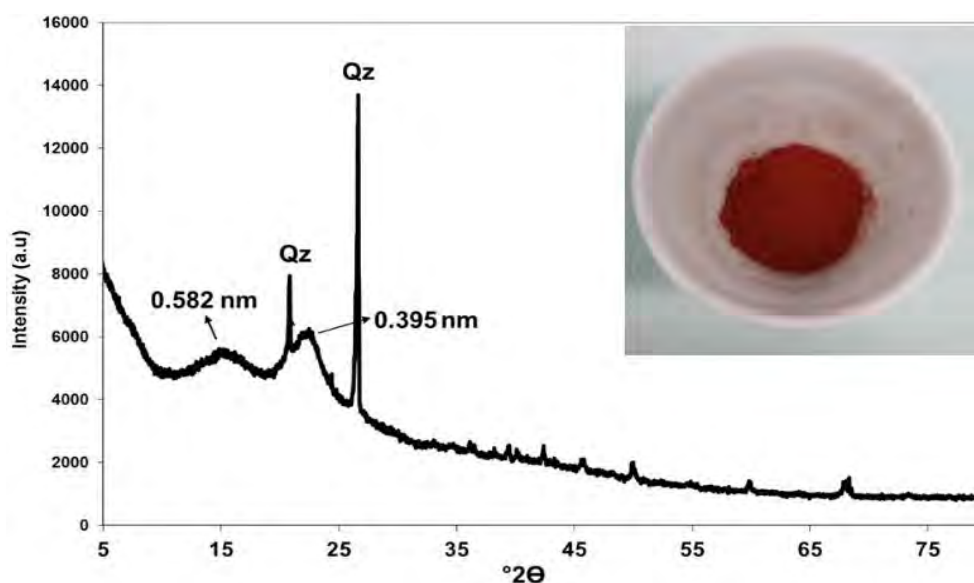
Figure 3.7: Diffractogram of kaolin from Gabon (inset: kaolin powder)

For the next identification of this kaolin, it will be analyzed by FTIR. Identification of organic funtional group on kaolin refer to the **Table 3.5**.

Table 3.5: Characteristic infrared bands of aliphatic hydrocarbons and oxygen containing compound

Wavenumber (cm^{-1})	Assignment
	Alkanes
2920	Methyl symetric C-H stretching
2930	Methylene asymetric C-H stretching
2870	Methyl asymetric C-H stretching
2850	Methylene symetric C-H stretching
1470	Methyl asymetric C-H bending
1465	Methylene scissoring
1380	Methyl symetrical C-H bending
1305	Methylene wagging
1300	Methylene twisting
720	Methylene rocking
	Alkenes
3100-3000	=C-H stretching
1680-1600	C=C stretching

1400	=C-H in-plane bending
	Alkynes
3300-3250	=C-H stretching
2260-2100	C=C stretching
700-600	=C-H bending
	Alcohol and phenol
3600	Alcohol O-H stretching
3550-3500	Phenol O-H stretching
1300-1000	C-O stretching
	Ethers
1100	C-O-C stretching
	Aldehydes and ketones
2900-2700	Aldehyde C-H stretching
1740-1720	Aliphatic aldhehyde C=O stretching
1730-1700	Aliphatic ketone C=O stretching
1720-1680	Aromatic aldehyde C=O stretching
1700-1680	Aromatic ketone C=O stretching
	Esters
1750-1730	Aliphatic C=O stretching
1730-1705	Aromatic C=O stretching
1310-1250	Aromatic C-O stretching
1300-1100	Aliphatic C-O stretching
	Carboxylic Acid
3300-2500	O-H stretching
1700	C=O stretching
1430	C-O-H in-plane bending
1240	C-O stretching
930	C-O-H out-of-plane bending
	Anhydrides
1840-1800	C=O stretching
1780-1740	C=O stretching
1300-1100	C-O stretching

Spectra infrared of kaolin (Figure 3.8) shown the OH stretching at 3435 cm^{-1} and the –OH bending at 1620 cm^{-1}. Quartz is identified at band 1031 cm^{-1} and 595 $cm^{-1.}$ There are bands at 2928, 1506 and 1462 cm^{-1}. Spectra at 2928 cm^{-1} correspond to the C-H streching in alkana (Carballo *et al*., 2008) and C-H bending at 1462 cm^{-1}. Almost all the natural clays associated with impurites

organic compounds as we described at the section before, and all the clays that we analysis before have this bands. But, the colors of four clays are not red. The specific band that unic and special is band at 1506 cm^{-1} which is identified as C=C stretching (Stuard, 1997). Band at 1620 cm^{-1} can related to the C=C stretching of alkenes, and =C-H put-of-plane identified at 595 cm^{-1}.
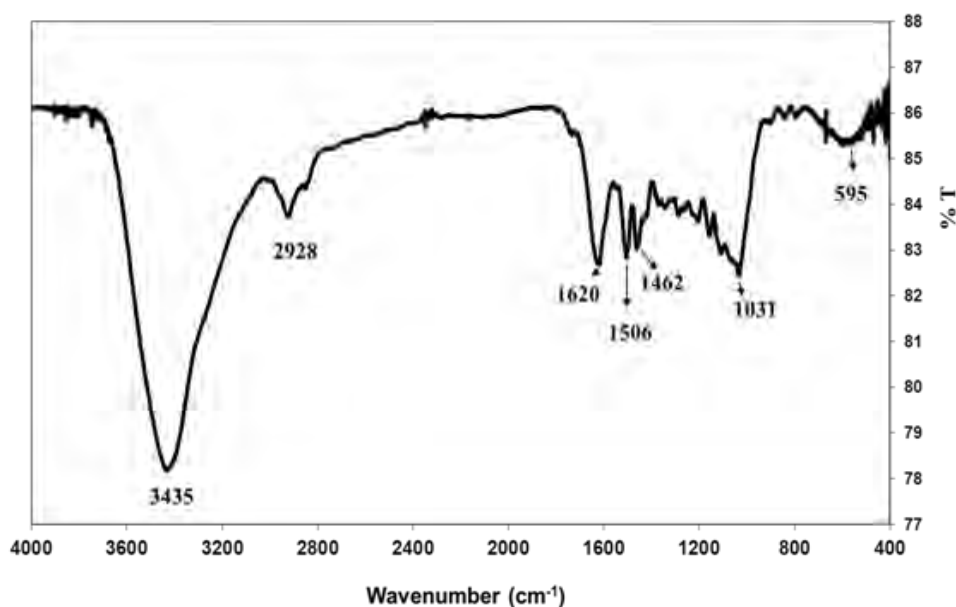
Figure 3.8: Spectra infrared of kaolin

This aliphatic organic molecule also confirmed by H-NMR (solvent: CDCl$_3$, deuterated chlorofom) and represented at Figure 3.9. The chemical shift (δ) at 0.9 ppm, 1.3 ppm, and 1.5 ppm correspond to RCH$_3$, R$_2$CH$_2$, and R$_3$CH, respectively (Pretsch *et al*., 2001). The other chemical shift at 2.1 ppm was related to the proton of C=C-H (ethylenic).
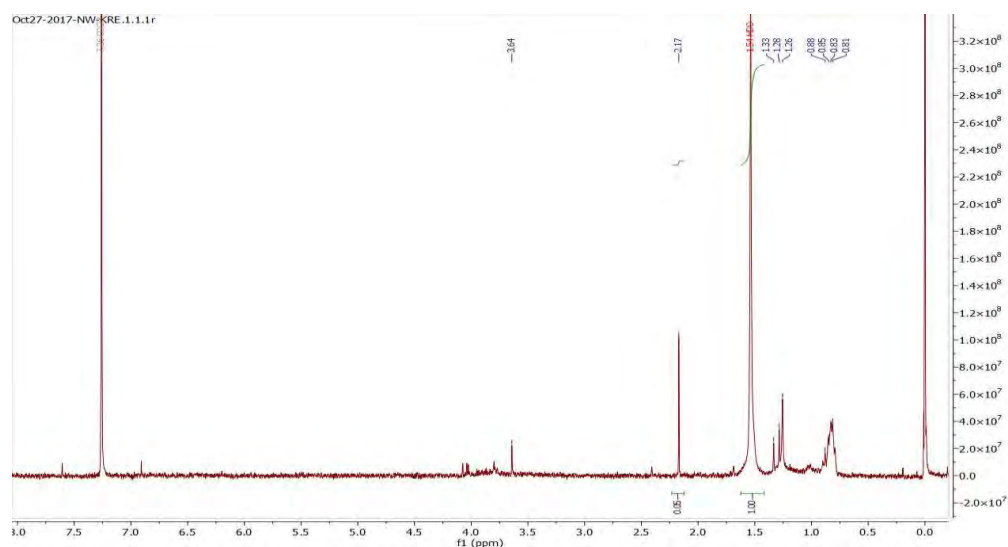
Figure 3.9 : Spectra H-NMR of kaolin from Gabon

Base on FTIR and H-NMR analysis, the organic compound in kaolin from Gabon has C=C, therefore the analysis will be continued using UV-visible to characterize the absorption spectrum. Sample kaolin was characterized using organic solvent with different polarizability: methanol, chlorofom, and acetone (Figure 3.10). Solubility of this kaolin decreased with the increase of the nonpolarity of the solvent. The solubility is in order, methanol > chlorofom > acetone, respectively. This is correlated with the composition of the red kaolin, which is consist of quartz and organic molecule. Quartz is not soluble in organic solvent. Therefore, the solubility is correspond to the polarity of the the organic molecule in kaolin. From this information, we known that the organic molecule are polar with functional group – OH as we seen at spectra infrared. The band- OH are came from the organic molecule not from H_2O in clay. The OH functional group caused the polarity of this organic molecule.
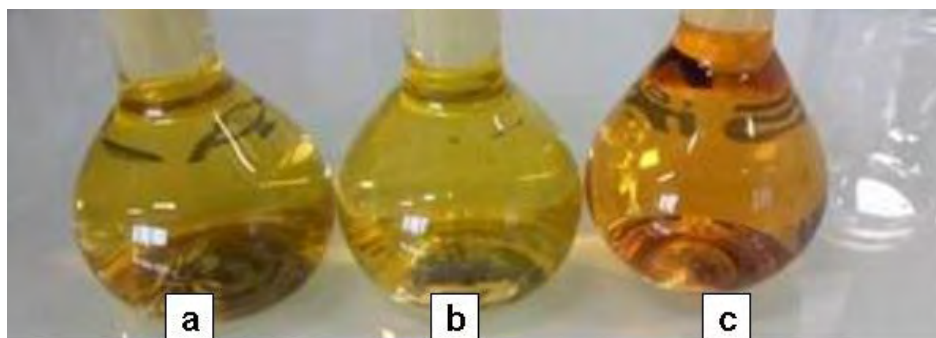
Figure 3.10: Kaolin from Gabon in different solvent: acetone (a), chloroform (b), and methanol (c)

Spectra UV absorption of kaolin in acetone has three peaks at range 441 nm, 468 nm, and 498 nm, while in chlorofom and methanol at 441 nm, 469 nm, 501 nm and 443 nm, 471 nm, 503 nm (Figure 3.11). The λ_{max} at methanol, chlorofom and acetone are 503, 469, and 468 nm, respectively. For carotenoid, the electron transition in $\pi \rightarrow \pi^*$ of C=C around 446-452 (Bouchouit *et al.*, 2010). The λ_{max} of organic compund (468-503 nm) in this research is more then carotenoid (lower energy), it was suggested correlate with to the more stabilize of this carotenoid due to interaction with silica or metal ion (Cu and Ca in kaolin). Then, the element contain of kaolin and the morphology will be analyzed.
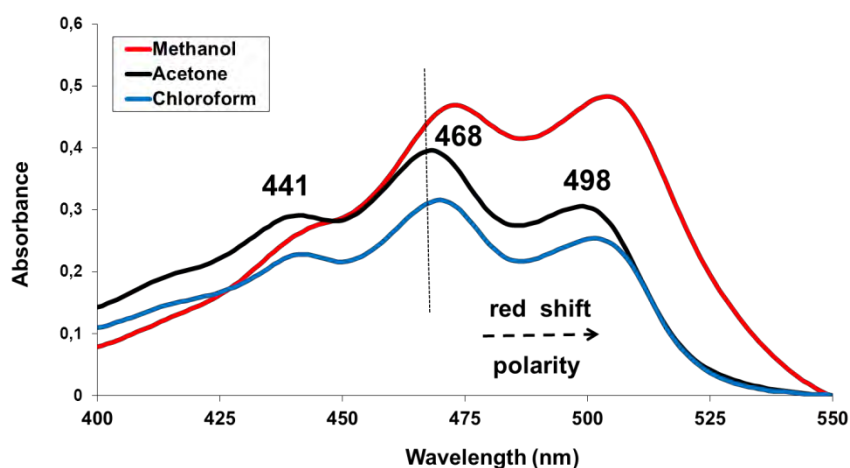
Figure 3.11: UV-Vis spectra of kaolin in different solvent

91

Carbon element in this material is 73% of the total mass, which is almost 4-fold than the natural clay from Congo. Also, there is Al, but in small quantity. Therefore, there is a possibility that there is mineral clay here but in very small fraction. The others metal element are Cu and Ca in significant quantity (Figure 3.12). Morphology of this material shown the large surface with the size is more than 10µm. This surface, maybe came from the organic molecule with arranged with quartz. The morpholody of kaolin with difference magnification are shown at Figure 3.13.
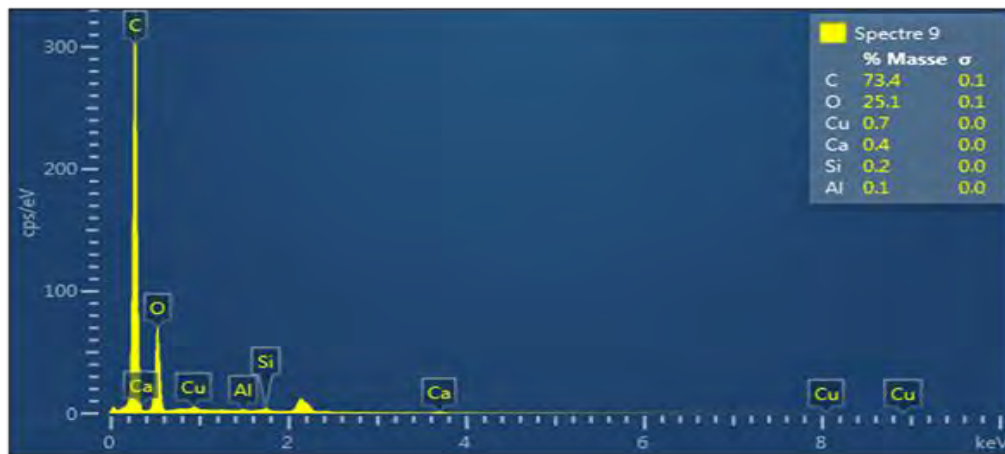
Figure 3.12: Percentage mass of the element in kaolin from SEM-EDS
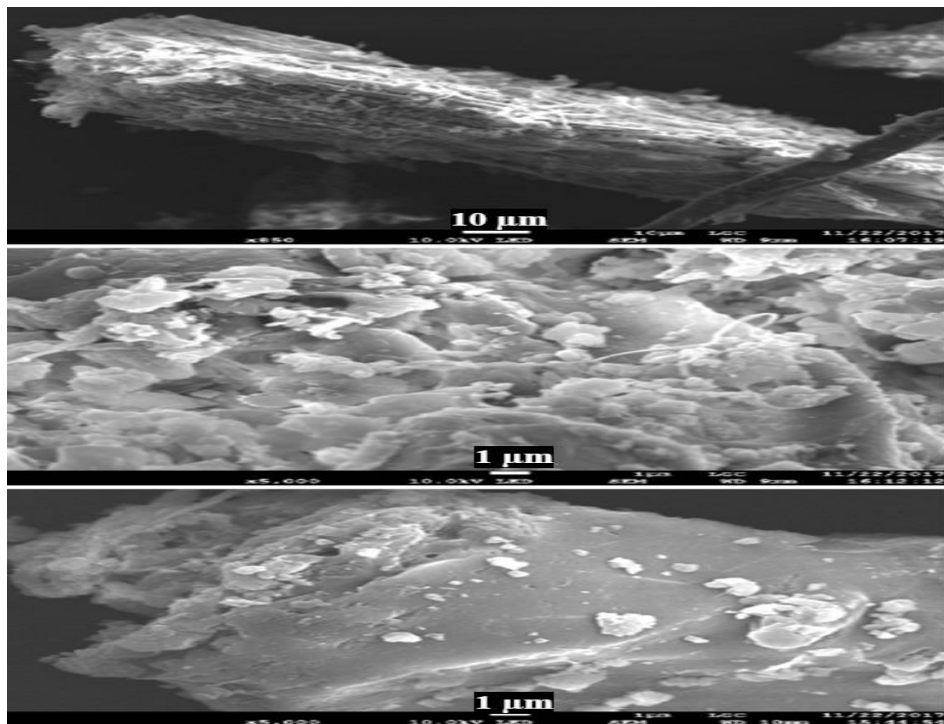
Figure 3.13: Morphology of kaolin

Surface area of kaolin is 4,95 m^2/g, total pore volume: 0,03 cm^3/g and mean pore volume 20,96 nm. The low of the surface area due to the major component in this material is the organic molecule.

3.2. Degradation of organic compound in kaolin

Degradation of kaolin under UV irradition is shown at Figure 3.14. The absorbance decreased significaly with the time exposer from 0 hour until nine hour.
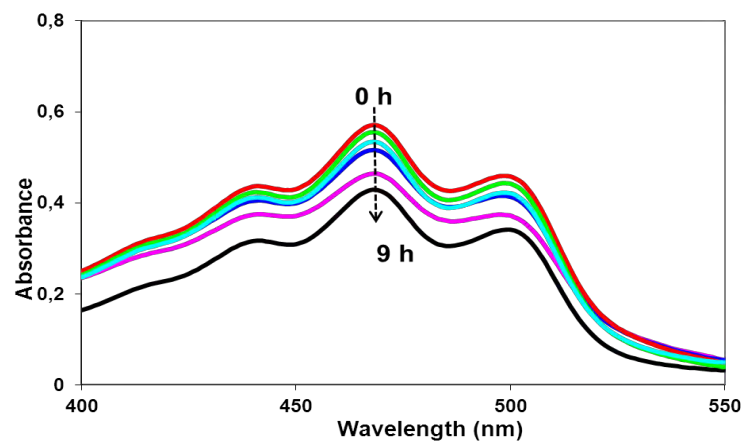
Figure 3.14: Photostability of organic compound in Gabon's kaolin

93

Kinetic experimental data were presented in a dimensionlless form using A and A_0 variables, where A was the absorbance at time t and A_0 was the initial absorbance. Degradation of red kaolin in acetone was described by the following equations (Xiao *et al*., 2018):

$$A - A_0 = -kt \qquad (3.3)$$

$$\ln(A/A_0) = -kt \qquad (3.4)$$

$$1/A - 1/A_0 = kt \qquad (3.5)$$

where k was the reaction rate constant, and t was the UV-irradiation time. Eqs. (3.3), (3.4), and (3.5) corresponded to zero-order, first-order, and second-order kinetics, respectively. The reaction rate constants were based on linear plots of $(A - A_0)$ vs. t, $\ln(A/A_0)$ vs. t, and $(1/A - 1/A_0)$ vs. t. The kinetic reaction order was determined by comparison of correlation coefficients and reperesented at Table 3.6. The kinetic reaction data shown that degradation of organic compound in kaolin was zero-order reaction with reaction rate constant 0.0155 h^{-1} and the half-life was 18.42 h. The half life of this material under UV-irradiation is higher then pure carotenoid compounds such as β-carotene and fucoxanthin. The half life of analytical grade of β-carotene and fucoxanthin on acetone were 1.43 h and 14.44 h, respectively (see chapter 5).

The higher photostability of organic compound, maybe correlated to the structure and properties of the organic molecule. Therefore, it is important to isolate and elucidate this organic compound to identify this molecule. The other possibility that caused the higher photostability of this organic molecule is correlated to the presence of metal Cu and Ca. Interaction organic molecule with metal ion can improve the stability (Zebib *et al*., 2010).

Table 3.6: Kinetic reaction order of kaolin from Gabon in acetone

Reaction order	Equation	Correlation coefficient, R^2	Reaction rate constant, k (h^{-1})	Half-life ,$t_{1/2}$ (h)
Zero-order	y=-0.0155x+0.005	0.9700	0.0155	18.42
First-order	y=-0.031x+0.0142	0.9589		
Second-order	y=0.0625x+0.0366	0.9455		

3.3 Electrochemical and photostability analysis

Information about energi band gap of the material is very important if will used in optoelectronic. Cyclic voltametry of red kaolin are represented at Figure 3.15. The LUMO energy is -0.82 eV and the HOMO is -0.52 eV. The electrochemical gap using equation 2.8 is -1.34 eV. This E_{gap}^{el} is lower than two carotenoids compounds, β-carotene (2.04 eV) , and fucoxanthin (2.02 eV).
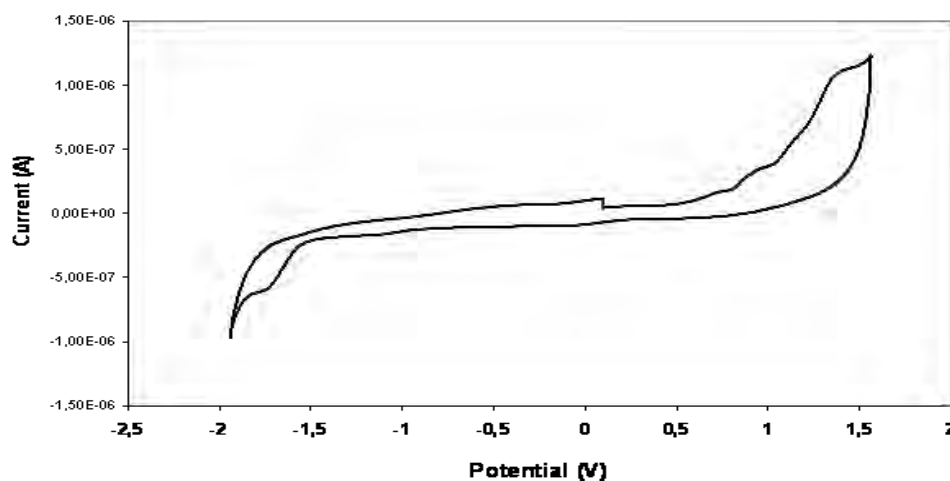
Figure 3.15: Cyclic voltammogram of organic compound in kaolin

Kaolin from Gabon is consist of aliphatic organic compound with C=C functional group, associated with quartz. Degradation of organic compound from this kaolin in acetone followed the zero-order reaction with the half-life 18.42 h. The electrochemical band gap of the aliphatic organic was 1.34 eV and lower than other carotenoid.

4.   Conclusions

Base on the characterization of natural clay, we can conclude that:

a.   Natural clays are kaolin type with different composition, almost associated with quartz. Kaolin from Capkala, Indonesia was kaolinite, and kaolin from Congo Brazzaville is nacritic. For the application, kaolin should be purification to increase the kaolinite or nacrite mineral. There is correlation of the color and the metal contain in kaolin, especially, ferric.

b.   Kaolin from Gabon consist of aliphatic carotenoid compound and quartz. It also has a characteristic properties in electrochemical properties and UV-photostability. This material can be a good candidate for optoelectronic devices and cosmetic (sunscreen) due to the half-life and the band gap electrochemical properties.

References

AL-Shameri, A.A. and Rong, L.X. (2009) Characterization and Evaluation of Algaof Kaolin Deposits of Yemen for Industrial Application. *American Journal of Engineering and Applied Sciences*, **2** (2), 292-296.

Aroke, U.O., Abdulkarim, A., and Ogubunka, R.O. (2013) Fourier-tranform infra red characterization of kaolin, granite, bentonite, and barite. *ATBU Journal of Enviromental Technology*, **6** (1), 42-52.

Awad, M.E., López-Galindob, A., Settid, M., El Rahmanya, M.M., and Iborrab, C.V. (2017) Kaolinite in pharmaceutics and biomedicine (Review). *International Journal of Pharmaceutics*, **533**, 34–48.

Buatier, M., Potdevi, J-L., Lopez, M., and Petit, S. (1996) Occurrence of nacrite in the Lodève Permian basin (France). *European Journal of Mineralogy*, **8**, 847-852.

Teresa Carballo, T., Gil, M.A., Gomez, X., Fernando Gonzalez-Andreas, F. And Antonio Moraan, A. (2008) Characterization of different compost extracts using Fourier-transform infra red spectroscopy (FTIR) and thermal analysis. *Biodegradatio*n, **19**, 815–830.

Cardona, C.M., Li, W., Kaifer, A.E., Stockdale, D., and Bazan, G.C. (2011) Electrochemical considerations for determining absolute frontier orbital energy levels of conjugated polymers for solar cell applications. *Advances Materials,* **23**, 2367–2371.

De Poe, W., Stelian, Pintea, S., Drnec, J., Carla, F., Felici, R., Mulder, P., Johannes, A.A.W., Elemans, W., Van Enckevort, W.J.P., Rowana, A.E., and Vlieg, E. (2014) Muscovite mica: Flatter than a pancake. *Surface Science*, **619**, 19-24.

Djomgoue, P. and Njopwouo, D. (2013) FT-IR Spectroscopy Applied for Surface Clays Characterization. *Journal of Surface Engineered Materials and Advanced Technology*, **3**, 275-282.

Ekosse, G-E. E. (2005) Fourier Transform Infra red Spectrophotometry and X-ray powder Diffractometry as Complementary Techniques in characterizing Clay size fraction of Kaolin. *Journal of Applied Science and Environmental Migitation*, **9** (2), 43-48.

Gadsen, J.A. (1975) Infra red spectra of minerals and related inorganic compounds, Butterworths, London.

Haq, A., Iqbal, Y., Khan, M.R. (2009) Phase and microstructural characterization of kaolin. *Journal Pakistan Material Society*, **3** (2), 77-88.

Jaafar, N., Naamen, S., Ben Rhaiem, H., and Ben Haj, A. (2015) Functionalization and structural characterization of a novel nacrite-LiCl nanohybrid material. *American Journal of Analytical Chemistry*, **6**, 202-215.

Jia, F., Sua, J., and Songa, S. (2015) Can Natural Muscovite be Expanded. *Colloids and Surfaces A: Physicochemical and Engineering Aspects*, **471**, 19–25.

Ke, S., Chen, C., Fu, N., Zhou, H., Ye, M., Lin, P., Yuan, W., Zeng, X., Chen, L., and Huang. (2016) Transparent indium tin oxide electrodes on muscovite mica for high-temperature-processed flexible optoelectronic devices. *Applied Materials & Interfaces*, **8**, 28406-28411.

Madejová, J. (2003) FTIR techniques in clay mineral studies. *Vibrational Spectroscopy*, **31**, 1–10.

Murray, H.H. (2000) Traditional and new applications for kaolin, smectite, and palygorskite: a general overview. *Applied Clay Science*, **17**, 207–221.

Murray, H.H. (2007) Applied clay mineralogy. First ed, Elsevieer, Amsterdam.

Nasrati, A., Addai-Mensah, J., and Skinner, W. (2012) Muscovite clay mineral particle interaction in aquest media. *Powder Technology*, **219**, 228-238.

Obaje, S.O., Omada, J.I., and Dambatta, U.A. (2013) Clays and their industrial applications: Synoptic review. *International Journal of Science and Technology*, **3** (5), 264-269.

Pretsch, E., Buhlmann, P., and Badertscher, M. (2009) Structure Determination of Organic Compounds. Fourth, Revised and Enlarged Edition, Springer-Verlag Berlin Heidelberg.

Robertson, I.D.M. and Eggleton, R.A. (1991) Wethering of granitic muscovite to kaolinite and halloysite of plagioclase-derived kaolinite, *Clays and Clay Minerals*, **39** (2), 113-126..

Saikia, B.J. and Parthasarathy, G. (2010) Fourier transform infra red spectroscopi characterization of kaolinite from Assam and Meghalaya, Northeastern India. *Journal of Modern Physisc*, **1**, 206-210.

Senoussi, H., Osmania, H., Courtois, C., and Bourahlia, M-H. (2016) Mineralogical and chemical characterizationof DD3 kaolin from the East of Algeria. *Boletín De La Siciedad Española de Cerámica y Vidrio*, **55**, 121-126.

Singh, B. and Gilkes, R.J. (1991) Weathering of a chromiun muscovite to kolinite. *Clays and Clay Minerals*, **39** (6), 571-579.

Stuart, B. (1997) Infra red Spectroscopy: Fundamentals and Applications. Wiley, Chichester, UK.

Vaculíková, L., Plevová, E., Vallova, S., and Kouttnik, I. (2011) Characterization and differentiation of kaolinites from selected Czech deposits using infra red spectroscopy and differential thermal analysis. *Acta Geodyamic and Geomaterials*, **8**, 59–67.

Xiao, Y-D., Huang, W-Y., Li, D-J., Song, J-F., Liu, C-Q., Wei, Q-Y., Zhang, M., and Yang, Q-M. (2018) Thermal degradation kinetics of all-trans and cis-carotenoids in a light-induced model system. *Food Chemistry*, **239**, 360-368.

CHAPTER IV

MODIFICATION AND CHARACTERIZATION KAOLIN FROM MOUBEYI CONGO BRAZZAVILLE AND WEST KALIMANTAN INDONESIA

CHAPTER IV

MODIFICATION AND CHARACTERIZATION KAOLIN FROM MOUBEYI IN CONGO BRAZZAVILLE AND WEST KALIMANTAN INDONESIA

1. Introduction

Physical and chemical properties of clay mineral have been studied by numerous researchers due to their application in many industries. Kaolin is one of the clay materials most widely used by human. Millions of tons of kaolin are used each years in the world for a large variety industry, likes ceramics, paper coating, paper filling, paint extender, rubber filler, plastic filler, cracking catalysis or cement (Murray, 2000; Jaafar *et al*., 2015).

The kaolin group is divided in three polytypes (kaolinite, nacrite, dickite) in addition to halloysite their hydrated analogue. Kaolinite, dickite, and nacrite have the same chemical composition of SiO_2 46.54%, Al_2O_3 39.50% and H_2O 13.96% with the chemical formula $Al_2SiO_2O_5(OH)_4$. Identification of kaolin polytypes can be done by X-Ray diffraction, infra red-spectroscopy, and differential thermal analysis (Shen *et al*., 1994; Ruiz Cruz, 1996; Buatier *et al*., 1996). Nacrite crystallized in monoclinic lattice with a Cc space group with the parameter a = 8.906 Å, b = 5.146 Å, c = 15.669 Å , β = 113.58 Å with a basal distance equal to d_{002} = 7.18 Å. Nacrite is generally considered as a high temperature polymorph (Jaafar *et al*., 2015).

The improvement of properties of kaolin can be done by two main different treatment such as (a) physical modification with thermal/microwave treatment, and (b) chemical treatment with acid, bases or organic compound. Physical modification involved alteration of chemical composition and crystalline structure by the high temperature, but in chemical modification usually by alteration of structure, surface functional groups and surface area (Kumar *et al*. 2013). Some researchers used thermal treatment and or chemical treatment to improved kaolinite properties.Thermal treatment, usually by calcinating, produce metakaolin that is more reactive clay than the origin ones.

Belver *et al* (2002) calcination kaolin at 600°C continuing activating by HCl yielded material with surface area 219 m^2/g. Other activation condition are using H_2SO_4 (Hattab *et al*., 2013), CH_3COOH, H_3PO_4, HCl, HNO_3 and base NaOH (Kumar *et al*., 2013). Activation metakaolinite with H_2SO_4 increased their dielectric permittivity. It can be used for filling the plastic or rubber-coating material on wires (Izci, 2014).

2. Characterization and modification clay from Congo Brazzaville in Central Africa

2.1 Characterization with XRD

The XRD patterns of natural clay from Moubeyi, Congo Brazzaville, Centra Africa are shown in Figure 4.1. The natural clay shows well-defined reflections at 2θ value of 12.308 (corresponding to the d value of 7.185 Å. These peaks are corresponding to the reflections from d_{002}, which are typically characteristic peaks of kaolin clay, nacrite. The others reflections are at 2θ= 21,438, doublet peaks at 2θ= 25.61 and 26, triplet peaks at 36.805; 37.9, and 38.802. These are matching with nacrite identified by Ruiz Cruz (1996). Chen *et al* (2001) whose reported nacrite from Taiwan, found that nacrite has special reflection in presence doublet at 2θ= 20.0- 20.4, and triplet reflection between 2θ= 34.8-35.7. Jaafar *et al* (2016) identified nacrite from 002, 004, 006 and 008 reflections which are correlated with 2θ= 12,310; 24,777; 37,546 and 50,771 in natural clay from Congo. From XRD determination based on profile fit method compare to the reference JCPDS database, it was clear that natural clay from Congo is kaolin type, which is consist of nacrite (Nct), quartz (Qz), anatase (Ant) and goethite (Go).

Nacrite is the rarest kaolin polymorph. Chen *et al* (2001) reported that nacrite was founded in Northern Taiwan. Another occurrence of nacrite has been reported at Northern Tunisia (Ben Haj *et al*., 1996), Lodève, France (Buatier *et al*., 1996), China (Shen *et al*., 1994), and Spain (Ruiz Cruz., 1996). Jaafar *et al* (2014) used amorphous nacrite clay hybrid from Tunisia as solid electrolyte for Li-ion batteries.

In this work, the structural change that occurred in nacrite after treated with calcination and chemical activating with ammonium hydroxide were studied using X-Ray diffraction technique. After calcined at 600°C, d-value at 7.185 Å disappeared. It mean, calcination at 600°C for 6 h caused the nacrite's layer (002 basal reflection) destroyed. Structural clay calcined not change after activated by ammonium hydroxide. The dehydroxylation process from nacrite to the metanacrite are decribed in this equation (Jaafar *et al*., 2016):

$$Al_2O_3.2SiO_2 \rightarrow Al_2O_3.2SiO_2 + 2H_2O \qquad (4.1)$$

nacrite   metanacrite
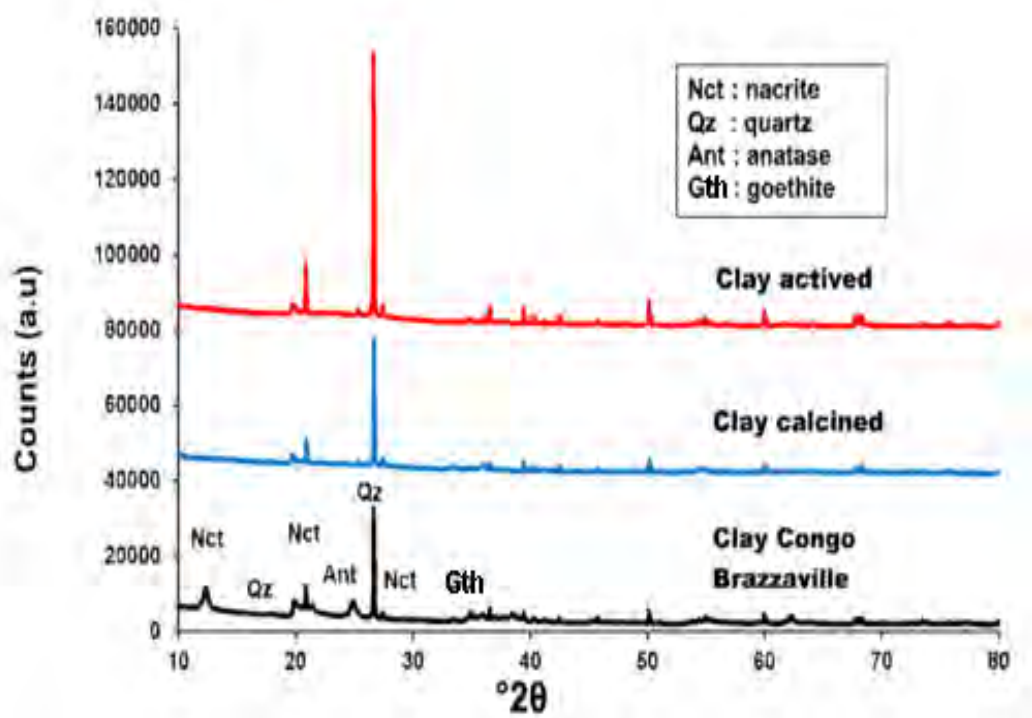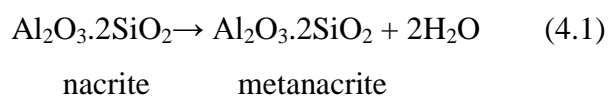
Figure 4.1: XRD pattern of natural, calcined, and activated of clay from Moubeyi, Congo Brazzaville

2.2. XRF characterization

The XRF analysis was done to know the chemical composition of the natural clay and the subsequent chemical changes that occurred after activation. Table 4.1 shows the results of chemical analysis of natural clay and treated clay. The natural clay from Congo Brazzaville contains silica and alumina which are in the major quantities whereas the other oxide such as ferric oxide, magnesium oxide, titanium oxide, potassium oxide, calcium oxide are present in trace amounts. The chemical weight percent composition of this fraction was follows: SiO_2= 57.86%; Al_2O_3= 35.21%; Fe_2O_3= 3.56%; MgO = 0.84%; TiO_2 = 0.93%; K_2O = 0.75% and CaO= 0.20%.

Table 4.1: Major oxide compositions of samples studied

Si/Al	CaO	K_2O	MgO	TiO_2	Fe_2O_3	Al_2O_3	SiO_2	Samples
Chemical content (% weight)								
1.64	0.20	0.75	0.84	0.93	3.56	35.21	57.86	Clay Congo
1.60	0.20	0.78	0.95	0.96	3.73	35.56	56.82	Clay Calcined
10.05	0.11	0.44	1.70	1.60	0.53	8.60	86.47	Clay Activated

After calcination at 600°C, it observed that the chemical compositions of clay not change significantly. But, activation process using ammonium hydroxide, caused Al_2O_3 and Fe_2O_3 decreased and SiO_2 content increased progressively. Decreasing in Al_2O_3 in clay activated can be described to the leaching of Al^{3+} ions from the octahedral sheet of nacrite due to the hydrolysis under base/alkaline condition (Belver *et al*., 2002; Kumar *et al*., 2013). Si/Al of clay activated enhanced from 1.64 up to 10.05, six fold than natural clay. Treatment of clay calcined with ammonium hydroxide, also decreased significantly the ferric content 6-fold lower than the origin. It was demonstrated that there is correlating about Fe contain in clay and their color, as we can see at Figure 4.2. Activating clay from Congo Brazzaville with NH_4OH increased the whiteness of this material. For industrial applications i.e filler or builder in paper and rubber, the whiteness properties of kaolin is very important.

Figure 4.2: Natural clay from Congo Brazzaville and their color changing after treated

2.3. FTIR characterization

The infrared spectra of NN, NC, and NA are shown in Figure 4.3 and the corresponding band assignments are listed in Table 4.2. The overall spectra of FTIR are divided into two general regions: 4000-1300 cm^{-1} (functional group region) and 1300-400 cm^{-1} (finger print region).

The band placed between 3697-3621 cm^{-1} regions correspond to OH stretching (hydroxyl sheet). Ben Haj (1996) identified nacrite from Tunisia at bands 3702, 3649, and 3630 cm^{-1}, while Prost *et al* (1989) at wavenumber 3692, 3688, 3629 and cm^{-1} and Buatier *et al* (1996) at 3700, 3648 and 3629 cm-^{1}. The band at 3697 cm^{-1} shows the free O-H stretching which correspond with 3700 cm^{-1} (Kumar *et al*. 2013) and 3702 cm^{-1} (Buatier *et al*., 1996). The 3621 cm^{-1} band corresponds to the inner layer OH (Al-O...H) stretching which close to 3629 cm^{-1} obtained by Ruiz Cruz (1996) and 3630 cm^{-1} (Buatier *et al*., 1996), respectively. The wavenumber band at 3421 cm^{-1} is assigned to H-O-H symmetrical stretching. This is falls close from that obtained by Jaafar *et al* (2015) as 3416 cm^{-1}.

The spectra regions between 2914 and 2850 cm^{-1} are indication of organic impurities in the clay sample (Aroke *et al*., 2013). The transmittance band at 1635 cm^{-1} is assigned to H-O-H bending (Burhan & Emin, 2009).

103
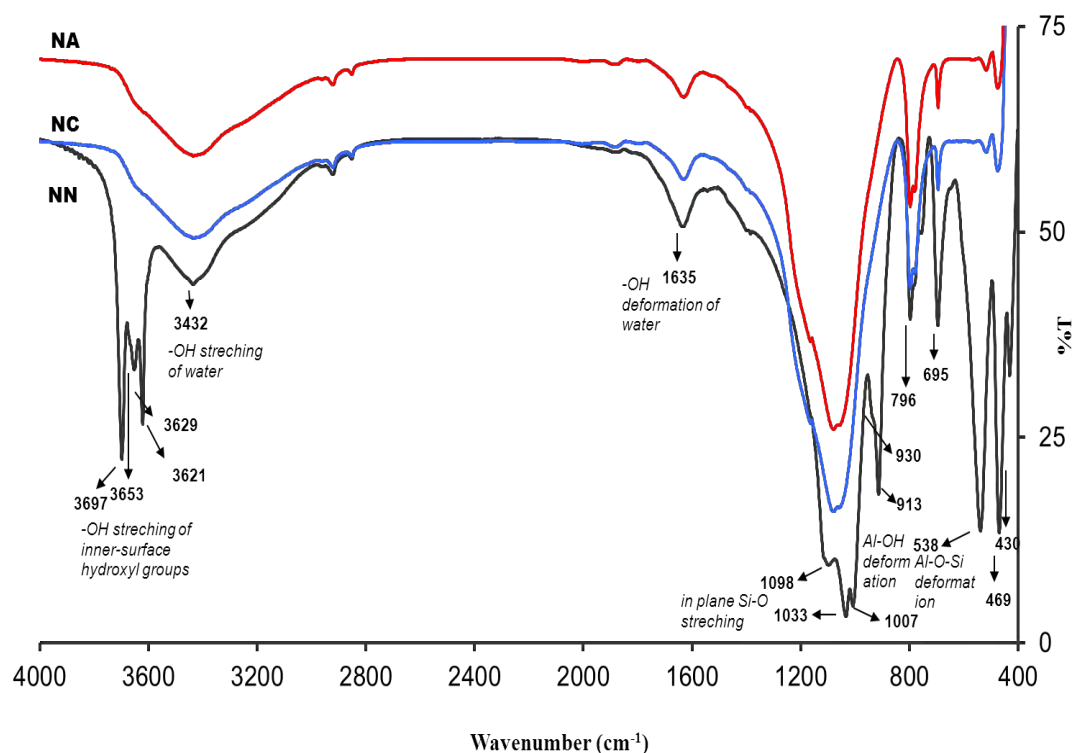
Figure 4.3: Spectra infrared of natural clay from Congo Brazzaville
and treated clay

Table 4.2: Frequencies and assignment of IR transmittance band in the 4000-400 cm[1] region for natural clay from Congo refer to the references

Natural clay from Congo Brazzaville (cm^{-1})	Band assignment
3697, 3653, 3629	AlO-H stretching
3421	Intercalated HOH symmetrical stretching
2914,2850	C-H stretching
1635, 1098, 1033, 1007	Intercalated HOH bending
1098, 1033, 1007	Si-O stretching
913,796, 695	Al-OH deformation
538, 469, 430	Al-O deformation

The wavenumber at 1098 cm^{-1}, 1033 cm^{-1}, and 1007 cm^{-1} are assigned to Si-O stretching which agree closely with 1135-1008 obtained by Jaafar (2015) and 1120-1037 (Buatier *et al*., 1996). Al-OH deformation band are identified at band at 913 cm^{-1}, 796 cm^{-1}, and 695 cm^{-1}, where the other researcher founded at band 918, 807, 757 cm^{-1} (Jaafar *et al*., 2015), and 912, 755, and 695. The wavenumber at 912 cm^{-1} is assigned to the inner surface of Al-OH deformation. The small band situated near 950 cm^{-1} is characteristic to nacrite mineral (Buatier *et al*., 1996; Prost *et al*., 1996), but this weak band in not clearly identified at natural clay's spectrum.

The presence of quartz was confirmed by the doublet around at 800 and 775 cm^{-1} (Vizcayno *et al*., 2010). These band appearances at 796 cm^{-1}. According to Aroke *et al* (2013) band at 780 cm^{-1} correspond to the Fe^{2+} and Fe^{3+} stretching, assigned to Fe^{2+}-OH and Fe^{3+}-OH stretching which is a sign of its impurity. The Al-O deformation is identified at band 538 cm^{-1} and 469 cm^{-1}, which suitable with Jaafar (2015), Buatier *et al* (1996) and Ben Haj *et al* (1996).

After calcined, there is significantly changing in transmittance of clay calcined, especially band correlated to the nacrite. The band assignment of AlO-H stretching in area 3700-3600 cm^{-1} and Si-O stretching 1098-1007 cm^{-1}. The band of AlO-H stretching is disappeared after calcined at 600°C. It also happened at band 913 cm^{-1} and 513 cm^{-1}. This decreasingly intensity of Al-O correlated to the XRD and XRF data of nacrite calcined, which is the layer nacrite destroyed and % mass of alumina decreased significantly. Calcination also gaved effluence to the silica contains. Decreasing significantly at band 538 cm^{-1} correlated to the changing band at 1098-1007 cm^{-1}. There is no difference significantly in spectra infrared of clay calcined and activated.

2.4. TGA/DTA analysis

The thermo gravimetric analysis/differential thermal analysis of natural clay shows three peaks at 70°C, 280°C and 470°C. The first one at 70°C and 280°C which is corelate to the loss mass of water molecules about 0.93% and 2.92%, respectively (Figure 4.4). The low temperature endothermic is due to the water out of the interlamellar space. The second loss mass at 270°C corresponds to the interlamellar water (Ben Haj *et al*., 1996). The strong mass loss center at 470°C (10.17%) is due to dehydroxylation.

Clay calcined also have three peaks at 120°C, 360°C and 770°C with lost mass 0.62%; 0.62%; and 0.16%, respectively, but clay activated only have two peaks at 70°C and 400°C with loss mass 7.26% and 3.05%.
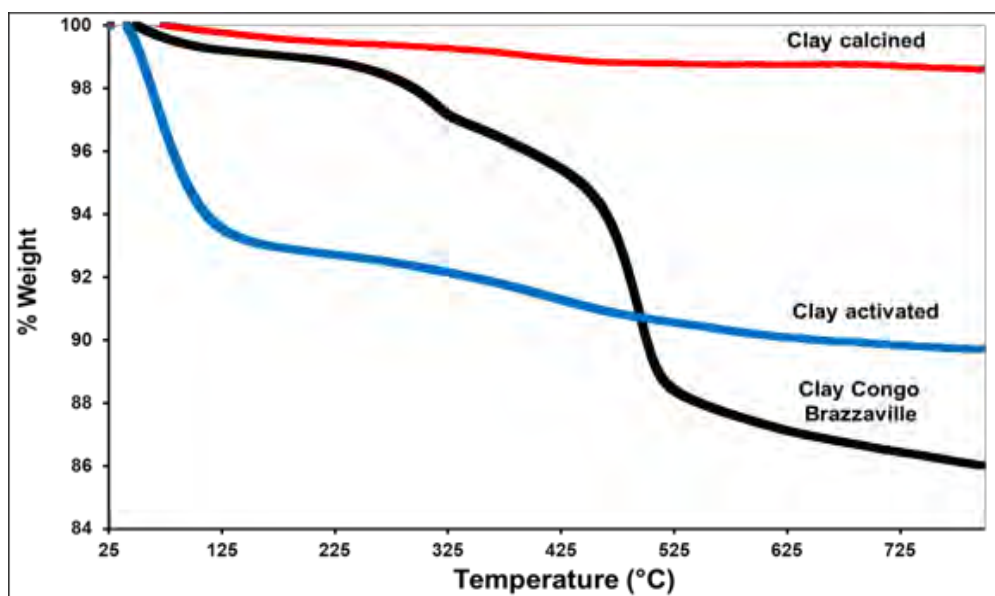
Figure 4.4: TGA of nacritic clay

2.5. SEM analysis

The scanning electron micrographs of natural clay from Congo Brazzaville is presented at Figure 4.5 which shows the morphological features. The SEM micrograph of natural clay showed nacrite with pseudohexagonal morphology. Ruiz Cruz (1996) who analyzed kaolin group from Spain, found that in sandstones nacrite showed blocky with pseudohexagonal morphology. The SEM reveals the presence of large particles that appeared to have been formed by several flaky particles stacked together in form aggregates. The SEM images of nacrite treated show no difference significantly especially at clay calcined. The micrograph of clay activated with ammonium hydroxide indicates the disaggregation.
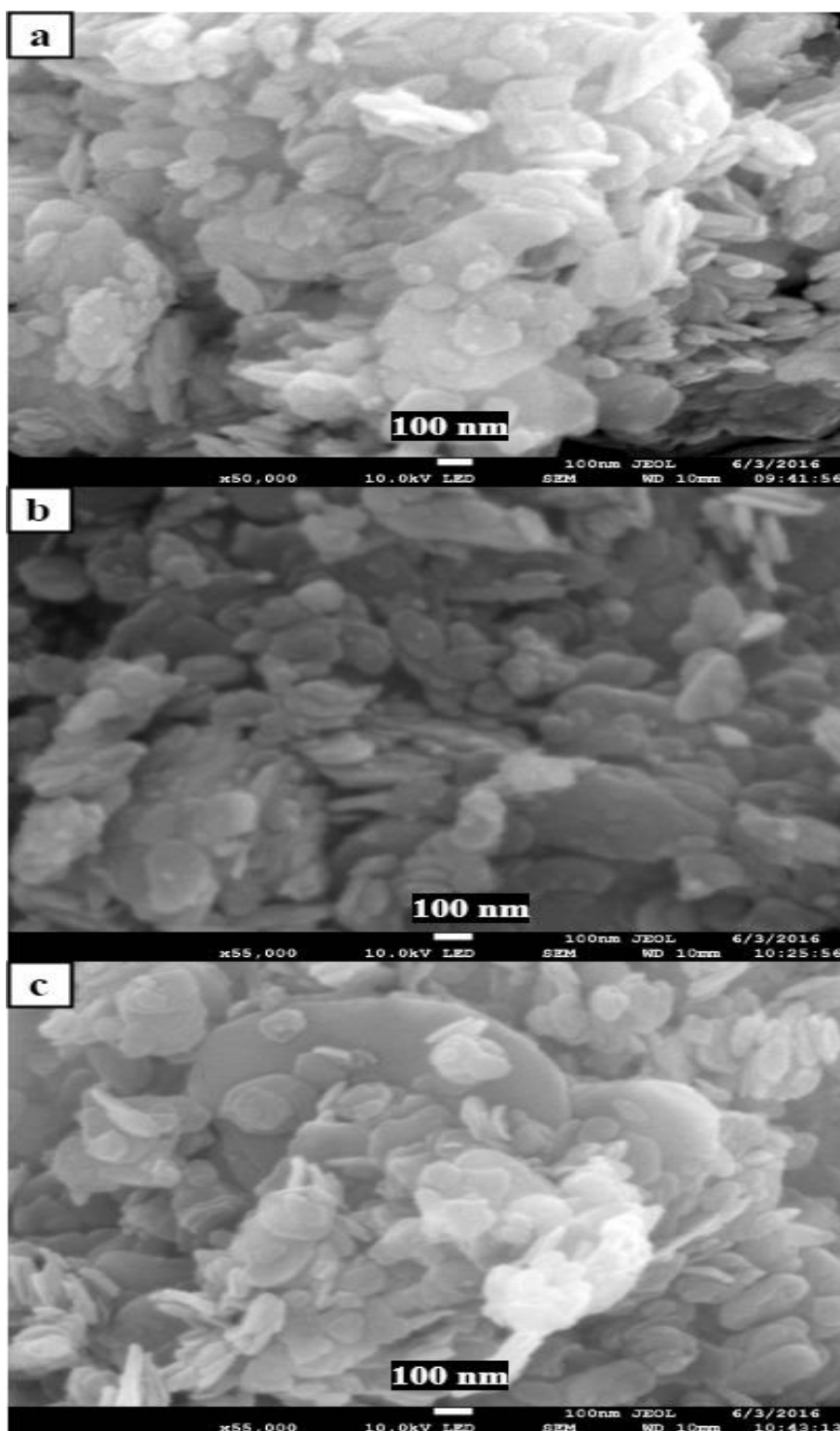
Figure 4.5: Scanning electron photomicrographs of natural clay from Congo Brazzaville (a), calcined (b), and activated (c)

2.6. BET surface area and pore volume analysis

Langmuir isotherm is classically isotherm for a homogenous flat of surface and most popular of all nonlinear isotherm with monolayer capacity approached at large concentration by assuming negligible interaction between adsorbed molecules. Basically, BET is an extension of the Langmuir treatment to multilayer adsorption on a homogeneous, flat surface. It is useful for gas-solid system in which condensation is approached (Kumar *et al*., 2013).

The surface area and pore volume of natural and treated clay from Congo Brazzaville obtained using N_2 adsorption-desorption isotherms summarized in Table 4.3. Calcination natural clay at 600°C for 6 hours increased surface area from 30.548 to 34.380 m^2/g. Activated nacrite calcined with ammonium hydroxide, enhanced surface area almost 8-fold than natural clay up to 239.69 m^2/g and decreased the mean pore diameter. Surface area of activated nacrite with ammonium hydroxide is relatively higher compared to the other researcher who using bases activator, such commercial kaolin activated NaOH with surface area 76 m^2/g (Kumar *et al*. 2013), kaolinite KOH 16.5 m^2/g (Belver *et al*., 2003). Activating methods using acid such as HCl resulting surface area 219 m^2g^{-1} (Belver *et al*., 2002).

Table 4.3: BET spesific surface area, volume pore and
mean pore diameter of nacritic

Parameter	Natural clay	Clay calcined	Clay activated
Specific surface area (m^2g^{-1})	30.548	34.380	239.68
Volume pore (cm^3g^{-1})	0.1589	0.1085	0.2120
Mean pore diameter (nm)	20.805	12.842	3.5384

Alkali treatment can increase the surface area and volume pore due to occurrence of the dealumination process and thus surface disintegration (Kumar *et al*., 2013). Under alkali treatment, finely dispersed Si oxides

produced after destruction and leaching of clay by removal some cations plugging the surface pores or interlamellar spaces, by formulation of surface pores and crack with accumulation of hydroxides of Mg and Ca (Jozefaciuk & Sarzynska, 2006).

With all these data, it is remarkable that natural clay from Congo Brazzaville is nacritic clay type. From XRD, we found that nacrite composition is less than quartz. For further application of nacrite, it is recomendated to do purification to increase the nacrite mineral fraction. Activation of nacritic enhanced the surface area up to 239.68 m^2/g. Natural nactitic clay untreated with NH4OH can be applicated in the manufacture of mud blocks for the construction of house (Shvarman *et al*., 2003).

3. **Characterization and modification kaolin from West Kalimantan, Indonesia**

West Kalimantan, Indonesia has abundance of mineral like quartz and kaolin clay (Destiarti *et al*., 2017). The application of kaolin a widely used industrial clay material, depend on its surface reactivity. Its common application e.g. filler in polymer, rubber, paper, cosmetic, medicines (Zsirka *et al*., 2015). Kaolin can also be used as adsorbents, catalysts, composites, nano-hybrids, and electrode coating (Araujo *et al*., 2014; Dedzo and Detellier, 2014; Matusik *et al*, 2011; Matusik and Matykowska, 2014; Mbaye *et al*., 2014; Tonlé *et al*., 2011). These applications, however, require modifications of the surface and their structure.

In this work, we characterized and modified kaolin from west Kalimantan, Indonesia. Before activated the natural kaolin was calcined at 600°C for 6 hours to product metakaolinite. Modification of metakaolinite was done by using $ZnCl_2$.

XRD pattern and infrared spectra of raw kaolin, metakaolinite and modified kaolinite represented in Figure 4.6 and Figure 4.7. The raw kaolin is composed of kaolinite associated with quartz and a small fraction of muscovite. The reflections observed at 7.15, 3.57 and 2.3 Å indicate the presence of a

second phase identified as kaolinite. The 001 basal distance of kaolinite is 7.2Å (Zsirka *et al*., 2015). Calcinating at 600˚C for 6 h caused 001 and 002 basal reflections of kaolinite destroyed and produced metakaolinite (MKaol). Modified metakaolinite with $ZnCl_2$, did not change significantly the XRD pattern of this material.
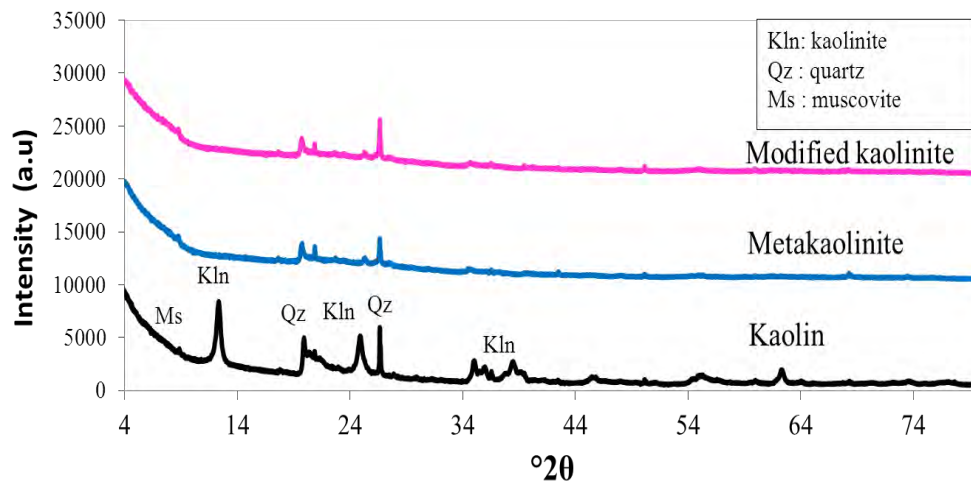
Figure 4.6: XRD pattern of raw kaolin, metakaolinite, and modified kaolinite

Metakaolinite was unstable phase of kaolinite. Metakaolinites formed by calcinating kaolinite with various temperature from 550-950˚C. Calcination condition affected the reactivity of metakolinite. Some researchers found the optimum condition for product metakolinite which almost reported from 600°C and 800°C. In this research, the temperature and residence time of calcination was adapted from Rahmalia (2016). Metakaolinite is an unstable phase of kaolinite, and its production can be represented as a simple equation (Ilić *et al*., 2010).

$$Al_2O_3 \cdot 2SiO_2 \cdot 2H_2O \quad \rightarrow \quad Al_2O_3 \cdot 2SiO_2 + 2H_2O\uparrow \quad (4.2)$$

Kaolinite   Metakaolinite

111
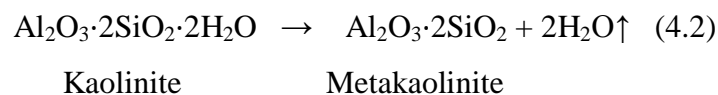
Spectra infrared of kaolin (K), metakaolinite (Mkaol) and modified kaolinite (MK) represented in Figure 4.7. The kaolin has wavenumber which identified of kaolinite at 3697 cm^{-1}, 3653 cm^{-1} and 3620 cm^{-1} which are stretching vibration of internal hydroxyl (Al..O..H) in octahedral sheet. The wavenumber at 3435 cm^{-1} was –OH stretching of H_2O, while the deformation at 1631 cm^{-1} (Sengupta *et al*., 2008). The wavenumber bands at 1112 cm^{-1}, 1032 cm^{-1} and 1000 cm^{-1} are assigned to Si-O stretching. Al-OH deformation band are identified at band at 912 cm^{-1} and 753 cm^{-1}. The Al-O-Si deformation identified at band 538 cm^{-1} and 470 cm^{-1} for Si-O-Si (Belver *et al*., 2002; Hattab *et al*., 2013; Kumar *et al*., 2013; Vaculikova *et al*., 2011). The presence of quartz was confirmed by the doublet around at 800 and 775 cm^{-1} (Vizcayno *et al*., 2010). After calcined, kaolinite converted into metakaolinite. It was clear that, the transmittance intensity of Al-O functional group decreased or the finger-print bands disappeared at spectra MKaol and MK.
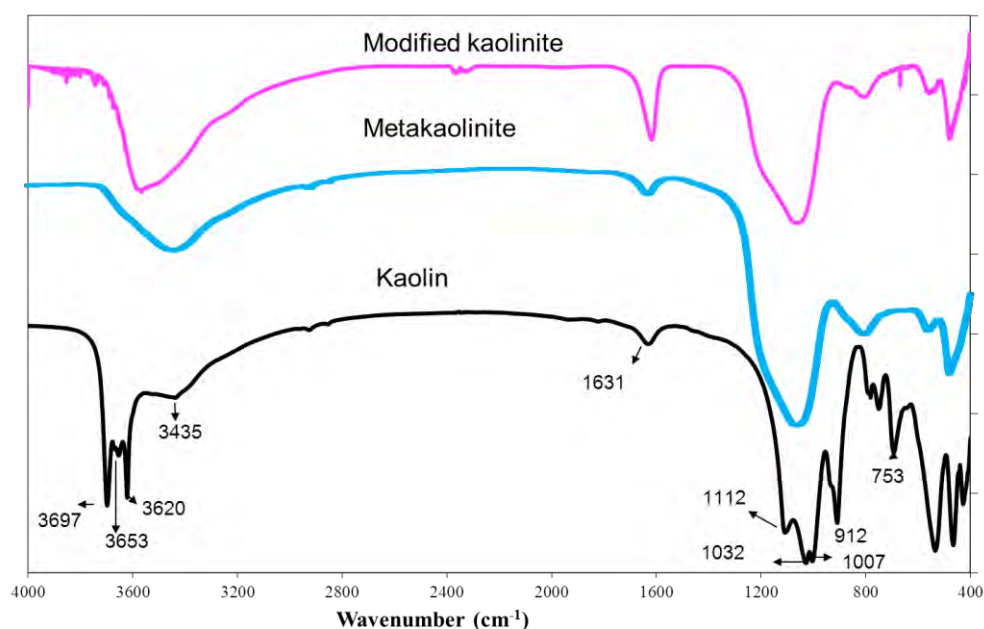
Figure 4.7: Spectra infra red of kaolin (K), metakaolinite (MKaol) and modified kaolinite (MK)

The morphological of kaolin from west Kalimantan, Indonesia shown at Figure 4.8. The SEM micrographs show a relatively homogeneous morphology consisting of small platelets of different sizes and pseudohexagonal or sometimes hexagonal, which is typical of kaolinite (Sengupta *et al*., 2008).

The characteristic randomly oriented platelets of kaolinite are stacked on one another to form large grains of a few micrometers size (Araujo *et al*., 2014). Modification metakolinite with zinc chloride is represented by the absence of Zn in modified kaolinite (Figure 4.9). From SEM-EDX analysis, the amount of zinc in modified kaolinite is 6.1%. In other words, almost 46.9% of the total zinc is impregnated onto the metakaolinite.
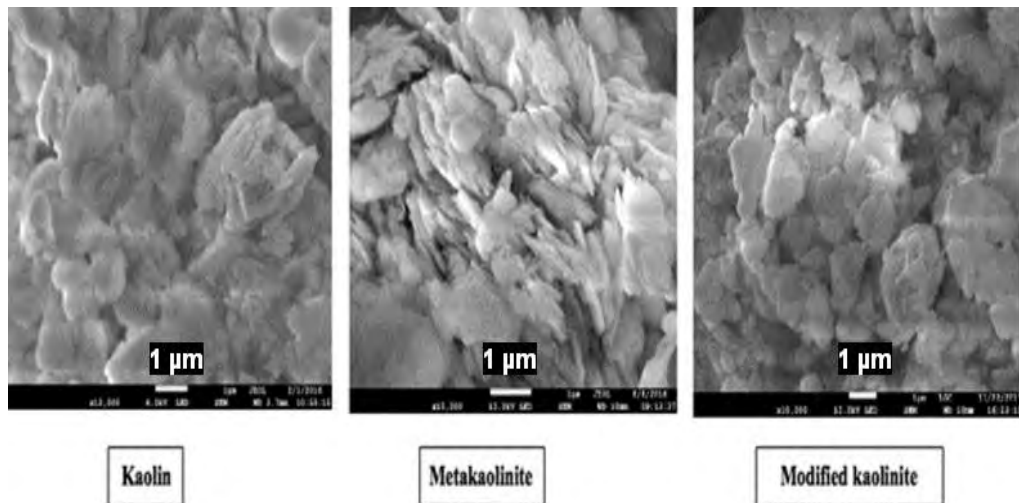
Figure 4.8: SEM micrographs of the kaolin, metakaolinite and modified kaolinite

Platelet of modified kaolinite is thicker than metakaolinite (Figure 4.8.b and c) and correlated to small increasing of surface area and decreasing of mean pore volume (Table 4.3). BET surface area analysis showed that heating kaolin decreased the specific surface area but increased the mean pore volume. According to BET surface area analysis (Table 4.3), calcination decreased the specific surface area, but increased total pore volume and mean pore volume. The surface area of kaolin decreased from 18.2 m^2/g into10.6

m^2/g during calcination at 600° for 10 h (Belver *et al*., 2002). While, Essomba *et al*. (2014) reported that calcinations kaolin at 700° for 6 h increased specific surface area and pore volume. The surface area to be 20.18 m^2/g and 33.83 m²/g, while pore volume from 0.0814 and 0.0935 cm^3/g, respectively. This present study was contrary with Essomba *et al* (2014) due to the chemical composition of natural kaolin was used. The major component is anatase associated with illite, quartz, kaolinite, and lepidocrocite. They studied the adsorption of cadmium onto metakaolinite and kaolinite and reported that the adsorption capacity of metakaolinite higher than kaolinite due the increasing the surface area and pore volume and hygroscopic property. In general, this research showed that modified kaolinite has higher mean pore volume, but lower surface area than kaolin.
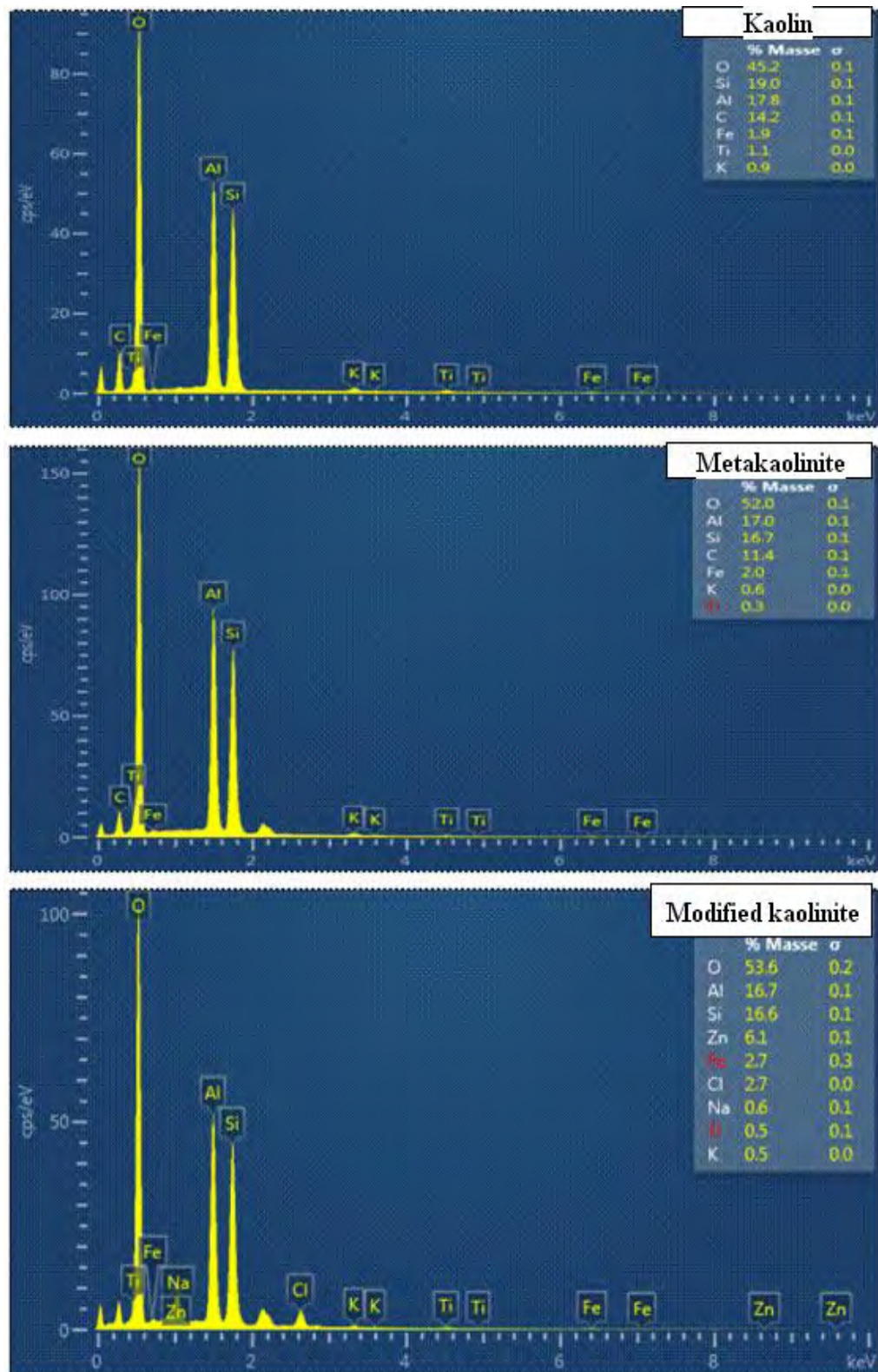
Figure 4.9: SEM-EDX of kaolinite, metakaolinite, and modified kaolinite

Table 4.3: BET surface area, total pore volume and mean pore volume of kaolinite

Samples	Surface area (m^2/g)	Total pore volume (cm^3/g)	Mean pore volume (nm)
Kaolin (K)	35.414	0.2006	22.660
Metakaolinite (MKaol)	23.193	0.2026	34.934
Modified kaolinite (MK)	23.805	0.1936	32.527

The thermo gravimetric analysis of kaolin shows two peaks, around 70°C and 490°C (Figure 4.10). The first one at 70°C, the loss mass of water molecules is 0.67%. The strong mass loss center at 490°C (11.52%) is due to dehydroxylation. Kaolin, metakolinite and modified kaolinite have total loss mass 12.19%, 1.05%, and 1.61 %, respectively.
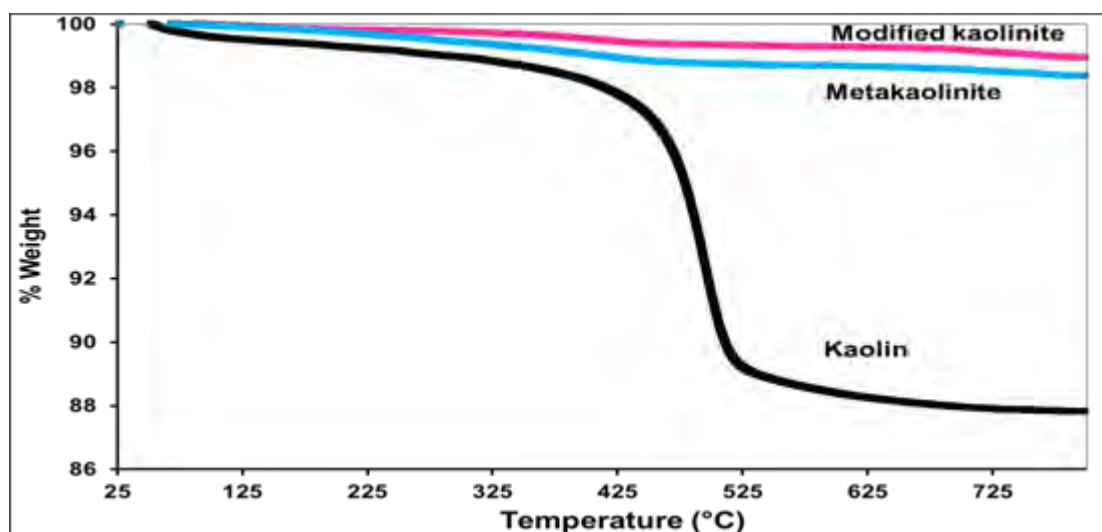
Figure 4.10: TGA of kaolin, metakaolinite and modified kaolinite

The permanent negative charge of kaolinite results from the isomorphic replacement of Si^{4+} in the silica tetrahedral sheet by Al^{3+} or the replacement of trivalent metal ions (such as Al^{3+}) by divalent ions (such as Fe^{2+} and Mg^{2+}) in the octahedral alumina sheet. Each substitution results in a single negative charge. Both the alumina sheet and the crystal edges have a pH-dependent variable charge caused by the protonation and deprotonation of surface

116

hydroxyl (SOH) groups (Srivastava *et al*., 2005). Metakaolinite is an unstable phase of kaolinite producted through dehydroxylation (Ilić *et al*., 2010). Dehydroxylation implies a reorganization and diffusion of hydroxyl group in the layer (Shvarzmana *et al*., 2003). Metakaolinite is more reactive than kaolin due to the structural disorder such as deformation of silica network or existence of 4-coordinated aluminium which is more reactive than 6-coordinated aluminium. The unstable metakaolinite, also still contains about 10% of the OH- groups initially present in the kaolin and is favourable to a surface dissolution of treated kaolin in cationic solution (Konan *et al*., 2009).The surface of the metakaolinite thus has some types of binding sites capable of interacting with Zn^{2+}. Essomba *et al*., (2014) studied the adsorption of cadmium onto kaolinite. They concluded that a chemisorption reaction or an activated process predominated in the rate-controlling step of the cadmium system. They also reported that metakaolinite had a higher adsorption capacity than kaolinite, due to its greater surface area, pore volume and hygroscopy.

Chai *et al*. (2017) reported that pH affected the mole fraction of hydrolyzed Zn^{2+} species relative to the total soluble metal concentration at 25°C. The main species present at pH values below 7 is $Zn^{2+.}$ Chai *et al*. also concluded that electronic attraction was the main mechanism of Zn^{2+} adsorption on kaolinite. Transition metals adsorb at permanent and variable charge sites. Sites with a permanent negative charge can undergo an exchange reaction with Zn^{2+} at high pH. At this present study, $ZnCl_2$ solution was allowed to interact with metakaolinite at pH= 6, therefore Zn^{2+} was probably adsorbed onto metakaolinite via a surface hydroxyl group (SOH).

$$SOH = SO^- + H^+ \qquad (4.3)$$
$$2SO^- + Zn^{2+} = Zn(SO)_2 + H^+ \quad (4.4)$$
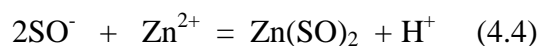
4. Characterization total acidity of kaolin

The acidic or base properties of solid surfaces are interesting aspects of the surfaces structure. The acidity of solid surface is an important aspect of ion exchange and catalysis (Alemdaroglu, 2001). Solid acids are classified according to acid strength, acid amount, acid-strength distribution, and type of acid site (Brőnsted or Lewis) (Matsuhashi and Arata., 2006).

Catalytic activity is determined by the chemical structure of the catalyst and its properties. There are some techniques to study the acidity of solid surface: titrations methods, the adsoprtion of basic probe molecule followed volumetrycally, gravimetrically, microcalometrically, with IR and NMR spectroscopy (Alemdaroglu, 2001). A method often used to determine the acidity of catalysts is gravimetric and IR spectroscopy with adsorbed ammonia (Nugrahaningtyas *et al*., 2017), pyridine (Zaki *et al*., 2001). Adsorption is a phenomenon involving the condensation of gas or liquid phase molecules onto the surface of solid. It is fundamentally an exothermic process. The heat generated in adsorption is measured as the heat of adsorption. The strength of interaction between an adsorbed molecule and the surface is reflected in the magnitude of the heat of adsorption. When there is an acid–base interaction between the adsorbed molecule and the surface, it is possible to evaluate the acid–base properties of the solid surface (Matsuhashi and Arata., 2006)

In particular in situ IR spectroscopy of adsorbed, usually used small base molecules, such as NH_3, pyridine (Py), CH_3CN, NO or CO molecules. The principle of the IR method is the characterization of surface acid sites via determination of changes conceded by the IR absorption features (frequency and intensity) of probe molecules there on adsorbed, and associated functional groups (e.g. OH-groups) of the surface. The acidity of the sites thus characterized can be determined by IR spectroscopic estimation of the isosteric heat of adsorption on each type of sites Py has been preferred as an IR probe base molecule for surface acid properties of metal oxides at room and higher temperature regimes, for it is (i) more stable and selective than NH_3, (ii) much

more strongly adsorbed than CO and CH_3CN and (iii) relatively more sensitive to the strength of Lewis sites than NO

The gravimetric analysis method was used to measure the total acidity. The method was carried out under standard pressure and temperature. At first, the porcelain crucible heated at 110°C for an hour. The crucible weight was labelled as W_1. Then 0.2 g of samples were placed into the porcelain crucible and heated at the same temperature for 1 hour. The weight of the porcelain crucible containing the sample was labeled as W_2. The crucible containing the sample was inserted into the desiccators. Then, soaked in 25 mL pyridine for 24 hour. The pyridine-adsorbed samples was dried at 130°C for 30 minutes to remove physically adsorpsed pyridine . The weight of porcelain was labelled as W_3. The pyridine was exposed to desiccators for 24 hours (before this treatment, the desiccators were made under vacuum conditions. This method modified methods from the reference ((Nugrahaningtyas *et al*., 2017; Joshi *et al*., 2011; Aboul-Gheit *et al*., 1997).

$$Total\ acidity = \frac{(W_3 - W_2)}{(W_2 - W_1).M} \qquad (4.5)$$

Where, M = molecular weight of pyridine (79.10 gram/mol)

The total acidity of clay from Congo Brazzaville and West Kalimantan Indonesia shown that relatif similar in total acidity around 0.5-0.6 mmol/g (Table 4.4). Calcined of nacritic decresed the acidity, but the total acidity increased twice after activated with amonium hydroxide. Modification kaolinite with $ZnCl_2$ enhanced the total acidity more then two fold. The increase of total acidity of modified kaolinite is due to the zinc presence in the modified kaolinite. The total acidity of modified kaolinite higher than nacrite active, and there is no correlation with the surface area.

Table 4.4: Total acidity of modified clay from Congo and
West Kalimantan Indonesia

Sample	Acidity (mmol/g)	Surface area (m^2/g)
Kaolin	0.60	35.414
Meta kaolin	0.89	23.193
Modified kaolin	1.95	23.805
Natural nacrite	0.55	30.548
Nacrite calcined	0.34	34.380
Nacrite actived	1.04	239.68

Figure 4.11 (a) display the FTIR spectra of the kaolin clay from Congo Brazaville after adsorbed pyridine. It has been long recognised that, in the complex mid-IR spectrum of adsorbed Py (whose 1700-1400 cm^{-1} range). There are two bands: centred at $\sim$1540 cm^{-1} (broad, and of m-intensity) and at $\sim$1445 cm^{-}1 (sharp, and of s-intensity) that are analytical of B-bound Py species (Py-B) and of L-bound py species (Py-L), respectively (Morterra *et al*., 2001). Acid Brönsted means that solid surface as a donor proton (H^+), while acid Lewis as a acceptor electron. There is no significant differencies at the 1700-1400 cm^{-1} range of spectra NN-Py, NC-Py, and NA-Py. But, after absorbed Py, Si-O band changed and bands at 1033 and 1007 cm^{-1} disappared (Figure 4.11b**).** Both of bands are correspond to the Si-O stretching in clay minerals (Gadsen, 1975). This spectra gave informatian that may be there is a weak interacting among NA and Py using proton (H) from Si-O-H and N in pyridine. At this case, NA as an acid Brönsted.
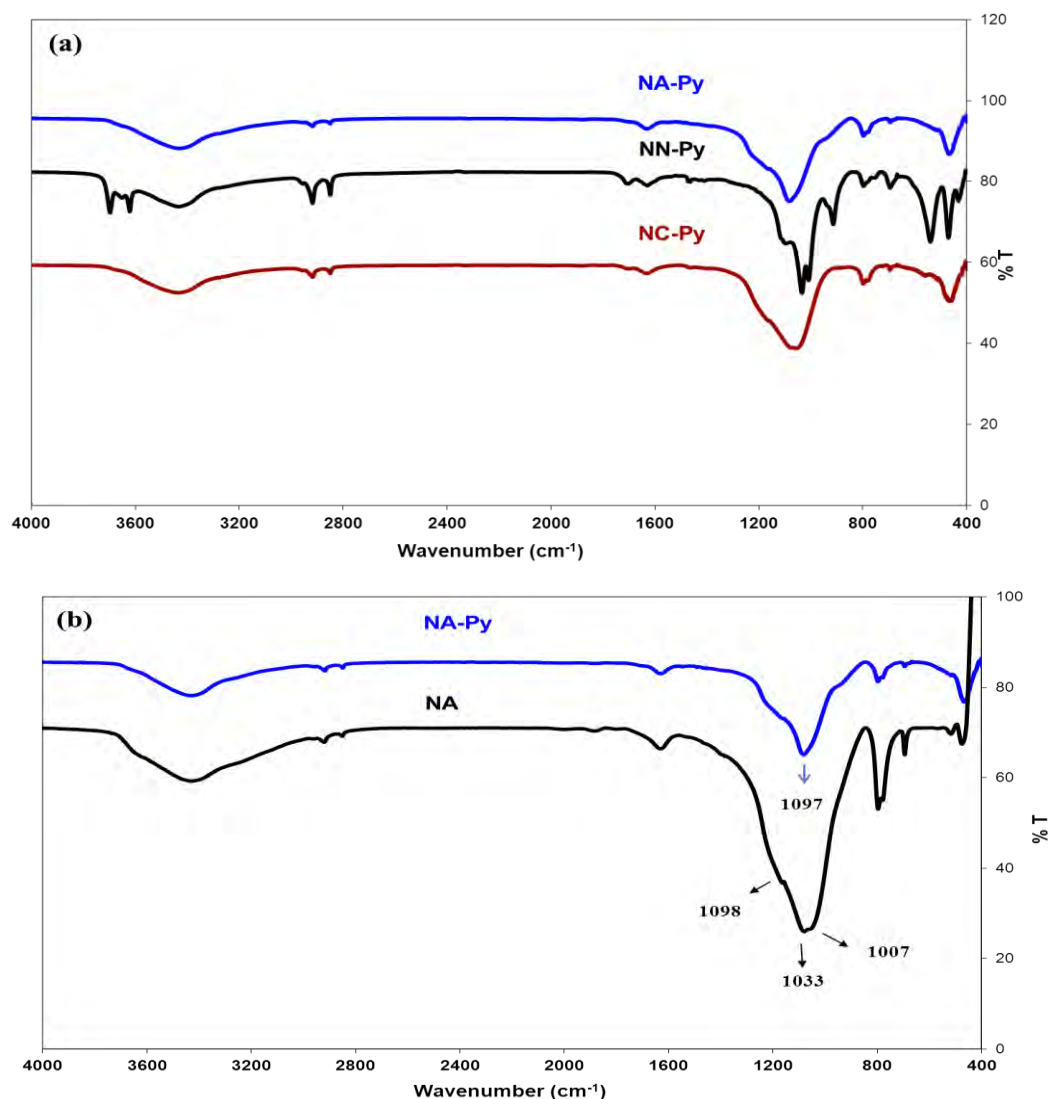
Figure 4.11: FTIR spectra of clay from Congo Brazzaville

Figure 4.12 (a) represented the spectra of kaolin and the modification after adsorbed Py. Lewis acid site at MK indicated by presence band at 1449 cm^{-1}. This Lewis acidity band close to 1450 cm^{-1} (Yurdakoç *et al*.,1999) or 1445 cm^{-1} (Morterra *et al*., 2001). Pyridine coordinated to the Lewis sites absorbed near at 1455 cm^{-1} and 1610-1625 cm^{-1} (Jankovic and Komadel, 2003). This research shown at 1608 cm^{-1}. The Lewis acid site came from Zinc in modified kaolinite. Pyridine influenced the Si-O site, it can be seen there are

two peaks at 1068 and 1044 cm^{-1}. At this spectra, we can see the –OH stretching of H_2O at 3450 cm^{-1}. It can be H_2O with interacted with Lewis site of pyridine molecule (Figure 4.12 b).
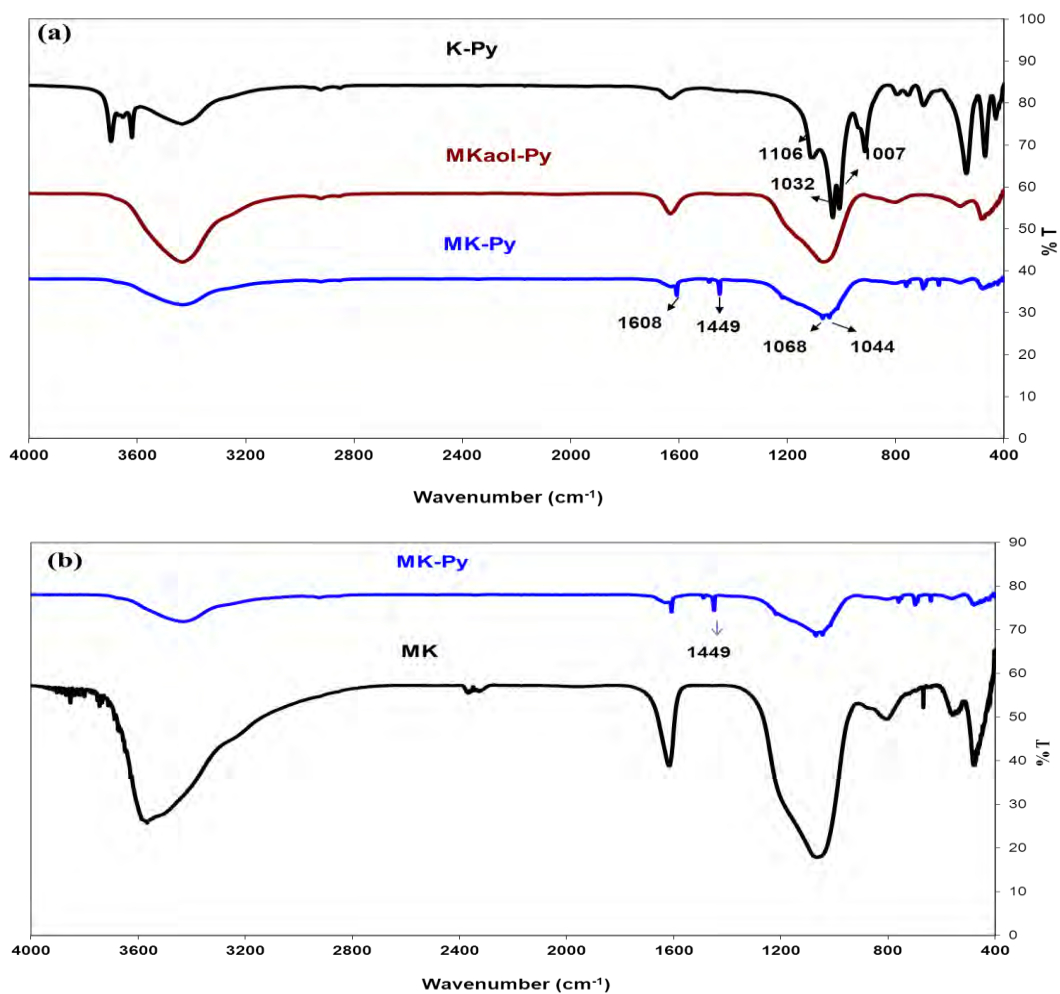
Figure 4.12: FTIR spectra of pyridine adsorbed on kaolin samples

5. Conclusions

Natural clay from Congo Brazzaville in Central Africa is a nacrite associated with quartz, anatase, and goethite. This natural clay has specific surface area 30.548 m^2g^{-1}. After activation with NH_4OH method, these values enhanced up to 239.68 m^2g^{-1}. Our study allowed us to define new method to obtain higher specific surface area of treated clay, which is calcined at 600°C for 6 hour, and continuing activating with 5 M ammonium hydroxide three times. The activated clay from Congo Brazzaville with high specific surface area can be used for adsorbents or support catalysts. This solid surface shows acidic sites of Brönsted.

From SEM, XRD and infrared analysis, we have observed that raw kaolin from West Kalimantan, Indonesia was kaolinite which associated with of quartz and small fraction of muscovite. Kaolinite has specific surface are 35.414 m^2g^{-1}. Modification of metakaolinite with $ZnCl_2$ decreased specific surface area but enhanced the mean pore volume of this solid material. Zinc as a Lewis acid site in modified kaolinite is identified at band 1449 cm^{-1}.

References

Aboul-Gheit, A.K. (1997) Reactivities of H-mordenite for the adsorption and oxidation of ammonia and pyridine. *Solid State Ionics*, **101-103**, 893-897.

Araujo, F.R., Baptitta, J.G., Marcal, L., Ciuffia, K.J., Nassara, E.J., Calefi, P.S., Vivcente, M.A., Trujilano, R., Rives, V., Gilc, A., Korilic, S., and De Faria E.H. (2014) Versatile heterogeneous dipicolinate complexes grafted into kaolinite: Catalytic oxidation of hydrocarbons and degradation of dyes. *Catalysis Today*, **227**, 105-115.

Aroke, U.O., El-Nafaty, U.A., and Osha, O.A. (2013) Properties and characterization of kaolin clay from Alkaleri, Nort-Eastern Nigeria. *International Journal of Emerging Technology and Advanced Engineering*, **3** (11), 387-392.

Alemdaroglu, L. (2001) Determination methods for the acidity of solid surfaces. *Communication of Faculty Science University Angkara: Series B*, **47**, 27-31

Belver, C., Banares., Munoz, M.A., and Vicente, M.A. (2002) Chemical activation of a kaolinite under acid and alkalinie conditions. *Chemical Materials*, **14**, 2033-2043.

Ben Haj, A.A., Ben Brahim, J., Ben Ayed, N., and Ben Rhaiem, H. (1996) Occurrance of nacrite in old Pb-Zn deposits from Northern Tunisia. *Clay Minerals*, **31**, 127-130.

Burhan, D. and Emin, C. (2009) Investigation of central Anatolian Clays by FTIR Spectroscopy. *International Journal of Natural and Engineering Sciences*, **3** (3), 154-161.

Chen, P.Y., Wang, M.K., and Yang, D.S. (2001) Mineralogy of dickite and nacrite from Norterm Taiwan. *Clay and Clay Minerals*, **49** (6), 586-595.

Buatier, M.D., Potdevin, J.L., Lopez, M., and Petit, S. (1996) Occurance of nacrite in the Lodève basin (France). *European Journal of Mineral*, **8**, 847-852.

Dedzo, G.K. and Detellier, C. (2014) Intercalation of two phenolic acids in an ionic liquid-kaolinite nanohybrid material and desorption studies. *Applied Clay Science*, **97-98**, 153-159.

Destiarti, L., Wahyuni, N., Prawatya, Y., and Sasri, R. (2017) Synthesis and characterization of mangan oxide coated sand from Capkala kaolin. International Conference on Chemistry, Chemical Process and Engineering, *AIP Conference Proceeding 1823*, **020023.**

Essomba, J.S., Ndi Nsami, J., Belibi Belibi, P.D., Tagne, G.M., and Ketcha Mbad, C.J. (2014) Adsorption of cadmium (II) ions from aqueous solution onto kaolinite and metakaolinite. *Pure and Applied Chemical Sciences*, **2**(1), 11-30.

Gadsen, J.A. (1975) *Infra red Spectra of Minerals and Related Inorganic Compounds*, Butterworths, London.

Hattab, A., Bagane, M., and Chlendi M. (2013) Characterization of Tataouinen's raw and activated clay. *Chemical Engineering & Process Technology*, **4** (4), 1-5.

Hiendro, A., Hadary, F., Rahmalia, W., and Wahyuni, N. (2012) Enhanced performance of bixin sensitized solar cells with activated kaolinite. *International Journal of Engineering Research and Innovation*, **4**, 40-44.

Ilić, B.R., Mitrović, A.A., and Miličić, L.R. (2010) Thermal treatment of kaolin clay to obtain metakaolin. Hemijska industrija, 64, 351–356.

Izci, E. (2014) Structural and dielectric properties of acid activated metakaolinite. Abstract for 11th GeoRaman International Conference, June 15-19 St. Louis, Missouri, USA.

Jaafar, N., Naamen, S., Ben Rhaiem, H., and Ben Haj, A.A. (2014) Elaboration of amorphous-clay hybrid: ($Al_2Si_2O_7$. 1/2 Li_2O) designed as a single ion conducting solid electrolyte for Li-ion batteries. *American Journal of Chemistry*, **5**, 1261.

Jaafar, N., Naamen, S., Ben Rhaiem, H., and Ben Haj, A.A. (2015) Functionalization and structural characterization of a novel nacrite-LiCl nanohybrid material. *American Journal of Analytical Chemistry*, **6**, 202-215.

Jaafar, N., Ben Rhaiem, H., and Ben Haj, A.A. (2016) Structural and electrochemical properties of cementitious and hybrid materials based on nacrite. Chapter 5:130-150.

Jankovic, L. and Komadel, P. (2003) Metal cation-exchanged montmorillonite catalyzed protection of aromatic aldehydes with AC_2O. *Journal of Catalysis*, **218** (1), 227-233.

Joshi, J., Mishra, M.K., and Srinivasarao, M. (2011) Silica-supported methanesulfonic acid - An efficient solid Brønsted acid catalyst for the Pechmann reaction in the presence of higher n-alkanes. *Canadian Journal of Chemistry*, **89** (6), 663-670.

Jozefaciuk, G. and Sarzynska, D.M. (2006) Effect of acid treatment and alkali treatment on nanopore properties of selected minerals. *Clays and Clay Minerals*, **54 (**2), 220-229.

Konan, K.L., Peyratout, C., Smith, A., Bonnet, J.-P., Rossignol, S., and Oyetola, S. (2009) Comparison of surface properties between kaolin and metakaolin in concentrated lime solutions. *Journal of Colloid and Interface Science*, **339**, 103–109.

Kumar, S., Panda, A.K., and Singh, R.K. (2013) Preparation and characterization of acid and alkali treated kaolin clay. *Bulletin of Chemical Reaction Engineering & Catalysis*, **8** (1), 61-69.

Matusik, J. and Matykowska, L. (2014) Behavior of kaolinite intercalation compounds with selected ammonium salts in aqueous chromate and arsenate solutions. *Journal of Molecular Structure,* **1071**, 52-59.

Matsuhashi, H. and Arata, K. (2006) Adsorption and desorption of small molecules for the characterization of solid acids. *Catalysis Surveys from Asia*, **10** (1), 1-7.

Mbaye, A., Diop, M.A., Miehe-Brendle, C.A.K., Senocq, J., Maury, F., and Francis. (2014) Characterization of natural and chemically modified kaolinite from Mako (Senegal) to remove lead from aqueous solutions. Clay Minerals, **49**, 527-539.

Md Saad, N.S.S., Nik Malek, N.A.N., and Chong, C.S. (2016) Antimicrobial activity of copper kaolinite and surfactant modified copper kaolinite against gram positive and gram negative. *Sciences & Engineering*, **78**, 127–132.

Morterra, C., Cerrato, G., Pinna, F., and Meligrana, G. (2001) Limits in the use of pyridine adsorption, as an analytical tool to test the surface acidity of oxidic systems: The case of sulfated zirconia catalysts. *Topics in Catalysis*, **15** (1), 53-60.

Murray, H.H. (2000) Traditional and new applications for kaolin, smectite, and palygorskite: A general overview. *Applied Clay Science*, **17**, 207-221.

Nugrahaningtyas, K.D., Hidayat, Y., Patiha., Prihastuti, N., Yelvi, B., and Nur Kalimah, R.U. (2017) Synthesis of the supported catalysts by co-impregnation and sequential impregnation methods. *IOP Conf. Series: Materials Science and Engineering*, **176**, 012024.

Prost, R., Dameme, A., Huard, E., Driad, J., and Leydecker, J.P. (1989) Infra red study of structural OH in kaolinite, dickite, nacrite, and poorly crystalline kaolinite at 5 to 600 K. *Clays and Clays Minerals*, **37** (5), 464-468.

Ruiz Cruz, M.D. (1996) Dickite, nacrite, and possible dickite/nacrite mixed-layers from the Betic cordilleras (SPAIN). *Clay and Clay Minerals*, **44** (3) 357-369.

Sengupta, P.C., Saiki, P.C., and Borthakur, P. (2008) SEM EDX characterization of an iron-rich kaolinite clay. *Journal of Scientific Industrial Research*, **67**, 812-818.

Shvarzman, A., Kovler, K., Grader, G.S., and Shter, G.E. (2003) The effect of dehydroxylation/amorphization degree on pozzolanic activity of kaolinite. *Cement and Concrete Research*, **33,** 405–416.

Shen, Z.Y., Wilson, M.J., Fraser, A.R., and Perason, M.J. (1994) Nacritic clay associated with the Jiangshan-Shaoxing deep fault in Zhejiang Province, China. *Clay and Clay Minerals*, **42** (5), 576-581.

Tonlé, I.K., Letaif, S., Ngameni, E., Walcarius, A., and Detellier, C. (2011) Square wave voltammetric determination of lead (II) ions using a carbon paste electrode modified by a thiol-functionalized kaolinite. *Electroanalysis*, **23**, 245-252.

Rahmalia, W. (2016) Paramètres de performances de photo-électrodes de TiO$_2$/kaolinite et d'électrolyte a base de carbonates biosourcés dans la cellule solaire sensibilisée par la bixine. Thèse, Institut National Polytechnique de Toulouse, France, 188 pp.

Vaculíková, L., Plevová, E., Vallova, S., and Kouttnik, I. (2011) Characterization and differentiation of kaolinites from selected Czech deposits using infra red spectroscopy and differential thermal analysis. *Acta Geodyamic and Geomaterials*, **8**, 59–67.

Vizcayno, C., Gutierrez, R.M., Castello, R., Rodriguez, E., and Guerrero, C.E. (2010) Pozzolan obtained by chemical and thermal treatments of kaolin. *Applied Clay Science*, **49**, 405-413.

Yurdakoç, M., Akçay, M., Tonbul, Y., and Yurdakoç, K. (1999) Acidity of silica-alumina catalysts by amine titration using Hammett indicators and FTIR study of pyridine adsorption. *Turkish Journal of Chemistry*, **23**, 319 -327.

Zaki, M.I, Hasan, M.A., Al-Sagheer, F.A., and Pasupulety, L. (2001) In situ FTIR spectra of pyridine adsorbed on SiO$_2$–Al$_2$O$_3$, TiO$_2$, ZrO$_2$ and CeO$_2$: General considerations for the identification of acid sites on surfaces of finely divided metal oxides. *Colloids and Surfaces A: Physicochemical and Engineering Aspects*, **190**, 261–274.

Zsirka, B., Horvath, E., Mako, E., Kurdi, R., and Kristof, J. (2015) Preparation and characterization of kaolinite nanostructure: Reaction pathways, morphology and structural order. *Clay minerals*, **50**, 329-340.

CHAPTER V

PHOTOSTABILTY OF CAROTENOIDS

CHAPTER V

PHOTOSTABILTY OF CAROTENOIDS

In this chapter, the photostability of carotenoids molecules with antioxidant and kaolinite will be studied. β-carotene and fucoxanthin are carotenoid molecules. We analyzed the effect of antioxidant types and the concentration. In the other subchapter, we studied the roll of modified kaolinite to improve the photostability of β-carotene.

1.   Introduction

The demand for β-carotene is increasing because this molecule can serve as a precursor of vitamin A, anticancer agent, nutraceutical, food colorant, in photoprotectant and cosmetic preparations, and for the prevention of age-related molecular degeneration (Palozza *et al*., 2004; Van Keulen *et al*., 2010; Wong *et al*., 2011; Freitas *et al*., 2015). These multiple uses are related to the antioxidant properties of carotenoids, which have a conjugated polyene structure that is highly effective for free radical and singlet oxygen scavenging (Siems *et al*., 2005; Mueller and Boehm, 2011). Natural β-carotene can be extracted from carrot (Suryana *et al*., 2013) or produced by biotechnological processes involving the use of filamentous fungi, yeasts, bacteria or microalgae (Thakur and Azmi, 2013). More than 85% the β-carotene available on the market is now produced through chemical synthesis (Van Keulen *et al*., 2010). β-carotene absorbs light at wavelengths of 415 to 508 nm. It could, therefore, potentially be used as a sensitizer in the dye sensitizer solar cell (DSSC) (Suryana *et al*., 2013). Photovoltaic based on organic semiconductors have been a dynamic area of research in the past twenty years ((Irimia-Vladu *et al*., 2012).

The π-conjugated molecules have emerged as potential candidates for applications in photonic devices due to its easy handling, environmental stability and structural flexibility (Vivas *et al*., 2011). Many organic materials have been shown to be biodegradable, safe, and nontoxic, including compounds of natural origin. Additionally, the unique features of such organic materials suggest they will be useful in biofunctional electronics. Such materials may lead to fully biodegradable and even biocompatible/ biometabolizable electronics for many low-cost applications (Głowacki *et al*., 2011).

The dye that is used as a photosensitizer plays an important role in the operation of DSSCs. The efficiency of the cell is critically dependent on the absorption spectrum of the dye and the anchorage of the dye to the surface of the semiconductor (El-Agez *et al*., 2012). Much work has been concentrated on organic dyes and organic metal complexes. Life time of the sensitizer is on the other challenging in this research field.

The long chain of alternating double bonds (conjugated) of β-carotene is responsible for its color. The axis of the carbon chain is curved, but the conjugated double bonds play an important role in ensuring that the molecule remains stable and rigid. Furthermore, the π-electrons in the chain are also delocalized, loosely held in place, and easily excited by low-energy visible light.

Baro and his colleagues studied the self-organisation of layers of β-carotene molecules on the surface of Cu111 and reported that β-carotene was a good electron transfer molecule. Within the multilayer structure, electrons flow easily from molecule to molecule within layers and to the layer below, due to the attractive interaction connecting the π-electron orbitals of adjacent molecules. They also reported the total length of the molecule to be 3.8 nm, with a height of 0.5 nm. A schematic molecular model of β-carotene is shown in Figure 5.1.
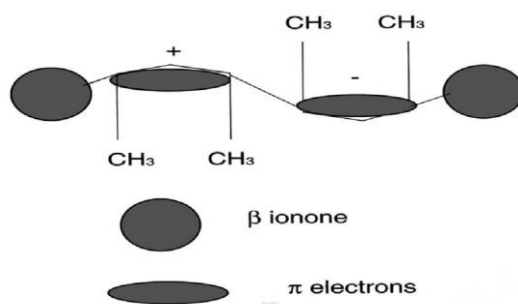
Figure 5.1: Schematic model of the β-carotene molecule, showing the curved backbone of the polyene chain, the methyl groups attached to it, the asymmetric corrugation attributed to π-electrons and the β-ionone rings (Baro *et al*., 2003).

β-carotene is sensitive to the light, temperature, and oxygen, and the mechanisms by which it is degraded have been investigated in many studies. The thermal degradation of β-carotene is responsible for the color change observed in pumpkin puree (Dutta *et al*., 2006). Visible changes in color have been shown to be a direct manifestation of changes in β-carotene content.

Following the absorption of ultraviolet (UV) light, organic compounds move from the ground state to singlet excited states, in which molecules may undergo intersystem crossing (ISC) to reach the triplet excited state or internal conversion (IC) back to the ground state. Thus, in terms of photostability, molecules displaying high rates of IC are the most desirable (Osterwalder and Herzog, 2009). Free radicals and photoproducts are generated by photochemical reactions in both the singlet and triplet excited states (Freitas *et al*., 2015). In previous studies, most of the photocatalytic products of β-carotene were identified in other systems, such as the thermal degradation of β-carotene. Esters, ketones, alcohols, and aldehydes are the principal degradation products of the photocatalytic degradation of β-carotene (Ge *et al*., 2015).

Some studies have focused on improving pigment stability. For example, the stability of curcumin was found to be increased by complexation with divalent ions such as Zn^{2+} (Zebib *et al*., 2010). The encapsulation of β-carotene

has been shown to improve its stability and facilitate the effective delivery of this molecule in various food systems and applications (Gul *et al*., 2015). The photostability of the natural pigment can be enhanced by the use of a photoprotector, such as gold nanoparticles (AuNPs), as demonstrated for chlorophyll-a (Chla). AuNPs bind to the nitrogen site of Chla, thereby preventing the binding of reactive oxygen species to this site, which is known to cause the photodegradation of Chla. The ability of AuNPs to protect Chla effectively, and not just through antioxidant properties, opens up new possibilities for increasing the photostability of other types of porphyrins. These molecules are widely used for industrial (in optoelectronic devices, such as OLEDs and photovoltaic devices) and medical (photodynamic therapy) applications (Barazzouk *et al*., 2012). The immobilization of bixin on activated kaolinite increased the photostability of pigment and this matrix has been used in DSSCs (Hiendro *et al.,* 2012; Rahmalia, 2016).The complexation of β-carotene with humic acid (hypothetically by π–π interaction) affects its chemical properties, increasing its photostability and water solubility (Martini *et al*., 2010).

Here, the stability properties of carotenoids molecules with two antioxidants and their electrochemical properties will be studied. The photostabilization of β-carotene also studied through the incorporation into the Zn-modified kaolinite.

2. Photostability of β-carotene

2.1 Photostability of β-carotene with antioxidant

Antioxidants are described as a substance that when present in low concentrations relative to the oxidable substrate significantly delayed or reduced oxidation of the substrate (Halliwell, 2006). Antioxidants sacrifice themselves by inhibiting further oxidation reactions that produce free radicals (Nimse and Pal, 2015). Free radicals are atoms, molecules or ions with unpaired electrons, which are highly active to chemical reactions with other

molecules. These free radicals are parts of groups of molecules called reactive oxygen species (ROS). ROS includes free radicals such as superoxide anion (O_2−•), perhydroxyl radical (HO_2•), hydroxyl radical (•OH), and other species such as hydrogen peroxide (H_2O_2), singlet oxygen ($^1O_2$), hypochlorous acid (HOCl).

Antioxidants may be molecules that can neutralize free radicals by accepting or donating electron(s) to eliminate the unpaired condition of the radical. The antioxidant molecules may directly react with the reactive radicals and destroy them, while they may become new free radicals which are less active, longer-lived and less dangerous than those radicals they have neutralized. They may be neutralized by other antioxidants or other mechanisms to terminate their radical status. Many antioxidants have aromatic ring structures and are able to delocalize the unpaired electron (Lü *et al*., 2010)

One antioxidant molecule can only react with a single free radical. Therefore, there is a constant need to replenish antioxidant resources endogenously or through supplementation. Many natural and synthetic compounds have been investigated over the decades for their efficacy to protect against oxidative stress (Heo and Jeon, 2009). Antioxidants from natural sources are preferred by consumers due to the concerns about the toxic and carcinogenic effects of synthetic antioxidants.

Plants contain a wide variety of antioxidant compounds, such as phenolics (phenol and polyphenols), flavonoids, carotenoids, steroids and thiol compounds (Lotito and Frei, 2006). Fucoxanthin is a major xanthophyll in algae which exhibits potential antioxidant activity (Sudhakar *et al*., 2013; Yan *et al*., 1999; Chuen-Fung, 2012; Waghmode and Kumbar, 2015; Zaelani. *et al*., 2015).

The other potential antioxidant compound is curcumin, the yellow pigment of turmeric and curry (Curcuma longa Linn) (Barzegar and Moosavi-Movahed, 2011). Curcumin has attracted much attention due to its significant medicinal potential and also its antioxidant properties (Silva-Buzanello *et al*.,

2016). The chemical structures of fucoxanthin and curcumin are shown in Figure 5.2.

Fucoxanthin (Kita *et al*., 2015)   Curcumin (Zebib *et al*., 2010)
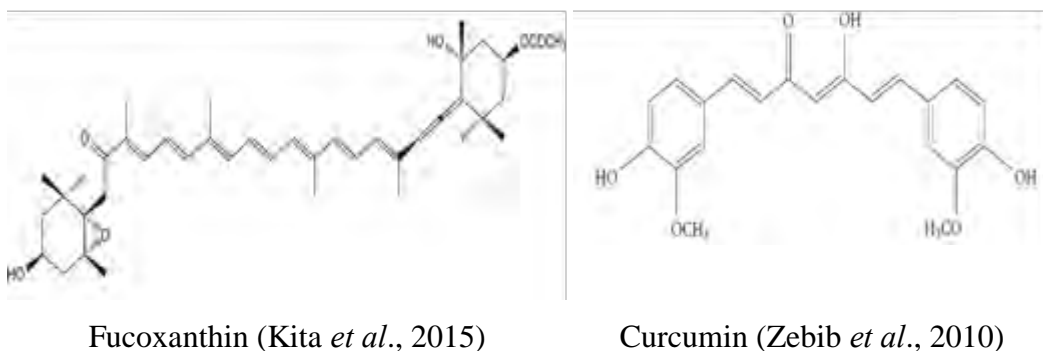
Figure 5.2: Molecular structure of fucoxanthin and curcumin

2.1.1   Characterization of biomolecules

Spectra infrared of biomolecules are represented at Figure 5.3. Identification of funtional group on those biomolecules refer to the Table 3.5 shown that β-carotene was aliphatic, while curcumin was aromatic. Band at 1530 cm^{-1} indicated the C=C aromatic, and band at 1439 cm^{-1} refer to C=C aliphatic. Fucoxanthin has C=O, identicated by the band at 1770 cm^{-1}. Those funtional groups related to the molecular structure.
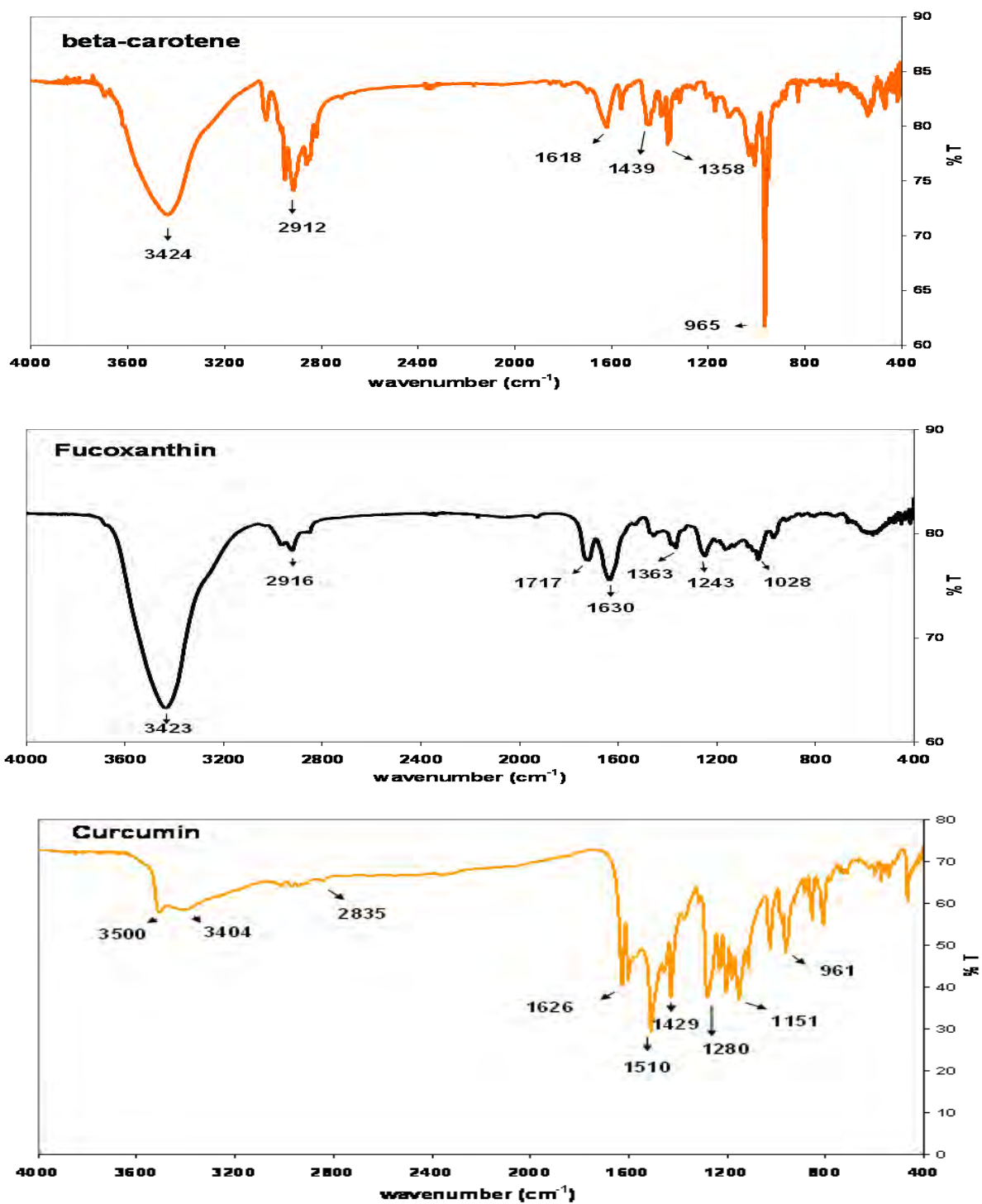
Figure 5.3: Spectra infrared of β-carotene, fucoxanthin, and curcumin

TGA/DTA analysis of biomolecules shown that β-carotene, fucoxanthin, and curcumin have total loss weight 90.34%, 97.54%, and 53.85%, respectively. β-carotene started loss its weight at 140°C (3.42%°) and continued at 317°C (86.92%),while fucoxanthin started at 40°C, and continued at 90°C, 220°C, and 340°C. The loss weight at each temperature were 10,85%, 8.31%, 21.83%, and 56.54%, respectively. Curcumin started loss its weight at 120°C (2.04%), then 290°C (28.91%), and finish at 370°C (22.89%). TGA of biomolecules are shown at Figure 5.4.

β-carotene   fucoxanthin   curcumin
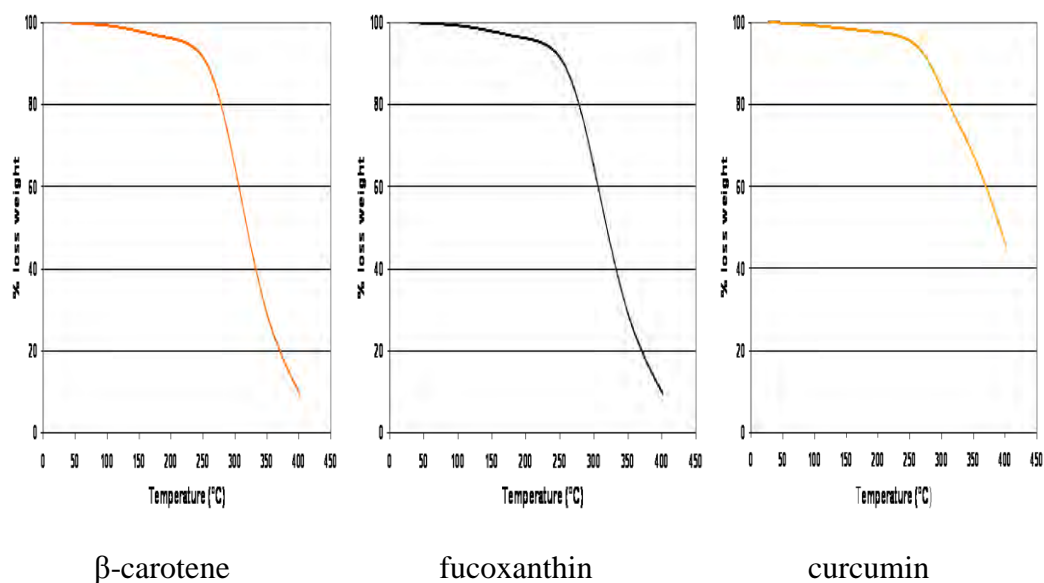
Figure 5.4 : TGA of biomolecules

2.1.2 Photostability and electrochemical properties of β-carotene with antioxidant

2.1.2.1 Photostability of β-carotene by coupling with antioxidant

The strong visible absorption band of carotenoid is known to be associated with the one photon allowing the $S_0(1^1A^{g-}) \rightarrow S_2(1^1B^{u+})$ transition, which can be determined from the maximum wavelength of the absorption spectrum (Christensen, 2004). The conjugated double bond system constitutes

the light absorbing chromophore of β-carotene (BC), fucoxanthin (Fx) and curcumin (Cur) resulting in the strong absorption band at 452 nm, 446 nm and 420 nm, respectively. For carotenoid, it is correlated to the electron transition in $\pi \rightarrow \pi^*$ (Bouchouit *et al*., 2010). Solvent influenced the maximum peaks of BC. In hexane solutions, its maximum peak at 448 nm (Chetkovic and Markovic, 2008). The absorbance maxima at 452 nm is closely to the isomer of BC, all-trans β-carotene at 450 nm (Henry *et al*., 1998). The others isomer, 13-cis β-carotene and 9-cis β –carotene identified at 446 and 447 nm, respectively. Absorption spectra of β-carotene, fucoxanthin and curcumin in acetone are represented in Figure 5.5.
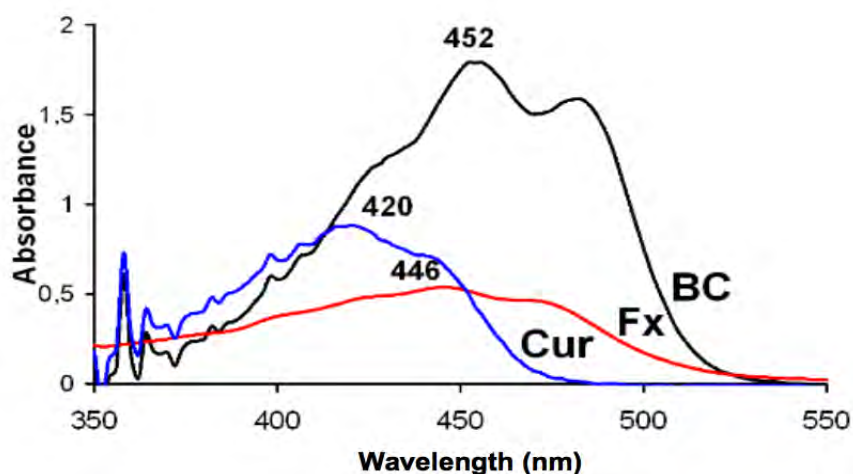
Figure 5.5:   Absorption spectra of β-carotene (BC), fucoxanthin (Fx) and curcumin (Cur)

Kinetic experimental data were presented in a dimensionlless form using A and A_0 variables, where A was the absorbance at time t and A_0 was the initial absorbance. Photodegradation and life-time of β-carotene was calculated using formula as described by Xiao *et al*. (2018).

The stability of β-carotene without irradiation were illusrated at Figure 5.6a and the photostability of β-carotene, fucoxanthin, and curcumin at Figure 5.6b, Figure 5.6c, and Figure 5.6d, respectively. The UV-irradiation of solution biomolecules in acetone were done at 0, 1, 3, 5,7 and 9 h. The life time of β-carotene (BC), fucoxanthin, and curcumin under UV- irradiation were 1.43 h,

17.72 h, and 14.44 h, respectively. This spectra shown that the life time of BC with UV 365 nm irradiation is short.
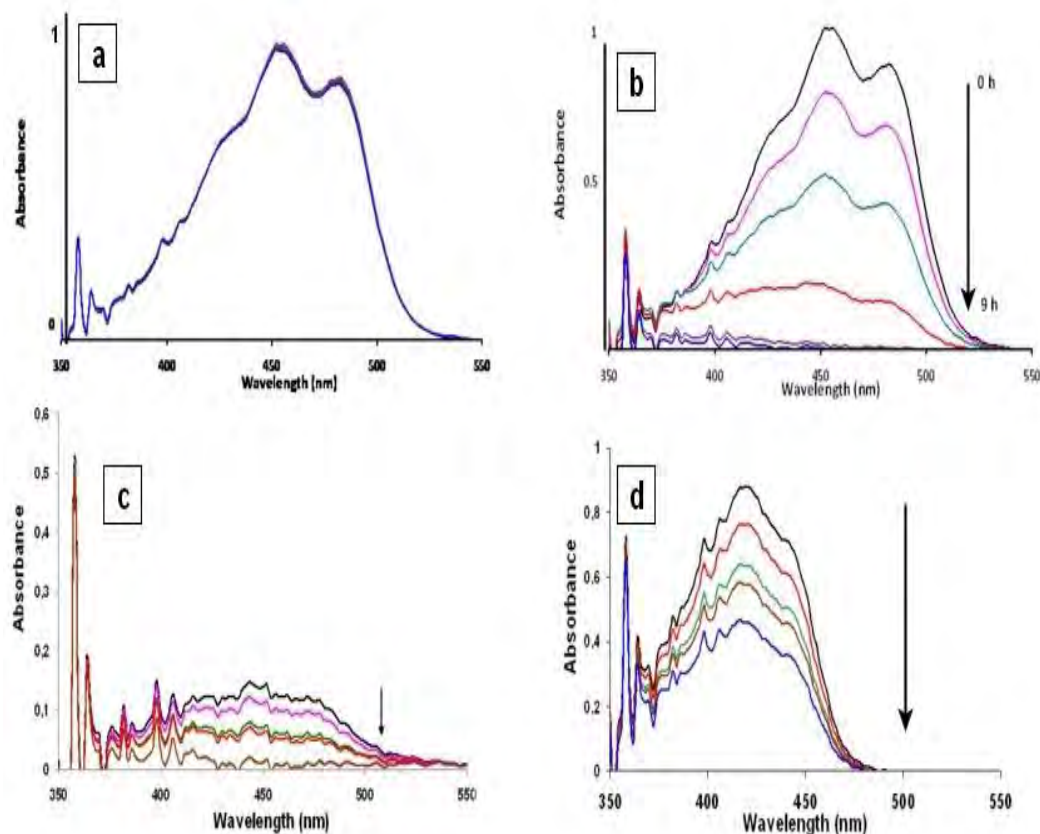
Figure 5.6: Stability of β-carotene without irradiation (a) and under uv light of β-carotene (b) fucoxanthin (c), curcumin (d)

Table 5.1 showed the first-order reaction data of β-carotene (BC), β-carotene/fucoxanthin (BC/Fx), and β-carotene/curcumin (BC/Cur). The antioxidant increased the photostability of β-carotene. Those antioxidants increased the half-life of BC from 1.43 to 3.55 and 6.35 hours by fucoxanthin and curcumin. The photoprotectan efficiency of antioxidant fucoxanthin and curcumin to the β-carotene at 5th hours were 10.17% and 11.91%, respectively, correlated to the more photostabilise of curcumin rather than fucoxanthin. Many antioxidants have aromatic ring structures and are able to delocalise the unpaired electron (Lü *et al*., 2010).

Table 5.1: First-order reaction data and photostablity of β-carotene and binary compound

Biomolecule	R^2	Degradation Rate constant, k (h^{-1})	Half-life time (h)	% photostability at 5th hours
β-carotene	0.99	0.4854	1.43	-
β-carotene/fucoxanthin	0.99	0.1951	3.55	10.17
β-carotene/curcumin	0.95	0.1091	6.35	11.91

There are two electrochemical analysis method using square wave voltametry and cyclic voltametry. From the square wave voltametry, anodic peak in the forward sweep is attributed to the one-electron oxidation of neutral species, whereas the cathodic peak in the back sweep originated from the one-electron reduction of the radical cation. The half-wave potentials of BC, Fx, and Cur were determined to be 0.522, 0.776 and 1.404 V, respectively. For β-carotene, this value is in aggrement with 0.54 V (Liu *et al*., 2000).

Table 5.2 showed the redox potential of β-carotene, fucoxanthin and curcumin. BC has two oxidation product at 0.522 (first oxidation stage) and 1.440 (second oxidation stage). The reduction product are identified at -1.802 and -1.719 V. The oxidation product of Fx are identified at 0.776; 0.962; 1,191; and 1.484 V, while the reduction at -1.443 and -0.803 V. Curcumin has one oxidation at 1.404 V and three reduction potentials at -1.765 V, -1.404 V and -1.184 V.

Table 5.2: Redox potential (V/SCE) of β-carotene, fucoxanthin and curcumin

Beta-carotene	Fucoxanthin	Curcumin	BC/Fx	BC/Cur
-1.802	-1.443	-1.765	-	-1.704
-1.719	-0.803	-1.404	-	-1.484
0.522	0.776	-1.184	-	-1.343
1.440	0.962	1.404	0.742	1.411
	1,191		0.869	
	1.484		0.996	
			1.477	

There is an significant changing in oxidation voltammograms of BC, BC/Fx and BC/Cur (Figure 5.7). The reduction voltammogram of BC/Fx is not good enough due to polimerization in Pt electrode. When Fx added to the BC, the second oxidation stage potential decresed significantly. New product arised at potential 0.742 V and other smaller potentials at 0.869 V; 0.996 V and 1.477 V which are correspond to the redox potentiol of Fx. This analysis shown that Fx in BC reduced the intensity of the second oxidation product of BC. Peak current is directly proportional to concentration (Kissinger, 1983). Curcumin protect β-carotene by reduce the second oxidation stage as same as fucoxanthin as seen that intensity (current) at 1.411 V decreased significantly. Effect antioxidant also to the potential of the binary compound. The BC/Cur decreased potential of the first oxidation stage from 1.440 V to the 1.411 V whic is contradiction with BC/Fx. The potential at the first oxidation stage of BC/Fx increased into 1.477 V.
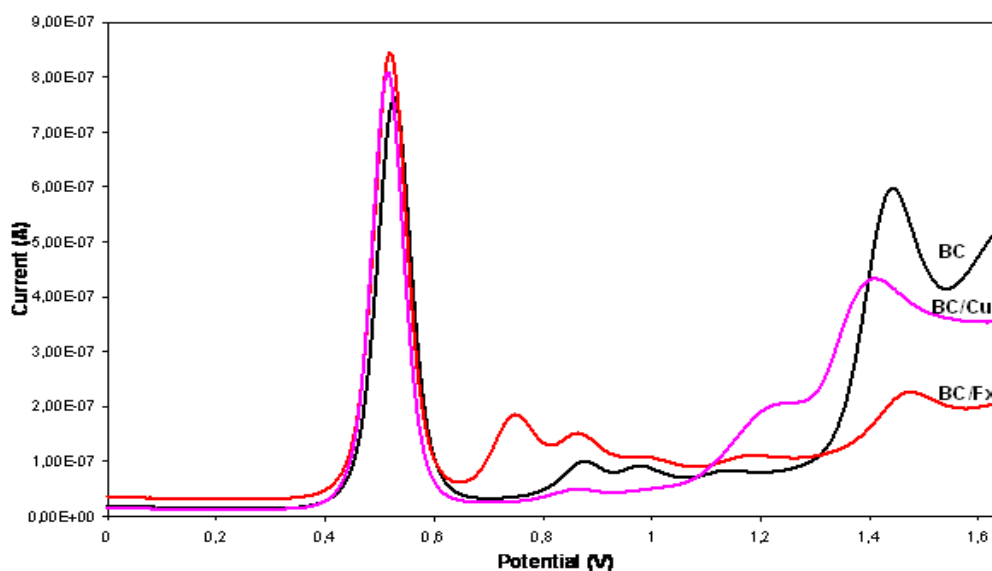
Figure 5.7: Oxidation voltammogram of carotene and BC/Fx and BC/Cur

Fucoxanthin and curcumin reduced the rate of forming reaction of the second oxidation stage from the first oxidation stage of β-carotene. The carbonyl in molecular structure of fucoxanthin and curcumin facilitate energy transfer by giving greater stability because they have less diradical character, thus transformation between excited states is easier (Delgado-Vargas *et al*., 2000). The phenolic hydroxyl group in curcumin gaved the more delocalized electron. Here, antioxidants sacrifice themselves by inhibiting further oxidation reactions that produce free radicals (Nimse and Pal, 2015).

The influence of curcumin to the β-carotene is more clearly by evaluated the reduction potential. BC has two reduction potential at -1.719 V and -1.802 V. The reduction potential of BC/Cur are -1.343 V ; -1.484 V and -1.704 V, respectively (Figure 5.8). Curcumin caused potential at -1.802 disappered, and two potentials arised at -1.343 V and -1.484 V. In another words, curcumin decreased the reduction energy level of the binary biomolecule. The ability of curcumin to protect β-carotene also by eliminate the reduction product of the binary compound at higher energy.
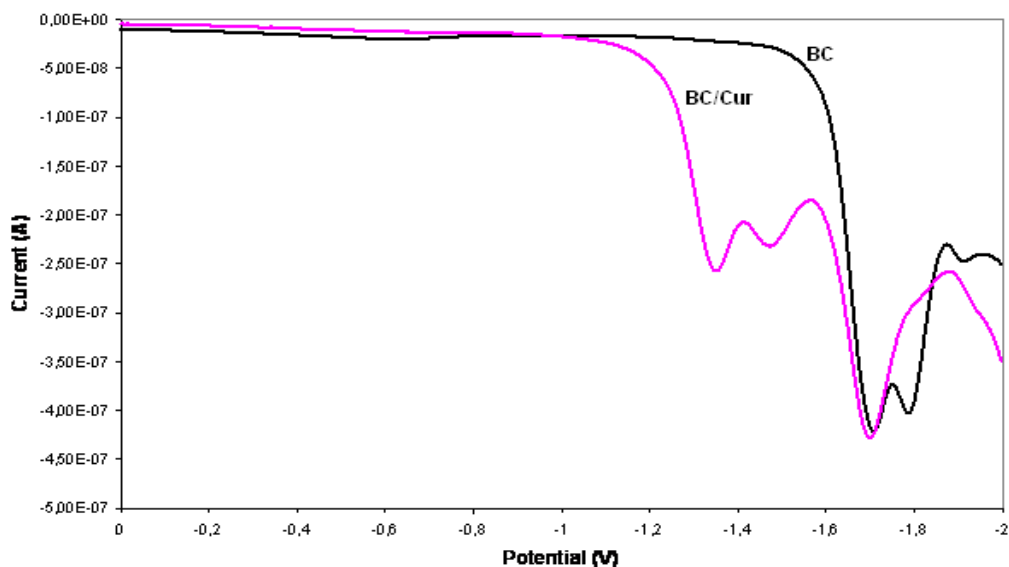
Figure 5.8: Reduction voltammogram of β-carotene and carotene-curcumin

Base on CV analysis, it suggested that there are two effect antioxidant to the BC: (1) reduce the intensity of first oxidation product of BC and (2) reduce/increase the oxidation-reduction potential. The more photostability BC by curcumin, due the more stabilize of Cur by reduce redox potential (rate formation of first oxidation-reduction product) rather than reduce the intensity/concentration of first oxidation product. The CV data in aggrement with kinetic analysis and photostability of the binary molecule that curcumin give the higher effect than fucoxanthin in enhancing the photostability of β-carotene.

2.1.2.2 Electrochemical properties of β-carotene with antioxidant

Electrochemical gap is one the important factor that to consider in using organic molecule in photo-optonic such as solar cells. Cyclic voltammetry (CV) is a methodology widely used by OPV researchers to obtain the HOMO and LUMO levels (Bard and Faulkner, 2001). Figure 5.9 represented the cyclic voltammograms of β-carotene (BC), fucoxanthin (Fx), and curcumin (Cur). The β-carotene has $E_{onset.ox}$= 0.45 V/SCE, and $E_{onset.red}$= -1.55 V/SCE. The $E_{onset.ox}$ and $E_{onset.red}$ for fucoxanthin and curcumin are 0.72; -1.30 and 1.40; -1.18 V/SCE, respectively. From equation 2.1, the electrochemical gap of β-carotene, fucoxanthin, and curcumin are -2.04; -2.02; and -2.58 eV, respectively. From CV analysis, we know that β- carotene and fucoxanthin almost have the same electrochemical gap. It was predicted from the absorption spectra that decribed before (Figure 5.5), both of them were carotenoid.
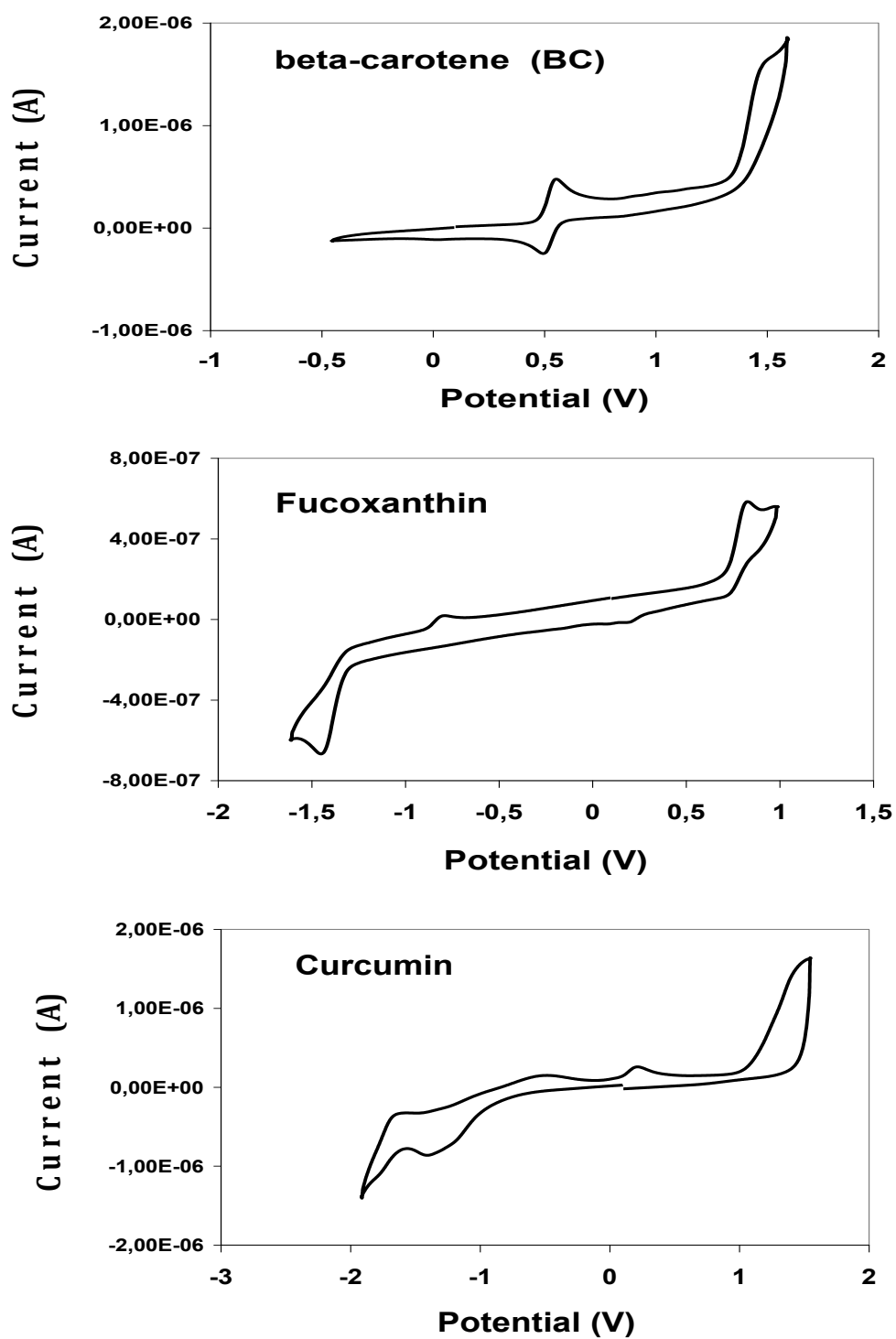
Figure 5.9: Cyclic voltammograms of β-carotene (BC), fucoxanthin (Fx), and curcumin (Cur)

142

Binary compound of β-carotene with antioxidant, BC/Fx and BC/Cur have $E_{onset.ox}$ and $E_{onset.red}$ 0.45; -1.30 and 0.36; -1.25 V, therefore the electrochemical gap of them are -1.75 and -1.61 eV, respectively (Figure 5.10). Antioxidants decreased the electrochemical gap of β-carotene. Curcumin reduced the electrochemical gap of β-carotene about 0.43 eV, while fucoxanthin 0.29 eV.
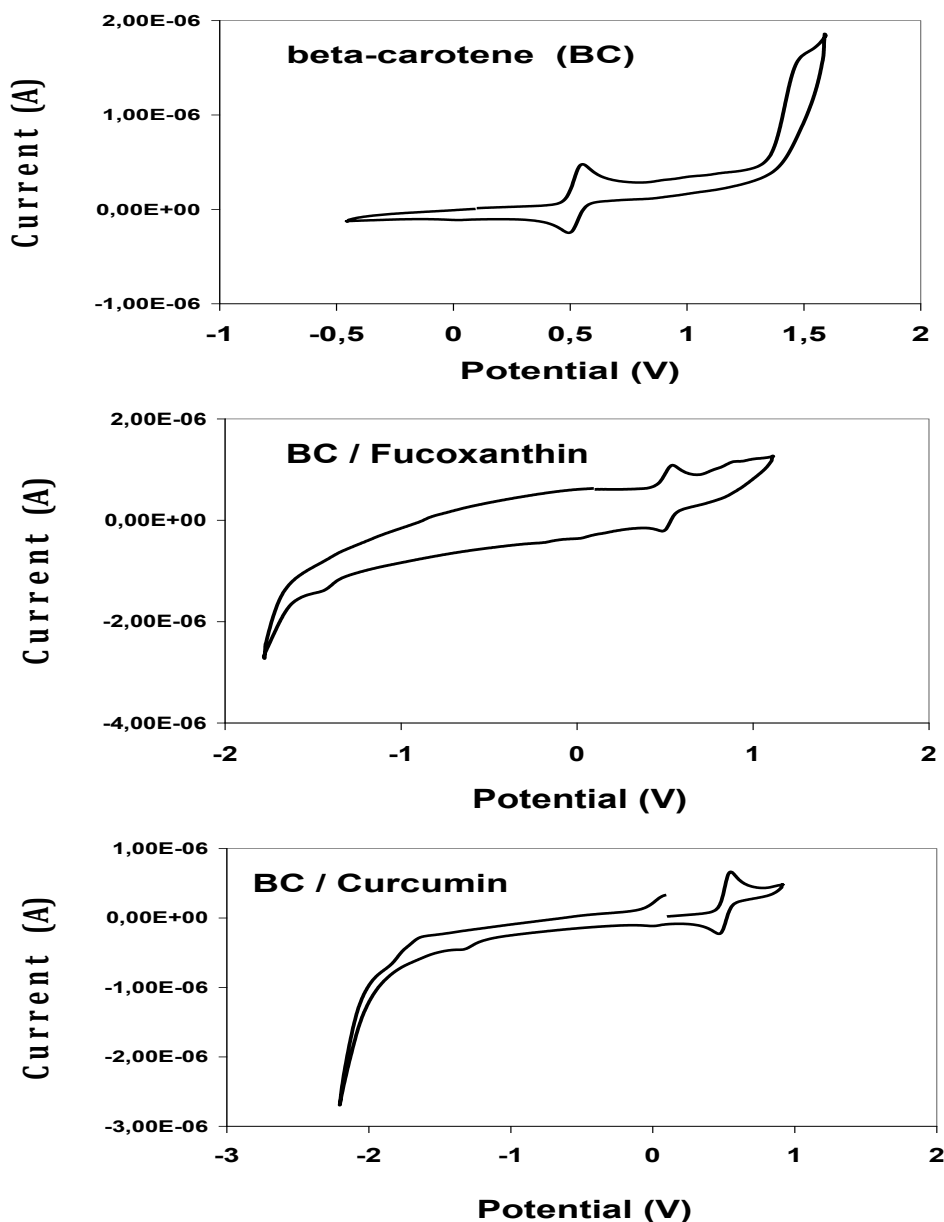
Figure 5.10: Cyclic voltammogram of BC, BC/Fx and BC/Cur

143

The values of anodic peak current (ipa) and cathodic peak current (ipc) in cyclic voltammogram characterised   simple reversible (fast) couple (Kissinger, 1983). Oxidation potential of β-carotene is reversible, but not for the reduction. Redox potential of BC/Cur is irreversible. Binary of BC/Fx has oxidation potential reversible but the reduction was nonreversible. Fucoxanthin can keep the reversibility of the first oxidation stage of β-carotene. For photo-electronic application, the reversibility of the first oxidation is very important, due to the capability of the electron transfer by the material (Barazzouk *et al.*, 2012; Sworakowski *et al.*, 2016).

CV analysis also can be used for determining energies of ionized levels in molecular solids. Table 5.3 represented the HOMO-LUMO energy level, solid-state ionization energy and solid-state electron affinity of fucoxanthin, curcumin, β-carotene and the mix biomolecule. The correlation between the electrochemical oxidation potential ($e\pi_{ox}$) and the solid-state ionization energy (I_c) and relation between the electrochemical reduction potential ($e\pi_{red}$) and the solid-state electron affinity (A_c) can be written as (Sworakowski *et al.,* 2016):

$$I_c = (1.15 \pm 0.09) \times (e\pi_{ox}) + (4.79 \pm 0.07)eV \qquad (5.1)$$

$$A_c = (1.18 \pm 0.05) \times (e\pi_{red}) + (4.83 \pm 0.10)eV \qquad (5.2)$$

Table 5.3: HOMO-LUMO energy and solid-state ionization and electron affinity

Biomolecule	HOMO (eV)[a]	LUMO (eV)[a]	I_c (eV)[b]	A_c (eV)[b]	Electrical gap (eV)[b]	Electrochemical gap (eV)[c]
Fx	-6.11	-4.09	-5.50	-3.30	2.20	2.02
Cur	-6.79	-4.21	-6.40	-3.44	2.96	2.58
BC	-5, 84	-3,84	-5,31	-3,00	2,31	2,04
BC/Fx	-5,84	-4,54	-5,31	-4,30	1,01	1,75
BC/Cur	-5,75	-4,50	-5,20	-4,41	0,79	1,61

[a]Estimated by CV with Fc/Fc$^+$ at 5.39 eV below vacuum using equation 2.9 and 2.10 [b]Estimated by CV using equation 5.1 and 5.2. [c]Measured in cyclic voltammetry in DCM solution with TBAPF$_6$.

The electrochemical and electrical/transport gap of the binary compound are lower than the BC only. Curcumin effect to the those properties of BC higher than fucoxanthin as the same as the photostability effect.

2.2 Photostability of β-carotene with fucoxanthin

The information about λ_{max} shifts is particularly important if we want to understand the modification of the $S_0 \rightarrow S_2$ transition energies of BC as sensitiser. These HUMO-LUMO (highest unoccupied molecular orbital- lowest unoccupied molecular orbital) energy changes provide important information about the various physical and organic reaction of BC. The sensitising dye which has the higher absorption coefficient and lower $S_0 \rightarrow S_2$ transition energy will give higher photoelectric conversion efficiencies of dyes sensitized solar cells (Ruiz-Anchondo *et al*., 2010). The spectra pure of BC and BC/Fx with concentration variation of Fx is shown in Figure 5.11.
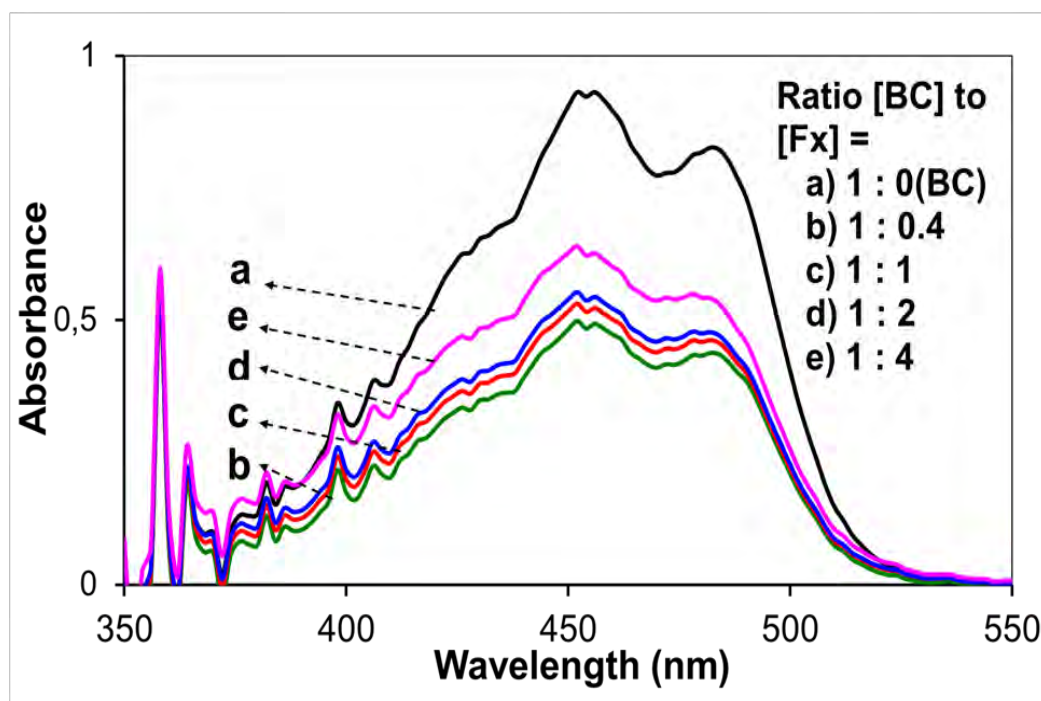
Figure 5.11: Spectra of β-carotene with different concentration of Fx

The solution of BC/Fx decreased the absorbance intensity at 452 nm, but did not changed the pattern of UV spectra. The λ_{max} of the mix solution of BC and Fx was still around 452 nm. The fucoxanthin solution did not give effect toward the energy transitition of BC, because both of them are caretonoids which have similar polarity and absorbted in the same wavelength range (Bouchouit *et al*., 2010). At this binary solution, BC remain at the original isomer, all-trans β-carotene.

The molecular hypochromic effect has been explained in terms of absorptive distortions due to molecular dipolar interactions or the physical overlap of π orbitals of stacked chromophores (Nonoyama *et al*., 2011).The higher the concentration of Fx, the lower the decreased of absorbance at λ_{max}. This hypocromic is caused by interference of two compound which correlated to absorbance intensity as we seen at Figure 5.11. The absorbance of BC almost three fold than Fx.
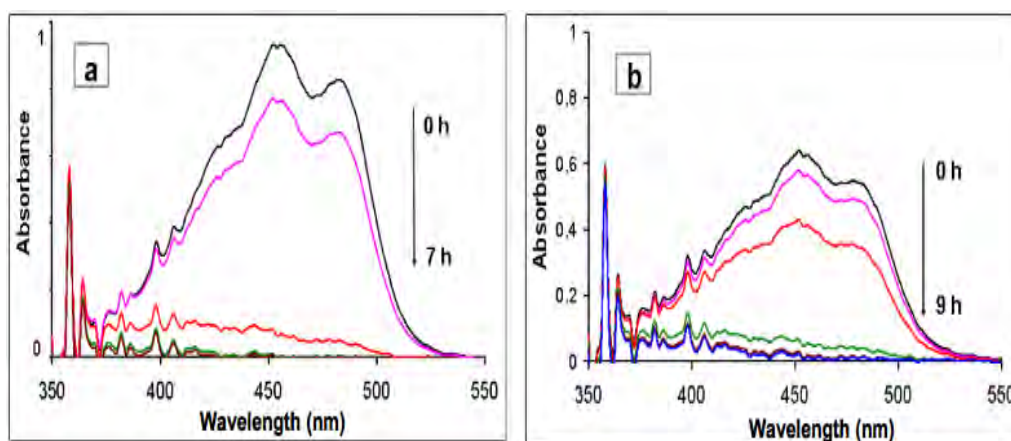
Figure 5.12: Spectra of BC (a) and and BC-Fx (b) under UV-irradiation

Spectra of BC and BC/Fx after irradition represented at Figure 5.12 and their photodegradation are illustrated at Figure 5.13. The degree of the photodegradation is expressed as the change in the main absorption band of β-carotene at 452 nm. The β-carotene concentration was relatively unchanged after being stored for nine hours at room conditions (temperature 25°C). Under irradiation, the absorbance of β-carotene (Figure 5.13a) decreased significantly

at 3 h, with absorbance reaching levels close to zero at 7 h. By contrast, the absorbance of Fx (Figure 5.13b) remained high for three hours, even under irradiation. After 3 h of irradiation, BC degraded only 41% in the presence of Fx (5 ppm). Fucoxanthin, therefore increased the photostability of β-carotene
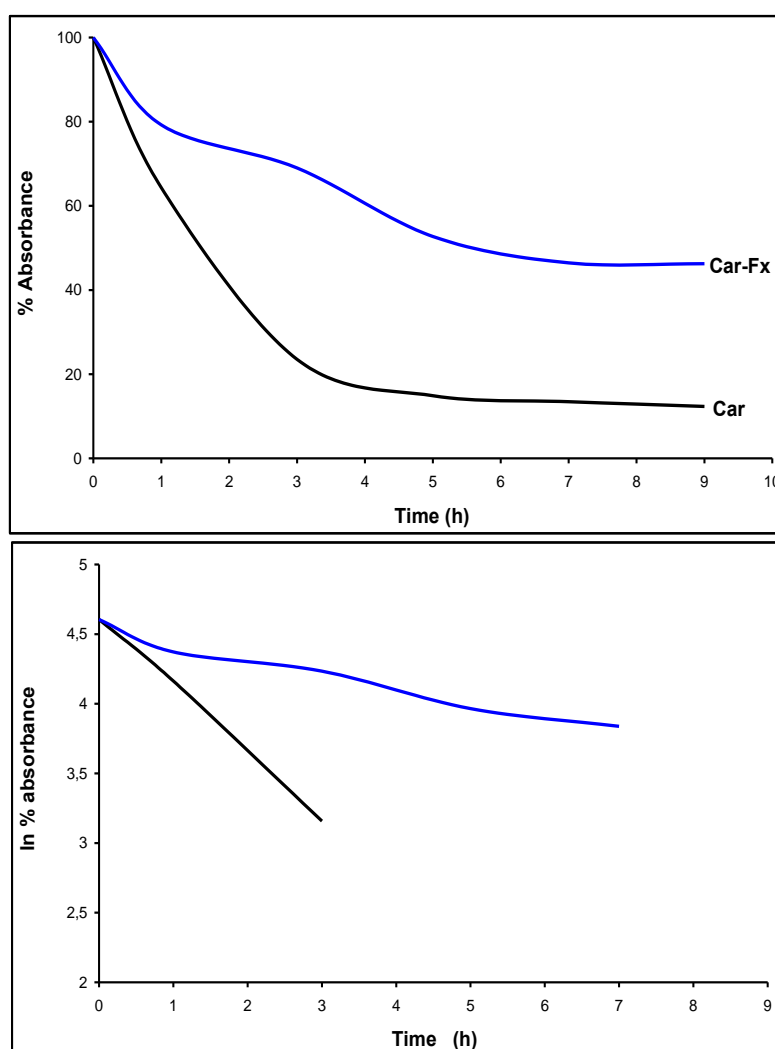
Figure 5.13: The photodegradadation of β-carotene in acetone solution (2.5 ppm) in the absence and presence of with fucoxanthin 5 ppm as function of irradiation time with UV light 365 nm (a) and their first order photodegradation kinetics (b)

The first-order reaction data and the protection efficiency provided of antioxidant Fx to the BC is represented in Table 5.4. The photodegradation of BC follows a first-order kinetic with the half-life times 1.43 and 6.96 hours in

the absence and presence of Fx, respectively, indicating an improvement in the photostability of BC by Fx.

Table 5.4: First-order reaction data of BC and BC-Fx

Ratio [BC] to[Fx]	R^2	Degradation rate constant, k (h^{-1})	Half-life (h)	% photostability at 5th hours
1 : 0 (BC)	0.99	0.4854	1.43	-
1 : 0.4	0.97	0.2089	3.32	4.78
1 : 1	0.99	0.1951	3.55	10.17
1 : 2	0.97	0.0995	6.96	38.56
1 : 4	0.93	0.1502	4.61	75.99

Futher, it is found that degradation of BC is dependent upon the Fx concentration. That is, the higher the concentration of Fx, the greater is the protoprotection provided to BC against UV-irradiation. In contrast with stability of BC which is represented with the half-life time. The maximum Fx concentration was added to BC was 2 times than BC concentration. If the Fx concentration increased, the half-life time of BC decreased. One antioxidant molecule can only react with a single free radical (Heo and Jeon, 2009). If the Fx concentration excess (BC : Fx = 1 : 4), the half-life time of BC-Fx represented the life time of Fx excess due to damage of BC.

Photodegradation of BC (half-life time of BC) represented the existence of BC molecule, while photostability is designed the capability of Fx to protect BC from photodamage. Base on this data, we concluded that Fx increased the half-life time of BC. The ratio maximum concentration BC to Fx was 1:2 and enhanced the stability of BC almost 5 fold. The percentage photostability by Fx (provide the BC) at 5th hours at this composition was 38.56%.

2.3.1. Photostability of β-carotene with curcumin

The λ_{max} of BC/Cur blue-shifted to the lower wavelength or higher energy with the increasing of curcumin concentration (Figure 5.14). This hypsocromic shift from 452 to the 446, 444, and 422 nm, respectively. At low

concentration of curcumin, the shifting wavelength maxima of BC/Cur from 452 to the 446 nm was observed. It indicated Cur caused isomerisation of BC from all-trans β-carotene to 13-cis β-carotene or 9-cis β –carotene (Henry *et al*., 1998). The blue shift was caused by some factors i.e. conjugation and polarity of solvent. When the curcumin concentration was increased (Figure 5.14c and Figure 5.14d), curcumin molecule was dominant. The blue shifted was caused by the less conjugation of curcumin structure in comparison to β-carotene structure (Reichardt, 1994).

The higher the concentration Cur, the λ_{max} of the mix solution (BC-Cur) shifted toward to lower wavelenght or higher energy. This shifting tend toward to the the λ_{max} of pure Cur (Figure 5.14d and Figure 5.14e) with the increasing of Cur concentration. It means, in this binary solution, the Cur molecule was dominant compare to the BC.
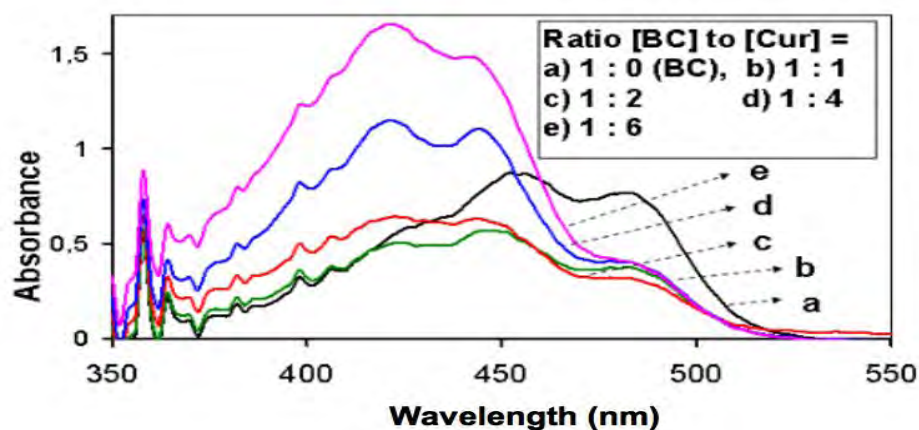
Figure 5.14: Spectra of β-carotene with variation of curcumin concentration

After 3 hours of irradiation, BC/Cur degraded only 31%, while after 5 h almost 98% of BC degraded in the absence of Cur compared to the 89% photodegradation (at 452 nm) in the presence of Cur (Figure 5.15). In other words, a protection of 11% of BC has been provided by 5 ppm of Cur. The photodegradation of BC/Cur also follows a first order kinetic with the half-life 14.81 hours (Table 5.5). The photostability enhancement of BC by Cur more than 10-fold.
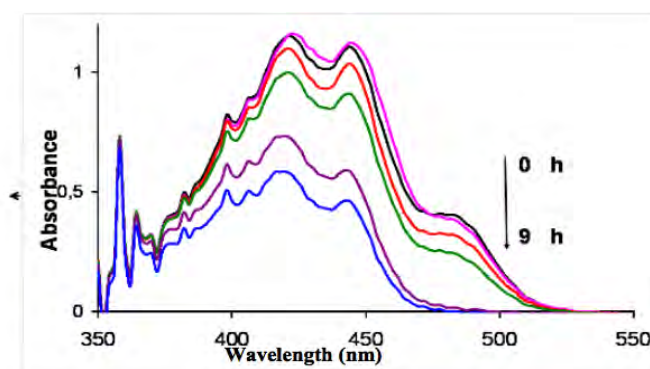
Figure 5.15: Spectra BC/Cur under UV-irradiation

Table 5.5: First-order reaction data of BC-Curcumin

Ratio [BC] to[Cur]	R^2	Degradation rate constant, k (h^{-1})	Half-life time (h)	% photostability at 5th hours
1 : 0 (BC)	0.99	0.4854	1.43	-
1 : 1	0.95	0.1091	6.35	11.91
1 : 2	0.99	0.0718	9.65	58.12
1 : 4	0.97	0.0468	14.81	88.13
1 : 6	0.99	0.0664	10.44	115.36

In view of this, the antioxidant increased the photostability of β-carotene. These antioxidants increased the half-life of β-carotene. The percentage photostability by the antioxidant of fucoxanthin and curcumin to the β-carotene (ratio BC to the antioxidant = 1:2) were 38.56% and 58.12%, respectively. The more stabilise of BC by curcumin due to the more capability of curcumin to absorpted UV-light rather fucoxanthin.

To analyzed the existance of curcumin in mix solid, the FTIR analyzed was done. Spectra IR of solid of β-carotene and curcumin respresented at Figure 5.16**.** The significant changing can be confirmed at band range from 800-1620 cm^{-1}**.** This solid consist of β-carotene and curcumin. It confirmed by the appearance band at 1429 cm^{-1} which is characterictif for β-carotene, and band at 1510 cm^{-1} from C=C aromatic of curcumin. There is no significantly differences if curcumin of concentration was increased, as we can see at Figure 5.17**.**
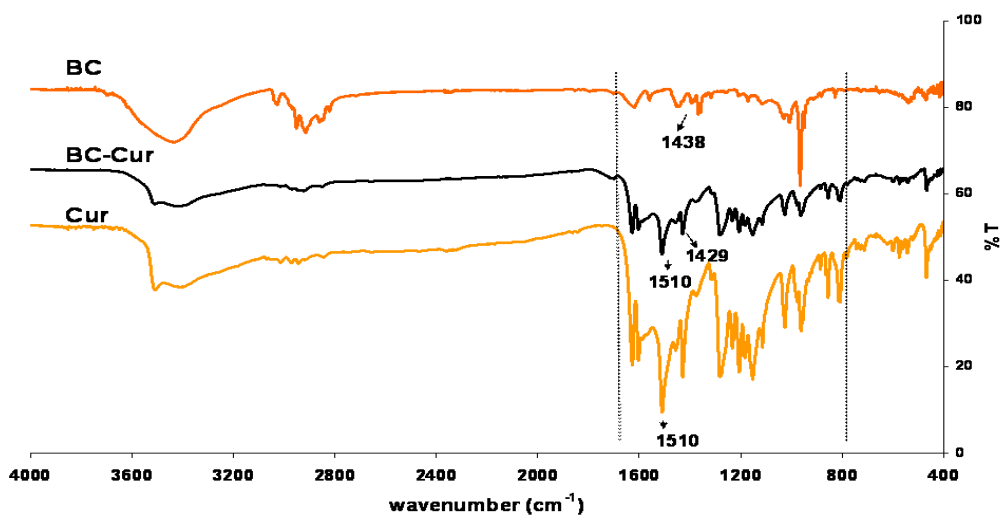
Figure 5.16: Spectra infrared solid BC, Cur and BC/Cur
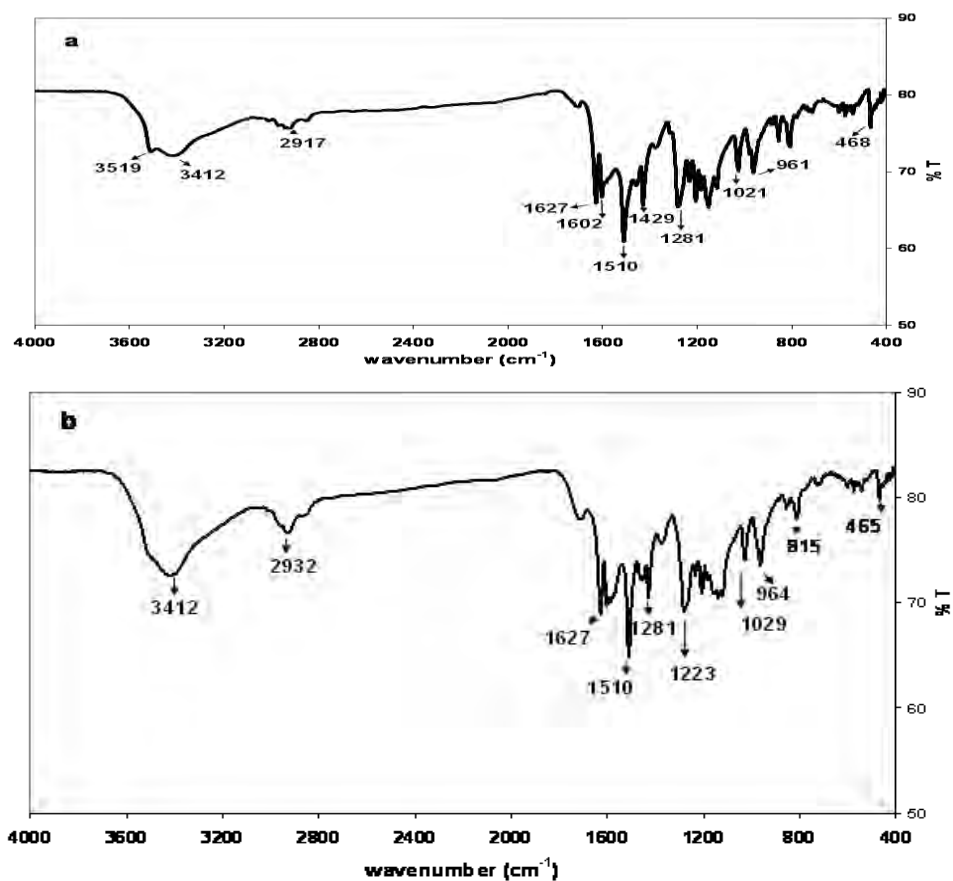
Figure 5.17: Spectra infrared of BC/Cur with different rasio (mol:mol) = 1:1 (a) and 1:2 (b)

151

The binary solid compound also confirmed from the DSC data (Figure 5.18). DSC of BC-Cur have endoterm peaks at 173°C and 181°C with energy around -24.6 J/g and -3.4 J/g. These peaks related to the composition of pure β-carotene at 183°C (-185,3 J/g) and curcumin at 175°C (-63.7 J/g).
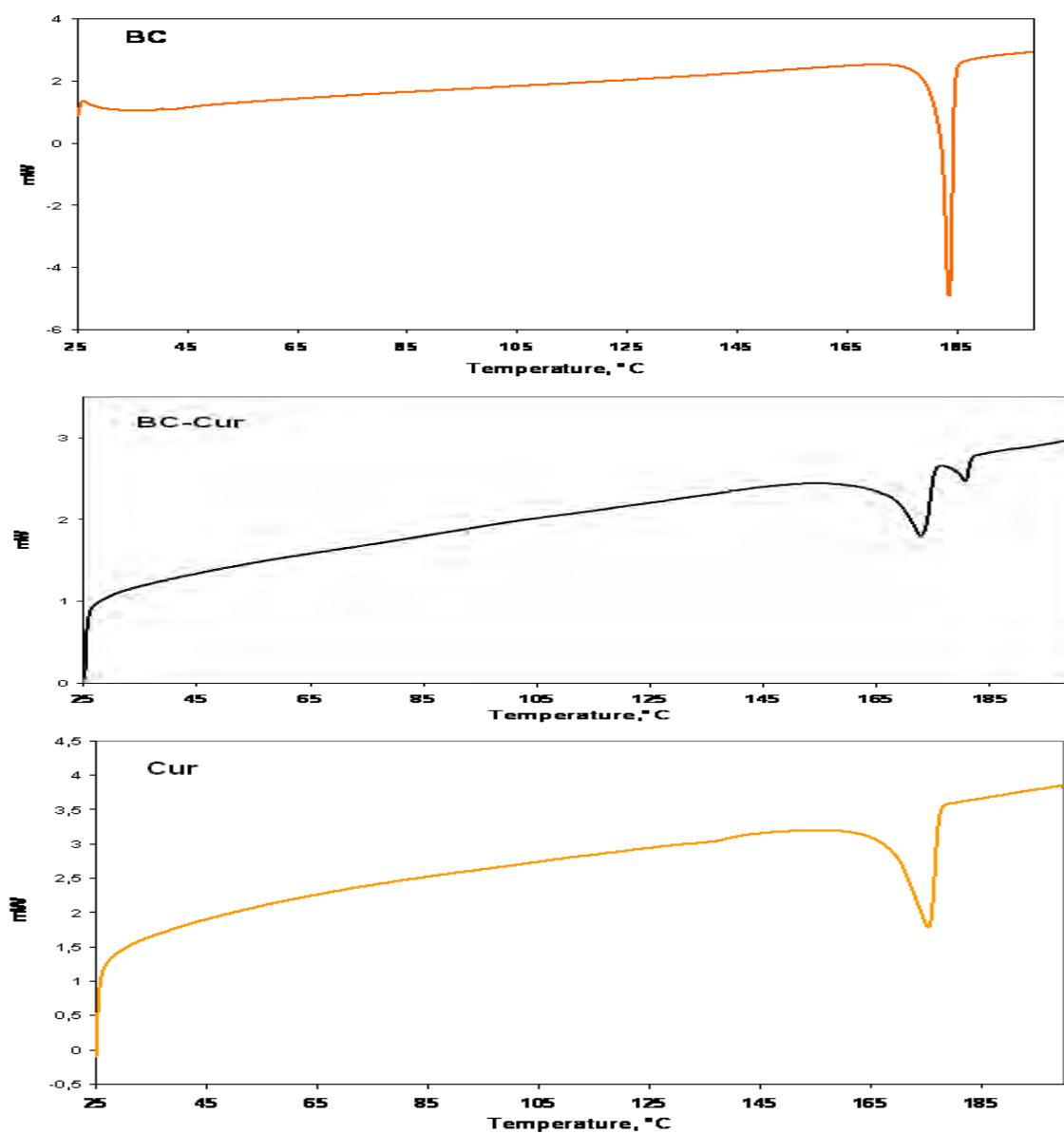
Figure 5.18: DSC of BC, BC-Curcumin and Curcumin

Curcumin stabilized the β-carotene also confirmed from TGA/DTA analysis. β-carotene have loss weight at 140°C (3.42%) and 317°C (86.92%). The total loss weight of at 120°C, 290°C, and 370°C were 2.04%, 28.91%, and 22.89%, respectively. And at BC-curcumin, the loss weight start at 120°C, continued at 290°C and 370°C. The percentage of loss weight at each temperature were 9.54%, 37.03%, and 22.16%, respectively. Therefore, the total weight of BC-Cur (68.74%) is lower than BC (90.34%), but higher than pure curcumin (53.85%). TGA of β-carotene, curcumin and BC-curcumin represented at Figure 5.19.

a   **b**   **c**
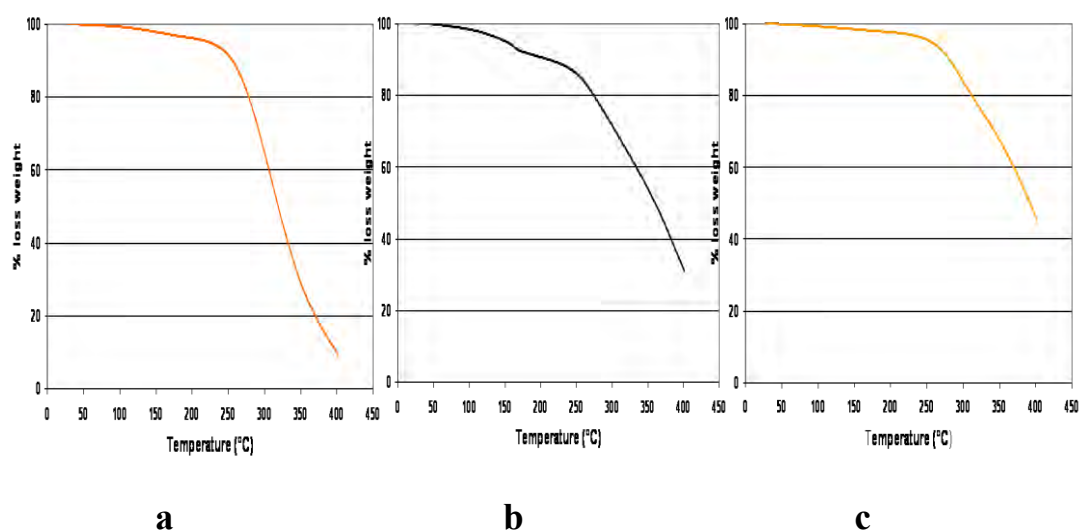
Figure 5.19: TGA of BC (a), BC-curcumin (b) and curcumin (c)

Curcumin in BC can trigger the isomerisation all-trans β-carotene prior to formation of 13-cis-β-carotene or 9-cis-β-carotene rather than 15,15'-cis-β-carotene (Henry *et al.*, 1998), but this geometric configuration did not affect to the stability significanly (Henry *et al.*, 1998; Xiao *et al.*, 2018). The isomerization BC as illustrated at Figure 5.20.
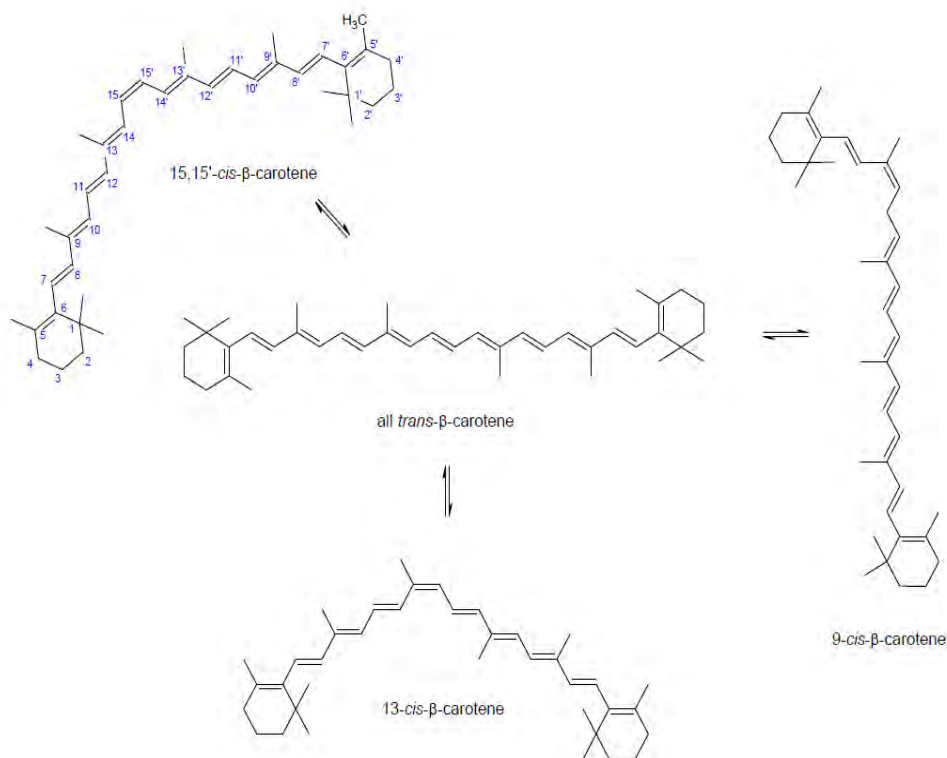
Figure 5.20: Cis-trans isomerisation of all-trans-β-carotene prior to formation
of the biradical (Mordi, 2015)

In photosensitized oxidation, carotenoids, i.e. β-carotene, are effective
quenchers of singlet oxygen ($^1O_2$). The quenching of $^1O_2$, by β-carotene can be
the physical quenching of (1) excited sensitizer molecules, or (2) singlet
oxygen. Physical quenching proceeds by energy transfer from $^1O_2$ to the
carotenoid molecule (Equation 5.3), leading to the formation of triplet-state
oxygen $^3O_2$. A similar process can occur between a carotenoid and an excited
sensitizer. If truly catalytic, the carotenoid should remain intact (equation 5.4),
however, usually a chemical reaction sets in, destroying the carotenoid
molecules (Bonnie and Choo, 1999).

$$^1O_2 + carotenoid \rightarrow {}^3O_2 + {}^3Carotenoid \tag{5.3}$$
$$^3Carotenoid \rightarrow Carotenoid + heat \tag{5.4}$$

154
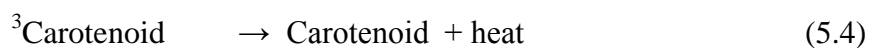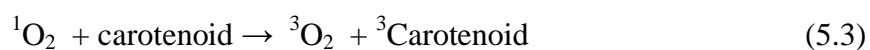
Light absorption by β-carotene (BC) results in the formation of its excited singlets (^{1}BC*). If not readily used photochemically, they get converted into triplet excited states (^{3}BC*). β-carotene triplet states are long-lived energetic species which can easily react with the triplet ground state of oxygen ($^{3}O_2$) to produce strongly photo-oxidative ROS. These ROS attack the 15C=C15 of the β-carotene and cause its photodegradation (Barazzouk *et al.*, 2012; Mordi, 2015). Antioxidant reduced the formation of the excited singlets (^{1}BC*) by absorption of UV light.

The more concentration antioxidant was added to the β-carotene, the half life time of β-carotene decrease. We seen the pro-oxidant effect of fucoxanthin to the BC solution at ratio concentration BC to the concentration Fx was 1 : 4, while curcumin was 1:6. The maximum photoprotectant of antioxidant fucoxanthin and curcumin to the β-carotene at BC-Fx and BC-Cur solution with the rasio BC to the antioxidant were 1:2 and 1 : 4. At this composition, the half-life time of BC-Fx and BC-Cur beyond to 6.96 and 14.81 hours, compare to the BC 1.43 hours and the percentage photostability of BC at 5 hours by the Fx and Cur were 38.56% and 88.13%. For carotenoids, prooxidant activity depends on pO$_2$ and the carotenoid concentration. Carotenoids exhibit prooxidant activity when in a high concentration and with high pO2 (Eghbaliferiz and Iranshah, 2016). The carotenoid loses its antioxidant activity and shows prooxidant behavior because of its autoxidation (Burton and Ingold, 1984). However, phenolics (in curcumin) can also act as prooxidants through autoxidation, in which semiquinone and superoxide (O2^{-}) radicals are formed (Mochizuki *et al.*, 2002) and depending on their concentration, pH and the presence or absence of transition-metal ions (Fukumoto and Mazza, 2000).

Fucoxanthin and curcumin are shown different effect to the photostability and electrichemical gap energy of β-carotene. Therefore, It will be very interesting to explore and study the properties of β-carotene with two

type of antioxidant and their luminescence properties (photo and electroluminescence).

2.4 Photostability of β-carotene with modified kaolinite

Photochemical damage to a substance is initiated by the compounds or photosensitizer absorption of energy. Many photochemical reactions are complex and may involve a series of competing reaction pathways in which oxygen may play a significant role. In fact, the great majority of photoreactions involve the consumption of molecular oxygen and are photosensitized oxidation processes. The photodegradation of BC is known to be mainly a photo-oxidative process, throught various reactive oxygen species (ROS), namely singlet oxygen, superoxide, etc (Barazzouk *et al*., 2012; Epe, 2012). The UV light absorption by BC results in the formation of its excited singlet (^{1}BC*). Mordi (1992) proposed the mechanism of degradation BC. The BC is degraded by cis-trans isomerization, followed by the formation of a singlet diradical. The oxygen attack on either side of the cis bond is enhanced giving the others type species radicals, followed by further reactions until final product.

Assessments of the stability of β-carotene without irradiation (Figure 5.21a) revealed a maximum peak for β-carotene in acetone at 452 nm, with other peaks observed at 486 nm and 426 nm. The degree of the photodegradation is expressed as the change in the main absorption band of β-carotene at 452 nm. The β-carotene concentration was relatively unchanged after being stored for nine hours at room conditions (temperature 25°C). Under irradiation, the absorbance of β-carotene (Figure 5.21b) decreased significantly at 5 h, with absorbance reaching levels close to zero at 7 h. By contrast, the absorbance of β-carotene /modified kaolinite (Figure 5.21c) remained high for nine hours, even under irradiation. Modified kaolinite therefore increased the photostability of β-carotene.
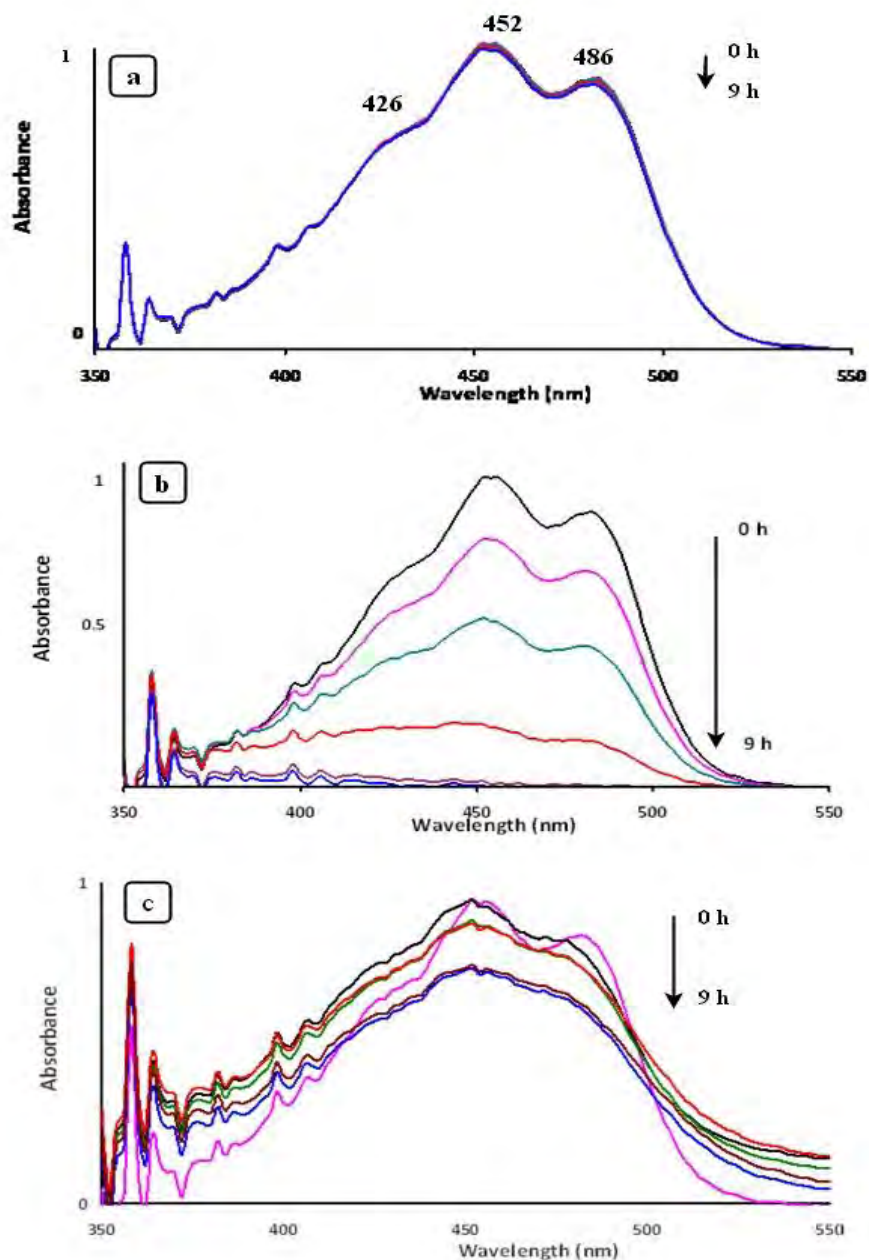
Figure 5.21: Absorption spectra of the products of BC without irradition (a) BC with UV irradiation (b) and BC/MK under UV irradiation (c)

Photodegradation and life-time of β-carotene with modified kaolinite calculated by determining the reaction rate constant by Santoso *et al*., (2007), modified from first-order rate equation from Lagergren's. The equation

purposed by Santoso *el al*., also can be used for system without adsorption interaction (the same with first order rate equation base on concentration in solution). Lagergren's first-order rate equation has been called pseudo-first-order to distinguish kinetic equation of liquid-solid phase adsorption base on adsorption capacity from concentration of solution (Qiu *et al*., 2009; Sejie *et al*., 2016). The change in the absorption at λ_{max} under visible light irradiation was expressed by the time dependence of the ratio A/A0 (A=absorption at time t, A0=absorption at time t=0). Plot of ln % absorbance (A/A0) to the irradiation time resulted a straight line can be obtained, where the slope is k, and $t_{1/2}$ is calculated.

The concentration of β-carotene is related to the amount of UV light energy is absorbed. The % absorbance is the percentage of absorbance value before irradiation at t=0 h to the absorbance decreased after irradiation at t hour. Photodegradation of β-carotene and β-carotene/modified kaolinite represented at Figure 5.22a. The rate constant of photodegradation β-carotene declined by the present of modified kaolinite (Figure 5.22b). Kinetic analyses of the photodegradation of β-carotene and β-carotene/modified kaolinite showed the half-life of β-carotene in the presence of modified kaolinite to be four times that in its absence (Table 5.6).The percentage photostability of 40 mL β-carotene with 1 g kaolinite (40 mL/1g) was 23.82%. Photostability increased to 52.76% and 61.87% for β-carotene interacting with metakaolinite and modified kaolinite, respectively. The percentage photostability reflects the amount of β-carotene adsorbed onto the kaolinite, metakaolinite or modified kaolinite. The amounts of β-carotene in kaolin, metakaolinite, and modified kaolinite were 1.46 ppm, 1.93 ppm, and 2.01 ppm. Therefore 58.34%, 77.31%, and 82.29% of the initial concentration β-carotene are photostabilized by the kaolin, metakaolinite, and modified kaolinite, respectively. The percentage photoprotection was calculated using equation 2.7 as described in the experimental section.
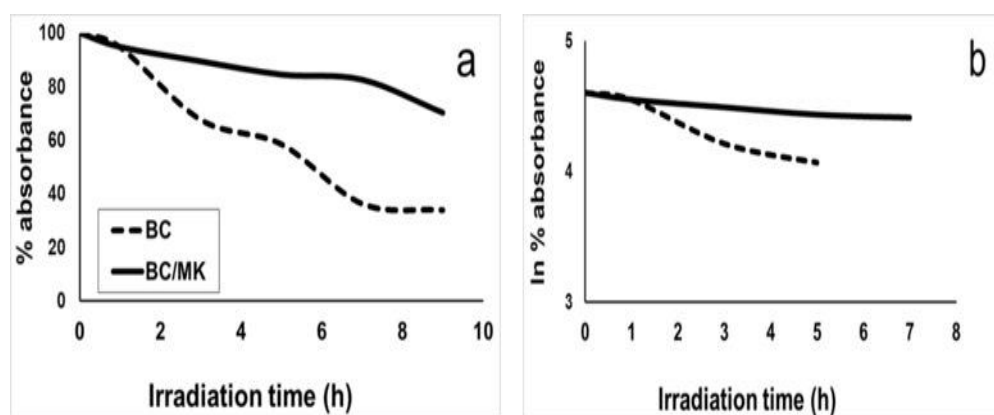
Figure 5.22: Kinetic photodegradation of β-carotene (BC) and
β-carotene/modified kaolinite (BC/MK)

Table 5.6: Pseudo-first-order reaction data of β-carotene (BC) with
kaolin (BC/K), metakaolinite (BC/MKaol) and modified
kaolinite (BC/MK)

Sample	Correlation coefficient (R^2)	Rate constant, k (h^{-1})	Half-life time (h)	% Photostability at 5th hours
BC	0.99	0.4854	1.43	-
BC/K	0.99	0.0833	8.32	23.82
BC/MKaol	0.96	0.0638	10.86	52.76
BC/MK	0.98	0.0325	21.32	61.87

According to BET surface area analysis (Table 5.7), calcination decreased the specific surface area, but increased total pore volume and mean pore volume. The surface area of kaolin decreased from 18.2 m^2/g into 10.6 m^2/g during calcination at 600° for 10 h (Belver *et al*., 2002). Essomba *et al*., (2014) reported that calcinations kaolin at 700° for 6 h increased specific surface area and pore volume. The surface area to be 20.18 and 33.83 m²/g, while pore volume from 0.081 and 0.093 cm^3/g respectively. They concluded that the chemisorption reaction or an activated process becomes more predominant in the rate-controlling step for the cadmium system. Adsorption capacity of cadmium ion on metakaolinite was correlated with the increasing of specific surface area and mean pore volume.

159

Table 5.7: BET surface area, total pore volume and mean pore volume of kaolinite

Samples	Surface area (m^2/g)	Total pore volume(cm^3/g)	Mean pore volume (nm)
Kaolin (K)	35.414	0.2006	22.660
Metakaolinite (MKaol)	23.193	0.2026	34.934
Modified kaolinite (MK)	23.805	0.1936	32.527

Carotene absorption occurred in meso-sized pores. This physical adsorption involved van der Waals forces. The higher adsorption capacity of metakaolinite than of kaolinite may be due to the presence of larger pores (Table 5.7). Metakaolinite pore size was markedly larger than the cross-sectional dimensions of the monomeric β-carotene molecule, consistent with the findings of Worasith *et al*. (2011), resulting in a large periodic multilayer (Baro *et al*., 2003). Srasra and Trabelsi-Ayedi (2000) proposed the possibility chemical interaction of β-carotene with the surface of the clay (Figure 5.23). This mechanism involved the hydrogen bonding of β-carotene to Bronsted sites and/or direct binding at Lewis sites through the formation of carbonium ions or coordinating bonds (Sarier and Güler, 1988). The interaction also involved the breaking of bonds in the dissolved octahedral and tetrahedral sheets (Adams, 1987).
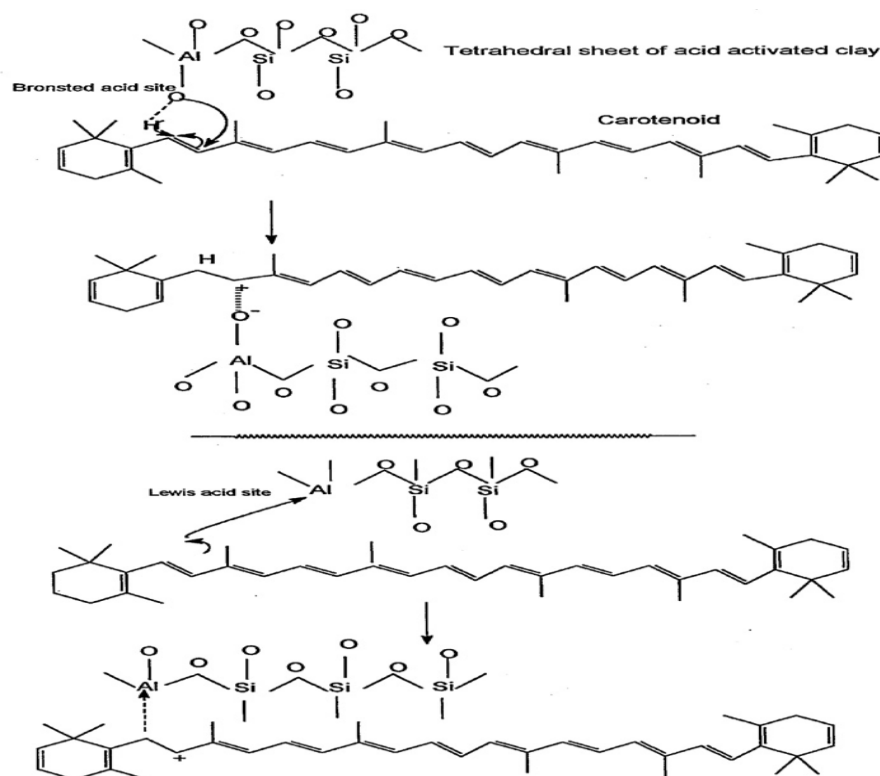
Figure 5.23: The mechanism of carotenoid adsorption on Brönsted and Lewis acid sites (Trabelsi-Ayebi and Srasra, 2000)

Zinc ions intercalate into metakaolinite by electronic attraction. The aggregation of metakaolinite particles results from the adsorption of positively charged Zn^{2+} ions onto the surfaces of this solid material (Chai *et al*., 2017). The presence of zinc ions in the metakaolinite increased the interaction of β-carotene with this solid material. The analysis of EDX spectra showed that the modified kaolinite contained 6.1% and identified as Lewis site (chapter IV). According to Zebib *et al*. (2010), who described a hypothetical mechanism of Zn^{2+} intercalation with curcumin and the structural model of β-carotene (Srasra and Trabelsi-Ayedi, 2000), interaction between modified kaolinite and β-carotene may modify complexation, with zinc as a Lewis site and β-carotene as the electron donor. This mechanism increases the adsorption capacity of β-carotene on modified kaolinite. Acid site contributed to the stabilization of dye on mesoporous material (Kohno *et al*., 2011).
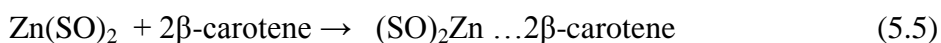
$$Zn(SO)_2 + 2\beta\text{-carotene} \rightarrow (SO)_2Zn \ldots 2\beta\text{-carotene} \tag{5.5}$$

No distinction was made between aluminol and silanol surface groups, but the SOH groups involved in adsorption were probably mostly those of aluminol and AlOH (Schindler *et al*., 1987). Spectra infra red of BC, MK and BC/MK shown that there is no significant differences from these spectra (Figure 5.24). Only, band at 668 cm^{-1} at MK disappered after contacted with β-carotene.
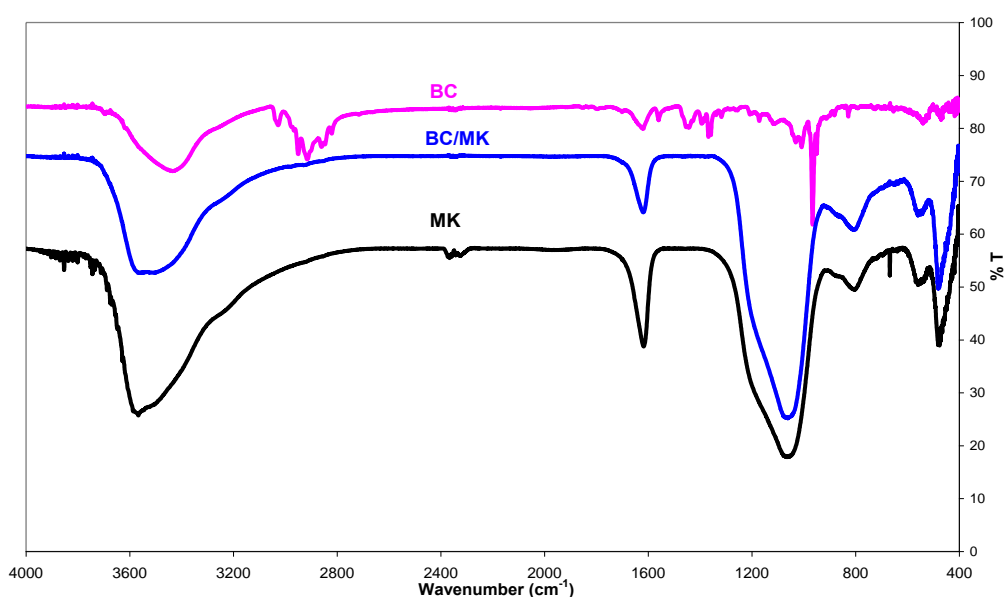
Figure 5.24: Spectra infra red of β-carotene, modified kaolinite, and BC/MK

The chemical interaction related to hydrogen bonding of BC with Brönsted sites and/or to direct binding at Lewis sites on clay surfaces by forming carbonium ions either by forming coordinating bonds (Sarier and Güler, 1988) as shown in Figure. 5.23. The other are come from the broken bonds in the dissolved octahedral and tetrahedral sheets (Adams, 1987). Physical adsorption, known as van der Waals adsorption related to absorbed of BC onto the mesopores between the particles of kaolinite. The higher adsorption capacity of metakaolinite compared to kaolin could be the result of it a having more bigger pores even though its specific surface area was lower than kaolin. This pore size is appreciably larger than the cross sectional

dimensions of the monomeric BC molecule and is consistent with the report by Worasith et al (2011) and leading to the completion of a large periodic multilayer (Baro *et al*., 2003).

The absorbance of BC/MK decreased after irradiation, but the λ_{max} was almost unchange. This fact indicating there was only a simple degradation, but not photochemical conversion such as isomerization (Henry *et al*., 1998; Kohno *et al*., 2009; Xiao *et al*., 2018). It has been reported that the stability of β-carotene related to order molecular association (Baro *et al*., 2003). As the spectral shift was not observed, only a little changing in shape spectral, it was suggested that β-carotenes formed aggregation with the disorder orientation. Aggregation also contributed to the stability improvement of dye, because the aggregation reduced the contact area to the oxygen (Kohno *et al*., 2015).

The modified kaolinite protected β-carotene from the effects of direct UV irradiation. Lower levels of triplet oxygen and ROS formation were observed in the presence of modified kaolinite. Carotenoid degradation was a direct result of irradiation. The shielding effect of the inorganic host material reduced the rate of degradation and also protected β-carotene against reactive oxygen species (Kohno *et al*., 2016). The carotenoid degradation caused directly by irradiation are reduced by shielding effect of opaque mineral and isolation from reactive oxygen species as well (Vítek *et al*., 2009).

The percentage photostability of β-carotene with mass variation modified kaolinite represented at Figure 5.25. The maximal percentage photostability of β-carotene was achieved with 1 g of modified kaolinite. The photostability of β-carotene decreased with decreases in the mass of modified kaolinite. The percentage photostability of this matrix was 61.87%. Increasing the mass of modified kaolinite to 2 g, decreased the percentage photostability of β-carotene significantly, due to a decrease in capacity of β-carotene to adsorb onto the modified kaolinite. Overlaps between adsorption sites or their aggregation as a result of overcrowding decreased the adsorption capacity of β-

carotene (Essomba *et al*., 2014; Ndongo Kounou *et al*., 2015). The lower level of adsorption at higher mass also reflects the increase in interactions between the particles of a material with mass. The excess of amount of cation caused the precipitation of dye aggregate (Kohno *et al*, 2015). Therefore, β-carotene photostability decreased with increasing the mass of modified kaolinite also due to excessive amounts of Zn^{2+}.
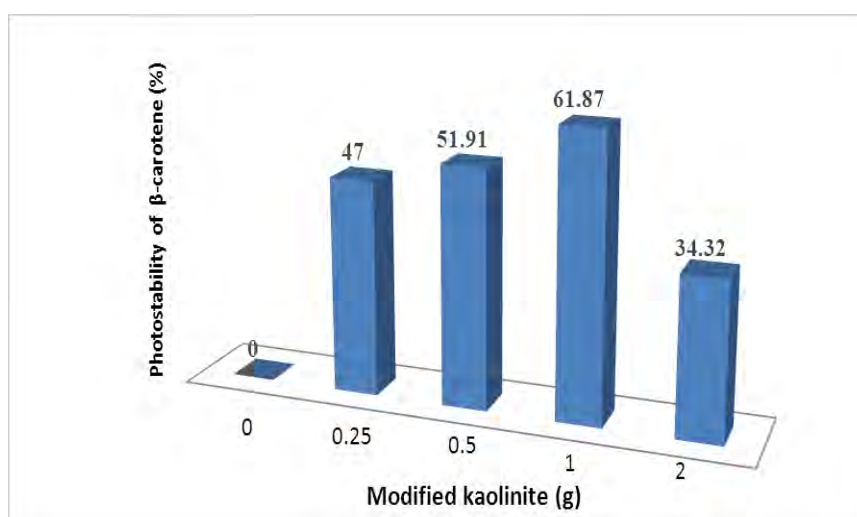
Figure 5.25: Photostability of β-carotene with different masses of modified kaolinite

However, this finding is not consistent with the results of Barazzouk *et al.,* (2012) who reported that the protection against Chla photodegradation afforded by AuNPs (gold nanoparticles) eventually reached a plateau. This phenomenon being correlated to photoprotector particle size. When modified kaolinite, which has micrometre-range particles, was used as photoprotector, the interactions between particles increased with mass. In the presence of excess modified kaolinite, the interaction of β-carotene with modified kaolinite decreased, and the β-carotene was irradiated with UV light.

2   Photostability fucoxanthin with curcumin

Fucoxanthin is an orange-colour carotenoid (Beppu *et al*., 2012) and a major xanthophyll which exhibits potential antioxidant activity (Sudhakar *et al*., 2013). Fucoxanthin can be extracted from seaweed (Waghmode and Kumbar, 2015; Zaelani *et al*., 2015).

The λ_{max} of Fx/Cur blue-shifted to the lower wavelength or higher energy (Figure 5.26). This hypsocromic shift from 446 to the 442, 420 nm. At very low concentration of curcumin,   the shifting wavelength maxima of Fx/Cur from 446 to the 442 nm was observed. The blue shift was caused by some factors i.e. conjugation and polarity of solvent. When the curcumin concentration was increased, curcumin molecule was dominant. The blue shifted was caused by the less conjugation of curcumin structure in comparison to fucoxanthin structure (Reichardt, 1994). This shifting tend toward to the the λ_{max} of pure Cur (Figure 5.26d and Figure 5.26e) with the increasing of Cur concentration. It means, in this binary solution, the Cur molecule dominant to the Fx.
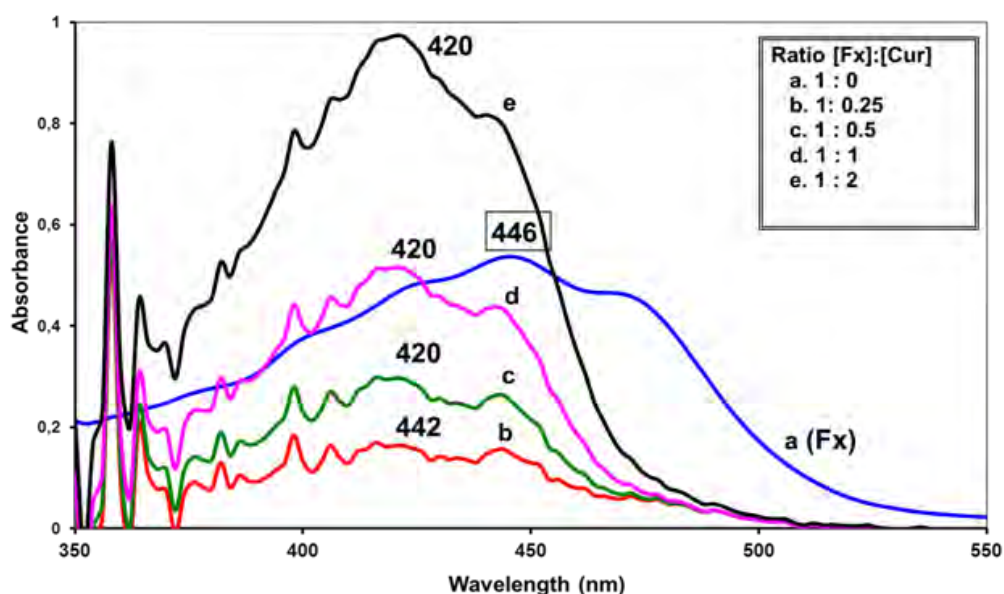
Figure 5.26: UV-spectra of Fx with variation curcumin concentration

The stability of fucoxanthin without irradiation were illustrated at Figure 5.27a, while fucoxanthin and fucoxanthin/curcumin at Figure 5.27b and Figure 5.27c, respectively**.** Under irradiation, the absorbance of Fx decreased significantly at 7 h, with absorbance reaching levels close to zero at 9 h. By contrast, the absorbance of Fx/Cur, remained high for nine hours, even under irradiation. Curcumin, therefore increased the photostability of fucoxanthin.
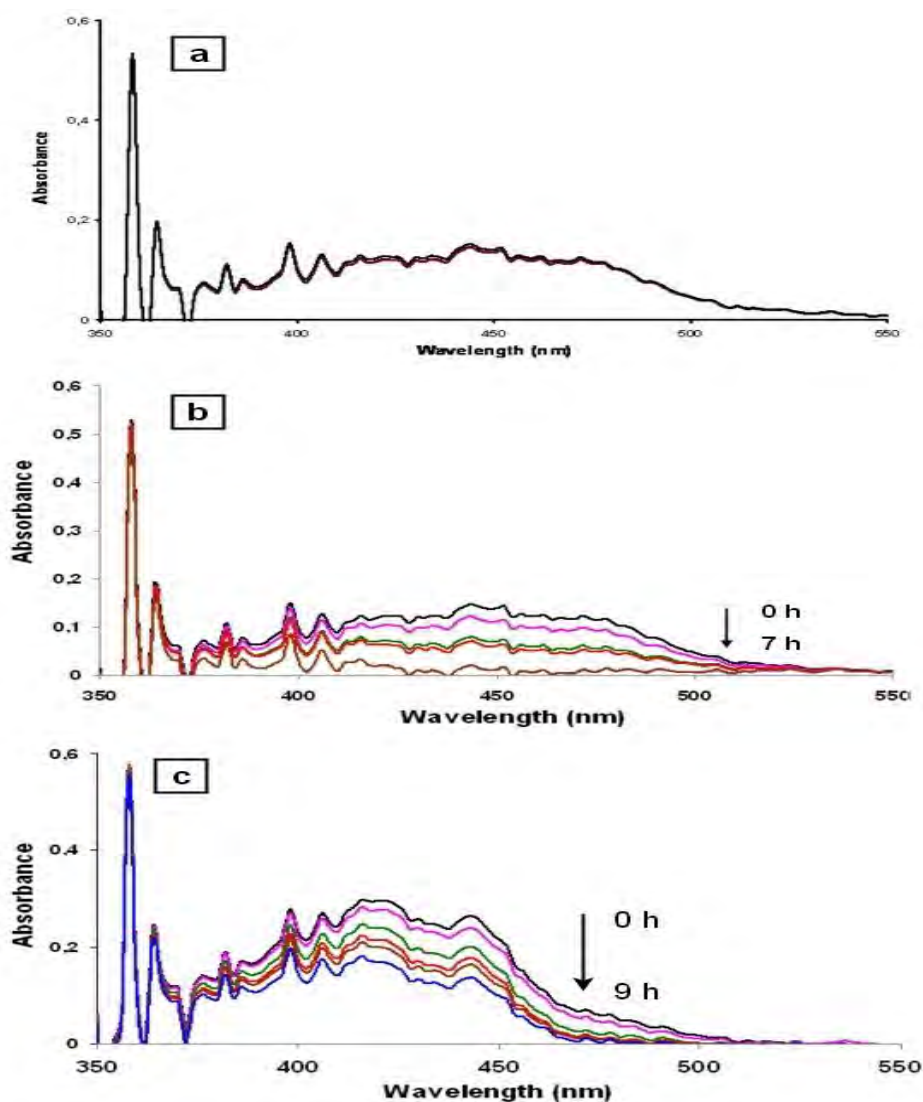
Figure 5.27: UV absorption spectra of Fx without irradiation (a), under irradiation of Fx (b), Fx/Cur (c)

The photodegradation of Fx/Cur also follows a first order kinetic with the half-life 38.5 hours (Table 5.8). The half-life enhancement of Fx by Cur almost 2.5 fold compared to the half-life of Fx which is only 14.44 h. The percentage of photostability at this composition was more than 100%.

Table 5.8: First-order reaction data of Fx and Fx/Cur

Ratio [Fx] to[Cur]	R^2	Degradation rate constant, k (h^{-1})	Half-life time (h)	% photostability at 5th hours
1 : 0 (Fx)	0.98	0.0008	14.44	-
1 : 0.25	0.96	0.0004	28.88	40
1 : 0.5	0.98	0.0003	38.50	136
1 : 1	0.99	0.0006	19.25	243
1 : 2	0.98	0 .0011	10.50	495

Table 5.9 showed the redox potential of fucoxanthin and Fx/curcumin. Fucoxanthin has four oxidation product and two for reduction one and Fx/Cur has more oxidation and reduction stage due to the present of curcumin.

Table 5.9: Redox potential (V/SCE) of fucoxanthin and Fx/Cur

Fucoxanthin	Curcumin	Fx/Cur
-1.958	-1.765	-1.958
-1.443	-1.404	-1.1772
-0.803	-1.184	-1.387
0.776	1.404	-1.069
0.962		0.732
1.191		0.942
1.484		1.147
		1.245
		1.377

There is an significant changing in oxidation voltammograms of Fx, Fx/Cur (Figure 5.28). Curcumin protect fucoxanthin by reduced the second oxidation stage around 0.7746 V and 1.191 V. The protection of fucoxanthin by curcumin also can be seen at reduction voltammogram. The reduction stage at - 1.443 V and -1.958 V decreased significantly.

167
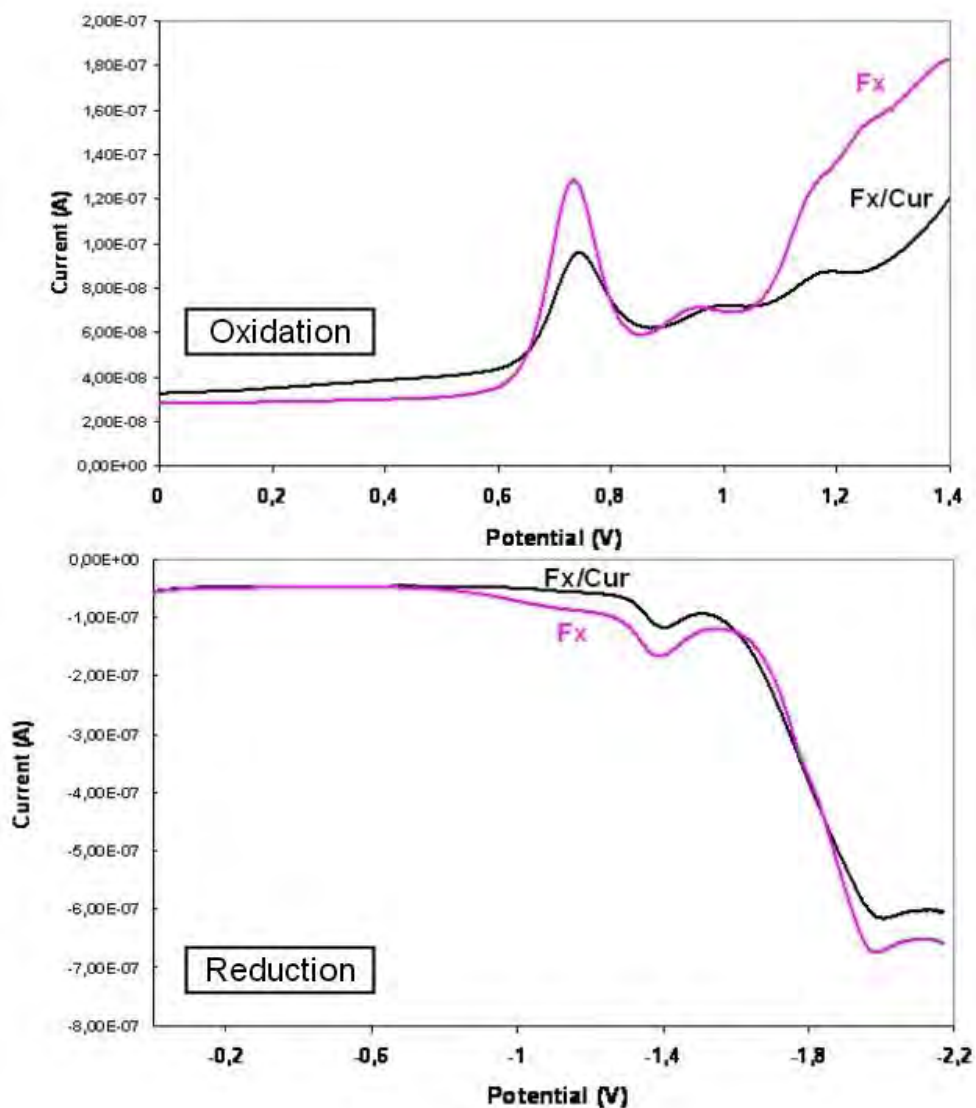
Figure 5.28: Redox voltammograms of fucoxanthin and Fx/Cur

Figure 5.29 represented the cyclic voltammograms of fucoxanthin (Fx), and Fx/Cur. Fucoxanthinhas $E_{onset.ox}$= 0.68 V/SCE, and $E_{onset.red}$= -1.33 V/SCE. The $E_{onset.ox}$ and $E_{onset.red}$ for FX/Cur were 0.68 and -0.85 V/SCE, respectively. Therefore, the electrochemical gap of fucoxanthin and Fx/Cur, were 2.02 eV and 1.64eV, respectively. The Fx/Cur has lower electrochemical gap than pure Fx. HOMO-LUMO energy level and solid-state ionization and electron affinity of fucoxanthin and fucoxanthin/curcumin are described at Table 5.10.
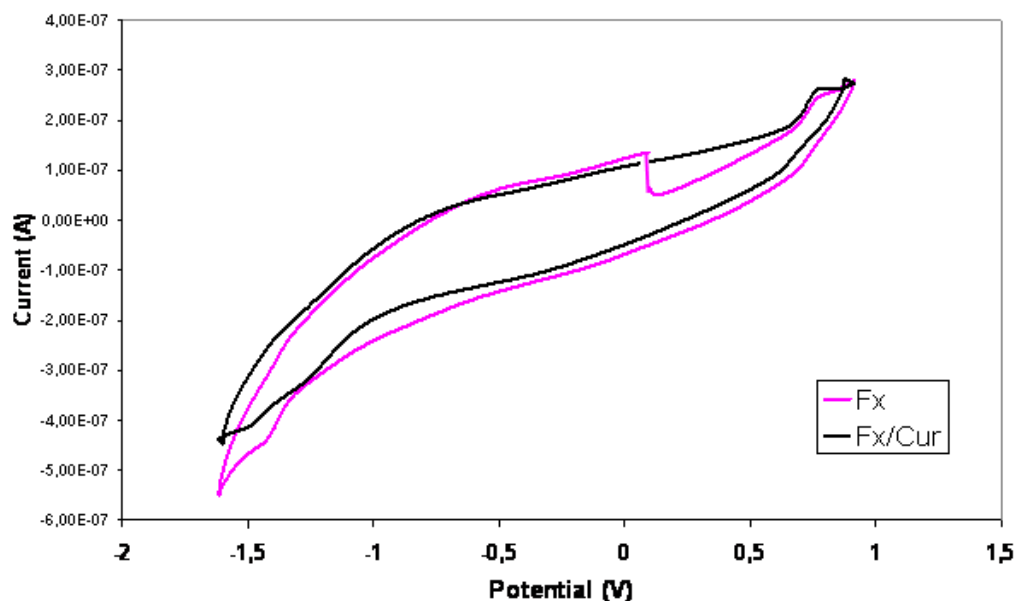
Figure 5.29: Cyclic voltammogram of Fx and Fx/Cur

Table 5.10: HOMO-LUMO energy and solid-state ionization and electron
affinity of fucoxanthin and Fx/curcumin, and BC/curcumin

Biomolecule	HOMO (eV)[a]	LUMO (eV)[a]	I_c (eV)[b]	A_c (eV)[b]	Electrical gap (eV)[b]	Electrochemical gap (eV)[c]
BC	-5, 84	-3,84	-5,31	-3,00	2,31	2,04
BC/Cur	-5,75	-4,50	-5,20	-4,41	0,79	1,61
Fx	-6.11	-4.09	-5.50	-3.30	2.20	2.02
Fx/Cur	-6.07	-4.54	-5.57	-3.83	0.74	1.53

Antioxidant curcumin improved photostability of carotenoid molecules. Effect of curcumin to the photostability of two type of carotenoid molecules represented at Table 5.11. Curcumin enhanced the half-life time of β-carotene almost 4.5-fold, while fucoxanthin only 1.3-fold. Photoprotectance of curcumin to β-carotene also better than fucoxanthin. The percentage photostability more than 100% represented that curcumin was dominant at that mix molecules. The CV analysis shown that curcumin reduced the electrochemical band gap and the first oxidation of both of mix biomolecules (BC/Cur and Fx/Cur) were irreversible.

Table 5.11: First-order reaction data and photostablity of carotenoid
with curcumin (ratio 1 : 1)

Biomolecule	R^2	Degradation Rate constant, k (h^{-1})	Half-life time (h)	% photostability at 5th hours
β-carotene	0.99	0.4854	1.43	-
Fucoxanthin	0.98	0.0008	14.44	-
β-carotene/curcumin	0.95	0.1091	6.35	11.91
Fucoxanthin/curcumin	0.99	0.0006	19.25	246.30

4. Conclusions

The present work clearly shows that curcumin can protect carotenoid molecules such as β-carotene and fucoxanthin. Photoprotection efficiency of β-carotene by curcumin was higher than fucoxanthin. The protecting ability of fucoxanthin and curcumin related to the ability of both of these antioxidants to delocalized of electron and transfer electron. The concentration of antioxidant influenced the stability of β-carotene. The half-life time of β-carotene enhanced by fucoxanthin (ratio BC to Fx = 1 : 2) and curcumin (Car: BC = 1 : 4) were almost five and seven fold, respectively, compare to the only β-carotene. The percentage photostability of β-carotene by each antioxidant were 38.56% and 88.13%.

Photoprotection efficiency of fucoxanthin by curcumin enhanced the half-life of fucoxanthin almost 3 fold from 14.44 h at ratio mol Fx to Cur = 1: 1. At percentage of photostability 40%, the half-life of Fx only increased 2 fold.

From cyclic voltametry analysis gived information that curcumin reduced the electrochemical gap of BC/Cur and Fx/Cur. Antioxidant fucoxanthin and curcumin decreased the electrochemical gap of the binary material. The electrochemical gap of carotene-curcumin is -1.61 eV, carotene-fucoxanthin is -1.75 eV compare to the only β-carotene -2.04 eV. Fucoxanthin can keep the first oxidation stage of beta-carotene still reversible, but not for curcumin.

Modified kaolinite decreased photodegradation of β-carotene by shielded and protected from direct UV irradiation and caused the half-life time enhanced almost fiftieth times. The mass of modified kaolinite influenced the photostability of β-carotene. The percentage photostability of β-carotene by modified kaolinite at 5 hour was 61.87% (40 mL/1 g). The amount of β-carotene which adsorbed onto kaolinite was related to the photostability.

Thus, the use of antioxidant and modified kaolinite offers us a new possibilities to increase the photostability of β-carotene has potential application in photovoltaic (DSSC) or opto-electronic device. β-carotene with curcumin can be used in cosmetic (sunscreen).

References

Araujo, F.R., Baptitta, J.G., Marcal, L., Ciuffia, K.J., Nassara, E.J., Calefi, P.S., Vivcente, M.A., Trujilano, R., Rives, V., Gilc, A., Korilic, S., De Faria, E.H. (2014) Versatile heterogeneous dipicolinate complexes grafted into kaolinite: Catalytic oxidation of hydrocarbons and degradation of dyes. *Catalysis Today*, **227**, 105-115.

Barazzouk, S., Bekalé, L., Hotchandani, S. (2012) Enhanced photostabillity of chlorophyll-a using gold nanoparticles as an efficient photoprotector. *Journal Materials Chemistry*, **22**, 25316-25324.

Bard, A.J. and Faulkner, L.R. (2001) Electrochemical Methods: Fundamental and Application, 2nd Edition, John Wiley & Son Inc, New York.

Baro, A.M., Hla S., and Rieder, K.H. (2003) LT-STM study of self-organization of β-carotene molecular layers on Cu (1 1 1). *Chemical Physics Letters*, **369**, 240–247.

Barzegar, A., Moosavi-Movahedi, A.A. (2011) Intracellular ROS protection efficiency and free radical-scavenging activity of curcumin. *PLoS ONE*, **6** (10), 26012.

Beppu, F., Hosokawa, M., Niwano, Y., and Miyshita, K. (2012). Effects of dietary fucoxanthin on cholesterol metabolism in diabetic/obese KK-Ay mice. *Lipid and Health Diseases*, **11** (112), 1-8.

Belver, C., Banares, M.A.,Vicente, M.A. (2002) Chemical activation of kaolinite under acid and alkaline conditions. *Chemical Materials*, **14**, 2033-2043.

Bonnie, T.Y.P. and CHOO, Y.M. (1999) Oxidation and thermal degradation of carotenoids. *Journal of Oil Palm Research*, **2** (1), 62-78.

Bouchouit, K., Derkowska, B., Migalska-Zalas, A., Abed, S.N., Benali-cherif, N., and Sahraoui, B. (2010) Nonlinear optical properties of selected natural pigments extracted from spinach: Carotenoids. *Dyes and Pigments*, **86**, 161-165.

Burton, G.W. and Ingold K.U. (1984) Beta-carotene: an unusual type of lipid antioxidant. *Science*, **224**, 569–573.

Cardona, C.M., Li, W., Kaifer, A.E., Stockdale, D., and Bazan, G.C. (2011) Electrochemical considerations for determining absolute frontier orbital energy levels of conjugated polymers for solar cell applications. *Advances Materials,* **23**, 2367–2371.

Chuen-Fung, A.Y. (2012) The Fucoxanthin content and antioxidant properties of undaria pinnatifida from Marlborough Sound, Auckland University of Technology University, New Zealand,. Thesis.

Christensen, L.R. (2014) in: Frank H. A., Young, A. J., Britton, G., and Cogdell, R. J, The Electronic States of Carotenoids. Kluwer Academic Publisher, New York, pp: 137–157.

Claes, H. (1960) Interaction between chlorophylls and carotenes with different chromophoric groups. *Biochemistry and Biophysics Research and Communication*, **3**, 585-590.

Cuquerella, M.C., Lhiaubet-Vallet, V., Cadet, J., Miranda, M.A. (2012) Benzophenone photosensitized DNA damage. *Account of Chemical Research*, **45**, 1558–1570.

Cvetkovic, D. and Markovic, D. (2008) Stability of carotenoids toward UV-irradiation in hexane solution. *Journal of Serbia Chemistry and Society,* **73** (1), 15–27.

Douiri, H., Louati, S., Baklouti, S., Arous, M., and Fakhfakh, Z. (2016) Enhanced dielectric performance of metakaolin–H_3PO_4 geopolymers. *Materials Letters*, 164, 299–302.

Dedzo, G.K. and Detellier, C. (2014) Intercalation of two phenolic acids in an ionic liquid-kaolinite nanohybrid material and desorption studies. *Applied Clay Science*, **97-98**, 153-159.

Delgado-Vargas, F., Jiménez, A.R., and Paredes-López O. (2000) Natural pigments: Carotenoids, anthocyanins, and betalains-characteristics, biosynthesis, processing, and stability. *Critical Reviews in Food Science and Nutrition.* **40** (3), 173–289.

Destiarti, L., Wahyuni, N., Prawatya, Y., and Sasri, R. (2017) Synthesis and characterization of mangan oxide coated sand from capkala kaolin. International Conference on Chemistry, Chemical Process and Engineering, *AIP Conference Proceeding 1823*, 020023 doi: 10.1063/1.4978096.

Dutta, D., Dutta, A., Raychaudhuri, U., and Chakraborty R. (2006) Rheological characteristics and thermal degradation kinetics of beta-carotene in pumpkin puree. *Journal of Food Engineering*, **76**, 538–546.

Eghbaliferiz, S. and Iranshahi, M. (2016) Prooxidant activity of polyphenols, flavonoids, anthocyanins and carotenoids: Updated review of mechanisms and catalyzing metals. *Phytotheraphy Research*, **30**, 1379–1391.

El-Agez, T.M., El Tayyan, A.A., Al-Kahlout, A., Sofyan, A., Taya, S.A. and Abdel-Latif, M.S. (2012) Dye-Sensitized solar cells based on ZnO films and natural dyes. *International Journal of Materials and Chemistry*, **2** (3), 105-110.

Epe, B. (2012) DNA damage spectra induced by photosensitization. *Photochemical and Photobiologycal Sciences*, **11**, 98-106.

Essomba, J.S., Ndi Nsami, J., Belibi Belibi, P.D., Tagne, G.M., and Ketcha Mbad C.J. (2014) Adsorption of cadmium (II) ions from aqueous solution onto kaolinite and metakaolinite. *Pure and Applied Chemical Sciences*, **2**(1), 11–30.

Fukumoto, L. and Mazza, G. (2000) Assessing antioxidant and pro-oxidant activities of phenolic compounds. *Journal of Agriculture and Food Chemistry*, **48**, 3597–3604.

Freitas, J.V., Lopes, N.P., and Gaspar, N.L. (2015) Photostability evaluation of five UV-filters, trans-resveratrol and beta-carotene in sunscreen. *European Journal of Pharmaceutical Science*, **78**, 79-89.

Ge, W., Chen, Y., Wang, L. and Zhang, R. (2015) Photocatalytic degradation of β-carotene with TiO_2 and transition metal ions doped TiO_2 under visible light irradiation. *Universal Journal of Chemistry,* **3**, 104-111.

Głowacki, E.D., Leonat, L., Voss, G., Bodea, M., Bozkurt, Z., Irimia-Vladu, M., Bauerf, S. and Sariciftci, N.S. (2011) Natural and nature-inspired semiconductors for organic electronics. *Proceeding of SPIE 8118.*

Gul, K., Tak, A., Singh, A.K., Singh, P., Yousuf, B. and Wani, A.A. (2015) Chemistry, encapsulation, and health benefits of β-carotene - A review. *Cogent Food & Agriculture*, **1**, 1-12.

Halliwell, B. (2006) Reactive Species and Antioxidants. Redox Biology Is a Fundamental Theme of Aerobic Life. *Plant Physiology*, **141**, 312-322.

Hattab, A., Bagane, M., and Chlendi, M. (2013) Characterization of Tataouinen's raw and activated clay. *Chemical Engineering & Process Technology*, **4**, 1-5.

Henry, L.K., Catigani, G.L., and Schwartz, S.J. (1998) Oxidative degradation kinetic of lycopene, lutein, and 9-cis and all-trans β-carotene. *Journal of the American Oil Chemists Society*, 7 (7), 823-829.

Heo, S-J. and Jeon, Y-J. (2009) Protective effect of fucoxanthin isolated from Sargassum siliquastrum on UV-B induced cell damage. *Journal of Photochemistry and Photobiology B Biology*, 95 (2), 101-107.

Hiendro, A., Hadary, F., Rahmalia, W., Wahyuni, N. (2012) Enhanced performance of bixin sensitized solar cells with activated kaolinite. *International Journal of Engineering Research and Innovation,* **4**, 40-44.

Irimia-Vladua, M., Głowacki, E.D., Voss, G., Bauera., S. and Sariciftci, N.Y. (2012) Green and biodegradable electronic. *Material Today*, **15** (7-8), 340-346.

Izci, E. (2014) Structural and dielectric properties of acid activated metakaolinite. Abstract for 11th GeoRaman International Conference, June 15-19 St. Louis, Missouri, USA.

Kissenger, P.T (1983) Cylic Voltammetry. *Journal of Chemical Education*, **60** (9), 702-705.

Kita, S., Fuji, R., Richard, J., Cogdell, R.J., and Hashimoto, H. (2015) Characterization of fucoxanthin aggregates in mesopores of silica gel: Electronic absorption and circular dichroism spectroscopies. *Journal of Photochemistry and Photobiology A: Chemistry,* **313**, 3–8.

Kohno,Y., Kinoshita, R., Ikoma, S., Yoda, K., Shibata, M., Matsushima, R.,Tomita, Y., Maeda, Y., and Kobayashi, K. (2009) Stabilization of natural anthocyanin by intercalation into montmorillonite. *Applied Clay Science*, **42**, 519–523.

Kohno, Y., Senga, M., Shibata, M., Yoda, K., Matsushima, R., Tomita, Y., Maeda, Y., and Kobayashi, K. (2011) Stabilization of flavylium dye by incorporation into Fe-containing mesoporous silicate. Microporous and Mesoporous Materials, **141**, 77–80.

Kohno, Y., Kato, Y., Shibata, M., Fukuhara, C., Maeda, Y., Tomita, Y., and Kobayashi, K. (2015) Enhanced stability of natural anthocyanin incorporated in Fe-containing mesoporous silica. *Microporous and Mesoporous Materials*, **203**, 232-237.

Kohno, Y., Kato, Y., Shibata, M., Fukuhara, C., Maeda, Y., Tomita, Y., and Kobayashi, K. (2016) Fixation and stability enhancement of beta-carotene by organo-modified mesoporous silica. *Microporous and Mesoporous Materials*, **220**, 1-6.

Kumar, S., Panda, A.K., Singh, R.K. (2013) Preparation and characterization of acid and alkali treated kaolin clay. *Bulletin of Chemical Reaction Engineering & Catalysis,* **8**, 61-69.

Larsen, D.S., Papagiannakis, E., Van Stokkum, I.H.M., Vengris, M., Kennis, J.T.M., and Van Grondelle, R. (2003) Excited state dynamics of β-carotene explored with dispersed multi-pulse transient absorption. *Journal of Applied Physic*, **109**, 103529.

Lim, H.W. and Draelos, Z.D. (2009) Clinical Guide to Sunscreens and Photoprotection. Informa Healthcare, USA, pp. 37-38.

Liu, D., Gao, Y. and Kispert, L.D. (2000) Electrochemical properties of natural carotenoids. *Journal of Electroanalytical Chemistry*, **488**, 140-1 50.

Lotito, S.B., Frei, B. (2006) Consumption of flavonoid-rich foods and increased plasma antioxidant capacity in humans: cause, consequence, or epiphenomenon. *Free Radical Biology and Medical*, **41**, 1727–46.

Lü, J.M., Lin, P.H., Yao, Q., and Chen, Q. (2010) Chemical and molecular mechanisms of antioxidants: experimental approaches and model systems. *Journal of Cellular and Molecular Medicine*, **14** (4), 840-860.

Martini, S., D'Addario, C., Bonechi, C., Leone, G., Tognazzi, A., Consumi, M., Magnani, A., and Rossi, C. (2010) Increasing photostability and water-

solubility of carotenoids: Synthesis and characterization of β-carotene–humic acid complexes. *Journal of Photochemistry and Photobiology B: Biology*, **101**, 355–361.

Matusik, J., Matykowska, L. (2014) Behavior of kaolinite intercalation compounds with selected ammonium salts in aqueous chromate and arsenate solutions. *Journal of Molecular Structure,* **1071**, 52-59.

Matusik, J., Stodak, E., and Baranowski, K. (2011) Synthesis of polylactide/clay composites using structurally different kaolinites and kaolinites nanotubes. *Applied Clay Sciences*, **51**, 102-109.

Md Saad, N.S.S., Nik Malek, N.A.N., and Chong, C.S. (2016) Antimicrobial activity of copper kaolinite and surfactant modified copper kaolinite against gram positive and gram negative. *Sciences & Engineering*, **78**, 127–132.

Mochizuki, M., S-i, Y., Kano, K., Ikeda, T. (2002) Kinetic analysis and mechanistic aspects of autoxidation of catechins. *Biochemical and Biophysical Acta*, **1569**, 35–44.

Mordi, R.C. (1992) Mechanism of β-carotene degradation. *BJ Letter*, **10**, 310.

Mordi, R.C. (2015) The involvement of free radicals in the mechanism of β-carotene degradation. *Covenant Journal of Physical and Life Sciences*, **3** (1), 26-35.

Morabito, K., Steeley, K.G., Shapley, N.C., Mello, C., Li, D., Calvert, P., and Tripathi, A. (2011) Proximal effects of ultraviolet light absorbers and polymer matrix in the photostability of β-carotene. *Dyes and Pigments*, **92**, 509-516.

Mueller, L. and Boehm, V. (2011) Antioxidant activity of β-carotene compounds in different in vitro assays. *Molecules*, **16**, 1055-1069.

Nimse, S.B. and Pal, D. (2015) Free radicals, natural antioxidants, and their reaction mechanisms. *RSC Advances*, **5**, 27986–28006.

Nonoyama, A., Garcia-Lopez, A., Garcia-Rubio, L.H., Leparc, G.F., and Potter, R.L. (2011) Hypochromicity in red blood cells: An experimental and theoretical investigation. *Biomedical Optic Express*, **2** (8), 2126-2143.

Osterwalder, U. and Herzog, B. (2009) Chemistry and properties of organic and inorganic uv filters. Pp. 11-38 in: Clinical Guide to Sunscreens and Photoprotection (H.W. Lim and Z.D. Draelos, editors). Informa Healthcare, New York.

Palozza, P., Serini, S., Nicuolo, F.D., and Calviello, G. (2004) Modulation of apoptotic signaling by carotenoids in cancer cells. *Arc Biochemistry and Biophy*sical, **430**, 104-109.

Qiu, H., LV, L., Pan, B-C., Zhang, Q-J ., Zhang, W-M, Zhang, Q-X. (2009) Critical review in adsorption kinetic models. *Journal of Zhejiang University SCIENCE A*, 10: 716-724.

Rahmalia, W. (2016) Paramètres de performances de photo-électrodes de TiO2/kaolinite et d'électrolyte a base de carbonates biosourcés dans la cellule solaire sensibilisée par la bixine. PhD Thesis, Institut National Polytechnique de Toulouse, Toulouse, France, 188 pp.

Reichardt, C. (1994) Solvatochromic dyes as solvent polarity indicators. *Chemical Reviews*: *1594*, *94,* 2319-2358.

Rodriguez-Amaya, D.B. (2002) A Guide to carotenoid analysis in food, ILSI Press, Washington.

Rudolph, T., Eisenberg, S., Grumelard, J., and Herzog, B. (2014) State-of-the-art light protection against reactive oxygen species. *International Journal for Applied Science*, **3**, 10-14.

Ruiz-Anchondo, T., Flores-Holguín, N., and Glossman-Mitnik, D. (2010) Natural carotenoids as nanomaterial precursors for molecular photovoltaics: A computational DFT study. *Molecules* , **15**, 4490-4510.

Santosa, S.J., Siswanta, D., Kurniawan, A., and Rahmanto, W.H. (2007) Hybrid of chitin and humic acid as high performance sorbent for Ni(II), *Surface Science*, 601, 5155–5161.

Sattar, A, de Man, J.M., Alexander, J.C. (1977) Wavelength effect on light-induced decomposition of vitamin A and β-carotene in solutions and milk fat. *Canadian Institute of Food Science and Technology Journal*, **10**, 56-60.

Sejie, F.P. and Nadiye-Tabbiruka, M.S. (2016) Removal of methyl orange (MO) from water by adsorption onto modified local clay (Kaolinite). *Physical Chemistry*, 6, 39-48.

Sengupta, P.C., Saiki, P.C., and Borthakur P. (2008) SEM EDX characterization of an iron-rich kaolinite clay. *Journal of Scientific Industrial Research*, **67**, 812-818.

Siems, W., Wiswede, I., Salerno, C., Crifo, C., Augustin, W., Schild, L., Langhans, C.D., and Sommerburg, O. (2005) β-carotene breakdown products may impair mitochondrial functions-potential side effects of high-dose β-carotene supplementation. *Journal of Nutricy and Biochemistry*, **16**, 385-397.

Silva-Buzanello, R.A., Souza, M.F., Oliveira, D.A., Bona, E., Leimann, F.V., Cardozo, L. F., Araújo, P.H.H., Ferreira, S.R.S., and Gonçalves, O.H. (2016) Preparation of curcumin-loaded nanoparticles and determination of the antioxidant potential of curcumin after encapsulation. *Polímeros,* **26** (3), 207-214.

Srivastava, P., Singh, B., and Angove, M. (2005) Competitive adsorption behavior of heavy metals on kaolinite. *Journal of Colloid and Interface Science*, **290**, 28–38.

Sudhakar, M.P., Ananthalakshmi, J.S. and Beena, B.N. (2013) Extraction, purification and study antioxidant properties of fucoxanthin from seaweeds. *Journal of Chemistry and Pharmatical Research*, **5** (7), 169-175.

Suryana, S., Khoiruddin., and Supriyanto, A. (2013) Beta-carotene dye of Daucus carota as sensitizer on dye-sensitized solar cell. *Materials Science Forum*, **737**, 15-19.

Tonlé, I.K., Letaif, S., Ngameni, E., Walcarius, A., and Detellier, C. (2011) Square wave voltammetric determination of lead (II) ions using a carbon paste electrode modified by a thiol-functionalized kaolinite. *Electroanalysis*, **23**, 245-252.

Vaculikova, L., Plevova, E., Vallova, S., and Kouttnik, I. (2011) Characterization and differentiation of kaolinites from selected Czech deposits using infrared spectroscopy and differential thermal analysis. *Acta Geodynamic and Geomaterials*, **8**, 59–67.

Van Keulen, F., Carolas, A.L., Brito, M.L., and Ferreira, B.S. (2010) Production of high-purity carotenoids by fermenting selected bacterial strains. US Patent. 2010/0145116 A1.

Vivas, M.G., Silva, D.L., de Boni, L., Zalesny, R., Bartkowiak, W., and Mendonca, C.R. (2011) Two-photon absorption spectra of carotenoids compounds**.** *Journal of Applied physics*, **109**, 103529.

Vizcayno, C., Gutierrez, R.M., Castello, R., Rodriguez, E., and Guerrero, C.E. (2010) Pozzolan obtained by chemical and thermal treatments of kaolin. *Applied Clay Science*, **49**, 405-413.

Vítek, P., Jehlička, J., Bezděk, J., Franců, E. (2009) Degradation of β-carotene under uv-rich irradiation conditions: implication for martian environmental. 40th Lunar and Planetary Science Conference.

Waghmode, A.V. and Kumba, R.R. (2015) Phytochemical screening and isolation of fucoxanthin content of Sargassum ilicifolium. *International Journal of Pure and Applied Biosciences,* **3** (6), 218-222.

Wong, I.Y.H., Koo, S.C.Y., and Chan, C.W.N. (2011) Prevention of age related macular degeneration. *International Journal of Optic and molecules*, **31**, 73-82.

Xiao, Y-D., Huang, W-Y., Li, D-J., Song, J-F., Liu, C-Q., Wei, Q-Y., Zhang, M., and Yang, Q-M. (2018) Thermal degradation kinetics of all-trans and cis-carotenoids in a light-induced model system. *Food Chemistry*, 239, 360-368.

Yan, X., Chuda, Y., Suzuki, M., and Nagata, T. (1999) Fucoxanthin as the major antioxidant in Hijikia fusiformis a common edible seaweed. *Bioscience, Biotechnology and Biochemistry*, **63** (3), 605-607.

Zaelani, K., Kartikaningsih, H., Kalsum ,U., and Sanjaya, Y.A. (2015) Fucoxanthin effect of pure sargassum filipendula extract toward hela cell damage. *International Journal of Pharmatechnology and Research*, **8**(3), 402-407.

Zebib, B., Mouloungui, Z., Noirot, V. (2010) Stabilization of curcumin by complexation with divalent cations in glycerol/water system. *Bioinorganic Chemistry and Applications*, **2010**, 1-8.

Zsirka, B., Horvath, E., Mako, E., Kurdi, R., and Kristof, J. (2015) Preparation and characterization of kaolinite nanostructure: Reaction pathways, morphology and structural order. *Clay minerals*, **50**, 329-340.

CHAPTER VI

FABRICATION OLED USING BIOMOLECULES

CHAPTER VI
FABRICATION OLED USING BIOMOLECULES

1.   Introduction

Organic light emitting diode (OLED) is monolithic, thin-film, semi conductive that emits light when voltage is applied to it (Zmija and Malachowski, 2009). The voltage applied on the electrode is very low from 2.5 to ~ 20 V and the active layer is very thin, ~10Å to 100 nm (Patel and Prajapati, 2014). Their low power consumption provides for maximum effeciency and helps minimize heat and electric interference in electronic devices. The active layer also has very high electric field in order of 105-107 V/cm.

In general, the OLEDs operate in the following manner: electrons are injected from cathode, and holes are injected from anode (typically transparent). The injected charges migrate against each other in the opposite direction, meet and recombine. Recombination energy is released and the molecule or polymer segment in which the recombination occurs, reaches an exited state. In OLED, it is desirable that all the excess excitation energy released as photon (light) not heat. This phenomenon known as organic electroluminescence (EL). Approximately 25% of the excitions are in the singlets states and 75% in the triplets states. The emission from the single states, is well-known as fluorescence, was believed to be the only applicable form of energy release. Therefore, the maximum internal quantum efficiency (IQE) of OLED is 25%.

The organic stack consist of series individual organic material tailored for specific funtionality, e.g. light emission and carrier transport (electron or hole). The guiding principle for choising the right composition of organic or polymer for EL device is that energetic position of the HOMO/LUMO (Highest Occupied Molecular Orbital/Lowest Unoccupied Molecular Orbital) (Zmija and Malachowski, 2009).

The first report on using biomolecule in OLED was initiated by Tajima *et al* (2003). They used cytochrome c as emitting layer. They obtained emission spectrum band of cytochrome c was 690 nm at applied voltage during the EL measurement 8 V. Their group research also used the other biomolecules such as chlorophyll a, myoglobin, hemin, Vitamin B_{12} (Tajima *et al*., 2006). Soltani Rad *et al*. (2015) fabricated OLED using curcumin which is the donor-acceptor (D-A) type of chromosphor type.

Carotenoids constitute an important class of linear π-conjugated molecules that exhibit high degree of electronic delocalization and ultrafast dynamic (Vivas *et al*., 2011). The β-carotene is one of the potential natural organic compound used as biofunctional electronic, as organic field effect transistors (OFETs) and organic photovoltaics (OPVs) (Głowacki *et al*., 2011; Suryana *et al*., 2013). The molecular structures of carotenoids present donor-p-acceptor forms which are very promising candidates for this applications. Bouchouit *et al* (2015) studied the non linear optical properties of some caretonoid compound and concluded the nonlinear optical properties of the studied pigments decrease in the order of β-carotene > violaxanthin > xanthophyll.

In this work, OLED will be fabricated using some biomolecules such as: β-carotene, fucoxanthin, curcumin, and chlorophyll a. The absorption and fluorescence properties of those molecules were resumed at Table 6.1.

Table 6.1: Absorption and fluorescence properties of biomolecules

Biomolecule and the system	Absortion maxima,λa (nm)	Fluorescence maxima, λ_{fl} (nm)	Fluorescence Quantum yield, Φ_{fl}	Fluorescence life time, τ_{fl} (ps)	Reff
β-carotene in chloroform	463	540			Van Riel *et al*., 1983
		430	6.1×10^{-5}		Jørgensen *et al*., 1991
		530		14 μs	Burke et al., 2000
Fucoxanthin in CS_2	476	685	5.0×10^{-5}	41	Katoh *et al*.,1991
Curcumin in acetone	418	513	0.159	0.182	Barik *et al*., 2004
Chlorophyll a in triton (acetone)	436-437	730		< 30 ps	Il'in and Borisov, 1981
Chlorophyll a in organic solvents			0.25	$<10^{-10}$s	Forster and Livington, 1952

2. Fabrication OLED

All the biomolecules were from Sigma Aldrich, France. Molecular structure of some material using in OLED are represented at Figure 6.1 and the informations about the HOMO-LUMO the material are listed at Table 6.2. Fabrication of OLED using Tecnische Instrument GmbH, Specbos 1201-JETI. Preparation and treatment of samples in glove with N_2 condition.

Alq₃   BAlq   MoO₃
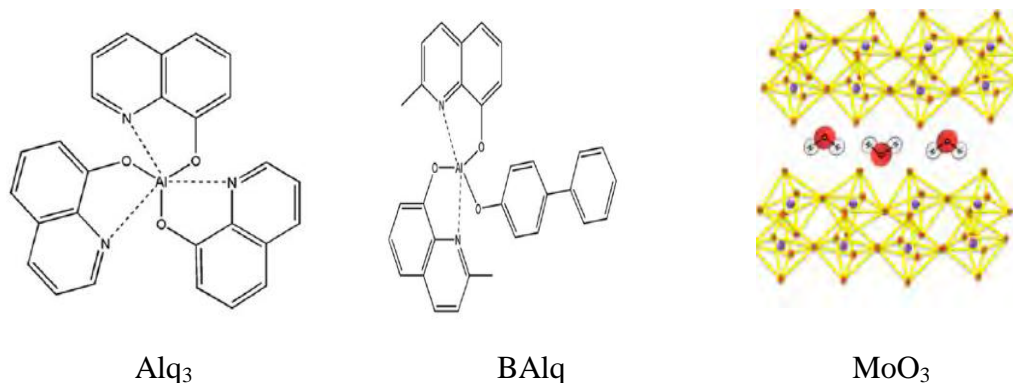
Figure 6.1: Molecular structure of materials used in OLED

Table 6.2: HOMO-LUMO materials used in fabrication OLED

Material	Abbreviation	HOMO (eV)	LUMO (eV)	Band gap (eV)	Reference
Indium Tin Oxide	ITO			-4.7 (Anode)	Parthasarathy *et al.*, 2003
Calcium	Ca			~ -3.0 (Cathode)	Brütting *et al.*, 2001
Molybdenum trioxide	MoO$_3$			-6.86	Kao and Chiu, 2015
4,4'-bis[N-(1-napthyl)-N-phenyl-amino] biphenyl	NPD	-5.7	-2.6	HTL	Parthasarathy *et al.*, 2003
Aluminum tris-(8-hydroxyquinoline)	Alq3	-5.7	-3.0	ETL	Chu *et al.*, 2005
Aluminum (III) bis(2-methyl-8-quninolinato) -4-phenylphenolate	BAlq	-5.9	-3.0	ETL	Chu *et al.*, 2005
Fucoxanthin	Fx	-6.60	0.39	EL	Premvardhan *et al.*, 2008
β-carotene	Car	-5.84	-3.54	HTL, EL	Głowacki *et al.*, 2011
Curcumin	Cur	-5.3	-2.04	EL	Soltani Rad *et al.*, 2015
Chlorophyll a	Chl	-5.009	-3.294	EL	Faiz *et al.*, 2018

HTL = hole transport layer, ETL =electron transport layer, EL = emitting layer

3. **Fucoxanthin as emitter material**

Schematic design in OLED fabrication is represented at Figure 6.2. Here, fucoxanthin used as emitter layer (EL), and three type of ETL were used: Bphen, Alq3 and BAlq. From the premier data, there was no difference emission spectra from NPD/Fx/Bphen and NPD/Bphen. Therefore, Figure 6.2 only represented fabrication OLED using Alq3 and BAlq.
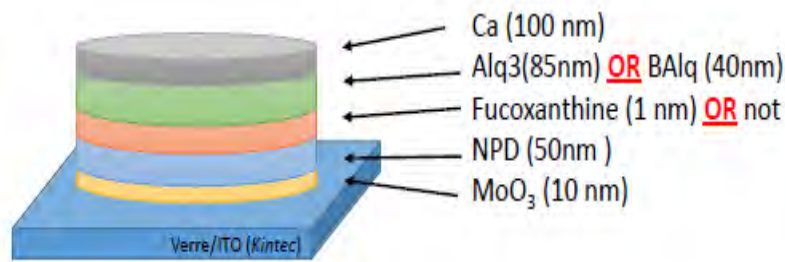
Figure 6.2: Schematic OLED fabrication using fucoxanthin

MoO_3 as p-type dopant was used to improve the conductivity of ETL and HTL material (Kao and Chiu, 2015). MoO_3 as a carrier of hole from anode to the HTL. The radiance spectra and CIE coordinate diagram of Alq3 with fucoxanthin is represented at Figure 6.3.

OLED desain with NPD(50nm)/Alq3 (85 nm) has wavelength maxima at 555 nm with CIE (x,y)= 0.416; 0.5212. The effect of using fucoxanthin to the the radiance spectra and CIE seem not too significant. The λ_{max} and CIE almost unchanged. If ETL was replaced by BAlq, fucoxanthin changed the λ_{max} of the radiance from 449 nm to 521 nm. The CIE diagram shifted from blue region to the green one (Figure 6.4).
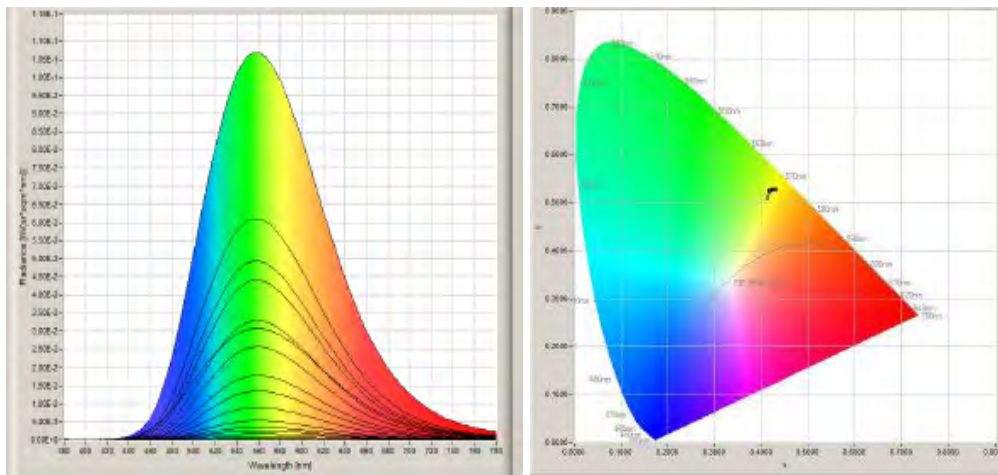
NPD(50nm)/Alq₃(85nm)
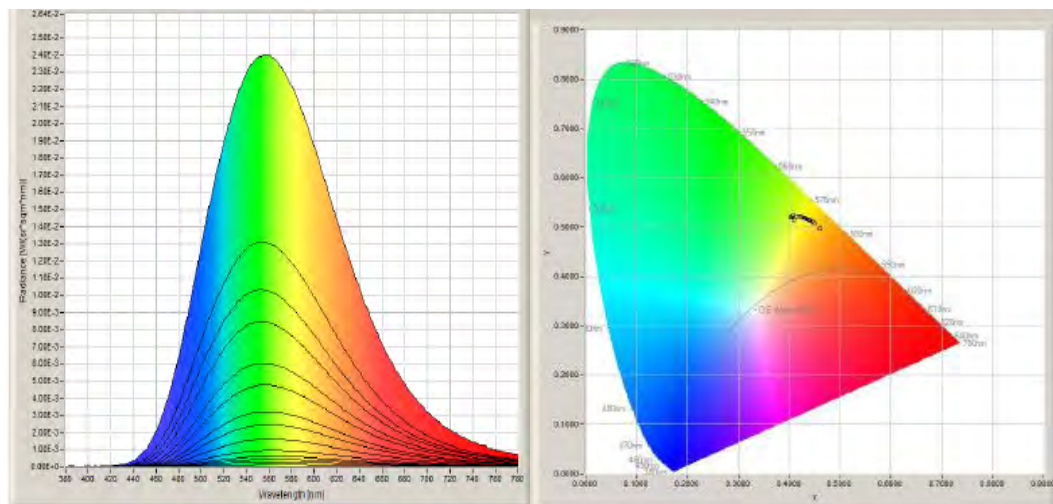
NPD(50nm)/Fx(1nm)/Alq₃(85nm)

Figure 6.3: The radiance spectra and CIE coordinate diagram Alq$_3$ with fucoxanthin

Figure 6.4 described the radiance spectra and CIE coordinate diagram of OLED NPD(50nm)/BAlq(50nm) and NPD(50nm)/Fx(1nm)/ BAlq(50nm). There is no different significantly in color at the OLED device using fucoxanthin or not. The CIE coordinate diagram at a yellow area.
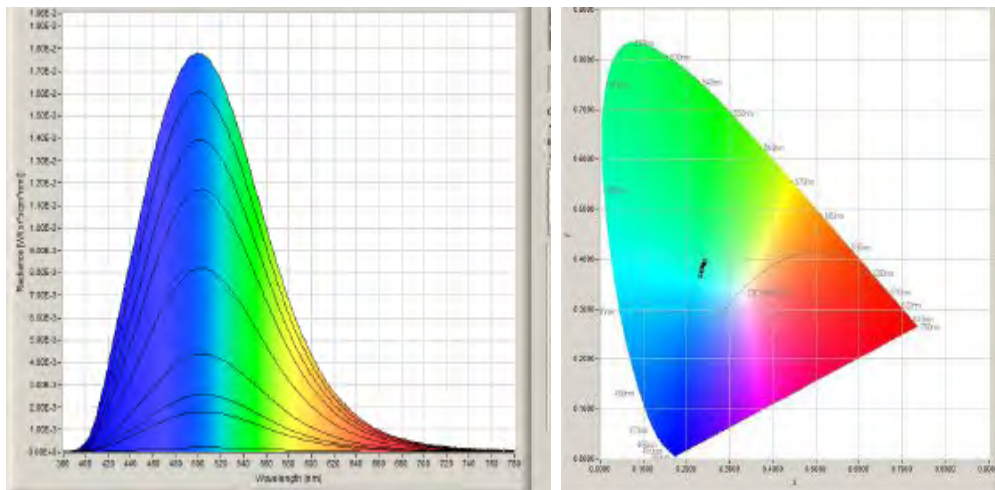
NPD(50nm)/BAlq(50nm)
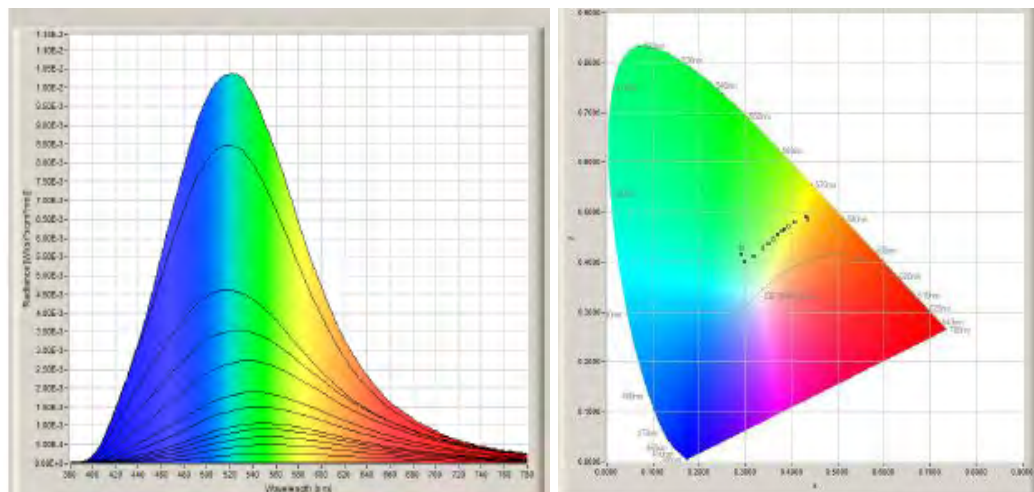
NPD(50nm)/Fx(1nm)BAlq(50nm)

Figure 6.4: Radiance spectra and CIE coordinate diagram of OLED using BAlq with fucoxanthin

Figure 6.5 shows the emission spectra of devices using   The peak emission wavelength is at $\lambda = 555$ nm for NPD/Fx/ Alq$_3$ and 520 nm for NPD/Fx/BAlq based device which indicate that fucoxanthin caused blue shifting.

NPD/Alq$_3$

NPD/Fx/Alq$_3$

NPD/BAlq

NPD/Fx/BAlq
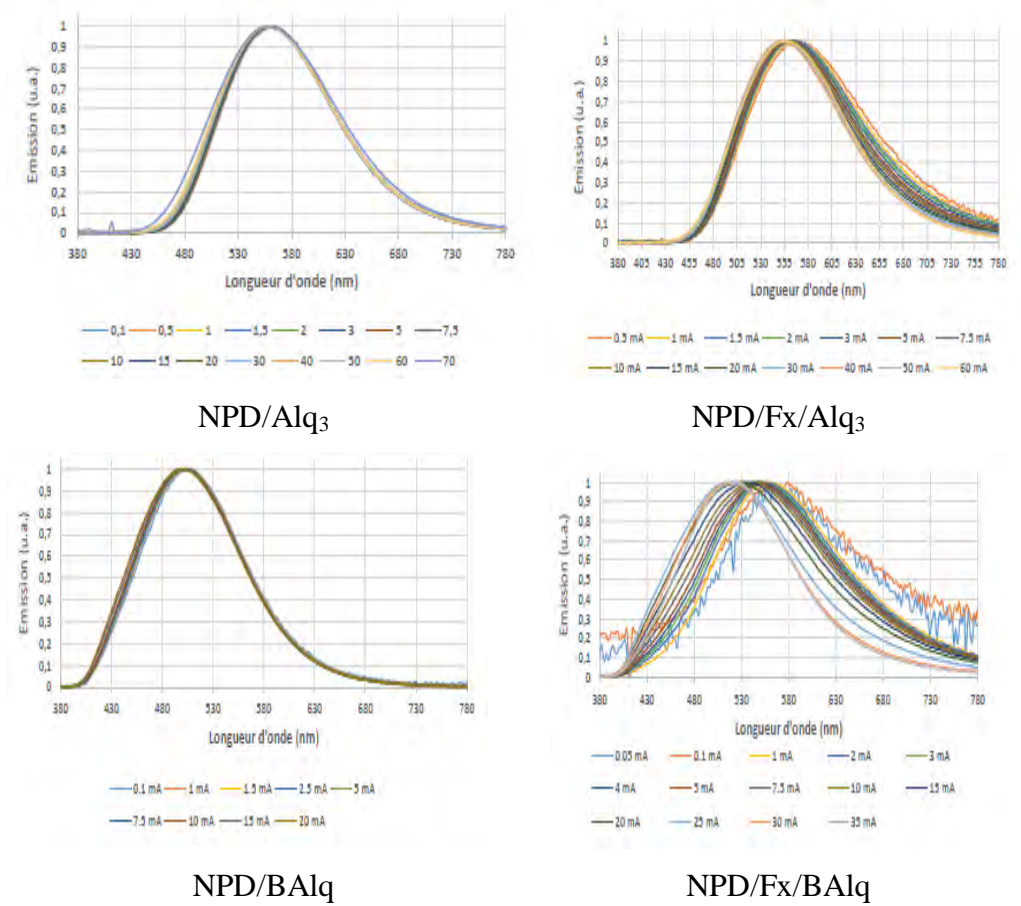
Figure 6.5: Emission spectra of OLED devices with different ETL

Figure 6.6 shows the current density (J) versus voltage (V) characteristics for devices based on NPD/Fx with two different ETL. All the devices turn on about 10 V. Fucoxanthin increased the voltage applied, especially when fabricated with BAlq.
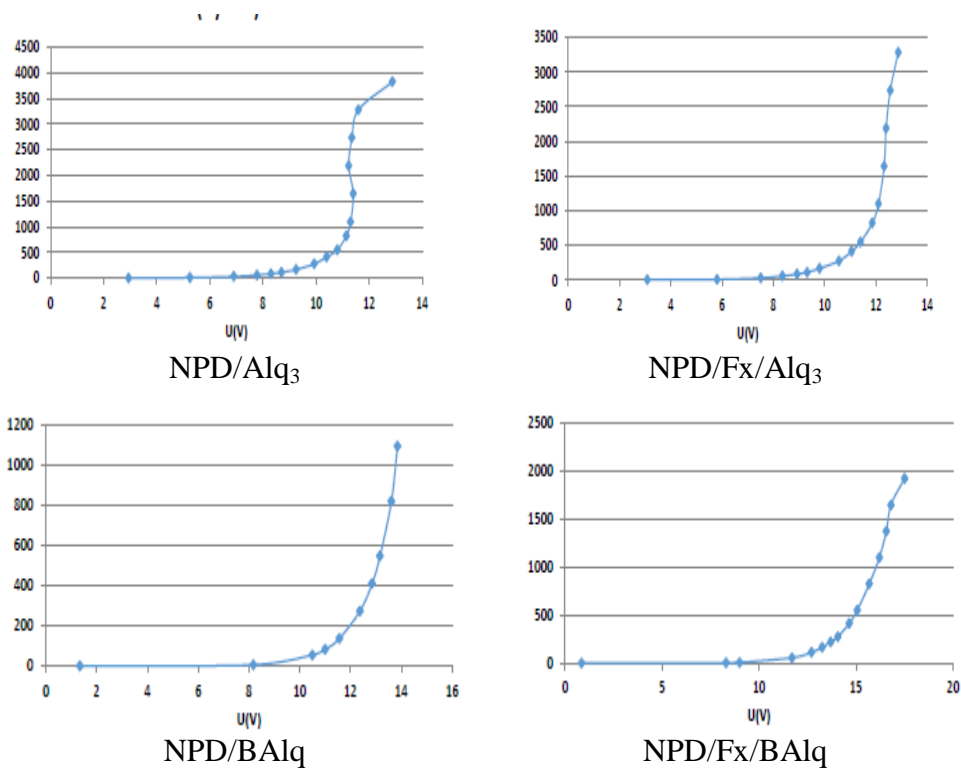
Figure 6.6: The Current Density (*J*) versus voltage (*V*) for fucoxanthin in OLED

The external quantum efficiency (EQE) was derived due to Sharbati *et al*. (2011). OLED device using fucoxanthin NPD/(50nm)/Fx(1nm)/Alq$_3$(85nm) yielded maximum EQE of ηEQE=0.12% and the optical measurement for all the composition are listed at Table 6.3.

Table 6.3: Characterization OLED devices using fucoxanthin

Devices	λ$_{max}$ (nm)	EQE (%) at 100 A/m^2	CIE (x,y)	Color
NPD(50nm)/Alq$_3$(85nm)	560	0.60	0.4160, 0.5212	yellow
NPD(50nm)/Fx(1nm)/Alq$_3$(85nm)	555	0.12	0.4160, 0.5302	yellow
NPD(50nm)/BAlq(50nm)	505	0.50	0.2312, 0.3648	blue
NPD(50nm)/Fx(1 nm)/Balq(50nm)	520	0.12	0.2925, 0.4287	green

Fucoxanthin reduced the EQE of all devices may be due to the higher band gap of fucoxanthin that contributed to the less mobility of electron. The other possibility is came from the molecular structure which has less π-electron conjugation (Bouchouit *et al*.,2015).

Base on the EQE value at Table 6.3, fabrication OLED using fucoxanthin is better with ETL Alq3 rather than BAlq. Although, fucoxanthin in device with ETL Alq3 reduced the EQE of the OLED more than BAlq, but it existence did not cause shifting. Therefore, the next step is to characterize the EQE of OLED devices by combine fucoxanthin with other biomolecules using Alq3 as ETL.

4. Biomolecules in OLED

HOMO-LUMO of all the materials used and OLED fabrication are schemed at Figure 6.7. At this device scheme, β-caroten used as HTL combine with other dyes as a EL materials. The device using only β-caroten did not give emission perfomance, but with combination with curcumin yielded external quantum effeciency, EQE at 100 A/m^2 = 0.02% (device A).
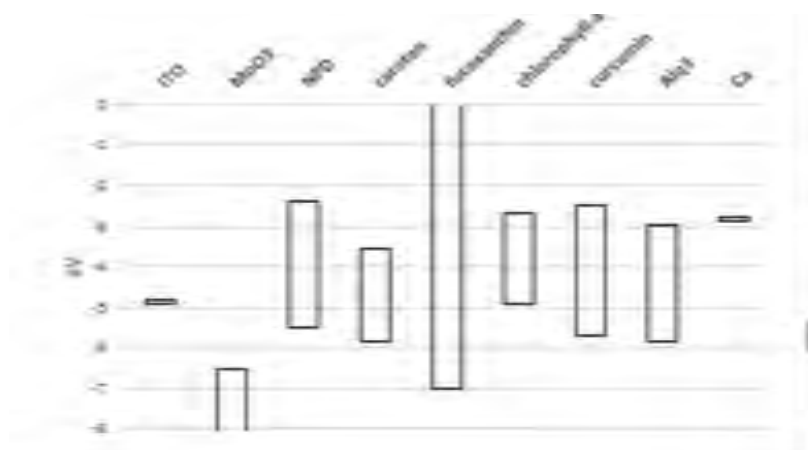
(a)
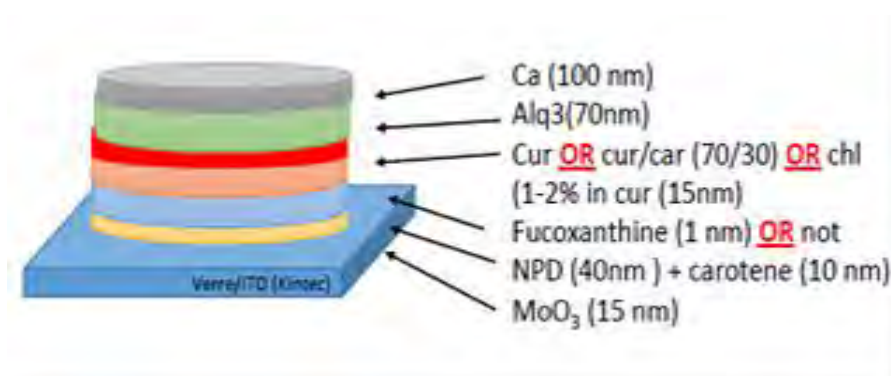
(b)

Figure 6.7: HOMO-LUMO energy level of materials used (a), and scheme of OLED fabrication using biomolecules (b)

The λ$_{max}$, EQE, CIE and color of OLED product were presented at Table 6.4. Device with only dyes β-carotene did not yielded emision, but combination with other dyes resulted with variation EQE from 0.0055-0.02%. The external quantum effeciency of OLED device using β-carotene with other dyes (B, C and D) were lower than device A.

The composition of OLED using β-carotene/curcumin in this research is MoO_3(15nm)+NPD(40nm)+Car(10nm)/Cur(15nm)/Alq3(70nm)/Ca(100nm). This device yielded the EQE about 0.02% which is almost the same with Soltani Rad *et al*. (2015). Soltani Rad *et al*. reported that the external quantum effeciency of the configuration ITO/4,4'-Bis(N-carbazolyl)-1,1'-biphenyl

(CBP) (45 nm)/ Curcumin (35 nm)/ 1,4-phenylenebis(triphenyl silan) (HGH2) (10 nm)/ Alq3(35 nm)/LiF(1 nm) /Al (100 nm) was 0.029% at 0.5-1 V. The applied voltage in our fabrication test is lower than 10V (about 8 V).

Binary compound of natural dyes (β-carotene and curcumin) resulted external quantum effeciency almost the same with OLED device using curcimin with dopant HGH2. This result shows give a new method to use natural dyes curcumin/ β-carotene at OLED fabrication without dopant.

Table 6.4: Fabrication OLED using biomolecules

Code	Devices	λ_{max} (nm)	EQE (%) at 100 A/m^2	CIE (x,y)	Color
A	MoO$_3$(15nm)+NPD(40nm)+Car(10nm)/ Cur(15nm)/Alq3(70nm)/Ca(100nm)	545	0.02	0.3867, 0.5155	yellow
B	MoO$_3$(15nm)+NPD(40nm)+Car(10nm)/ Fx(0.8nm)+Cur-Car(15nm)/Alq3(70nm)/Ca(100nm)	550	0.035	0.3832, 0.5304	yellow-green
C	MoO$_3$(15nm)+NPD(40nm)+Car(10nm)/Chl in Cur(15 nm)/Alq3(70nm)/Ca(100nm)	720	0.002	0.4590, 0.4787	yellow-red
D	MoO$_3$(15nm)+NPD(40nm)+Car(10nm)/Fx(0.8nm)+Chl in Cur(15 nm)/Alq3(70nm)/Ca(100nm)	700	0.0055	0.4358, 0.4800	yellow-red

5. Conclusions

Fucoxanthin in OLED devices NPD/Fx/ETL reduced significantly the EQE (%) almost 80% in Alq$_3$ and 76% in BAlq. Fucoxanthin device using BAlq change the color from blue into green. OLED device NPD(50nm)/Fx(1nm)/Alq3(85nm) has EQE 0.12% and CIE (0.4160, 0.5302). Fabrication OLED using fucoxanthin is not good enough related to band gap of fucoxanthin, which is very large and can be an isolator. Fabrication OLED using binary compound of β-carotene as HTL and curcumin as EL layer resulted yellow color with EQE 0.02%.

References

Barik, A., Goel, N.K., Priyadarsini, K.I., and Mohan, H. (2004) Effect of Deuterated Solvents on the Excited State Photophysical Properties of Curcumin. Journal of Photoscience, **11**(3), 95-99.

Burke, M., Land, E.J., McGarvey, D.J., and Truscott, T.G. (2000) Carotenoid triplet state lifetimes. *Journal of Photochemistry and Photobiology B: Biology*, **59**, 132–138.

Brütting, W., Berleb, S., and Mückel, A.G. (2001) Device physisc of organic light-emitting diode based on molecular materials. *Organic Electronics*, **2**, 1-36.

Chithambararaj, A., Yogamalar, N.R., and Bose, A.C. (2016) Hydrothermally Synthesized h-MoO_3 and α-MoO_3 Nanocrystals: New Findings on Crystal-Structure-Dependent Charge Transport. *Crystal Growth & Design*, **16**, 1984−1995.

Chu, T-Y., Wu, Y-S., Chen, J-F., and Chen, C.H. (2005) Characterization of electronic structure of aluminum (III) bis(2-methyl-8-quninolinato)-4 phenylphenolate (BAlq) for phosphorescent organic light emitting devices. *Chemical Physics Letters*, **404**, 121–125.

Faiz, M.R., Widhiyanuriyawan, D., Siswanto, E., and Wardana, I.N.G. (2018) Theoretical study on the effect of solvents in chlorophyll solution for Dye-Sensitized Solar Cell. IOP Conf. Series: Materials Science and Engineering 299, 012089.

Forster, L.S. and Livingston, R. (1952) The Absolute Quantum Yields of the Fluorescence of Chlorophyll Solutions. *The Journal of Chemical Physics*, **20**, 1315.

Głowacki, E.D., Leonat, L., Voss, G., Bodea, M., Bozkurt, Z., Irimia-Vladu, M., Bauerf, S. and Sariciftci, N.S. (2011) Natural and nature-inspired semiconductors for organic electronics. Proceeding of SPIE 8118.

Il'ina, M.D and Borisov, A.Y. (1981) The fluoresence lifetime and quantum yield of chlorophyll a in tritonx-100 solutions. *Biochimica et Biophysica Acta*, **637**, 540-545.

Jorgensen, K., Stapelfeldt, H., and Skibsted. L.H. (1992) Fluorescence of carotenoids. Effect of oxygenation and cis/trans isomerization. *Chemical Physical Letters*, **190** (5), 514-519.

Kao, P-C and Chiu, C-T. (2015) MoO_3 as p-type dopant for Alq_3-based p–i–n homojunction organic light-emitting diodes. *Organic Electronics*, **26**, 443–450.

Katoh,T., Nagashima, U., and Mimuro, M. (1991) Fluorescence properties of the allenic carotenoid fucoxanthin: Implicationfor energy transfer in photosynthetic pigment systems. *Photosynthesis Research*, **27**, 221-226.

Parthasarathy, G., Liu, J., and Duggal, A.R. (2003) Organic light emitting devices from displays to lighting**.** *The Electrochemical Society Interface*, Summer, 42-47.

Patel, B.N. and Prajapati, M.M**. (**2014) OLED: A Modern Display Technology. *International Journal of Scientific and Research Publications*, **4** (6), June.

Premvardhan, L., Sandberg, D.J., Fey, H., Robert R. Birge, R.R., Büchel, C., and Rienk van Grondelle, R. (2008) The charge-transfer properties of the S2 state of fucoxanthin in solution and in fucoxanthin chlorophyll-a/c2: protein (FCP) based on stark spectroscopy and molecular-orbital theory. *Journal. Physical Chemistry B*, **112***,* 11838–11853.

Soltani Rad, M.N., Sharbati, M.T., Behrouz, S., and Nekoei, A.R. (2015) Fabrication of non-doped red organic light emitting diode usingnaturally occurring Curcumin as a donor-acceptor-donor (D-A-D) emitting layer with very low turn-on voltage. *Iranian Journal of Science & Technology,* **39A3**, 297-304.

Suryana, S., Khoiruddin., and Supriyanto, A. (2013) Beta-carotene dye of Daucus carota as sensitizer on dye-sensitized solar cell. *Materials Science Forum*, **737**, 15-19

Tajima, H., Ikeda, S., Matsuda, M., Hanasaki, N., Oh, J.W., and Akiyama, H. (2003) A light-emitting diode fabricated from horse-heart cytochrome c . *Solid State Communications*, **126**, 579–581.

Tajima, H., Shimatani, K., Komino, T., Ikeda, S., Matsuda, M., Ando, Y., and Akiyama, H. (2006) Light-emitting diodes fabricated from biomolecular compounds. *Colloids and Surfaces A: Physicochemical and Engineering Aspects,* **284–285**, 61–65.

Vivas, M.G., Silva, D.L., de Boni, L., Zalesny, R., Bartkowiak, W., and Mendonca, C.R. (2011) Two-photon absorption spectra of carotenoids compounds. *Journal of Applied physics*, **109**, 103529.

Zmija, J. and Maachowski, M.J. (2009) Organic light emitting diodes operation and application in displays. *Archives of Materials Science and Engineering,* **40** (1), 5-12.

GENERAL CONCLUSIONS AND FUTURE WORK

GENERAL CONCLUSIONS AND FUTURE WORK

GENERAL CONCLUSION

The objective of this thesis was to improve the photostability of carotenoid using antioxidant and modified kaolinite for fabrication OLED. In general conclusions, in this work, two type of carotenoids were used: β-carotene and fucoxanthin. Curcumin and fucoxanthin were used as antioxidant. There are four main step were done at the research activity: (1) characterization of natural clay from Congo, Gabon and Indonesia, (2) modification and characterization of kaolin clay, (3) study photostability of β-carotene with antioxidant and modified kaolinite, and (4) fabrication of OLED using biomolecules.

Natural clays from Central Africa (Congo Brazaville and Gabon) also Indonesia are kaolin types with different composition, almost associated with quatz. Kaolin from Capkala, Indonesia was kaolinite, and kaolin from Congo was nacritic. Red kaolin from Gabon consist of aliphatic carotenoid compound and quartz.

Activation nacritic clay from Congo Brazzaville with NH_4OH enhanced up the specific surface area from 30.548 m^2g^{-1} to 239.68 m^2g^{-1}. This is a new method to obtain higher specific surface area of treated clay, which is calcined at $600°C$ for 6 hour, and continuing activating with 5 M ammonium hydroxide. Modification metakaolinite from West Kalimantan with $ZnCl_2$ decreased specific surface area but increase the mean pore volume of this solid material. Zinc as a Lewis acid site in modified kaolinite is identified at band 1449 cm^{-1}.

Photoprotection efficiency of β-carotene by curcumin was higher than fucoxanthin. The protecting ability of fucoxanthin and curcumin related to the ability of both of these antioxidants to delocalized of electron and transfer electron. The concentration of antioxidant influenced the stability of β-

carotene. The percentage photostability of β-carotene by each antioxidant were 38.56% and 88.13%. Photoprotection efficiency of fucoxanthin by curcumin enhanced the half-life of fucoxanthin almost 3 fold and photostability 40%.

From cyclic voltametry analysis gived information that curcumin reduced the electrochemical gap of BC/Cur and Fx/Cur. Antioxidant fucoxanthin and curcumin decreased the electrochemical gap of the mix material. The electrochemical gap of carotene/curcumin is -1.61 eV, carotene/fucoxanthin is -1.75 eV compare to the only β-carotene -2.04 eV. Fucoxanthin can keep the first oxidation stage of β-carotene and still reversible, but not for curcumin.

Modified kaolinite also decreased photodegradation of β-carotene by shielded and protected from direct UV irradiation and caused the half-life time enhanced almost fiftieth times. The amount of β-carotene which adsorbed onto kaolinite was related to the photostability.

Fabrication OLED using fucoxanthin is not good enough related to band gap of fucoxanthin, which is very large and can be an isolator. Fucoxanthin in OLED devices NPD/Fx/ETL reduced significanly the EQE (%) almost 80% in Alq_3 and 76% in BAlq. NPD(50nm)/Fx(1nm)/Alq3(85nm) has EQE 0.12% and CIE (0.4160, 0.5302). Fucoxanthin in OLED devices with BAlq changed the color emission from blue into green. Fabrication OLED using β-carotene as HTL and curcumin as EL resulted yellow color with EQE 0.02%.

In conclusion, photostability of carotenoid can be enhanced by antioxidant and modified kaolinite. OLED can be fabricated using carotenoid fucoxanthin and β-carotene. For application of β-carotene in OLED device, its perfomance can be improved by using curcumin at the fabrication.

FUTURE WORK

First, concerning the result show from fabrication OLED using biomolecule which is not good enough due to the limitation of the fluoresence quantum yield of the dyes. Maximum only 25% from total emition as fluoresence. There are possibility to use delay-fluoresence compound to convert phosphorescence into fluoresecence. The other necessary study is to make fabrication with different HTL and ETL materials.

Second, β-carotene/modified kaolinite will be used as material in OLED fabrication with laser coating. Evaporation methode is not suitable to evaporate clay. In addition it will necesarry to study the activity acid site of this material using temperature programed desorption (TPD) analysis.

Third, natural clays are kaolin type with different composition, almost associated with quartz. Clay from Gabon is nacritic which is a very potential material for making a solid battery. But, the purification proces is needed to to increase fraction of nacrite mineral.

The other interisting material is 'red kaolin' from Gabon which is contain aliphatic carotenoid compound with a good electrochemical properties and UV-photostability. It will be interisting to isolate and elucidate this molecule because it can be used in optoelectronic and cosmetic (sunscreen) due to the half-life and the band gap electrochemical properties.

And fourth, activated nacritic clay with high surface can be applicated as adsorbent metal ion such as zinc (II) and its capability to improve the photostability of carotenoid or the the other natural dyes can be studied.

ANNEXE I

PUBLICATIONS

1. CHARACTERIZATION OF ACID SITES ON MODIFIED KAOLINITE BY FTIR SPECTRA OF PYRIDINE ADSORBED (*ACCEPTED, PROSIDING THE 2ND IC3P3, IN PRESS*)

2. PHOTOSTABILITY OF BETA-CAROTENE/MODIFIED KAOLINITE (*ACCEPTED, CLAYS AND CLAY MINERALS*)

Characterization of acid sites on modified kaolinite by FTIR spectra of pyridine adsorbed

Nelly Wahyuni, Georges Zissis, and Zéphirin Mouloungui

Characterization of Acid Sites on Modified Kaolinite by FTIR Spectra of Pyridine Adsorbed

Nelly Wahyuni [1,4,a)], Georges Zissis[2], and Zéphirin Mouloungui[1,3,b)]

[1]*Université de Toulouse, INP-ENSIACET, LCA (Laboratoire de Chimie Agro-industrielle),*
4 Allée Monso, F-31030 Toulouse, France
[2] *Université de Toulouse, Université de Toulouse, LAPLACE (Laboratoire Plasma et Conversion d'Energie), UPS,*
INPT, 118 route de Narbonne, F-31062 Toulouse, France
[3] *INRA, UMR 1010 CAI, F-31030, Toulouse, France*
[4]*Department of Chemistry, Mathematic and Natural Science, Tanjungpura University,*
Jl. Prof. H. Hadari Nawawi, Pontianak 78124, Indonesia

a) nelly.wahyuni@ensiacet.fr
b) zephirin.mouloungui@ensiacet.fr

Abstract. FTIR spectroscopy of adsorbed probe molecules has been existent for some decades and well-developed technique for analysis the composition and structure of the functional groups. In this research, we studied the surface structure of functional groups on modified kaolinite using pyridine. Modified kaolinite is made by a simple process, impregnation metakaolinite with zinc chloride and characterized by SEM-EDX and thermal gravimetric analysis. Zinc as a Lewis acid site is identified on modified kaolinite at 1449 cm^{-1}.

INTRODUCTION

Clay minerals are well-known and recognized as natural inorganic materials with good rheological and thermal characterictic as well as structural adsorption [1,2]. Kaolin is a 1:1 type of clay that is widely used in industry because of its low-cost, abundant availability, high adsorption properties, non-toxicity, large potential for ion exchange, surface charges, large surface area, charge density, hydroxyl groups on the edges, silanol groups of crystalline defects or broken surfaces, and Lewis and Brönsted acidity [3-6]. Kaolin has been used as an adsorbent for heavy metals (e.g. Cd^{2+}, Cu^{2+}, Pb^{2+}, and Zn^{2+} [7-10], gas (e.g. SO_2) [11], and dye molecules (e.g. bixin) [12,13]. Kaolin also has been widely accepted as an adsorbent because of its high adsorption capacity of the kaolinite due to the surface structure and edges.

In general, adsorption can be classified as either chemical sorption or physical sorption. Chemical adsorption or chemisorption is explained by the formation of strong chemical interactions between molecules or ions of adsorbate to adsorbent surface, which is generally due to the exchange of electrons. Thus, chemical sorption usually is irreversible. Physical adsorption (physisorption) is indicated by weak Van der Waals intraparticle bonds between adsorbate and adsorbent, and thus reversible. The physical forces controlling adsorption are Van der Waals forces, hydrogen bonds, polarity, and dipole–dipole π–π interaction [14].

In applications, some treatments have been used to enhance the properties of kaolinite. In general, there are two principal modifications: physical and chemical treatments. Physical modification with heating or microwave treatment can be used due to changes in chemical composition and crystalline structure at high temperature. Chemical modifications with acids, bases or organic compounds, usually through changes the structure, surface functional groups and surface area [15]. Calcined and followed by acid-activated kaolin is a favorable adsorbent for uranium (VI) removal from aqueous solutions [16] or adsorbent for dye molecule [17]. Rahmalia *et al*. studied

adsorption of bixin with acid and base-treated kaolin on aprotic solvent [17]. They concluded that electrostatic interactions between bixin and with acid and base-treated kaolin took place in two forms: one was between the carboxylic group of the bixin with Si of the treated kaolin and the other was between the carboxyester group of the bixin with Al of the treated kaolin.

In this research, we characterized the modified kaolinite, which was treated by calcination followed by impregnation with zinc chloride. The FTIR of the pyridine adsorbed was measured to evaluate the surface properties (Lewis and Brönsted acid sites) of the modified kaolinite. Brönsted and Lewis acid sites could be distinguished from the IR spectrum of the pyridine adsorbed on the clay surface. The spectrum showed well resolved and characteristic bands for the pyridine adsorbed on both types of the acid sites [18].

MATERIALS AND METHODS

Materials. The raw material of kaolin was from the Capkala Sub-district, District of Bengkayang, West Kalimantan, Indonesia. Zinc chloride and pyridine were both from Sigma Aldrich.

Methods. Modification of kaolin. Raw kaolin (K) was calcined at 600°C for 6 hours to convert it into metakaolinite (MKaol). 125 mL of 0.08 M $ZnCl_2$ was added to 5 g of metakaolinite and then stirred for six hours at room temperature. The mixture was then decanted. The solid fraction was later dried (MK) and characterized.

Characterization of modified kaolinite

Kaolin, metakaolinite, and modified kaolinite were characterized by scanning electron microscopy (SEM-EDX) and thermal gravimetric analysis (TGA). Micrographs and element content were obtained with a JEOL-JSM 7100 F, at an accelerating voltage of 10 kV. The samples were deposited on a sample holder with adhesive carbon foil and sputtered with gold. Thermal analysis was performed on Mettler-Toledo AG Analytical. All measurements were carried out at a heating rate of 10°C/min from room temperature until 800°C under the flow of N_2.

Characterization of total acidity of the kaolin, metakaolinite, and modified kaolinite were conducted under standard pressure and temperature. The porcelain crucible was heated at 110°C for an hour and the crucible weight was labelled as W_1. Then 0.2 g of samples were placed into the porcelain crucible and heated at the same temperature for 1 hour. The weight of the porcelain crucible containing the sample was labeled as W_2. The crucible containing the sample was inserted into the desiccators and then soaked in 25 mL of pyridine for 24 hours. The pyridine-adsorbed samples were dried at 130°C for 30 minutes to physically remove the adsorbed pyridine. The weight of porcelain was labelled as W_3. The pyridine was exposed to desiccators for 24 hours (before this treatment, the desiccators were made under vacuum conditions. This method modified methods from the references [19-21]. The gravimetric analysis method was used to measure the total acidity using this formula:

$$\text{Total acidity} = \frac{(W_3 - W_2)}{(W_2 - W_1) \cdot M} \qquad (1)$$

Where, M = molecular weight of pyridine (79.10 gram/mole)
The FTIR spectra of the samples were recorded using Shimadzu 8201 PC FTIR spectroscopy with KBr method.

RESULTS AND DISCUSSION

Characterization of kaolin from West Kalimantan shows that the main component is kaolinite associated with quartz and muscovite [22]. Morphology of the samples shows hexagonal platelets (Fig 1). Therefore, thermal treatment [23] and impregnation with zinc chloride do not drastically modify the morphology. Modification of metakaolinite with zinc chloride is represented by the absence of Zn in modified kaolinite (Fig 2). From SEM-EDX analysis, the amount of zinc in modified kaolinite is 6.1%. In other words, almost 46.9% of the total zinc is impregnated into the metakaolinite.
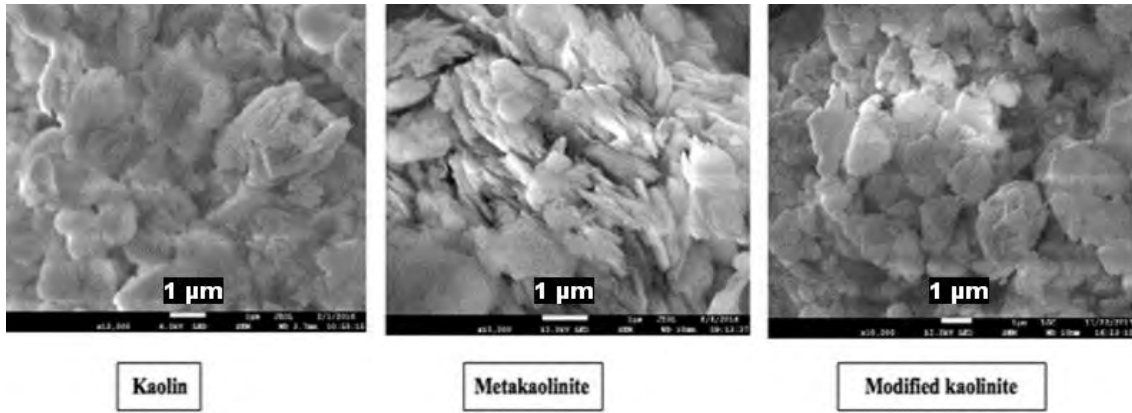
FIGURE 1. SEM micrographs of kaolinite, metakaolinite and modified kaolinite
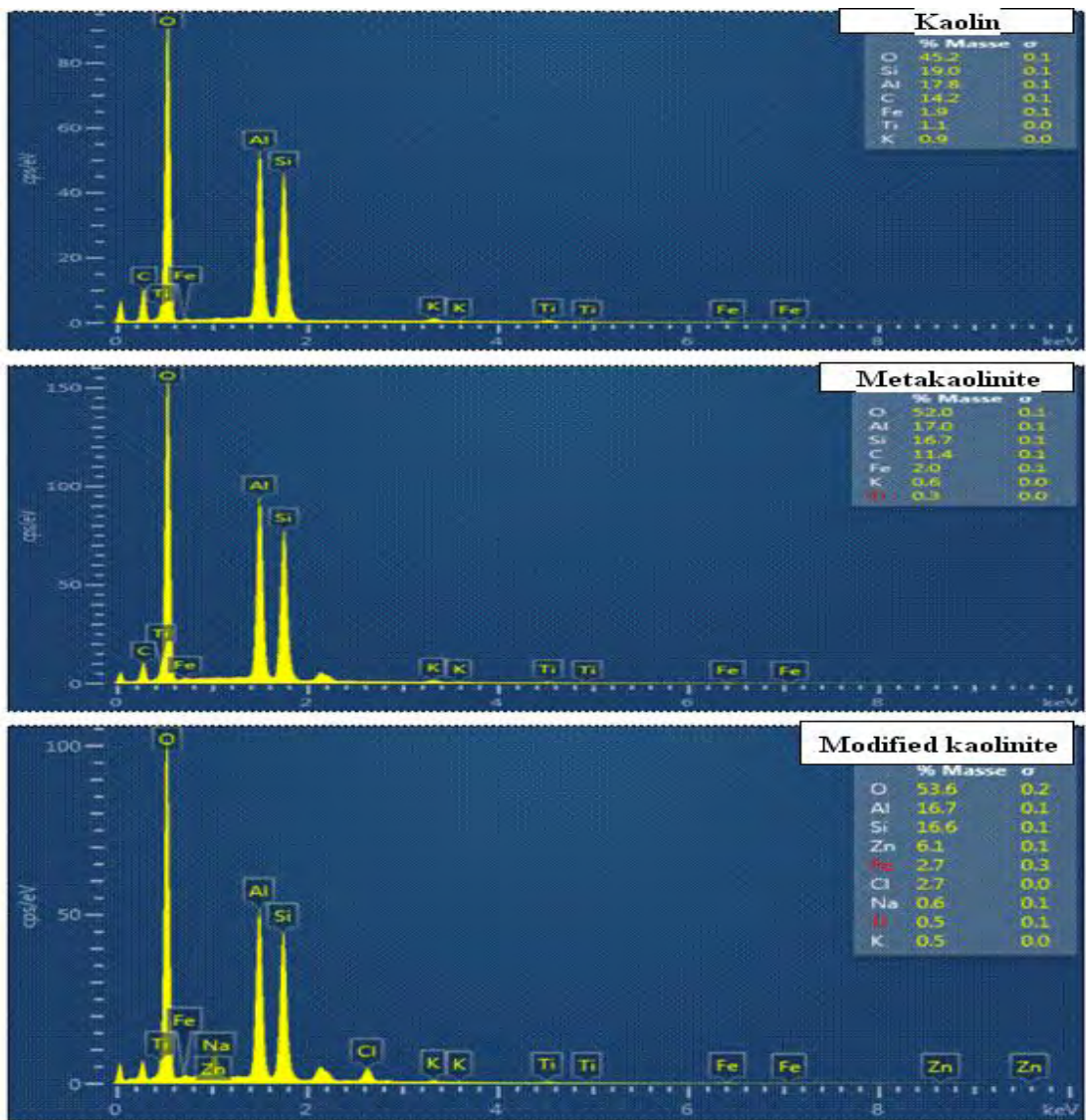
FIGURE 2. SEM-EDX of kaolin, metakaolinite and modified kaolinite

Base on SEM-EDX analysis, silicon and aluminum were rich in the samples. Si and Al contents were only slightly decreased after calcination and impregnation by zinc chloride (Table 1). This shows the persistence of natural kaolinite to heating and chemical treatment.

TABLE 1. Si and Al contents

Samples	Si	Al	Si/Al
Kaolin	19.0	17.8	1.07
Metakaolinite	17.0	16.7	1.02
Modified kaolinite	16.6	16.7	0.99

Thermo gravimetric analysis (TGA) of kaolin shows two peaks, i.e. around 70°C and 490°C (Fig 3). The first one at 70°C shows that the loss of mass of water molecules is 0.67%. The strong mass loss center at 490°C (11.52%) is due to dehydroxylation. Kaolin, metakaolinite and modified kaolinite have total loss mass 12.19; 1.05; and 1.61 %, respectively. This indicated that dehydroxylation in metakaolinite and modified kaolinite are lower than kaolin. For the dehydroxylation of kaolin and metakaolinite, the weight loss is equal to 12.62 [23]. Dehydroxylation means a reorganization and diffusion of hydroxyl group in the layer [24]. Metakaolinite is more reactive than kaolin due to the structural disorder. The structural disorder can be in the form of a deformation of silica network or existence of 4-coordinated aluminum. Both of those structural disorder is more reactive than 6-coordinated aluminum [23]. The reactive metakaolinite still contains about 10% of the OH- groups initially present in the kaolin and is suitable to a surface dissolution of metakaolinite in cationic solution such as Zn^{2+}.
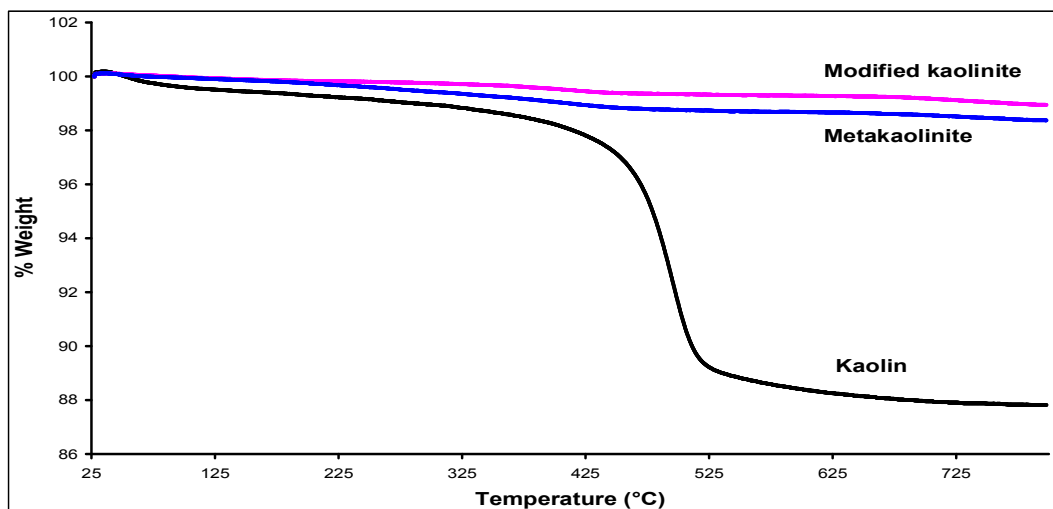
FIGURE 3. TGA of kaolin, metakaolinite, and modified kaolinite

Fig 4.a represents the FTIR spectra of the kaolin and the modification after adsorbing pyridine (Py). It has been well recognised that complex of adsorbed Py identified at mid-IR spectrum in range around 1700 cm^{-1} until 1400 cm^{-1}. There are two specific bands centre at 1540 cm^{-1} (broad and of m-intensity) and at 1445 cm^{-1} (sharp and of s-intensity). These bands correspond to the Brönsted and Lewis sites bound with pyridine, (B-Py) and (L-Py), respectively [25].

Lewis acid site at MK is revealed by the presence of a band at 1449 cm^{-1} (Fig 4.b). This Lewis acidity band is close to 1450 cm^{-1} [26] or 1445 cm^{-1} [25]. Pyridine coordinated to the Lewis sites is absorbed at near 1455 cm^{-1} and near 1610-1625 cm^{-1} [27]. This research also shows a band at 1608 cm^{-1}. The Lewis acid site comes from Zinc in modified kaolinite. Pyridine impact to the Si-O site as can be seen by the presence of two peaks at 1068 and 1044 cm^{-1}. It can be related to weak Brönsted bound (B-Py) due to the interaction of pyridine with Si-OH in modified kaolinite. The appearance of bands in range 1030-1035 cm^{-1} can be correlated to the Si-O stretching in kaolin [28].
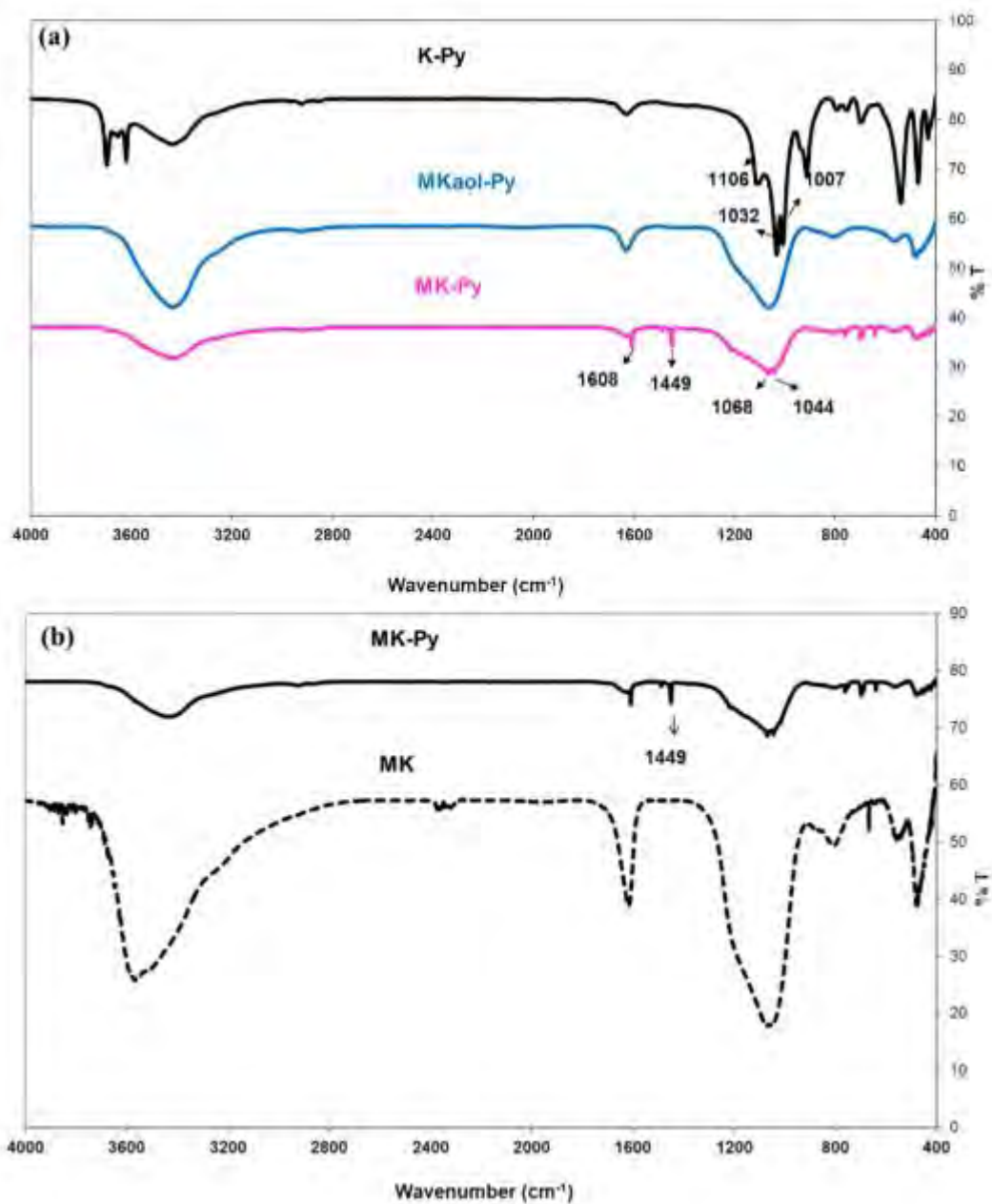
FIGURE 4. Spectra infrared of pyridine (Py) adsorbed onto kaolin (K), metakaolinite (Mkaol), and modified kaolinite (MK)

Modification of metakaolinite with $ZnCl_2$ enhances the total acidity more than three-fold (Table 2). Converting kaolin into metakaolinite does not significantly increase the total acidity. Modification of metakaolinite with $ZnCl_2$ improves the total acidity almost two-fold. The increase of total acidity of modified kaolinite is due to the zinc presence in the modified kaolinite.

TABLE 2. Total acidity of sample kaolin and the modification

Sample	Total acidity (mmol/g)
Kaolin	0.60
Metakaolinite	0.89
Modified kaolinite	1.95

This research clearly shows that modified kaolinite has Lewis acid site which can be identified from the infrared spectra of pyridine adsorbed. Lewis acid site is indicated by the existence of a band at 1449 cm^{-1} due to the zinc in modified kaolinite. Identification of acid site is important not only for catalytic application, but also in adsorption.

ACKNOWLEDGMENTS

REFERENCES

1. T. Ngulube, J. R. Gumbo, V. Masindi and A. Maity, J. Environ. Manag. **191,** 35-57 (2017).
2. D-W. Cho, C-M. Chon, Y. Kim, B-H. Jeon, F. W. Schwartz and E. S. Lee, Chem. Eng. J. **175**, 298-305 (2011).
3. T-J. Rong and J. Xiao, Mater. Lett. 57, 297– 301 (2002).
4. X. Liu, X. Lu, M. Sprik, J. Cheng, E. J. Meijer and R. Wang, Geochim. Cosmochim. Acta **117,** 180–190 (2013).
5. V. Vimonses, S. Lei, B. Jin , C. W. K. Chow and C. Saint, Appl. Clay Sci. **43,** 465–472 (2009).
6. M. N. Timofeeva, V. N. Panchenko, K. P. Volcho, S. Z. Zakusin, V. V. Krupskaya, A. Gil, O. S. Mikhalchenko and M. A. Vicente, J. Mol. Catal. A **414**, 160–166 (2016).
7. P. Srivastava, B. Singh and M. Angove, J. Colloid Interface Sci. **290**, 28–38 (2005).
8. M. A. K. Diop, C. A. K. Miehe-Brendle, J. Senocq, F. Maury and Francis, Clay Miner. **49**, 527-539 (2014).
9. J. S. Essomba, J. Ndi Nsami, P. D. Belibi Belibi, G. M. Tagne and J. Ketcha Mbadcam, Pure Appl. Chem. Sci **2**, 11-30 (2014).
10. W. Chai, Y. Huang, S. Su, G. Han, J. Liu and C. Y. Yijun, Physicochem. Probl. Miner. Process. **53**, 264−278 (2017).
11. C. Volzone and J. Ortiga. J. Environ. Management, **92**, 2590-2595 (2011).
12. A. R. Tehrani-Bagha, H. Nikkar, N. M. Mahmoodi, M. Markazi and F. M. Menger, Desalination **266**, 274–280 (2011).
13. A. Hiendro, F. Hadary, W. Rahmalia and N. Wahyuni, Enhanced performance of bixin sensitized solar cells with activated kaolinite. Inter.J. Eng. Research Innov. **4**, 40-44 (2012).
14. M. T. Yagub, T. K. Sen, S. Afroze and H. M. Ang, Adv Colloid Interface Sci. **209**, 172–184 (2014).
15. S. Kumar, A. K. Panda and R. K. Singh, Bull. Chem. React. Eng. Catal. **8**, 61-69 (2013).
16. G. Wang, X. Wang, X. Chai, J. Liu and N. Den, Appl. Clay Sci. **47**, 448–45 (2010).
17. W. Rahmalia, J. Fabre, T. Usman and Z. Mouloungui, Bioinorg. Chem. Appl. **2018**, 3805654 (2018).
18. C. R. Reddy, Y. S. Bhat, G. Nagendrappa and B. S. J. Prakash, Catal. Today **141**, 157–160 (2009).
19. K. D. Nugrahaningtyas, Y. Hidayat, Patiha, N. Prihastuti, B. Yelvi and R.U. N. Kalimah, ” Synthesis of the supported catalysts by co-impregnation and sequential impregnation methods,” in *International Conference on Advanced Materials for Better Future 2016* , IOP Confer Series: Mater. Sci. Eng. 176 (IOP Publishing 2017), 012024.
20. J. Joshi, M. K. Mishra and M. Srinivasarao, Can. J. Chem., **89**, 663-670 (2011).
21. A. K. Aboul-Gheit A. K, Solid State Ionics **101-103**, 893-897 (1997).
22. N. Wahyuni, G. Zissis and Z. Mouloungui, “Photostability beta-carotene/modified kaolinite from West Kalimantan, Indonesia,” in *16th International Clay Conference*-2017, Scientific Research Abstract 7, Edited by A. L. Galindo (Digilabs Pub, Bari, Italy, 2017), pp. 801.
23. K. L. Konan, C. Peyratout, A. Smith, J.-P. Bonnet, S. Rossignol and S. Oyetola, J. Colloid Interface Sci. **339**, 103-109 (2009).

24. A. Shvarzman, K. Kovler, G. S. Grader and G. E. Shter, Cem. Concr. Res. **33**, 405-416 (2003).
25. C. Morterra, G. Cerrato, F. Pinna and G. Meligrana, Top. Catal. **15**, 53-60 (2001).
26. M. Yurdakoç M. Akçay, Y. Tonbul and K. Yurdakoç, Turkish J. Chem. **23**, 319 -327 (1999).
27. L. Jankovič and P. Komadel, J. Catal. **218**, 227-233 (2003).
28. U. O. Aroke, A. Abdulkarim and R. O. Atbu, J. Environmental Techn. **6**, 42-52 (2013).

PHOTOSTABILITY OF β-CAROTENE/MODIFIED KAOLINITE

Nelly Wahyuni[1,4] Georges Zissis[2] Zéphirin Mouloungui[1,3]*

[1]Université de Toulouse, INP-ENSIACET, LCA (Laboratoire de Chimie Agro-industrielle),

4 Allée Monso, F-31030 Toulouse, France

[2] Université de Toulouse, Université de Toulouse, LAPLACE (Laboratoire Plasma et

Conversion d'Energie), UPS, INPT, 118 route de Narbonne, F-31062 Toulouse, France

[3] INRA, UMR 1010 CAI, F-31030, Toulouse, France

[4]Department of Chemistry, Mathematics and Natural Sciences, Tanjungpura University,

Jl. Prof. H. Hadari Nawawi, Pontianak 78124, Indonesia

*zephirin.mouloungui@ensiacet.fr

Abstract: β-carotene (BC), a natural organic compound, is very highly sensitive to light. The stability of BC can be improved by various methods. The aim of this study was to propose a simple method for improving the photostability of BC with modified kaolinite (MK). MK was produced by kaolin modification, through calcination and interaction with $ZnCl_2$. The characteristics of the MK were determined by using scanning electron microscope–energy dispersive X-ray spectroscopy (SEM-EDX), X-ray diffraction (XRD), infrared spectroscopy (IR), and surface area analyzer. The photostability of BC was measured with a UV-spectrophotometer. The XRD patterns of the kaolinite showed layer disruption during calcination at 600°C, leading to metakaolinite production. Surface area analysis and IR-spectroscopy revealed an increase in mean pore volume in the MK and a shift of the signal for the –OH group, respectively. MK decreased the photodegradation of BC, and increased

1

the half-life of this molecule by almost 15-fold than the only BC 1.44 h. The amount of BC

photostabilized by MK expressed as percentage of photostability, at five hours it was 61.87%.

The amount of BC adsorbed onto the kaolinite was related to the photostability of BC.

Key-words: β-carotene, half-life, kaolin, metakaolinite, modified kaolinite, photodegradation,

photostability

INTRODUCTION

The demand for β-carotene (BC) is increasing, as this molecule can serve as a

precursor of vitamin A, anticancer agent, nutraceutical, food colorant, in photoprotectant and

cosmetic preparations, and for the prevention of age-related molecular degeneration (Palozza

et al., 2004; Van Keulen *et al*., 2010; Wong *et al*., 2011; Freitas *et al*., 2015). These multiple

uses are related to the antioxidant properties of carotenoids, which have a conjugated polyene

structure that is highly effective for free radical and singlet oxygen scavenging (Siems *et al*.,

2005; Mueller and Boehm, 2011). Natural BC can be extracted from carrot (Suryana *et al*.,

2013) or produced by biotechnological processes involving the use of filamentous fungi,

yeasts, bacteria or microalgae (Thakur and Azmi, 2013). More than 85% the BC available on

the market is now produced through chemical synthesis (Van Keulen *et al*., 2010). BC

absorbs light at wavelengths of 415 to 508 nm. It could, therefore, potentially be used as a

sensitizer in the dye sensitizer solar cell (DSSC) (Suryana *et al*., 2013).

The long chain of alternating double bonds (conjugated) of BC is responsible for its

color. The axis of the carbon chain is curved, but the conjugated double bonds play an

important role in ensuring that the molecule remains, stable, and rigid. Furthermore, the π-

2

electrons in the chain are also delocalized, loosely held in place, and easily excited by low-energy visible light.

Baro and his colleagues studied the self-organisation of layers of BC molecules on the surface of Cu_{111} and reported that BC was a good electron transfer molecule. Within the multilayer structure, electrons flow easily from molecule to molecule within layers and to the layer below, due to the attractive interaction connecting the π-electron orbitals of adjacent molecules. They also reported the total length of the molecule to be 3.8 nm, with a height of 0.5 nm. A schematic molecular model of BC is shown in Figure 1.

BC is sensitive to the light, temperature, and oxygen, and the mechanisms by which it is degraded have been investigated in many studies. The thermal degradation of BC is responsible for the color change observed in pumpkin puree (Dutta *et al*., 2006). Visible changes in color have been shown to be a direct manifestation of changes in BC content.

Following the absorption of ultraviolet (UV) light, organic compounds move from the ground state to singlet excited states, in which molecules may undergo intersystem crossing (ISC) to reach the triplet excited state or internal conversion (IC) back to the ground state. Thus, in terms of photostability, molecules displaying high rates of IC are the most desirable (Osterwalder and Herzog, 2009). Free radicals and photoproducts are generated by photochemical reactions in both the singlet and triplet excited states (Freitas *et al*., 2015). In previous studies, most of the photocatalytic products of BC were identified in other systems, such as the thermal degradation of BC. Esters, ketones, alcohols, and aldehydes are the principal degradation products of the photocatalytic degradation of BC (Ge *et al*., 2015).

3

Some studies have focused on improving pigment stability. For example, the stability of curcumin was found to be increased by complexation with divalent ions such as Zn^{2+} (Zebib *et al*., 2010). The encapsulation of BC has been shown to improve its stability and facilitate the effective delivery of this molecule in various food systems and applications (Gul *et al*., 2015). The photostability of the natural pigment can be enhanced by the use of a photoprotector, such as gold nanoparticles (AuNPs), as demonstrated for chlorophyll-*a* (Chla). AuNPs bind to the nitrogen site of Chla, thereby preventing the binding of reactive oxygen species to this site, which is known to cause the photodegradation of Chla. The ability of AuNPs to protect Chla effectively, and not just through antioxidant properties, opens up new possibilities for increasing the photostability of other types of porphyrins. These molecules are widely used for industrial (in optoelectronic devices, such as organic light emitting diodes (OLEDs) and photovoltaic devices) and medical (photodynamic therapy) applications (Barazzouk *et al*., 2012). The immobilization of bixin on activated kaolinite increased the photostability of pigment and this matrix has been used in DSSCs (Hiendro *et al*., 2012; Rahmalia, 2016).The complexation of BC with humic acid (hypothetically, a π–π interaction) affects its chemical properties, increasing its photostability and water solubility (Martini *et al*., 2010).

Minerals, such as quartz, and kaolin clay are abundant in West Kalimantan, Indonesia (Destiarti *et al*., 2017). Kaolin is widely used for processes requiring clays in industry. The applications for which it is suitable depend on its surface reactivity. Kaolin is most frequently used as a filler in polymers, rubber, paper, cosmetics, and medicines (Zsirka *et al*., 2015). However, it can also be used as an adsorbent, catalyst, composite, nanohybrid, and electrode

4

coating (Tonlé *et al.*, 2011; Matusik *et al.*, 2011; Araujo *et al.*, 2014; Dedzo and Detellier, 2014; Matusik and Matykowska, 2014), provided that the surface and its structure are modified.

The properties of kaolinite can be improved by two principal treatments: (a) physical modification, and (b) chemical treatment with acids, bases, or organic compounds. Heating or microwave treatment can be used to induce physical modifications due to changes in chemical composition and crystalline structure at high temperature. Acids, bases, or organic compounds can be used for chemical modification, usually through changes to structure, surface functional groups, and surface area (Kumar *et al.*, 2013).

Thermal and chemical treatments have been used to improve the properties of kaolinite. Calcination, at type of thermal treatment, generates metakaolinite, which is more reactive than the original substance. Kaolin from Navalacruz, Zamora province, west of Spain has a Brunauer-Emmett-Teller (BET) surface area of 18 m^2/g. The calcination of this kaolin at 600°C followed by activation with HCl yields a material with a specific surface area of 219 m^2/g (Belver *et al.*, 2002). Other reported activation conditions have involved the use of H_2SO_4 (Hattab *et al.*, 2013), CH_3COOH, H_3PO_4, HCl, HNO_3, and NaOH (Kumar *et al.*, 2013). Metakaolinite has been activated by H_3PO_4, to increase dielectric performance by reducing dielectric permittivity and electrical conductivity, making this geopolymers suitable for use as encapsulating materials (Douiri *et al.*, 2016).

Kaolin and metakaolin have been used as cheap adsorbents for the removal of metal ions, such as Cd^{2+}, Cu^{2+}, Pb^{2+}, and Zn^{2+} (Srivastava *et al.*, 2005; Mbaye *et al.*, 2014; Chai *et al.*, 2017). The conversion of kaolin into metakaolin increases its ability to adsorb metal ions,

5

by increasing its surface area, pore volume or ability to take up water (Esomba *et al*., 2014).

Dyes molecules are stabilized by inorganic host materials due to the solid acidity and shielding effect from external circumtances by incorporation into the *nano-space* of clay, zeolit or mesoporous (Kohno *et al.*, 2011). The introduction of Al^{3+} and Fe^{3+} to mesoporous silicas forms acid sites, resulting in the sufficient stabilization of the flavylium. Since the stability enhancement of the BC using mesopores silica due to the inclusion of this molecule deep inside the mesopore contributed to the stabilization and tight fixation of this molecule (Kohno *et al*., 2016), the stabilization of the this dye can be expected through the incorporation into the Zn-modified kaolinite.

The objectives of this research were to study the photostability and degradation kinietic of BC with modified kaolinite (MK) under UV irradiation. Metakaolinite-Zn is expected increase the interaction of BC with MK, which correlate to the amount of BC absorbed. The unabsorbed BC related to the stability of this natural dye.

MATERIALS AND METHODS

The raw kaolin used came from Capkala region, West Kalimantan province, Indonesia. Separation was performed by aqueous decantation (3 times) and centrifugation at 6000 rpm for 10 min for enrichment of the clay fraction. The chemical composition of this fraction was follows: 51.82% SiO_2, 43.91% Al_2O_3, 1.19% MgO, 0.91% TiO_2, 0.87% Fe_2O_3, 0.10% CaO, and loss by ignition. According to the BET theory, the specific surface area of kaolin (K) was 35.414 m^2/g. BC (purity > 97%) used is a United Stated Pharmacopeia (USP) reference standard. The chemical reagents were analytical grade with purity more than 98% for $ZnCl_2$ and acetone > 99.5%. The chemical reagents and BC were obtained from Sigma

6

Aldrich (Saint Louis, Missouri, USA). Kaolin (250 mesh) was calcined in a furnace at 600°C

for 6 h to produce metakaolinite (MKaol) which was then modified by incubation with $ZnCl_2$.

In total, 5 g MKaol was modified by interaction with 125 mL 0.08 M $ZnCl_2$ (pH = 6), with

stirring, for 6 h. The mixture was decanted to separate out the solid fraction, which was dried

(MK). BC (2.5 ppm in acetone) was interacted with the MK (BC/MK = 40 mL/1 g) for 1 h

and then irradiated with UV light at 365 nm (flux = 1.6 W/m^2) for 9 h. The effluent was

centrifuged for 5 min at 5000 rpm to separate the solid particle thus only liquid (BC) will be

analyzed. Around 3 mL of the effluent were mesured with UV-VIS spectrophotometer. The

absorption spectra of BC were identified until 9 h of UV irradiation. BC concentration before

and after irradiation were determined with a standard curve equation : $y = 0.279x + 0.167$ ($x =$

BC concentration (ppm), $y =$ absorbance, and the correlation coefficient, $R^2 = 0.997$).

The raw kaolin was characterized by scanning electron microscopy- energy dispersive

X-ray spectroscopy (SEM-EDX), X-ray diffraction (XRD), infrared spectroscopy (IR), and

nitrogen adsorption. Micrographs were obtained with SEM model JSM 7100 F, manufactured

by Jeol, Origon, USA, at an accelerating voltage of 10 kV. The samples were deposited on a

sample holder with adhesive carbon foil and sputtered with gold. The mineral phases were

investigated with XRD instrumentation by Bruker AXS GmbH (Billerica, Massachussets,

USA) using Ni filtered CuKα radiation (λ = 0.154 nm) in Bragg-Bretano geometry with a

scanning rate of 10°/min from 4° to 80° (2θ). The patterns obtained were analysed with

Bruker-D8 software. The IR spectra were recorded for the 4000-400 cm^{-1} region, with a

Perkin-Elmer SHIMADZU IR spectrometer and the KBr pellet technique. The apparatus used

was fabricated by SHIMADZU at Kyoto, Japan. Textural analyses were performed on the

7

corresponding nitrogen adsorption-desorption isotherms at 77 K (BET method). The nitrogen

adsorption isotherms were obtained from BELSORP-max manufacturer by BEL JAPAN Inc,

Osaka, Japan. Nitrogen adsorption data were obtained with about 0.2 g of sample. The

samples were degassed for one hour at 90°C, with heating at a rate of 4°C/min. BET

equations were applied to the isotherms to determine the specific surface area. The absorption

spectrum of BC was obtained with a UV-1800, UV-VIS spectrophotometer by Shimadzu

Scientific Instrumentation Inc, Kyoto, Japan.

Photodegradation and life-time of BC calculated by determining the reaction rate

constant by Santoso *et al*. (2007), modified from first-order rate equation from Lagergren's.

Lagergren's first-order rate equation has been called pseudo-first-order to distinguish kenetic

equation of liquid-solid phase adsorption base on adsorption capacity from concentration of

solution (Qiu *et al*., 2009; Sejie *et al*., 2016). The change in the absorption at λ_{max} under

visible light irradiation was expressed by the time dependence of the ratio A/A_0

(A=absorption at time t, A_0=absorption at time t=0). Plot of ln % absorbance (A/A_0) to the

irradiation time resulted a straight line can be obtained, where the slope is k, and $t_{1/2}$ is

calculated.

The percentage photostability of BC in the presence of the MK was then calculated as

previously described (Claes, 1960), with the following formula:

$$\frac{E_3 - E_2}{E_1 - E_2} \times 100 \tag{1}$$

where E_1, E_2, and E_3 are the concentrations (or absorbances) of BC before irradiation, after

irradiation without MK, and after irradiation in the presence of MK, respectively.

8

RESULTS

The kaolin from West Kalimantan, Indonesia (Figure 2) used here had a reasonably homogeneous morphology. It consisted of small platelets of different sizes, pseudohexagonal or hexagonal in shape, as typically observed for kaolinite (Sengupta *et al*., 2008). The characteristic randomly oriented platelets of kaolinite were stacked to form large grains of a few micrometres in size (Figure 2b) (Araujo *et al*., 2014).

The XRD patterns of K, MKaol, and MK are shown in Figure 3. The raw kaolin consisted of kaolinite associated with quartz and a small muscovite fraction. The reflections observed at 7.15, 3.57, and 2.3 Å indicated the presence of a second phase, identified as kaolinite. The 001 basal distance of kaolinite is 7.2 Å (Zsirka *et al*., 2015). Calcination at 600°C for 6 h gave 001 and 002 basal reflections of destroyed kaolinite, indicating a collapse of the structure of the material and production of MKaol through dehydroxylation. MKaol is an unstable phase of kaolinite, and its production can be represented as a simple equation (Ilić *et al*., 2010).

$$Al_2O_3 \cdot 2SiO_2 \cdot 2H_2O \rightarrow Al_2O_3 \cdot 2SiO_2 + 2H_2O\uparrow \qquad (2)$$
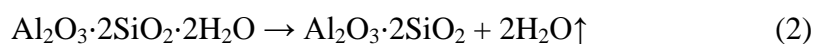
The modification of MK with $ZnCl_2$ had no significant effect on the XRD pattern. Md Saad *et al*. (2016) found that copper ions were adsorbed onto kaolinite with no change in structure.

On the IR spectrum of K (Figure 4), absorption peaks at 3697 cm^{-1}, 3653 cm^{-1}, and 3620 cm^{-1} were identified as corresponding to the stretching vibration of internal hydroxyl bonds (Al..O..H) in the octahedral sheet identified as kaolinite. The wavenumber at 3435 cm^{-1} corresponds to the stretching vibration for the –OH bond of H_2O, whereas a deformation of

this bond is observed at 1631 cm^{-1} (Sengupta *et al*., 2008). The bands at 1112 cm^{-1}, 1032 cm^{-1}, and 1000 cm^{-1} were assigned to Si-O stretching. Al-OH deformation bands were identified at 912 cm^{-1} and 753 cm^{-1}. Al-O-Si deformation was detected at 538 cm^{-1} and Si-O-Si deformation at 470 cm^{-1} (Belver *et al*., 2002; Hattab *et al*., 2013; Kumar *et al*., 2013; Vaculikova *et al*., 2011). The presence of quartz was confirmed by the doublet at about 800 and 775 cm^{-1} (Vizcayno *et al*., 2010).

Calcination converted the kaolinite into MKaol, as demonstrated by the disappearance of the band at 3697-3620 cm^{-1}, confirming the dehydroxylation of kaolinite. The presence of a band at 1631 cm^{-1}, corresponding to H_2O molecules on the MKaol reflects the hygroscopic nature of MKaol after heating at 600°C (Tchakouté *et al*., 2012). Furthermore, the transmittance intensity of the Al-O functional group decreased or the fingerprint bands disappeared on the spectra for MKaol and MK.

Assessments of the stability of BC without irradiation (Figure 5a) revealed a maximum peak for BC in acetone at 452 nm, with other peaks observed at 486 nm and 426 nm. The degree of the photodegradation is expressed as the change in the main absorption band of BC at 452 nm. The BC concentration was relatively unchanged after being stored for nine hours at room condition. Under irradiation, the absorbance of BC (Figure 5b) decreased significantly at 5 h, with absorbance reaching levels close to zero at 7 h. By contrast, the absorbance of BC/MK (Figure 5c) remained high for nine hours, even under irradiation. MK therefore increased the photostability of BC.

The rate constant of photodegradation BC declined by the present of MK (Figure 6b). Kinetic analyses of the photodegradation of BC and BC/MK showed the half-life of BC

10

in the presence of MK to be four times that in its absence (Table 1).The percentage

photostability of 40 mL BC with 1 g MK (40 mL/1g) was 23.82%. Photostability increased to

52.76% and 61.87% for BC interacting with MKaol and MK, respectively. The percentage

photostability reflects the amount of BC adsorbed onto the K, MKaol, or MK. The amount of

BC absorbed onto K, MKaol, and MK were 1.46 ppm, 1.93 ppm, and 2.01 ppm. Therefore

58.34%, 77.31%, and 82.29% of the inisial concentration BC are photostabilized by the K,

MKaol, and MK, respectively.

The percentage photoprotection was calculated using equation (1), as described in the

experimental section.

The maximal percentage photostability of BC (Figure 7) was achieved with 1 g of

MK. The photostability of BC decreased with decreases in the mass of MK. The percentage

photostability of this matrix was 61.87%.

DISCUSSION

The permanent negative charge of kaolinite results from the isomorphic replacement

of Si^{4+} in the silica tetrahedral sheet by Al^{3+} or the replacement of trivalent metal ions (such

as Al^{3+}) by divalent ions (such as Fe^{2+} and Mg^{2+}) in the octahedral alumina sheet. Each

substitution results in a single negative charge. Both the alumina sheet and the crystal edges

have a pH-dependent variable charge caused by the protonation and deprotonation of surface

hydroxyl (SOH) groups (Srivastava *et al.,* 2005). MKaol is an unstable phase of kaolinite

produced through dehydroxylation (Ilić *et al*., 2010). Dehydroxylation implies a

reorganization and diffusion of hydroxyl group in the layer (Shvarzman *et al*., 2003). MKaol

is more reactive than K due to the structural disorder such as deformation of silica network or

11

existence of 4-coordinated aluminium, which is more reactive than 6-coordinated aluminium. The unstable MKaol, also still contains about 10% of the OH-groups initially present in the K. Therefore, it is favourable to a surface dissolution of treated kaolin in cationic solution (Konan *et al*., 2009).The surface of the MKaol thus has some types of binding sites capable of interacting with Zn^{2+}. Essomba *et al*. (2014) studied the adsorption of cadmium onto kaolinite. They concluded that a chemisorption reaction or an activated process predominated in the rate-controlling step of the cadmium system. They also reported that metakaolinite had a higher adsorption capacity than kaolinite, due to its greater surface area, pore volume and hygroscopy.

Chai *et al*. (2017) reported that pH affected the mole fraction of hydrolyzed Zn^{2+} species relative to the total soluble metal concentration at 25°C. The main species present at pH values below 7 is Zn^{2+}. Chai *et al.* also concluded that electronic attraction was the main mechanism of Zn^{2+} adsorption on kaolinite. Transition metals adsorb at permanent and variable charge sites. Sites with a permanent negative charge can undergo an exchange reaction with Zn^{2+} at high pH. At this present study, $ZnCl_2$ solution was allowed to interact with MKaol at pH= 6, therefore Zn^{2+} was probably adsorbed onto MKaol via a SOH group.

$$SOH = SO^- + H^+ \qquad\qquad (2)$$

$$2SO^- + Zn^{2+} = Zn(SO)_2 + H^+ \qquad\qquad (3)$$
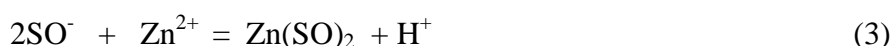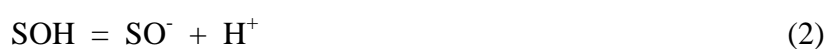
The absorption of energy by a compound or photosensitizer triggers photochemical damage to the substance concerned. Many photochemical reactions are complex and may involve serial competition for reaction pathways in which oxygen plays a significant role. Indeed, the vast majority of photoreactions involves the consumption of molecular oxygen
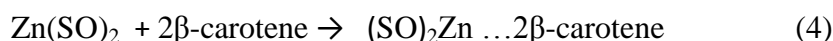
12

and is photo-oxidative processes. The photodegradation of BC is known to be essentially photo-oxidative, and is brought about by various reactive oxygen species (ROS), such as singlet oxygen and superoxide (Barazzouk *et al*., 2012). The absorption of UV light by BC results in the formation of its excited singlet (^{1}BC*). Mordi proposed a mechanism for BC degradation in which BC is degraded by *cis-trans* isomerization, followed by the formation of a singlet diradical. The oxygen attack on either side of the *cis* bond is enhanced, through the generation of other types of radical species, and further reactions occur until the final product is produced (Mordi, 1992).

According to BET surface area analysis (Table 2), calcination decreased the specific surface area, but increased total pore volume and mean pore volume. The surface area of kaolin decreased from 18.2 m^2/g into10.6 m^2/g during calcination at 600° for 10 h (Belver *et al*., 2002). Essomba *et al*. (2014) reported that calcination kaolin at 700° for 6 h increased specific surface area and pore volume. The surface area to be 20 and 33 m²/g, while pore volume from 0.0814 and 0.0935 cm^3/g, respectively. Therefore, the decreasing of surface area is consistent with Belver *et al*., but contradiction with Esomba *et al*., due to the chemical composition of natural kaolin was used. The major component was anatase associated with illite, quartz, kaolinite, and lepidocrocite (Esomba *et al*., 2014).

BC absorption occurred in meso-sized pores. This physical adsorption involved van der Waals forces. The higher adsorption capacity of MKaol than of K may be due to the presence of larger pores (Table 2). MKaol pore size was markedly larger than the cross-sectional dimensions of the monomeric BC molecule, consistent with the findings of Worasith *et al.* (2011), resulting in a large periodic multilayer (Baro *et al*., 2003). Srasra and

13

Trabelsi-Ayedi (2000) proposed the possiblity chemical interaction of BC with the surface of the clay (Figure 8). This mechanism involved the hydrogen bonding BC to Brönsted sites and/or direct binding at Lewis sites through the formation of carbonium ions or coordinating bonds (Sarier and Güler, 1988). The interaction also involved the breaking of bonds in the dissolved octahedral and tetrahedral sheets (Adams, 1987).

Zinc ions intercalate into MKaol by electronic attraction. The aggregation of MKaol particles results from the adsorption of positively charged Zn^{2+} ions onto the surfaces of this solid material (Chai *et al*., 2017). The presence of zinc ions in the MKaol increased the interaction of BC with this solid material. The analysis of EDX spectra showed that the MK contained 6.1%. According to Zebib *et al*. (2010), who described a hypothetical mechanism of Zn^{2+} intercalation with curcumin and the structural model of BC (Srasra and Trabelsi-Ayedi, 2000), interaction between MK and BC may modify complexation, with zinc as a Lewis site and BC as the electron donor. This mechanism increases the adsorption capacity of BC on MK. Acid site contributed to the stabilization of dye on mesoporous material (Kohno *et al.*, 2011). No distinction was made between aluminol and silanol surface groups, but the SOH groups involved in adsorption were probably mostly those of aluminol and AlOH (Schindler *et al*., 1987).

$$Zn(SO)_2 + 2\beta\text{-carotene} \rightarrow (SO)_2Zn \ldots 2\beta\text{-carotene} \qquad (4)$$

The absorbance of BC/MK decreased after irradiation, but the λ_{max} was almost unchange. This fact indicating there was only a simple degradation, but not photochemical conversion such as isomerization (Henry *et al*., 1998; Kohno *et al*., 2009; Xiao *et al*., 2018). It has been reported that the stability of BC related to order molecular association (Baro *et al*.,

14

2003). As the spectral shift was not observed, only a little changing in shape spectral, it was suggested that BC formed aggregation with the disorder orientation. Aggregation also contributed to the stability improvement of dye, because the aggregation reduced the contact area to the oxygen (Kohno *et al*., 2015).

The MK protected BC from the effects of direct UV irradiation. Lower levels of triplet oxygen and ROS formation were observed in the presence of MK. Carotenoid degradation was a direct result of irradiation. The shielding effect of the inorganic host material reduced the rate of degradation and also protected BC against ROS (Kohno *et al*., 2016).

Increasing the mass of MK to 2 g (Figure 7) decreased the percentage photostability of BC significantly, due to a decrease in capacity of BC to adsorb onto the MK. Overlaps between adsorption sites or their aggregation as a result of overcrowding decreased the adsorption capacity of BC (Essomba *et al*., 2014; Ndongo Kounou *et al*., 2015). The lower level of adsorption at higher mass also reflects the increase in interactions between the particles of a material with mass. The excess of amount of cation caused the precipitation of dye aggregate (Kohno *et al*, 2015). Therefore, BC photostability decreased with increasing the mass of MK also due to excessive amounts of Zn^{2+}.

However, this finding is not consistent with the results of Barazzouk and coworkers, who reported that the protection against Chla photodegradation afforded by AuNPs eventually reached a plateau (Barazzouk *et al*., 2012), this phenomenon being correlated to photoprotector particle size. When MK, which has micrometre-range particles, was used as photoprotector, the interactions between particles increased with mass. In the presence of

15

excess MK, the interaction of BC with MK decreased, and the BC was irradiated with UV light.

No significant difference was observed between the infrared spectra of MK and BC/MK (not shown).

CONCLUSIONS

SEM, XRD, and IR analysis showed that raw kaolin from West Kalimantan, Indonesia consisted of kaolinite associated with quartz and a small fraction of muscovite. The conversion of kaolinite to MKaol by calcination and the modification of MKaol with Zn^{2+} decreased the photodegradation of BC by shielding and protecting it against direct UV irradiation, leading to a 15-fold increase in half-life. The mass of MK influenced the photostability of BC. The percentage photostability of BC with MK at 5 h was 61.87% (40 mL BC/g MK). Photostability was related to the amount of BC adsorbed onto the kaolinite. The use of MK as a photostabiliser of BC is a new method in which MKaol-zinc can be used. This method could also be applied to other metal ions and pigments. This composite material has potential applications in cosmetics (sunscreen) or in photovoltaics (DSSCs).

ACKNOWLEDGMENT

References

Adams, J.M. (1987) Synthetic organic chemistry using pillared, cation-exchanged and acid-treated montmorillonite catalysts – A review. *Applied Clay Science*, **2**, 309 – 342.

Araujo, F.R., Baptitta, J.G., Marcal, L., Ciuffia, K.J., Nassara, E.J., Calefi, P.S., Vivcente,

M.A., Trujilano, R., Rives, V., Gilc, A., Korilic, S., and De Faria, E.H. (2014) Versatile heterogeneous dipicolinate complexes grafted into kaolinite: Catalytic oxidation of hydrocarbons and degradation of dyes. *Catalysis Today*, **227**, 105-115.

Baro, A.M., Hla, S., and Rieder, K.H. (2003) LT-STM study of self-organization of β-carotene molecular layers on Cu (1 1 1). *Chemical Physics Letters*, **369**, 240–247.

Barazzouk, S., Bekalé, L., and Hotchandani, S. (2012) Enhanced photostability of chlorophyll-*a* using gold nanoparticles as an efficient photoprotector. *Journal Materials Chemistry*, **22**, 25316-25324.

Belver, C., Banares, M.A., and Vicente, M.A. (2002) Chemical activation of a kaolinite under acid and alkaline conditions. *Chemistry of Materials*, **14**, 2033-2043.

Chai, W., Huang, Y., Su, S., Han, G., Liu, J., and Yijun, C.Y. (2017) Adsorption behavior of Zn(II) onto natural mineral minerals in wastewater. A comparative study of bentonite and kaolinite. *Physicochemical Problems of Mineral Processing*, **53**, 264−278.

Claes, H. (1960) Interaction between chlorophylls and carotenes with different chromophoric groups. *Biochemical and Biophysical Research Communications*, **3**, 585-590.

Dedzo, G.K. and Detellier, C. (2014) Intercalation of two phenolic acids in an ionic liquid-kaolinite nanohybrid material and desorption studies. *Applied Clay Science*, **97-98**, 153-159.

Destiarti, L., Wahyuni, N., Prawatya, Y., and Sasri, R. (2017) Synthesis and characterization of mangan oxide coated sand from Capkala kaolin. *International Conference on Chemistry, Chemical Process and Engineering*, AIP Conference Proceeding **1823**, 020023 doi: 10.1063/1.4978096.

17

Douiri, H., Louati, S., Baklouti, S., Arous, M., and Fakhfakh, Z. (2016) Enhanced dielectric performance of metakaolin–H_3PO_4 geopolymers. *Materials Letters*, **164**, 299–302.

Dutta, D., Dutta, A., Raychaudhuri, U., and Chakraborty, R. (2006) Rheological characteristics and thermal degradation kinetics of beta-carotene in pumpkin puree. *Journal of Food Engineering*, **76**, 538–546.

Essomba, J.S., Ndi Nsami, J., Belibi Belibi, P.D., Tagne, G.M., and Ketcha Mbadcam, J. (2014) Adsorption of cadmium (II) ions from aqueous solution onto kaolinite and metakaolinite. *Pure and Applied Chemical Sciences*, **2**, 11-30.

Freitas, J.V., Lopes, N.P., and Gaspar, N.L. (2015) Photostability evaluation of five UV-filters, trans-resveratrol and beta-carotene in sunscreen. *European Journal of Pharmaceutical Science*, **78**, 79-89.

Ge, W., Chen, Y., Wang, L., and Zhang, R. (2015) Photocatalytic degradation of β-carotene with TiO_2 and transition metal ions doped TiO_2 under visible light irradiation. *Universal Journal of Chemistry*, **3**, 104-111.

Gul, K., Tak, A., Singh,A.K., Singh, P., Yousuf, B., and Wani, A.A. (2015) Chemistry, encapsulation, and health benefits of β-carotene - A review. *Cogent Food & Agriculture*, **1,** 1018696.

Hattab, A., Bagane, M., and Chlendi, M. (2013) Characterization of Tataouinen's raw and activated clay. *Chemical Engineering & Process Technology*, **4**, 1-5.

Henry, L.K., Catigani, G.L., and Schwartz, S.J. (1998) Oxidative degradation kinetic of lycopne, lutein, and 9-cis and all-trans β-carotene. *Journal of the American Oil Chemists Society*, **7**, 823-829.

18

Hiendro, A., Hadary, F., Rahmalia, W., and Wahyuni, N. (2012) Enhanced performance of

bixin sensitized solar cells with activated kaolinite. *International Journal of Engineering*

Research and Innovation, **4**, 40-44.

Ilić, B.R., Mitrović, A.A., and Miličić, L.R. (2010) Thermal treatment of kaolin clay to

obtain   metakaolin. *Hemijska industrija*, **64**, 351–356.

Kohno,Y., Kinoshita, R., Ikoma, S., Yoda, K., Shibata, M., Matsushima, R.,Tomita, Y.,

Maeda, Y., and Kobayashi, K. (2009) Stabilization of natural anthocyanin by intercalation

into montmorillonite. *Applied Clay Science*, **42**, 519-523.

Kohno, Y., Senga, M., Shibata, M., Yoda, K., Matsushima, R., Tomita, Y., Maeda, Y., and

Kobayashi, K. (2011) Stabilization of flavylium dye by incorporation into Fe-containing

mesoporous silicate. *Microporous and Mesoporous Materials*, **141**, 77-80.

Kohno, Y., Kato, Y., Shibata, M., Fukuhara, C., Maeda, Y., Tomita, Y., and Kobayashi, K.

(2015) Enhanced stability of natural anthocyanin incorporated in Fe-containing

mesoporous silica. *Microporous and Mesoporous Materials*, **203**, 232-237.

Kohno, Y., Kato, Y., Shibata, M., Fukuhara, C., Maeda, Y., Tomita, Y., and Kobayashi, K.

(2016) Fixation and stability enhancement of beta-carotene by organo-modified

mesoporous silica. *Microporous and Mesoporous Materials,* **220**, 1-6.

Konan, K.L., Peyratout, C., Smith, A., Bonnet, J.-P., Rossignol, S., and Oyetola, S. (2009)

Comparison of surface properties between kaolin and metakaolin in concentrated lime

solutions. *Journal of Colloid and Interface Science*, **339**, 103-109.

Kumar, S., Panda, A. K., and Singh, R. K. (2013) Preparation and characterization of acid

and alkali treated kaolin clay. *Bulletin of Chemical Reaction Engineering & Catalysis*, **8**, 61-69.

Martini, S., D'Addario, C., Bonechi, C., Leone G., Tognazzi, A., Consumi, M., Magnani, A., and Rossi, C. (2010) Increasing photostability and water-solubility of carotenoids: Synthesis and characterization of β-carotene–humic acid complexes. *Journal of Photochemistry and Photobiology B: Biology*, **101**, 355–361.

Matusik, J., Stodak E., and Baranowski, K. (2011) Synthesis of polylactide/clay composites using structurally different kaolinites and kaolinite nanotubes. *Applied Clay Sciences*, **51**, 102-109.

Matusik, J. and Matykowska, L. (2014) Behavior of kaolinite intercalation compounds with selected ammonium salts in aqueous chromate and arsenate solutions. *Journal of Molecular Structure,* **1071**, 52-59.

Mbaye, A., Diop, M.A.K., Miehe-Brendle, C.A.K., Senocq, J., Maury, F., and Francis. (2014) Characterization of natural and chemically modified kaolinite from Mako (Senegal) to remove lead from aqueous solutions. *Clay Minerals*, **49**, 527-539.

Md Saad, N.S.S., Nik Malek, N.A.N., and Chong, C.S. (2016) Antimicrobial activity of copper kaolinite and surfactant modified copper kaolinite against gram positive and gram negative bacteria. *Sciences & Engineering*, **78**, 127–132.

Mordi, R.C. (1992) Mechanism of β-carotene degradation. *Biochemical Journal Letter* , 310.

Mueller, L. and Boehm, V. (2011) Antioxidant activity of β-carotene compounds in different *in vitro* assays. *Molecules*, **16**, 1055-1069.

Ndongo Kounou, G., Ndi Nsami, J., Belibi Belibi, D.P., Kouotou, D., Tagne, G.M., Dina Joh, D.D., and Ketcha Mbadcam, J. (2015) Adsorption of zinc (II) ions from aqueous solution onto kaolinite and metakaolinite. *Der Pharma Chemica*, **7**, 51-58.

Osterwalder, U. and Herzog, B. (2009) Chemistry and properties of organic and inorganic uv filters. Pp. 11-38 in: *Clinical Guide to Sunscreens and Photoprotection* (H.W. Lim and Z.D. Draelos, editors). Informa Healthcare, New York.

Palozza P., Serini, S., Nicuolo, F.D., and Calviello, G. (2004) Modulation of apoptotic signaling by carotenoids in cancer cells. *Archives of Biochemistry and Biophysics*, **430**, 104-109.

Qiu, H., LV, L., Pan, B-C., Zhang, Q-J ., Zhang, W-M, Zhang, Q-X. (2009) Critical review in adsorption kinetic models**.** *Journal of Zhejiang University SCIENCE A*, **10**, 716-724.

Rahmalia, W. (2016) Paramètres de performances de photo-électrodes de TiO_2/kaolinite et d'électrolyte a base de carbonates biosourcés dans la cellule solaire sensibilisée par la bixine. PhD Thesis, Institut National Polytechnique de Toulouse, Toulouse, France, 188 pp.

Santosa, S.J., Siswanta, D., Kurniawan, A., and Rahmanto, W.H. (2007) Hybrid of chitin and humic acid as high performance sorbent for Ni(II). *Surface Science*, **601**, 5155-5161.

Sarier, N. and Güler, C. (1988) B-carotene adsorption on acid activated montmorillonite. *Journal of American Oil Chemists Society*, **66**, 917–923.

21

Schindler, P.W., Liechti, P., and Westall, J.C. (1987) Adsorption of copper, cadmium and lead from aqueous solution to the kaolinite/water interface. *Netherlands Journal of Agricultural Science,* **35**, 219-330.

Sejie, F.P. and Nadiye-Tabbiruka, M.S. (2016) Removal of methyl orange (MO) from water by adsorption onto modified local clay (kaolinite). *Physical Chemistry*, **6**, 39-48.

Sengupta, P.C., Saiki, P.C., and Borthakur, P. (2008) SEM EDX characterization of an iron-rich kaolinite clay. *Journal of Scientific Industrial Research*, **67**, 812-818.

Shvarzman, A., Kovler, K., Grader, G.S., and Shter, G.E. (2003) The effect of dehydroxylation/amorphization degree on pozzolanic activity of kaolinite. *Cement and Concrete Research*, **33**, 405-416.

Siems, W., Wiswedel, I., Salerno, C., Crifo, C., Augustin, W., Schild, L., Langhans, C.D., and Sommerburg, O. (2005) β-carotene breakdown products may impair mitochondrial functions-potential side effects of high-dose β-carotene supplementation. *The Journal of Nutritional Biochemistry*, **16**, 385-397.

Srasra, E. and Trabelsi-Ayedi, M. (2000) Textural properties of acid activated glauconite, *Applied Clay Science*, **17**, 71–84.

Srivastava, P., Singh, B., and Angove, M. (2005) Competitive adsorption behavior of heavy metals on kaolinite. *Journal of Colloid and Interface Science*, **290**, 28–38.

Suryana, R., Khoiruddin., and Supriyanto, A. (2013) Beta-carotene dye of *Daucus carota* as sensitizer on dye-sensitized solar cell. *Material Science Forum*, **737**, 15-19.

Tchakoute K, H., Elimbi, A., Mbey, J.A., Ngally, S.C., and Njopwouo, D. (2012) The effect of adding alumina-oxide to metakaolin and volcanic ash on geopolymer products: A

comparative study. *Construction and Building Materials*, **35**, 960-969.

Thakur, M. and Azmi, W. (2013) Nutraceutical β-carotene from natural non-conventional sources and its applications. *Annals of Phytomedicine*, **2**, 59-73.

Tonlé, I.K., Letaif, S., Ngameni, E., Walcarius, A., and Detellier, C. (2011) Square wave voltammetric determination of lead (II) ions using a carbon paste electrode modified by a thiol-functionalized kaolinite. *Electroanalysis*, **23**, 245-252.

Vaculikova, L., Plevova, E., Vallova, S., and Kouttnik, I. (2011) Characterization and differentiation of kaolinites from selected Czech deposits using infrared spectroscopy and differential thermal analysis. *Acta Geodynamica et Geomaterialia*, **8**, 59–67.

Van Keulen, F., Carolas, A.L., Brito, M.L., and Ferreira, B.S. (2010) Production of high-purity carotenoids by fermenting selected bacterial strains. US Patent. 2010/0145116 A1.

Vizcayno, C., Gutierrez, R.M., Castello, R., Rodriguez, E., and Guerrero, C.E. (2010) Pozzolan obtained by chemical and thermal treatments of kaolin. *Applied Clay Science*, **49**, 405-413.

Wong, I.Y.H., Koo, S.C.Y., and Chan, C.W.N. (2011) Prevention of age related macular degeneration. *International Journal of Ophthalmology*, **31**, 73-82.

Worasith, N., Goodman, B.A., Jeyashoke, N., and Thiravetyan, P. (2011) Decolorization of rice bran oil using modified kaolin. *Journal of the American Oil Chemists' Society,* **88**, 2005-2014.

Xiao, Y-D., Huang, W-Y., Li, D-J., Song, J-F., Liu, C-Q., Wei, Q-Y., Zhang, M., and Yang, Q-M. (2018) Thermal degradation kinetics of all-trans and cis-carotenoids in a light-induced model system. *Food Chemistry*, **239**, 360-368.

Zebib B., Mouloungui Z., and Noirot V. (2010) Stabilization of curcumin by complexation with divalent cations in glycerol /water system. *Bioinorganic Chemistry and Applications*, 1-8.

Zsirka, B., Horvath, E., Mako, E., Kurdi, R., and Kristof, J. (2015) Preparation and characterization of kaolinite nanostructure: Reaction pathways, morphology and structural order. *Clay Minerals*, **50**, 329-340.
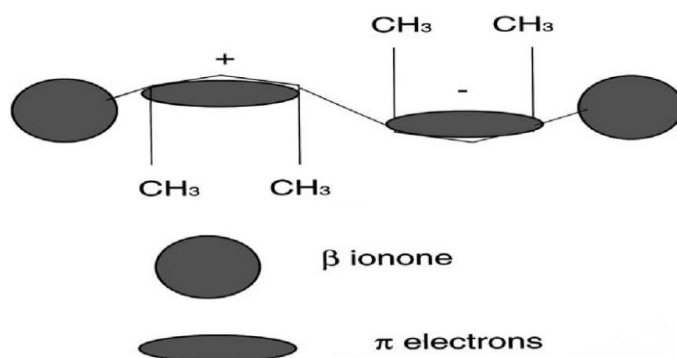
Figure 1. Schematic model of the β-carotene molecule, showing the curved backbone

of the polyene chain, the methyl groups attached to it, the asymmetric

corrugation attributed to π-electrons and the β-ionone rings (Baro *et al*., 2003)

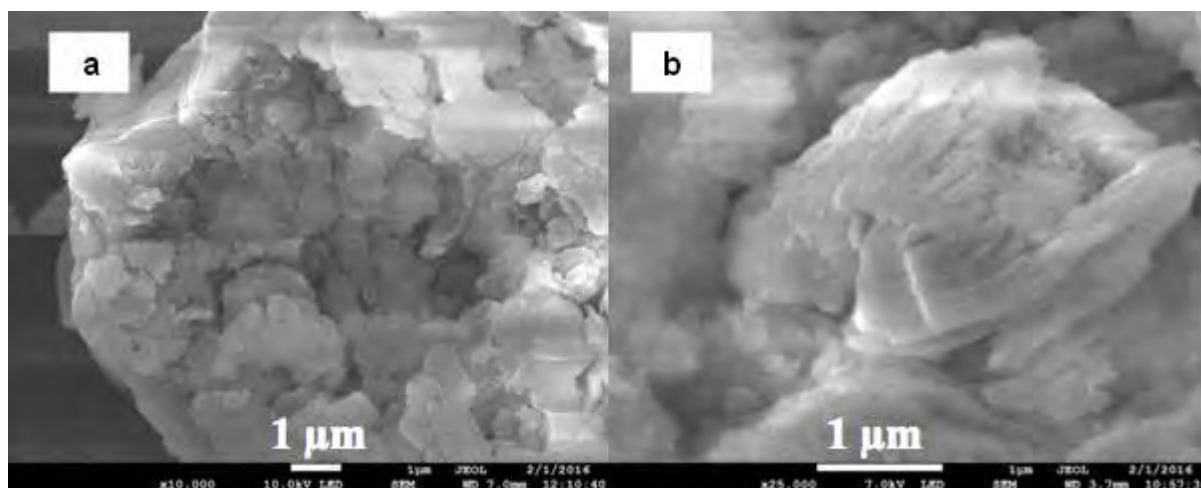Figure 2. SEM micrographs of the kaolin from West Kalimantan, Indonesia at magnifications

of (a) 10,000x and (b) 25,000x. Each of images showed a booklet morphology

consisting of platelet sheet of kaolinite mineral with estimated average particle size

about 2,0 μm.

25
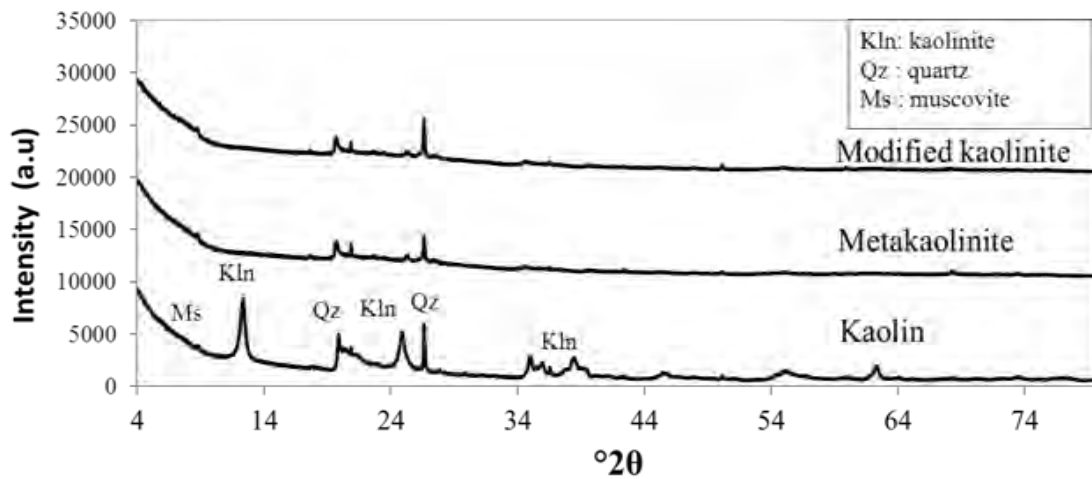
Figure 3. XRD pattern of kaolin, metakaolinite, and modified kaolinite
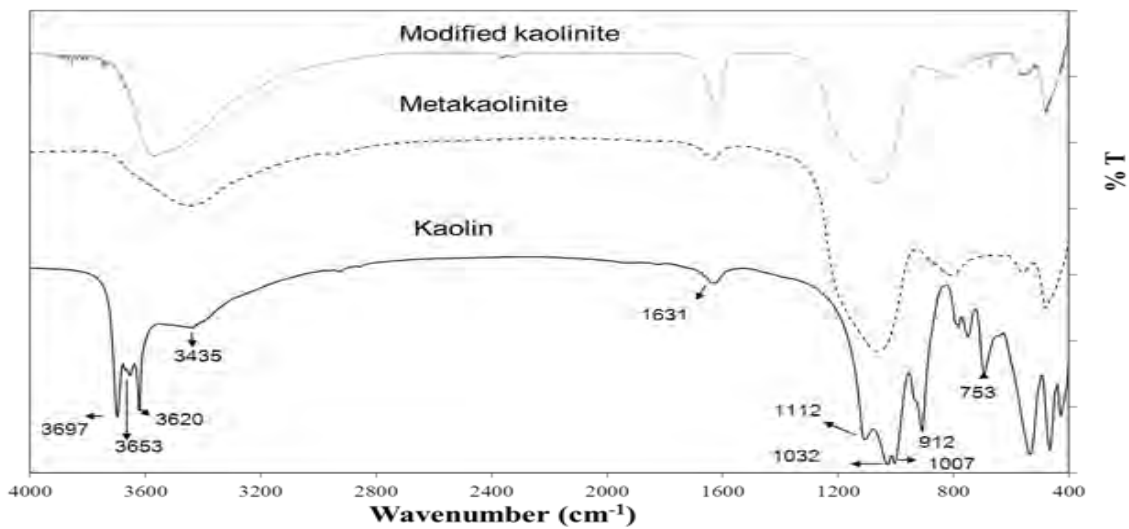
Figure 4. Infrared spectra of kaolin, metakaolinite, and modified kaolinite

26
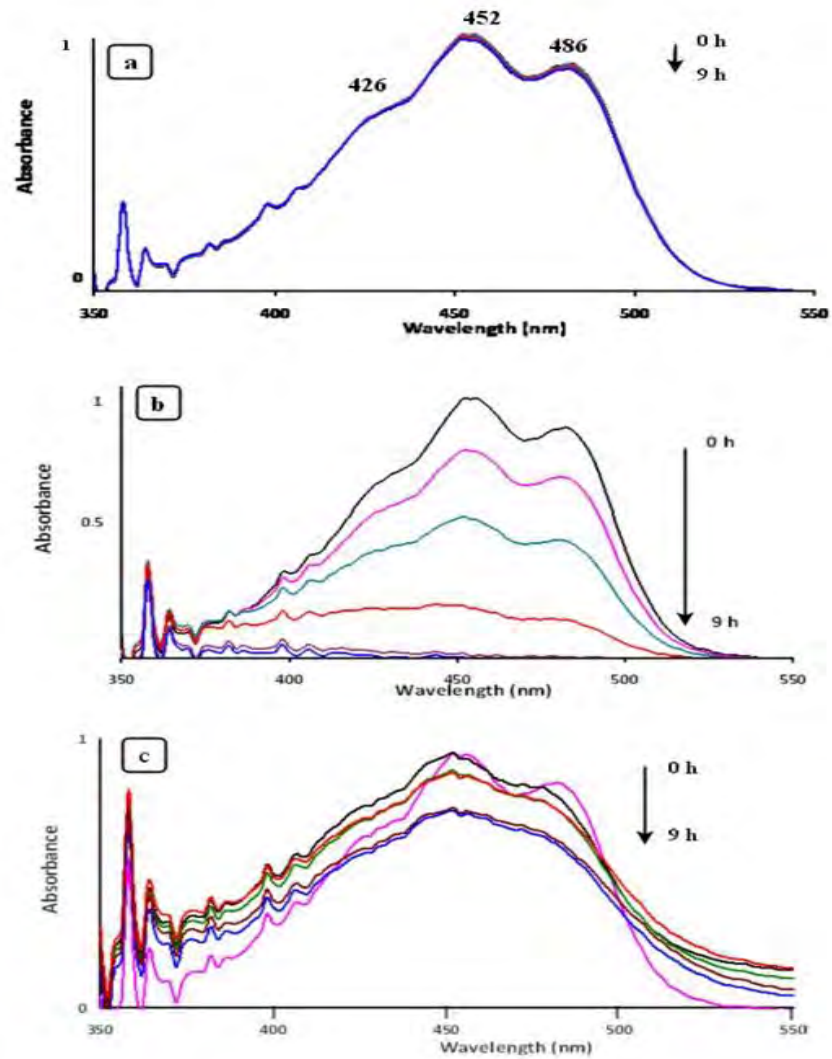
Figure 5. Absorption spectra of the products of (a) BC without irradition

(b) BC with UV irradiation, and (c) BC/MK under UV irradiation

27
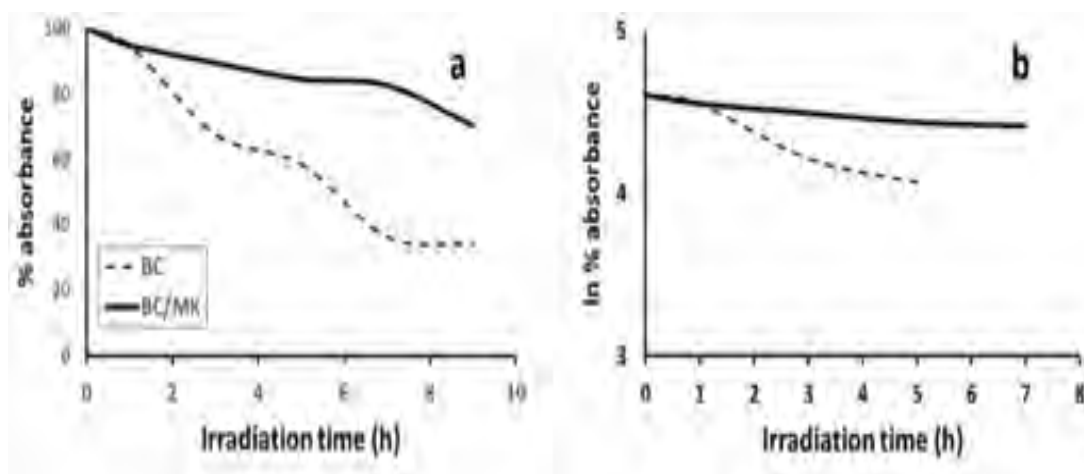
Figure 6. Kinetic photodegradation of β-carotene (BC) and β-carotene/modified kaolinite (BC/MK)
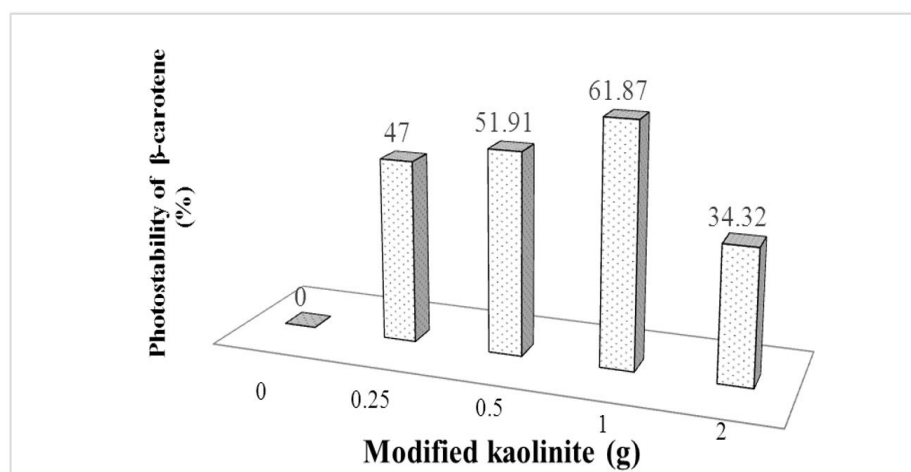
Figure 7. Photostability of β-carotene with different masses of modified kaolinite

28
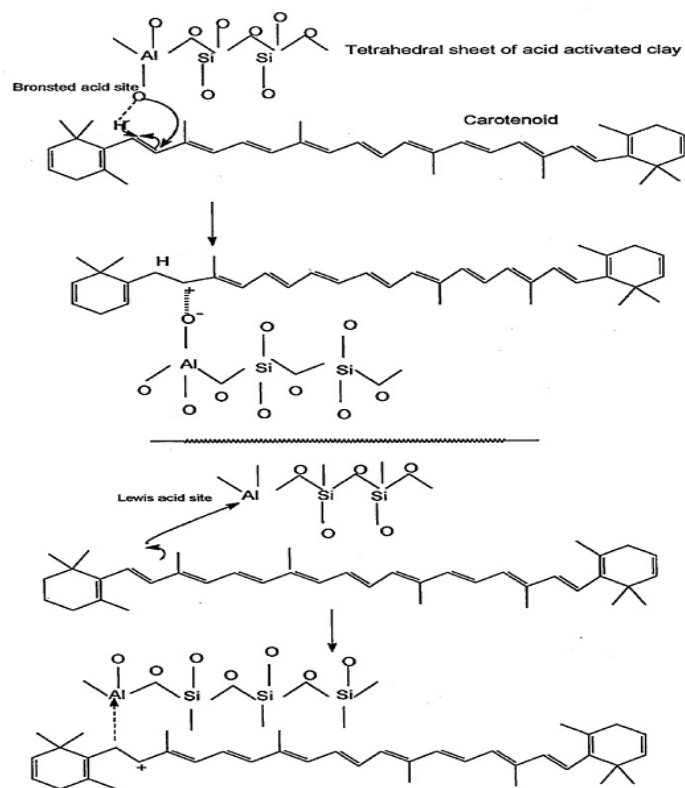
Figure 8. The mechanism of carotenoid adsorption on Brönsted and Lewis acid sites

(Srasra and Trabelsi-Ayedi, 2000)

29

Table 1. Pseudo-first-order reaction data for β-carotene (BC), β-carotene with kaolin (K),

metakaolinite (MKaol), and modified kaolinite (MK)

Sample code	Correlation coefficient (R^2)	Rate constant, k (h^{-1})	Half-life, (h)	% Photostability at 5 h
BC	0.99	0.4854	1.43	-
BC/K	0.99	0.0833	8.32	23.82
BC/MKaol	0.96	0.0638	10.86	52.76
BC/MK	0.98	0.0325	21.32	61.87

Table 2. BET specific surface area, total pore volume, and mean pore size

Sample	Specific surface area (m^2/g)	Total pore volume (cm^3/g)	Mean pore volume (nm)
Kaolin	35.414	0.2006	22.660
Metakaolinite	23.193	0.2026	34.934
Modified kaolinite	23.805	0.1936	32.527

30

ANNEXE II

RÉSUMÉ de THÈSE

RÉSUMÉ de THÉSE

Propriétés d'absorption et de luminescence du caroténoïdes à l'aide un antioxydant et le kaolin modifié et son application dans les diodes électroluminescentes organiques (OLED)

Nelly WAHYUNI

Résumé

Les crises énergétiques, en particulier celles liées aux combustibles fossiles, conduisent à une utilisation accrue des nouvelles énergies renouvelables. De plus, les recherches visent également à utiliser des matériaux de stockage de l'énergie qui sont plus efficace, tels que les batteries, et à utiliser des matériaux économes en énergie. Une OLED (diode électroluminecente organique)) est une diode émettrice la lumière (LED) qui sont connues grâce leur potentiel élevé dans les applications d'affichage, de signalisation et d'éclairage.

Parmi ces matériaux organiques, les caroténoïdes constituent une classe importante de molécules linéaires conjuguées qui présentent un degré de délocalisation électronique élevé et de dynamique ultra-rapide. Le colorant joue un rôle important dans le fonctionnement des cellules solaires à pigment photosensible (CSPP) ou d'autres matériaux bi fonctionnels.

Dans cette recherche, nous avons étudié la photostabilité des caroténoïdes (β-carotène et fucoxanthine) à l'aide du kaolin modifié et de l'antioxydant. La photostabilité du β-carotène et de la fucoxanthine peut être améliorée par la kaolinite modifiée et l'antioxydant.

La fabrication OLED utilisant la fucoxanthine n'est pas suffisante à cause de la bande interdite de la fucoxanthine (Fx) qui est très grande et peut être un isolant. NPD (50 nm) / Fx (1 nm) / Alq_3 (85 nm) a un EQE de 0,12% et un CIE (0,416 ; 0,5302). Les dispositifs OLEDs en utilisant le ß-carotene comme couche de transport du trou et la curcumine comme couche émettrice ont donné une couleur jaune avec un EQE de 0,02%.

Mots-clés: antioxydant, bêta-carotène, curcumine, fucoxanthine, kaolinite, OLED, photostabilité

INTRODUCTION GÉNÉRALE

Les crises énergétiques, en particulier celles liées aux combustibles fossiles, entraînent une utilisation accrue des nouvelles énergies renouvelables.

1

Cela encourage les chercheurs à développer de nouveaux types d'énergie renouvelables. En outre, la recherche est également orientée vers une utilisation de l'énergie qui sont plus efficace grâce au développement de matériaux de stockage de l'énergie, tels que des batteries, et à l'utilisation de matériaux économes en énergie. L'électronique organique est toujours un domaine technologique jeune qui comprend des applications diverses comme les illuminants, le photovoltaïque, l'électronique imprimée et les piles. La matière organique a la capacité à transforme la lumière en courant électrique (photovoltaïque) et en courant électrique en lumière (diodes lumineuses). Les dispositifs électroniques à base de diodes électroluminescentes organiques sont en train de développer aujourd'hui. Une OLED (diode électroluminecente organique) est une diode émettrice la lumière (LED) qui sont connues grâce leur potentiel élevé dans les applications d'affichage, de signalisation et d'éclairage. L'OLED est une diode électroluminescente dans laquelle la couche électroluminescente émissive est un film de composé organique qui émet la lumière en réponse à un courant électrique (Zissis et Bertoldi, 2014). Les OLEDs sont connues grâce à leur potentiel élevé dans les applications d'affichage, de signalisation et d'éclairage (Zmija *et al*., 2009; Kathirgamanathan *et al*., 2012; Karzazi, 2014, Scholz *et al*., 2015).

L'électronique naturelle est un domaine de recherche qui cherche des biomolécules d'origine naturelle ou naturelle pour remplacer les matériaux de synthèse traditionnels dans l'électronique organique à l'état solide (Irimia-Vladu, 2014). Les biomolécules ont souvent des propriétés électriques et optiques naturelles qui sont affinées pour améliorer les performances de l'appareil (Irimia-Vladu *et al*., 2011; Hagen *et al*., 2006; Steckl *et al*., 2011, Gomez *et al*., 2014; Soltani Rad *et al*., 2015). L'utilisation de biomolécules prend également en charge l'électronique renouvelable et respectueuse de l'environnement, avec potentiellement une réduction des coûts concomitante (Muhl *et al*., 2014).

Les écrans d'OLEDs sont basés sur des composants contenant des matériaux électroluminescents organiques (fabriqués par de petites molécules ou des polymères) qui émettent de la lumière lorsqu'ils sont stimulés par l'électricité. La conduction en couche organique est induite par la délocalisation des électrons π provoqués par la conjugaison sur tout ou partie de la molécule organique (Kathirgamanathas *et al*, 2012).

Les matériaux organiques ont des groupes fonctionnels carbonyle peuvent améliorer la stabilité de l'OLED. Parmi ces matériaux organiques, les caroténoïdes constituent une classe importante de molécules linéaires à conjugaison π qui présentent un degré élevé de délocalisation électronique et de dynamique ultrarapide (Vivas *et al*., 2011). La longue chaîne de doubles liaisons alternées (conjuguées) est responsable de la couleur orange du β-carotène. Leur absorption de lumière bleue-verte correspond à une transition électronique de l'état fondamental (S0) $1A^{-g}$ à l'état $1B^{u}$ (S2) (Larsen *et al*., 2003). Les électrons π de la chaîne sont délocalisés, faiblement tenus et facilement excités par la lumière visible à faible énergie.

Les informations sur orbital moléculaire inoccupé élevé - orbital moléculaire inoccupé inférieur (HOMO-LUMO ou OMIÉ-OMII) sont particulièrement importantes si nous voulons comprendre la modification des énergies de transition S0 $\rightarrow$ S2 du β-carotène en tant que sensibilisateur. Le colorant sensibilisant qui présente le coefficient d'absorption le plus élevé et une énergie de transition S0 $\rightarrow$ S2 inférieure donnera des rendements de conversion photoélectrique plus élevés des cellules solaires sensibilisées aux colorants (Ruiz-Anchondo *et al*., 2010).

La photostabilité du β-carotène a été étudiée par certains chercheurs. Sa complexation avec les acides humiques (en tant qu'interaction $\pi - \pi$) a pu affecter fortement ses propriétés chimiques en raison de la photostabilité supérieure (Martini *et al*., 2010). La mince couche de les minéraux opaques (régolithe martien) peut protéger la dégradation du β-carotène provoquée directement par irradiation (Vítek *et al*., 2009). Barazzouk *et al*. (2012) ont

signalé que les antioxydants augmentaient la photostabilité de la chlorophylle-a. La stabilité aux UV du β-carotène peut être améliorée par l'addition d'un photostabilisant qui absorbe la lumière au-dessous de 465 nm (Morabito *et al*., 2011; Sattar *et al*., 1977).

Le Kalimantan Ouest, l'Indonésie et Afrique Centrale ont une abondance de minéraux comme le quartz et l'argile kaolinique (Mbaye *et al*., 2014; Destiarti *et al*., 2017). L'application du kaolin, un matériau d'argile industriel largement utilisé, dépend de sa réactivité de surface. Son application commune, par ex. charge dans le polymère, le caoutchouc, le papier, les cosmétiques, les médicaments (Zsirka *et al*., 2015). Le kaolin peut également être utilisé comme adsorbant, catalyse, composites, nanohybrides et revêtement d'électrode (Araujo *et al*., 2014; Dedzo et Detellier, 2014; Matusik *et al*, 2011; Matusik et Matykowska, 2014; Tonlé *et al*., 2011, Samyn *et al*., 2015). L'électrolyte solide des batteries Li-ion était fabriqué à partir d'hybride amorphe d'argile nacrite originaire de Tunisie (Jaafar *et al*., 2014). Ces applications nécessitent toutefois des modifications de la surface et de leur structure.

Sur la base de l'historique décrit, l'objectif de cette thèse est :
(1) Caractérisation de l'argile naturelle du Congo, du Gabon et d'Indonésie
(2) Modification et caractérisation de l'argile kaolin
(3) Etude de la photostabilité du β-carotène avec la antioxydante et kaolinique modifiée
(4) Fabrication d'OLED à l'aide de biomolécules

En général, cette thèse comporte huit parties: (1) introduction générale, (2) bibliographie, (3) méthodologie, (4) caractérisation de l'argile naturelle d'Afrique Centrale et d'Indonésie, (5) modification et caractérisation du kaolin modifié du Congo Brazzaville et d'Indonésie, (6) photostabilité du caroténoïde, (7) fabrication l'OLED à l'aide de biomélécules, et (8) conclusions générales et les perpectives.

CHAPITRE I: BIBLIOGRAPHIE

1. Les Diodes électroluminescente organiques (OLEDs)

Une OLED est une technologie de pointe utilisant des matériaux organiques (petits moléculaires ou polymères) pour générer de la lumière (Zhou, 2007). Chauhan *et al* (2014) ont repris les avantages de l'OLED, tels que: (1) lumière diffuse de grande surface, source, (2) mince, plat, léger, (3) liberté de conception, (4) mise en marche rapide, entièrement aimable, (5) beaucoup de couleurs, inclut les blancs, (6) source robuste (pas de fils à l'intérieur), (7) transparent, aspect miroir, noir ou blanc, (8) technologie basse tension, (9) potentiellement haute efficacité, (10) produit vert (économe en énergie, recyclable) et (11) fabrication potentiellement bon marché. Par conséquent, les dispositifs OLED utilisant de nombreuses applications telles que la lumière (Pang *et al*., 2014), l'affichage (Ammermann *et al*., 1995), le capteur (Shinar et Shinar, 2008) et l'électronique imprimée organique (Sekine *et al*. 2014). La structure de base du dispositif comprend un substrat en verre sur lequel est formée une électrode transparente (Figure 1).
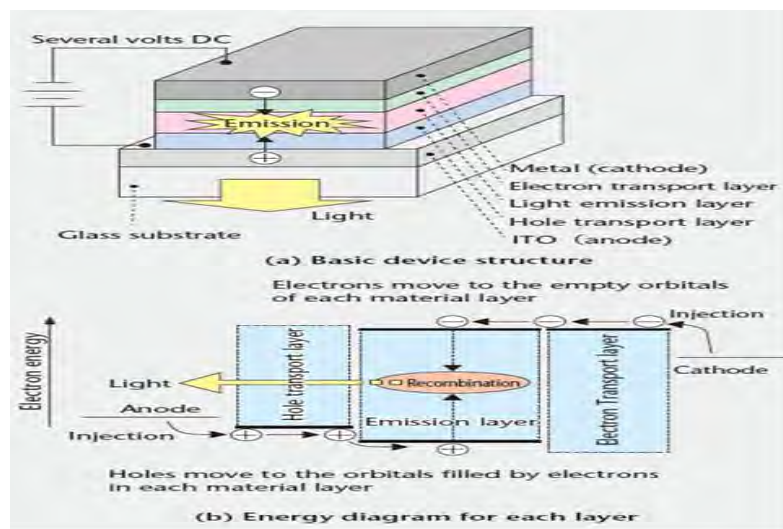

Figure 1: Principe de l'électroluminescence dans l'OLED (Shimizu, 2014)

2. Les **Bioled de biomolécules (BIODE) et colorants naturels dans OLED**

Le premier rapport sur l'utilisation de biomolécules comme couche émettrice dans les OLEDs a été initié par Tajima *et al*. (2003), dont les spectres du cytochrome c. Ils ont obtenu une bande spectrale d'émission du cytochrome c de 690 nm à la tension appliquée pendant la mesure LE 8 V. Ils ont également fabriqué des OLED en utilisant d'autres biomolécules: ITO/ biomolécule/Al, utilisant la chlorophylle a, cytochrome c, myoglobine, hémine et vitamine B12. L'autre BIODE a été réalisé par Ohtani *et al*. (2011). Ils ont utilisé des chlorophylles qui ont été extraites des épinards. Ils ont fabriqué de l'ITO (150 nm) / PPV-chlorophylles (100 nm) / Al (150 nm) et la surface de cette OLED était de 2 x 2 mm2. L'application du type de chromosphère de curcumine du type donneur-accepteur (D-A) a été réalisée par Soltani Rad et al. (2015). Gomez *et al*. (2014) ont utilisé des bases d'ADN thymine et adénine dans des diodes électroluminescentes bio-organiques.

2. Composé l'organique naturel

Le β-carotène est l'un des caroténoïdes colorés ayant une activité antioxydant. C'est un pigment rouge-orange fortement coloré présent dans de nombreuses plantes et fruits, comme les carottes, les citrouilles ou les patates douces. Le β-carotène est la provitamine de la vitamine A et est largement utilisé comme colorant dans les aliments et les boissons. C'est un composé hydrocarboné lipophile hautement conjugué non polaire (Figure 2).
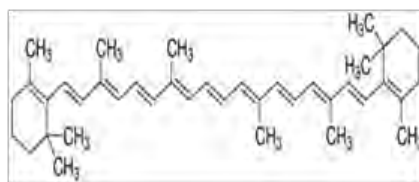

Figure 2: Structure moléculaire du β-carotène (Delgado-Vargas *et al*., 2000)

La fucoxanthine (Figure 3), un important caroténoïde marin, est présente en abondance dans certaines macro et micro algues et représente plus de 10% de la production totale estimée de caroténoïdes dans la nature. La curcumine est une poudre cristalline jaune orangé composée de trois

composants colorants en différentes parties qui sont tous des dérivés du dicinnamoyiméthane (Mainum et Shashikala, 2014). La curcumine peut être extraite de curcuma (Curcuma longa) (Kulkarni *et al*,.2012; Kandasamy et Subramanian, 2013; Van Nong *et al*., 2016) ou de Curcuma xanthorriza (Taher et Sarmidi, 2015). En raison de la conscience environnementale et des effets nocifs de la toxicité ou de la nature non biodégradable des colorants synthétiques, les colorants naturels pensent globalement du fait que la majorité des sources sont plus sûres, plus respectueuses de l'environnement, la curcumine (Hasan *et al* 2014). Soltani Rad *et al*. (2015) ont utilisé la curcumine comme couche émettrice dans les OLEDs.

Récemment, on s'est beaucoup intéressé aux antioxydants naturels contenus dans les matières végétales pour remplacer les antioxydants synthétiques présents dans les produits alimentaires (Taher et Sarmidi, 2015) ou médicaux (Zaelani *et al*, 2015) tels que la fucoxanthine et la curcumine. La structure de la fucoxanthine et de la curcumine est représentée à la Figure 3.
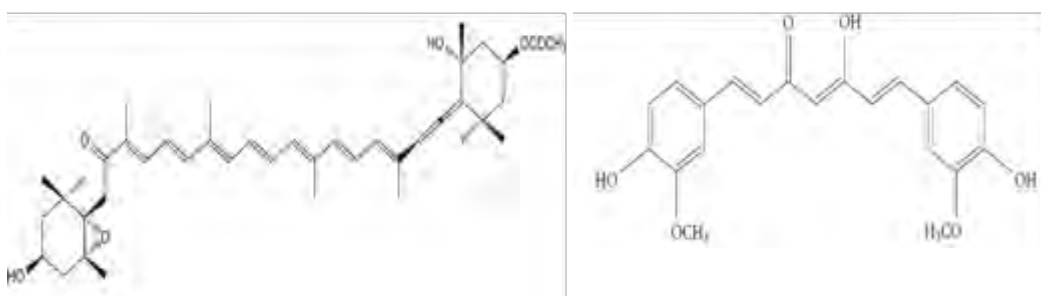
Fucoxanthine (Kita *et al*., 2015)   Curcumine (Zebib *et al*., 2010)

Figure 3: Structure moléculaire de la fucoxanthine et de la curcumine

L'argile est un groupe minéral naturel de philo silicatés cristallins à structure stratifiée dont la taille est inférieure à 2 micromètres. Selon Leroy et Revil (2004), les minéraux argileux sont classés en huit groupes principaux, sur la base du type de couche (1: 1 ou 2: 1). Les applications industrielles des trois principaux types de minéraux argileux sont variées et dans la plupart des cas très différentes. Cela est principalement dû aux différences de propriétés

physiques et chimiques, qui dépendent de la structure et de la composition (Murray, 2000).

Le groupe kaolin (type 1: 1) est divisé en trois poly typés (kaolinite, nacrite, dickite) en plus de l'halloysite, son analogue hydraté. La kaolinite (Figure 4) apparaît normalement sous forme de plaquettes pseudo-hexagonales empilées, de taille <2 µm, avec une forme de livret commune.
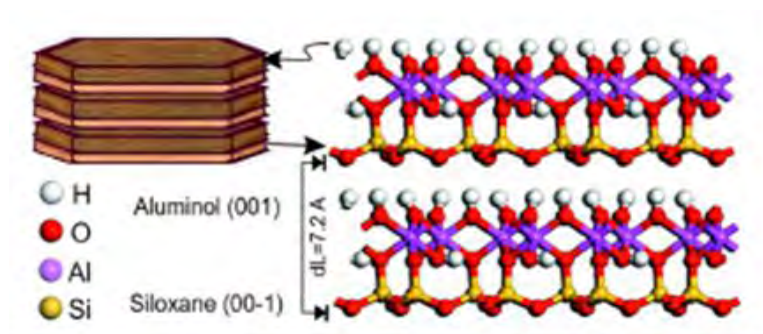

Figure 4: Modèle de simulation moléculaire de la structure de la kaolinite (cellules $1 \times 2 \times 2$ unités) montrant les surfaces en siloxane et en aluminol

L'application du kaolin, un matériau d'argile industriel largement utilisé, dépend de sa réactivité de surface. Son application commune, par ex. charge dans le polymère, le caoutchouc, le papier, les cosmétiques, les médicaments (Zsirka *et al*., 2015). Ces applications nécessitent toutefois des modifications de la surface et de leur structure.

2. Biodes de biomolécules (BIODE) et colorants naturels dans OLED

Le premier rapport sur l'utilisation de biomolécules comme couche émettrice dans les OLEDs a été initié par Tajima *et al*. (2003), dont les spectres EL du cytochrome c. Ils ont obtenu une bande spectrale d'émission du cytochrome c de 690 nm à la tension appliquée pendant la mesure LE 8 V. Ils ont également fabriqué des OLED en utilisant d'autres biomolécules: jonctions ITO / biomolécule / Al utilisant la chlorophylle a, cytochrome c, myoglobine, hémine, vitamine B12. L'autre BIOLED a été réalisé par Ohtani *et al*. (2011). Ils ont utilisé des chloropylles qui ont été extraites des épinards. Ils ont fabriqué de l'ITO (150 nm) / PPV-chlorophylles (100 nm) / Al (150 nm) et la

surface de cette OLED était de 2 x 2 mm2. L'application du type de chromosphore de curcumine du type donneur-accepteur (D-A) a été réalisée par Soltani Rad et al. (2015). Gomez et al. (2014) ont utilisé des bases d'ADN thymine et adénine dans des diodes électroluminescentes bio-organiques.

CHAPITRE II: MÉTHODOLOGIE

Quatre grandes étapes de la conduite de cette recherche sont: (1) préparation et caractérisation de l'argile naturelle, (2) modification du kaolin avec NH_4OH et $ZnCl_2$, (3), caractérisation du kaolin modifié, (4) analyse de la photostabilité du caroténoïde avec kaolinite modifiée, et (5) fabrication l'OLED en utilisant des biomolécules.

CHAPITRE III: CARACTÉRISATION DE L'ARGILE NATURELLE

L'argile naturelle a été caractérisée par des études Diffraction des rayons X (DRX), Fluorescence X Ray (FXR), Infrarouge (IR), Analyse Gravimétrique Thermique/Analyse Thermique Différentielle (AGT/ATD), Microscope électronique à balayage (MEB) et par absorptiomètre utilisant de l'azote. Les propriétés physiques de l'argile naturelle sont représentées à la Figure 5. La couleur de l'argile provenant de l'ouest de l'Indonésie (Capkala et Sintang) et de l'argile du Gabon est blanche et grise. La couleur de ces argiles est significativement différente avec l'argile du Congo Brazzaville. L'argile du Congo Brazzaville ressemble à du brun-vert. Le kaolin est généralement blanc ou presque blanc.

Figure 5: Argile d'Indonésie, du Congo Brazzaville et du Gabon

Les diagrammes DRX ont montré que tous les échantillons sont constitués de kaolin (Figure 6). L'argile d'Indonésie, de Capkala et de Sintang est de type kaolinite.
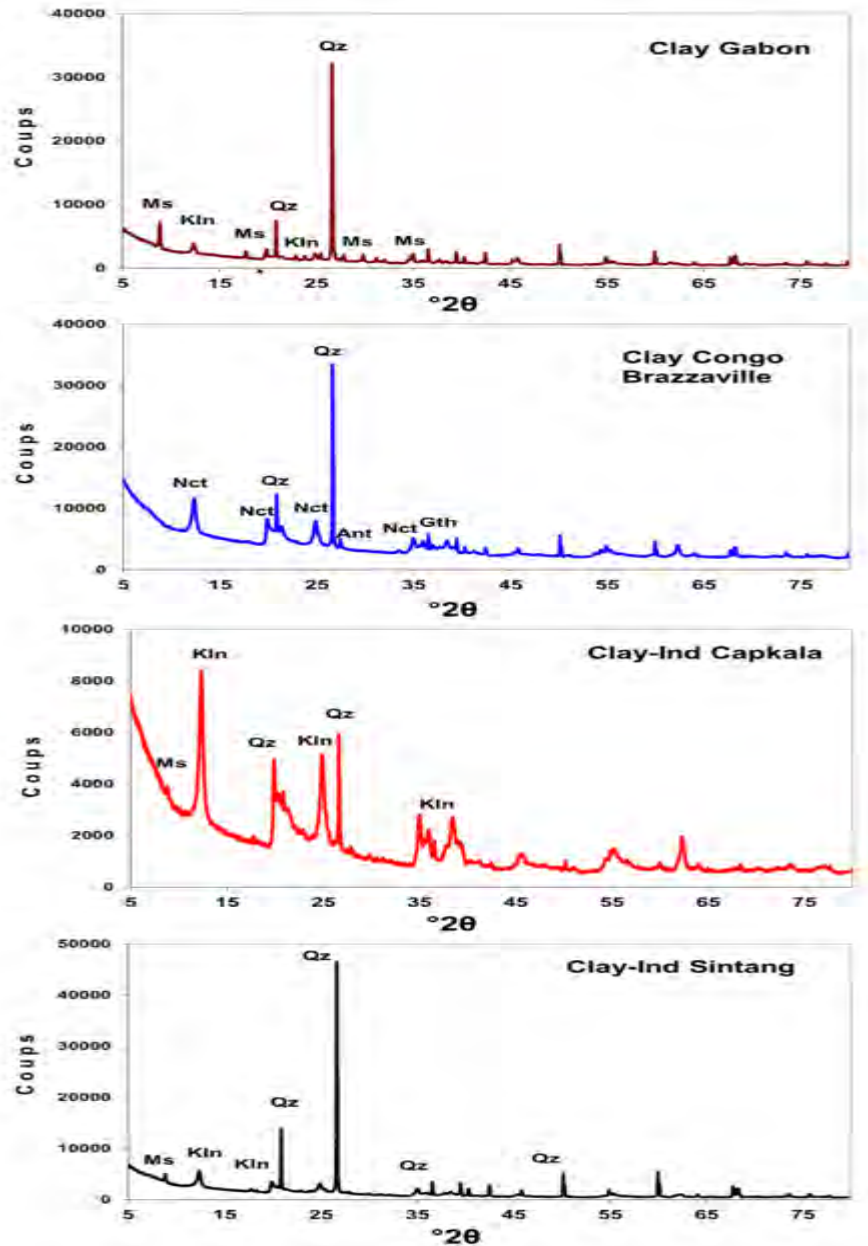
Figure 5: Spectres DRX d'argile naturelle (Ms: muscovite; KIn: kaolinite; Qz: quartz; Nct: nacrite; Ant; anatase; Gth: goethite)

La morphologie de toute l'argile naturelle (Figure 6) avec différents grossissements montre que les cristaux de kaolinite sont pseudo-hexagonaux avec des plaques, des livres plus gros et des empilements vermiculaires (Murray, 2000). 1991; Singh et Gilkes, 1991).

Figure 6: MEB de l'argile provenant de Sintang (A, B), Capkala (C, D), Congo Brazzaville (E, F) et Gabon (G, H)

L'DRX de l'argile rouge montre qu'il existe des pics avec une haute cristallinité et que les autres sont brodés (Figure 7). Le pic mince correspond au 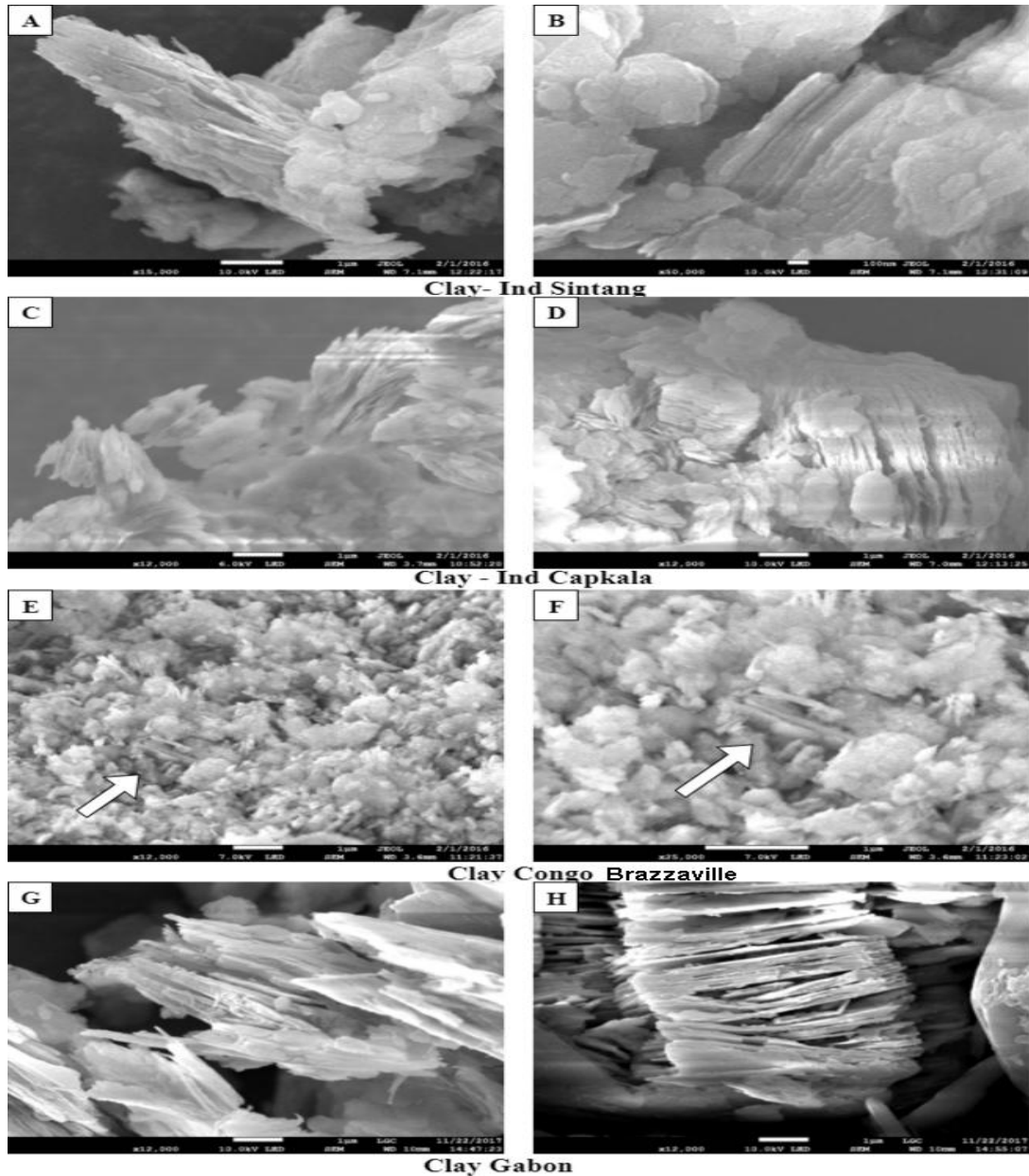quartz (Qz) et le plus large peut être un composé organique. Cette molécule organique aliphatique est également confirmée par IR et H-RMN. L'élément de carbone dans ce matériau est supérieur à 70%, soit près de 4 fois plus que l'argile naturelle du Congo Brazzaville. Les données de la réaction cinétique ont montré que la dégradation du kaolin rouge dans l'acétone était une réaction d'ordre zéro avec une vitesse de réaction constante de 0,0155 h^{-1} et une demi-vie de 18,42 h. L'écart électrochimique utilisant -1,34 eV est inférieur à deux composés caroténoïdes, le β-carotène (2,04 eV) et la fucoxanthine (2,02 eV).
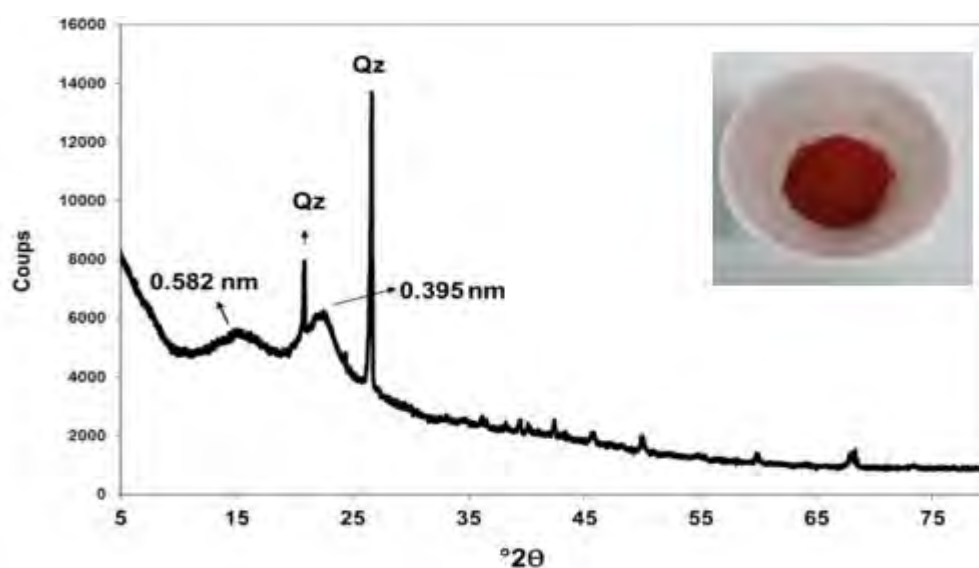
Figure 7: Difratogramme du kaolin du Gabon (encadré: poudre de kaolin)

HAPITRE IV: MODIFICATION ET CARACTÉRISATION KAOLIN DE L'AFRIQUE DU CONGO ET DE L'INDONÉSIE DE KALIMANTAN OUEST

1. Caractérisation et modification de l'argile naturelle du Congo Afrique

Les motifs DRX de l'argile naturelle du Moubeyi,Congo Brazzaville, en Afrique Central, montrent des réflexions bien définies à une valeur de 2θ2 de 12,308 (correspondant à la valeur d de 7,185 Å. Ces pics correspondent aux

réflexions de d002, qui sont typiquement des pics caractéristiques de l'argile kaolinique, de la nacrite.

L'activation de l'argile du Congo avec NH_4OH a augmenté la blancheur de ce matériau (Figure 8). Pour les applications industrielles comme les charges ou les adjuvants dans le papier et le caoutchouc, les propriétés de blancheur du kaolin sont très importantes.

Figure 8: Argile naturelle du Congo Brazzaville et changement de couleur après traitement

Nacrite activée calcinée avec de l'hydroxyde d'ammonium, augmentation de la surface presque 8 fois supérieure à celle de l'argile naturelle jusqu'à 239,69 m2 /g et diminution du diamètre moyen des pores. La surface de nacrite activée avec de l'hydroxyde d'ammonium (Tableau 1) est relativement supérieure à celle de l'autre chercheur utilisant un activateur de base, tel que le NaOH activé par le kaolin commercial ayant une surface de 76 m^2 /g (Kumar et al. g (Belver *et al*., 2003). Méthodes d'activation utilisant un acide tel que HCl, surface de surface résultante 219 m^2g^{-1} (Belver *et al*., 2002).

Tableau 1: surface spécifique BET, volume des pores et diamètre des pores des narcotiques

Paramètre	L'Argile naturelle	L'Argile calcinée	L'Argile activée
Aire de surface spécifique (m^2g^{-1})	30,548	34,380	239,68
Volume pore (cm^3g^{-1})	0,1589	0,1085	0,2120
Diamètre moyen des pores (nm)	20,805	12,842	3,5384

2. Caractérisation et modification du kaolin de Kalimantan Ouest, Indonésie

Dans cette recherche, nous avons caractérisé et modifié le kaolin de l'ouest du Kalimantan, en Indonésie. Avant activation, la kaolinite naturelle était calcinée à 600 ° C pendant 6 heures pour donner de la métakaolinite. La modification de la métakaolinite a été effectuée en utilisant $ZnCl_2$. Le diagramme de DRX montre que ce matériau est composé de kaolinite associée à du quartz et à une petite fraction de muscovite.

La métakolinite de modification avec le chlorure de zinc est représentée par l'absence de Zn dans la kaolinite modifiée. D'après l'analyse MEB-RDE, la quantité de zinc dans la kaolinite modifiée est de 6,1%. En d'autres termes, près de 46,9% du zinc total est imprégné sur la métakaolinite. L'analyse de la surface BET a montré que le chauffage du kaolin diminuait la surface spécifique mais augmentait le volume moyen des pores. Selon l'analyse de la surface BET, la calcination diminue la surface spécifique, mais augmente le volume total des pores et le volume moyen des pores.

3. Caractérisation de l'acidité totale du kaolin

La Figure 9 (a) représente les spectres du kaolin et la modification après adsorption de Py. Site acide de Lewis à MK (kaolinite modifiée) indiqué par bande de présence à 1449 cm^{-1}. Cette bande d'acidité de Lewis est proche de 1450 cm^{-1} (Yurdakoç *et al*., 1999), 1445 cm^{-1} (Morterra *et al*., 2001). La pyridine coordonnée aux sites de Lewis a absorbé près de 1455 cm^{-1} et 1610-1625 cm^{-1} (Jankovic et Komadel, 2003). Cette recherche a montré à 1608 cm^{-1} à 1608 cm^{-1}. Le site acide de Lewis provient du zinc dans la kaolinite modifiée.
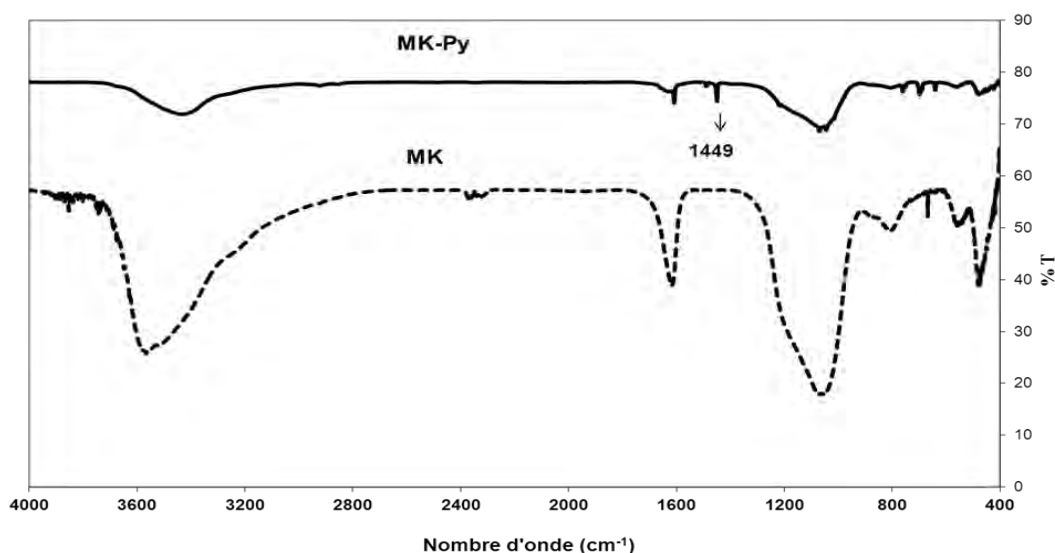
Figure 9: Spectres IR de pyridine adsorbés sur des échantillons de kaolin

CHAPITRE V: PHOTOSTABILITÉ DU CAROTÉNOÏDE

1. Photostabilité du β-carotène avec un antioxydant

La stabilité du β-carotène sans irradiation a été illustrée à la figure 10a et la photostabilité du β-carotène, de la fucoxanthine et de la curcumine aux figures 10b, 10c et 10d. L'irradiation UV des biomolécules en solution dans l'acétone a été effectuée à 0, 1, 3, 5, 7 et 9 heures. La durée de vie du β-carotène (BC), de la fucoxanthine et du curcumi sous irradiation UV était respectivement de 1,43 h; 17,72 h et 14,44 h.
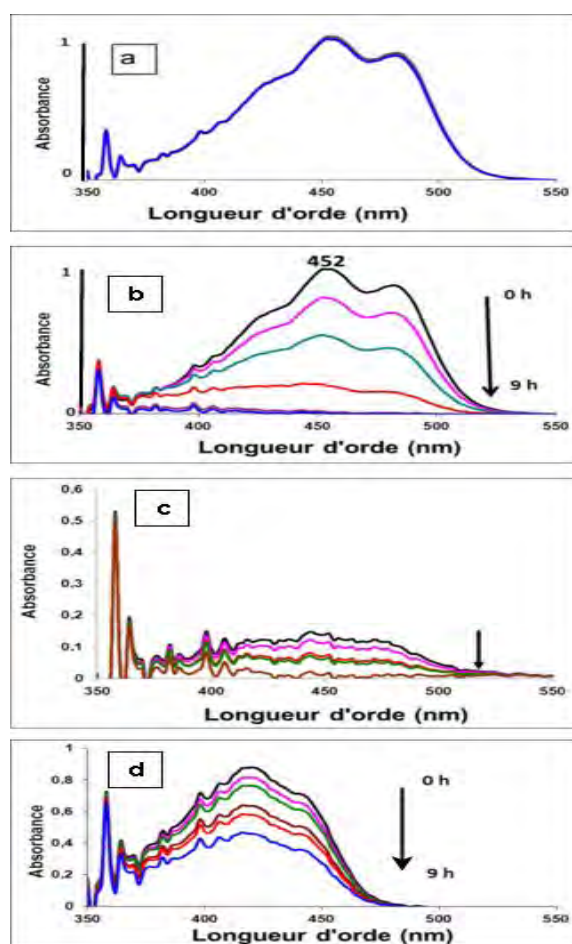
Figure 10: Stabilité du β-carotène sans irradiation (a) et sous lumière UV: de β-carotène (b) fucoxanthine (c), curcumine (d)

Le Tableau 2 montre les données de réaction de premier ordre du β-carotène (BC), de la β-carotène / fucoxanthine (BC/Fx) et du β-carotène / curcumine (BC /Cur). L'antioxydant augmente la photostabilité du β-carotène

Tableau 2: Données de réaction de premier ordre et photostablité du β-carotène et mélange composé

Biomolécule	R^2	Taux de dégradation constant, k (h^{-1})	Demi-vie (h)	% photostabilité à 5eme h
β-carotene	0.99	0.4854	1.43	-
β-carotene/fucoxanthin	0.99	0.1951	3.55	10.17
β-carotene/curcumin	0.95	0.1091	6.35	11.91

La photodégradation de la BC/Fx (période de demi-vie) représentait l'existence de la molécule de BC, tandis que la photostabilité est conçue comme la capacité de Fx à protéger le BC du photodamage. Nous avons conclu que Fx augmentait la demi-vie de la BC. La concentration maximale de rasio BC à Fx était de 1: 2 et augmentait la stabilité de BC d'environ 5 fois. Le pourcentage de photostabilité par Fx (fournir le BC) à 5 heures à cette composition était de 38,56%. La concentration maximale de rasio BC à Cur était de 1: 4 avec un pourcentage de photostabilité de 88,13%.

D'un mélange de β-carotène avec un antioxydant, BC / Fx et BC / Cur ont Eonset.ox et Eonset.red 0,45; -1,30 et 0,36; -1,25 V, donc l'intervalle électrochimique de ceux-ci sont respectivement -1,75 et -1,61 eV. Les antioxydants diminuent la lacune électrochimique du β-carotène. La curcumine a réduit l'intervalle électrochimique du β-carotène à environ 0,43 eV, tandis que la fucoxanthine à 0,29 eV.

Le Tableau 3 représente le niveau d'énergie HOMO-LUMO , l'énergie d'ionisation à l'état solide et l'affinité électronique à l'état solide de la fucoxanthine, de la curcumine, du β-carotène et de la biomolécule mélangée.

Tableau 3: Énergie HOMO-LUMO et ionisation à l'état solide et affinité électronique

Biomolécule	OMIE (eV)[a]	OMII (eV)[a]	I_c (eV)[b]	A_c (eV)[b]	Espace électrique (eV)[b]	Électrochimique écart (eV)[c]
Fx	-6.11	-4.09	-5.50	-3.30	2.20	2.02
Cur	-6.79	-4.21	-6.40	-3.44	2.96	2.58
BC	-5, 84	-3,84	-5,31	-3,00	2,31	2,04
BC/Fx	-5,84	-4,54	-5,31	-4,30	1,01	1,75
BC/Cur	-5,75	-4,50	-5,20	-4,41	0,79	1,61

[a]Estimé par voltamétrie cyclique (VC) avec Fc / Fc + à 5,39 eV sous le vide (Cardona *et al*., 2011)
[b]Estimé par VC (Sworakowski *et al*., 2016). [c]Moturé en voltamétrie cyclique dans une solution de DCM avec TBAPF6.

3. Photostabilité du β-carotène avec la kaolinite modifiée

La photodégradation du β-carotène et du β-carotène / kaolinite modifiée représentée à la Figure 5.11a. La constante de vitesse de la photodégradation du β-carotène a diminué par la présence de kaolinite modifiée (Figure 5.11b).
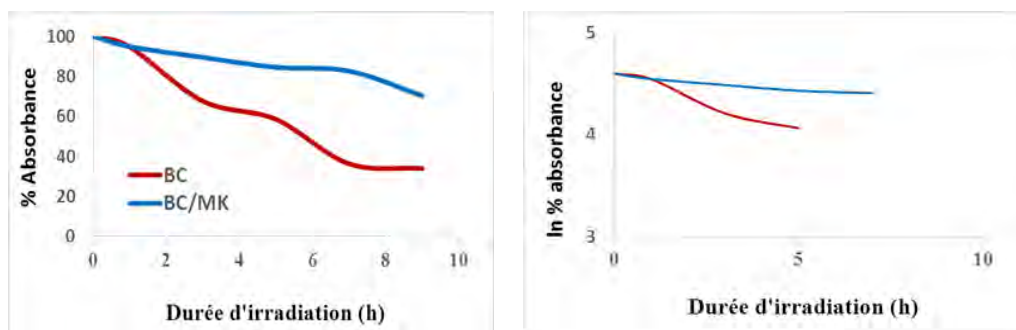

Figure 5.11: Photodégradation cinétique du β-carotène (BC) et β-carotène/kaolinite modifiée (BC/MK)

La kaolinite modifiée a diminué la photodégradation du β-carotène par protection et protection contre l'irradiation UV directe et a provoqué une demi-vie presque 50 fois plus longue. La masse de kaolinite modifiée a influencé la photostabilité du β-carotène. Le pourcentage de photostabilité du β-carotène par la kaolinite modifiée à 5 heures était de 61,87% (40 mL / 1 g). La quantité de β-carotène adsorbée sur la kaolinite était liée à la photostabilité.

4. Photostabilité fucoxanthine avec curcumine

Le λ_{max} de Fx/Cur est décalé vers la longueur d'onde inférieure ou l'énergie supérieure (Figure 12). Cet hypsocromic passe de 446 à 442, 420 nm. Le décalage en bleu était dû à la moindre conjugaison de la structure de la curcumine par rapport à la structure de la fucoxanthine (Reichardt, 1994). Ce décalage tend vers le λmax de la courbe pure (Figure 12d et Figure 12e) avec l'augmentation de la concentration de Cur. Cela signifiait dans cette solution de mélange la molécule Cur qui domine le Fx.
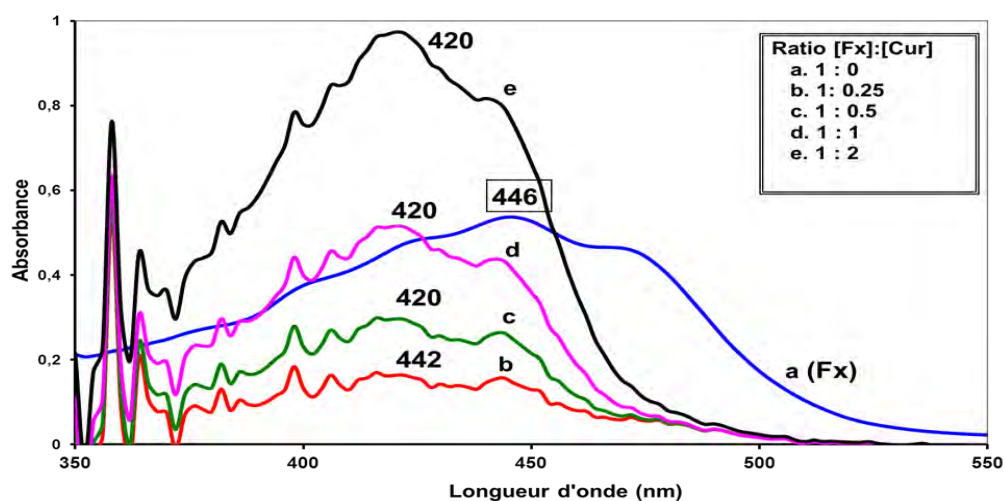
Figure 12: Spectre UV de Fx avec variation de la concentration de curcumine

L'efficacité photoprotectrice de la fucoxanthine par la curcumine a augmenté de près de 3 fois la demi-vie de la fucoxanthine de 14,44 h au rasio mol Fx à Cur = 1: 1. Avec un pourcentage de photostabilité de 40%.

CHAPITRE VI: FABRICATION OLED À L'AIDE DE BIOMOLÉCULES

Toutes les biomolécules provenaient à Sigma Aldrich, à l'exception de la curcumine à la Probe, en France. La structure moléculaire de certains matériaux utilisant OLED est représentée à la Figure 13. Fabrication OLED à l'aide de Tecnische Instrument GmbH, Specbos 1201-JETI. Préparation et traitement des échantillons dans un gant en condition N_2.

Alq₃   BAlq   MoO₃
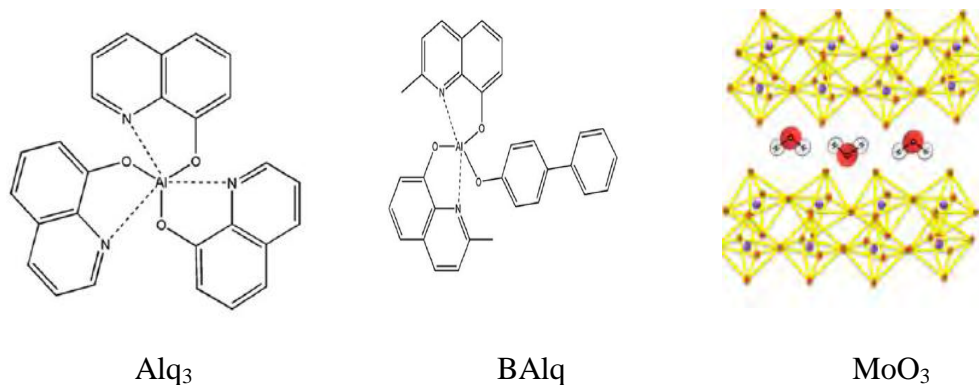
Figure 13: Structure moléculaire des matériaux utilisés dans les OLEDs
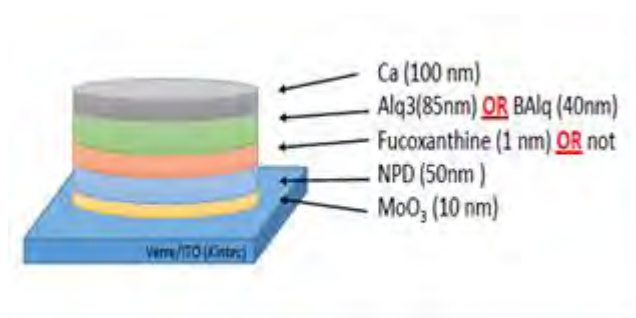
Figure 14: Fabrication l'OLED schématique utilisant la fucoxanthine

Figure 14 illustre la description schématique de la fabrication ODEL. Ici, la fucoxanthine utilisée comme matériau de couche d'émetteur (MCE) et trois types d'CTE (couche de transport d'électrons) ont été utilisés: Bphen, Alq3 et BAlq.

MoO₃ en tant que dopant de type p a été utilisé pour améliorer la conductivité des matériaux CTE et HTC, Trou de transport couche (Kao et Chiu, 2015). MoO₃ comme porteur de trou de l'anode au HTC. Le spectre de luminance et le diagramme de coordonnées CIE de Alq3 avec la fucoxanthine sont représentés à la Figure 15.
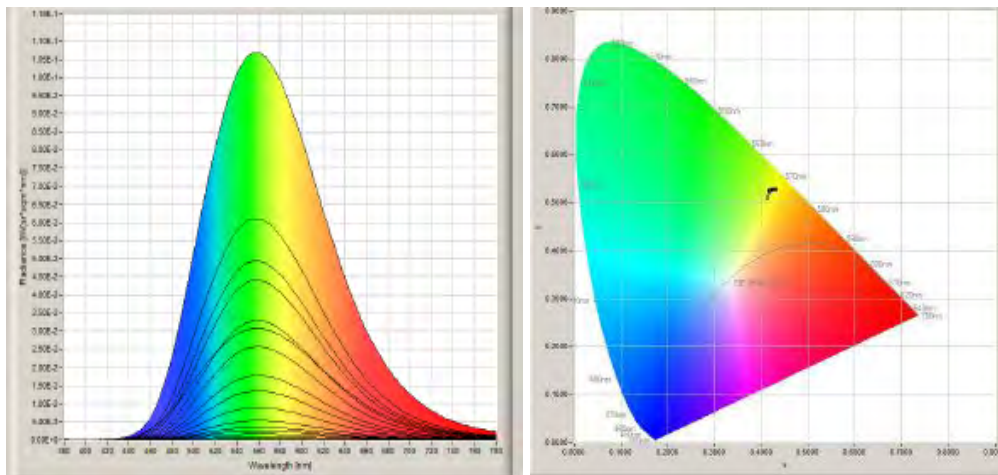
NPD(50nm)/Alq₃(85nm)
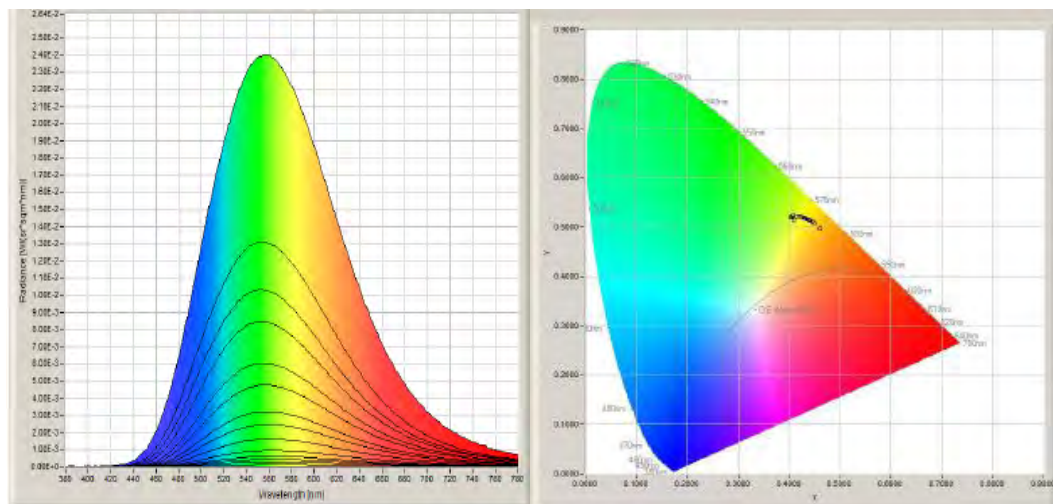
NPD(50nm)/Fx(1nm)/Alq₃(85nm)

Figure 15: Spectres de luminance et diagramme de coordonnées CIE Alq3 avec fucoxanthine

Le desain de OLED avec NPD (50 nm) / Alq3 (85 nm) a des maxima de longueur d'onde à 555 nm avec CIE (x, y) = 0,416; 0,5212. L'effet de l'utilisation de la fucoxanthine sur les spectres de luminance et CIE ne semble pas trop significatif. Le λmax et le CIE sont pratiquement inchangés. Si CTE était remplacé par BAlq, la fucoxanthine changeait le λmax de la luminance de 449 nm à 521 nm. Le diagramme CIE est passé de la région bleue à la zone verte.

Les caractéristiques de densité de courant (J) en fonction de la tension (V) pour les appareils basés sur NPD / Fx avec deux CTE différents. Tous les appareils s'allument à environ 10 V. La fucoxanthine augmente la tension appliquée, en particulier avec BAlq. La fabrication des ODEL utilisant la fucoxanthine a donné un maximum d'EQE de ηEQE = 0,12% et est indiquée dans le Tableau 4.

Tableau 4: Dispositifs ODEL de caractérisation utilisant la fucoxanthine

Dispositifs	λ_{max} (nm)	EQE (%) at 100 A/m^2	CIE (x,y)	Couleur
NPD (50nm)/Alq$_3$(85nm)	560	0,60	0,4160; 0,5212	jaune
NPD (50nm)/Fx(1nm)/Alq$_3$(85nm)	555	0,12	0,4160; 0,5302	jaune
NPD(50nm)/BAlq(50nm)	505	0,50	0,2312; 0,3648	bleu
NPD(50nm)/Fx(1 nm)/Balq(50nm)	520	0,12	0,2925; 0,4287	vert

Le dispositif n'utilisant que des β-carotènes n'a pas donné de performance en matière d'émision, mais avec une association avec la curcumine, il a donné un EQE à 100 A / m^2 = 0,02% (dispositif A). La combinaison des β-carotènes avec d'autres colorants (dispositifs B, C et D) a considérablement réduit l'EQE. En règle générale, tous les appareils se trouvent dans une zone jaune ou rouge jaune (Tableau 5).

Tableau 5: Fabrication l'ODEL à l'aide de biomolécules

Code	Dispositifs	λ_{max} (nm)	EQE (%) at 100 A/m^2	CIE (x,y)	Couleur
A	MoO$_3$(15nm)+NPD(40nm)+Car(10nm)/ Cur(15nm)/Alq3(70nm)/Ca(100nm)	545	0.02	0.3867, 0.5155	jaune
B	MoO$_3$(15nm)+NPD(40nm)+Car(10nm)/ Fx(0.8nm)+Cur-Car(15nm)/Alq3(70nm)/Ca(100nm)	550	0.035	0.3832, 0.5304	Jaune- vert
C	MoO$_3$(15nm)+NPD(40nm)+Car(10nm)/Chl in Cur(15 nm)/Alq3(70nm)/Ca(100nm)	720	0.002	0.4590, 0.4787	Jaune-rouge
D	MoO$_3$(15nm)+NPD(40nm)+Car(10nm)/Fx(0.8nm)+Chl in Cur(15 nm)/Alq3(70nm)/Ca(100nm)	700	0.0055	0.4358, 0.4800	Jaune-rouge

CONCLUSIONS GÉNÉRALES ET PERSPECTIVE

1. Conclusions générales

Les argiles naturelles du Congo Brazzaville, du Gabon et d'Indonésie sont des types de kaolin de composition différente, presque associés à la quatz. Le kaolin de Kaolin de Capkala, en Indonésie, et le kaolin du Congo Brazaville étaient nacritiques. Le kaolin rouge du Gabon se compose de composé caroténoïde aliphatique et de quartz.

L'argile nacritique d'activation du Congo Brazzaville avec NH_4OH augmentait la surface spécifique de 30,548 m^2g^{-1} à 239,68 m^2g^{-1}. La modification du métakaolinite du Kalimantan Ouest avec $ZnCl_2$ a diminué la surface spécifique mais a augmenté le volume moyen des pores de ce matériau solide. Le zinc en tant que site acide de Lewis dans la kaolinite modifiée est identifié à la bande 1449 cm^{-1}.

Le pourcentage de photostabilité du β-carotène par la fucoxanthine et la curcumine antioxydants était respectivement de 38,56% et de 88,13%. L'efficacité photoprotectrice de la fucoxanthine par la curcumine a augmenté de près de 3 fois la demi-vie de la fucoxanthine et de 40% la photostabilité. La kaolinite modifiée a également diminué la photodégradation du β-carotène par protection et protection contre l'irradiation UV directe et a provoqué une demi-vie presque 50 fois plus longue.

La fucoxanthine dans les dispositifsOLED: NPD / Fx / CTT a considérablement réduit l'EQE (%) de près de 80% dans Alq3 et de 76% dans BAlq. NPD (50 nm) / Fx (1 nm) / Alq3 (85 nm) a EQE 0,12% et CIE (0,4160, 0,5302). La fabrication d'OLED utilisant du ß-carotene comme CTL et de la curcumine comme a couche émettrice (CE) eu pour résultat une couleur jaune avec EQE 0,02%.

En conclusion, la photostabilité du caroténoïde peut être renforcée par la kaolinite modifiée et antioxydante. Basée sur l'efficacité quantique externe, la fabrication d'ODEL utilisant la fucoxanthine et la combinaison avec d'autres

colorants organiques naturels ne sont pas bonnes à bonnes, liées à la bande passante et au rendement quantique de fluorescence des colorants.

2. Perspective

Tout d'abord, en ce qui concerne le résultat, il ressort de la fabrication les OLEDs utilisant une biomolécule qui n'est pas assez bonne en raison de la limitation du rendement quantique de fluorescence des colorants. Le maximum 25% seulement de l'émission totale sous forme de fluorescence. Il est possible d'utiliser un composé à fluorescence retardée pour convertir la phosphorescence en fluorescence. L'autre étude nécessaire consiste à fabriquer des matériaux CTE et CTT différents.

Références

Ammermann, D,. Böhler, A., and Kowalsky, W. (1995) Multilayer Organic Light Emitting Diodes for Flat Panel Displays. Annual report Institut Hochfrequenztechnik, TU Braunschweig, 47-58.

Araujo, F.R., Baptitta, J.G., Marcal, L., Ciuffia, K.J., Nassara, E.J., Calefi, P.S., Vivcente, M.A., Trujilano, R., Rives, V., Gilc, A., Korilic, S., and De Faria E.H. (2014) Versatile heterogeneous dipicolinate complexes grafted into kaolinite: Catalytic oxidation of hydrocarbons and degradation of dyes. *Catalysis Today*, **227**, 105-115.

Barazzouk, S., Bekalé, L., and Hotchandani, S. (2012) Enhanced photo stability of chlorophyll-a using gold nanoparticles as an efficient photoprotector. *Journal of Materials Chemistry*, **22**, 25316-25324.

Belver, C., Banares, M.A.,Vicente, M.A. (2002) Chemical activation of kaolinite under acid and alkaline conditions. *Chemical Materials*, **14**, 2033-2043.

Cardona, C.M., Li, W., Kaifer, A.E., Stockdale, D., and Bazan, G.C. (2011) Electrochemical considerations for determining absolute frontier orbital energy levels of conjugated polymers for solar cell applications. *Advances Materials*, **23**, 2367–2371.

Dedzo, G.K. and Detellier, C. (2014) Intercalation of two phenolic acids in an ionic liquid-kaolinite nanohybrid material and desorption studies. *Applied Clay Science*, **97-98**, 153-159.

Delgado-Vargas, F., Jiménez, A.R., and Paredes-López, O. (2000) Natural pigments: Carotenoids, anthocyanins, and betalains-characteristics, biosynthesis, processing, and stability.*Critical Reviews in Food Science and Nutrition*, **40** (3), 173–289.

Destiarti, L. Wahyuni, N., Prawatya, Y., and Sasri R. (2017) Synthesis and characterization of mangan oxide coated sand from Capkala kaolin. *International Conference on Chemistry, Chemical Process and Engineering (IC3PE) AIP Conf. Proc.* 1823, 020023-1–020023-5.

Gomez, E.F., Venkatraman, V., Grote, J.G., and Steckl, A.J. (2014) DNA bases thymine and adenine in bio-organic light emitting diodes. *Scientific Report*, **4**, 7105.

Hagen, J.A., Li, W., Steckl, A.J., and Grote, J.G. (2006) Enhanced emission efficiency in organic light-emitting diodes using deoxyribonucleic acid complex as an electron blocking layer. *Applied Physical Letters*, **88**, 171109.

Hasan, M.M., Hossain, M.B., Azim, M.A., Ghosh, A.Y., and Reza, M.S (2014) Application of purified curcumin as natural dye on cotton and polyester. *International Journal of Engineering & Technology*, **14** (05), 17-23.

Irimia-Vladu, M. (2014) ''Green'' electronics: Biodegradable and biocompatible materials and devices for sustainable future. *Chemical Society Reviews*, **43**, 588–610.

Irimia-Vladu, M., Sariciftci, N.S., and Bauer, S. (2011) Exotic materials for bio-organic electronics. *Journal Materials Chemistry*, **21**, 1350–1361.

Jaafar, N., Naamen, S., Ben Rhaiem, H., and Ben Haj, A.A. (2014) Elaboration of amorphous-clay hybrid: ($Al_2Si_2O_7$. $1/2Li_2O$) designed as a single ion conducting solid electrolyte for Li-ion batteries. *American Journal of Chemistry*, **5**, 1261.

Kandasamy, J. and Subramanian, M. (2013) Validation method for estimation of curcumin from different varieties of curcuma longa. *International Journal of Pharma and Bio Sciences*, **4**(1), 1004-1010.

Karzazi, Y. (2014) Organic light emitting diodes: devices and applications. *Journal of Materials and Enviromental Science,* **5** (1), 1-12.

Kathirgamanathan, P., Surendrakumar, S., Antipan-Lara, J., Ravichandran, S., Chan, Y.V., Arkley, V., Ganeshamurugan, S., Kumaraverl, M., Paramswara, G., Partheepan, A., Reddy, V.G., Bailey, G., and Blake, A.J. (2012) Lithium schiff-base cluster complexes as electron injectors: Synthesis, crystal structure,

thin film characterisation and their performance in OLEDs. *Journal of Materials Chemstry*, **22**, 6104.

Kita, S., Fuji, R., Richard, J., Cogdell, R.J., and Hashimoto, H. (2015) Characterization of fucoxanthin aggregates in mesopores of silica gel: Electronic absorption and circular dichroism spectroscopies. *Journal of Photochemistry and Photobiology A: Chemistry*, **313**, 3–8.

Kulkarni, S.J, Maske, K.N., Budre, M.P., and Mahajan, R.P. (2012) Extraction and purification of curcuminoids from Turmeric (curcuma longa L.). *International Journal of Pharmacology and Pharmaceutical Technology*, **1** (2), 81-84.

Kumar, S., Panda, A.K., Singh, R.K. (2013) Preparation and characterization of acid and alkali treated kaolin clay. *Bulletin of Chemical Reaction Engineering & Catalysis*, **8**, 61-69.

Larsen, D.S., Papagiannakis, E., Van Stokkum, I.H.M., Vengris, M., Kennis, J.T.M., and Van Grondelle, R. (2003) Excited state dynamics of β-carotene explored with dispersed multi-pulse transient absorption. *Journal of Applied Physic*, **109**, 103529.

Leroy, P. and Revil, A.A. (2004) Triple-layer model of the surface electrochemical properties of clay minerals. *Journal of Colloid andInterface Sciences*, **70**, 371–380.

Mainum, S.H. and Shashikala P. (2014) Extraction, nanoformulation and evaluation of curcumin. *International Journal of Pharmacognosy*, 1 (8), 520-527.

Matusik, J., Stodak E., and Baranowski, K. (2011) Synthesis of polylactide/clay composites using structurally different kaolinites and kaolinite nanotubes. *Applied Clay Sciences*, **51**, 102-109.

Matusik, J. and Matykowska, L. (2014) Behavior of kaolinite intercalation compounds with selected ammonium salts in aqueous chromate and arsenate solutions. *Journal of Molecular Structure*, **1071**, 52-59.

Mbaye, A., Diop, M.A.K., Miehe-Brendle, C.A.K., Senocq, J., Maury, F., and Francis. (2014) Characterization of natural and chemically modified kaolinite from Mako (Senegal) to remove lead from aqueous solutions. *Clay Minerals*, **49**, 527-539.

Morabito, K., Steeley, K.G., Shapley, N.C., Mello, C., Li, D., Calvert, P., and Tripathi, A. (2011) Proximal effects of ultraviolet light absorbers and polymer matrix in the photostability of β-carotene. *Dyes and Pigments*, **92**, 509-516.

Mühl, S. and Beyer, B. (2014) Bio-organic electronics–Overview and prospects for the future. *Electron*, **3**, 444-461.

Murray, H.H. (2000) Traditional and new applications for kaolin, smectite, and palygorskite: a general overview. *Applied Clay Science*, **17**, 207–221.

Ohtani, N., Kitagawa, N., and Matsuda, T. (2011) Fabrication of organic light-emitting diodes using photosynthetic pigments extracted from spinach. *Japananese Journal of Applied Physisc*, 50, 1-3.

Pang, H., Michalski, L., Weaver, M.S., Ma, R., and Brown, J.J. (2014) Thermal behavior and indirect life test of large-area OLED lighting panels. *Journal of Solid State Lighting*, **1**,7-9.

Ruiz-Anchondo, T., Flores-Holguín, N., and Glossman-Mitnik, D. (2010) Natural carotenoids as nanomaterial precursors for molecular photovoltaics: A computational DFT study. *Molecules*, **15**, 4490-4510.

Samyn, P., Schoukens, G., and Stanssens, D. (2015) Kaolinite nanocomposite platelets synthesized by intercalation and imidization of poly(styrene-*co*-maleic anhydride). *Materials,* **8**, 4363-4388.

Sattar, A, de Man, J.M., Alexander, J.C. (1977) Wavelength effect on light-induced decomposition of Vitamin A and β-carotene in solutions and milk fat. *Canadian Institute of Food Science and Technology Journal*, **10**, 56-60.

Shimizu, T. (2014) Trends in research on organic light emitting diode. Broadcast Technology, 58, Autumn.

Shinar, J. and Shinar, R. (2008) Organic light-emitting devices (OLEDs) and OLED-based chemical and biological sensors: An overview. *Journal of Physics D: Applied Physics*, **41**, 133001.

Silva-Buzanello, R.A., Souza, M.F., Oliveira, D.A., Bona, E., Leimann, F.V., Cardozo, L.F. Araújo, P.H.H., Ferreira, S.R.S., and Gonçalves, O.H. (2016) Preparation of curcumin-loaded nanoparticles and determination of the antioxidant potential of curcumin after encapsulation. *Polímeros,* **26** (3), 207-214.

Soltani Rad, M.N., Sharbati, M.T., Behrouz, S., and Nekoei, A. R. (2015) Fabrication of non-doped red organic light emitting diode using naturally

occurring curcumin as a donor-acceptor-donor (D-A-D) emitting layer with very low turn-on voltage. *Iranian Journal of Science & Technology*, **39A3***, 297-304.

Steckl, A.J., Spaeth, H., You, H., Gomez, E., and Grote, J. (2011) DNA as an optical material. *Optical Photon News*, **22**, 34–39.

Sworakowski, J., Lipinski, J., and Krzysztof, J. (2016) On the reliability of determination of energies of HOMO and LUMO levels in organic semiconductors from electrochemical measurements. *Organic Electronics*, **33**, 300-310.

Taher, Z.M. and Sarmidi, M.R. (2015) Optimization processing parameters for curcuma xanthorriza oleoresin yield and its antioxidant activity. *International Journal of Biotechnology for Wellness Industries*, **4**, 97-102.

Tajima, H., Ikeda, S., Matsuda, M., Hanasaki, N., Oh, J.W., and Akiyama, H. (2003) A light-emitting diode fabricated from horse-heart cytochrome c . *Solid State Communications*, **126**, 579–581.

Tonlé, I.K., Letaif, S., Ngameni, E., Walcarius, A., and Detellier, C. (2011) Square wave voltammetric determination of lead (II) ions using a carbon paste electrode modified by a thiol-functionalized kaolinite. *Electroanalysis*, **23**, 245-252.

Vivas, M.G., Silva, D.L., de Boni, L., Zalesny, R., Bartkowiak, W., and Mendonca, C.R. (2011) Two-photon absorption spectra of carotenoids compounds. *Journal of Applied physics*, **109**, 103529.

Zebib, B., Mouloungui, Z., Noirot, V. (2010) Stabilization of curcumin by complexation with divalent cations in glycerol/water system. *Bioinorganic Chemistry and Applications*, **2010**, 1-8.

Zhou, Z. (2007) Combinatorial fabrication & studies of small molecular organic light emitting devices (OLEDs) and structurally integrated OLED-based chemical and biological sensors. Iowa State University. Ames, Iowa. 121 pp

Zissis, G. and Bertoldi, G. (2014) Status Report on Organic Light Emitting Diodes (OLED). 2014 Status Report on Organic Light Emitting Diodes (OLED). JRC Science and policy Report, 1-33.

Zsirka, B., Horvath, E., Mako, E., Kurdi, R., and Kristof, J. (2015) Preparation and characterization of kaolinite nanostructure: Reaction pathways, morphology and structural order. *Clay minerals*, **50**, 329-340.

Zmija, J. and Maachowski, M.J. (2009) Organic light emitting diodes operation and application in displays. *Archives of Materials Science and Engineering,* **40** (1), 5-12.